STUDIES ON

SELF-COMPACTING CONCRETE CONTAINING GGBS

Mohammed Majeed Alkuhly

B.Sc., M.Sc.

A thesis submitted in fulfilment of the requirement for the degree of Doctor of Philosophy

School of Engineering

Cardiff University, UK

October 2021

In the Name of God

The Most Compassionate and the Most Merciful

DEDICATION

For my country IRAQ,

For people who believe my goals and support my efforts

Mohammed Alkuhly

ACKNOWLEDGEMENTS

I would here like to express my immeasurable appreciation and deepest gratitude for the help and support extended to me by all those who gave me the chance to accomplish this thesis. I deeply appreciate my loved country Iraq represented by the; The Higher Committee of Education Development in Iraq, Ministry of Higher Education and Scientific Research and Local administration of Karbala for their support during the study period.

I would here like to express my thanks to the people who have been very helpful to me during the time it took me to achieve research work and write this thesis. I have been very fortunate with my supervisor, Professor Jefferson is more than I can express in words. It has been an honour to be his PhD. student. I appreciate his support, suggestions, valuable discussions and continuous provisions that benefited me much in completion and success of this study. Without his support, I could not have finished my dissertation successfully.

I would like also to express my gratitude to my co-supervisors Prof Grosvenor and Dr Davies who has been always helpful. I am deeply grateful to them for valuable discussions we had during my research project.

My thanks also go to the staff of research office (lovely Miss Aderyn Raid and Miss Janette White) and the technical staff of concrete laboratory, (Mr Carl Wadsworth) at Cardiff University / School of Engineering for their help and support.

Special thanks for student support team who have been very helpful and supportive in difficult times when I needed and on the top of them Miss Linda Hellard.

Warm and special thanks are expressed to my wife and children, parents, brother and sister for their support during the period of this research.

Finally, special thanks go to my friends, on the top Mohammed, Alaa, Assel and Abbas

SUMMARY

A new procedure for designing self-compacting concrete (SCC) mixes with high levels of ground granulated blast furnace slag (ggbs) as a cement replacement material is proposed. The research to produce and validate this procedure comprises three main parts. In the first part, an existing micromechanical model for the plastic behaviour of fluids with inclusions is adapted to compute the plastic viscosity of SCC. The model is needed because rheometers are unable to reliably measure the plastic viscosity of liquids with multiple inclusions of different sizes. The effects of including high levels of ggbs in an SCC on the yield stress of plastic mixes are also investigated. The second part of the research considers the hardened properties of SCC. A combined hydration and strength development model is adapted and validated for SCC mixes with high levels of ggbs, and new formulae are developed for predicting the compressive strength at 28 days and at full hydration. This combined model allows the strength of a SCC to be predicted at any time after casting. The final part of the work brings together the research on plastic and hardened properties and presents a design procedure for proportioning SCC mixes with ggbs cement replacement levels from 0 to 80%. The work involved the production of a series of graphs and tables that allow the proportions of an SCC mix to be determined for a given target plastic viscosity. The strength prediction formulae are arranged so that multiple strength criteria (i.e. strengths at different times after casting) can be used to determine the required ggbs level and water-binder ratio. The mix design procedure is successfully validated using a series of experiments. The research highlights the potential of SCC blended with high proportions of ggbs to reduce the amount of cement used in the production of this type of concrete. Overall, the work provides a way to maximise the use of ggbs in SCC and thereby produce more sustainable and environmentally friendly concrete.

NOTATIONS

SCC	Self-compacting concrete
NVC	Normal vibrated concrete
CA	Coarse aggregate ≤ 20 mm
cm	Cementitious materials
CRMs	Cement replacement materials
FA	Fine aggregate ≤2 mm
fcu	Cube compressive strength, MPa
ggbs	Ground granulated blast furnace slag
LP	Limestone powder ≤ 125µm
SP	Super-plasticizer
t500	Time taken for SCC to spread 500mm in the flow test, s
t500 j	Time taken for SCC to spread 500mm in the J-ring test, s
tstop	Time taken for SCC to spread stop in the flow test, s
VMAs	Viscosity modifying agents
SP/b	Superplasticiser/ binder ratio %
w/cm	Water to cementitious material ratio, %
w/p	Water to powder ratio, %
fc	Cylinder strength, MPa
η	Plastic viscosity, Pa s
τ_y	Plastic yield strength parameter, Pa
ϕ_m	Maximum possible volume fraction
Ĥ	Numerical factor is equal to 2.5 for rigid spherical particles and to 1 for spherical air bubbles that are packed randomly in a hexagonal arrangement
ψ	Numerical factor that depends on the plastic shear rate
ϕ	Volume fraction
sf	Silica fume
FA	Fly ash
CSF	Condensed silica fume
SSD	Saturated surface dry
HRWRs	High-range water-reducing admixtures
C-S-H	Calcium–silicate hydrate
α	Degree of hydration
SF	Consistence classes expressed by slump-flow
VS	Viscosity classes expressed by T500
VF	Viscosity classes expressed by V-Funnel time

TABLE OF CONTENTS

Chapter 1 Introduction

1.1 Introduction

This chapter presents the scope of the research, highlights the research objectives and methodology, describes the structure of the thesis and outlines the research outputs.

1.2 Scope of the research

The increasing growth of the world's population and expansion of cites in recent decades has led to the need for new structural design ideas and a rise in the demands on reinforced concrete structures. Forms and sections of construction members have become more complex, and their reinforcement has become more clustered and denser, posing problems when pouring, casting, compacting and filling concrete elements. With growing complexity, the durability problem of concrete structures has become a crucial matter facing engineers. Durable concrete structures can be created when sufficient compaction is achieved by skilled labour. In the 1980s, the lack of skilled site operatives and consequential poor quality of construction caused serious concerns in Japan (Okamura and Ouchi, 2003). The need for improved concrete quality assurance and better working conditions has driven progressive innovation in concrete construction. In 1986, a Japanese researcher (Okamura) efficaciously pioneered what is now known as "self-compacting concrete" (SCC). Since its early use in Japan, SCC has become an alternative to vibrated concrete (VC) across the world as it offers numerous economic and technical advantages over VC (Omran and Khayat, 2016). These include: overcoming obstacles associated with cast-in-situ concrete, ensuring good structural implementation and robustness, shortening execution time, and contributing to a safe and healthy working environment by minimizing the use of vibration equipment and noise levels.

Self-compacting concrete is a deliquescent material suspension that can compact itself by means of its own weight with no requirement for vibration. It is able to fill the gaps in heavily congested reinforcement and geometrically complicated structural members without any segregation and bleeding (EFNARC, 2005).

Thus, it can achieve the following requirements: filling ability, passing ability and segregation resistance. This is accomplished by correctly designing the volumetric fractions of the mix constituents. SCC has passed from the research stage to real applications. However, until recently no specific systematic design method had been developed for proportioning SCC mixes. The existing methods relied on trial and error approaches that were both time-consuming and wasteful in materials. The design process would be altogether more efficient if a comprehensive systematic design approach for SCC was available. The author's predecessors at Cardiff (Abo Dhaheer et al, 2016b) developed the first systematic approach to SCC mix design but this was limited in the range of mixes that it covered (See Chapter 2).

The volume fractions of the mix ingredients i.e. cement, cement replacement materials, aggregates, water and admixtures have a substantial effect on the rheology of SCC, and also play a pivotal role in its hardened properties. SCC's flowing ability is its main characteristic; thus, to understand SCC fully requires an understanding of its rheology. Good quality control and accurate prediction of SCC rheology are both crucial for successful SCC production and deployment. Understanding SCC's flow behaviour is not a simple matter, particularly when the flow path is impeded by heavy reinforcement and involves complex shapes

Regardless of its fresh state, the characteristics of SCC in its hardened state cannot be neglected since its structural performance is governed by its hardened properties. There is much literature on SCC but a significant proportion of this has focused on its properties in the fresh state with less attention having been being given to its long-term time-dependent hardened properties.

Compressive strength remains the most widely-used parameter to characterise solid concrete, playing a key role in assessing its strength and giving an indication of its overall quality (Neville, 1995).

Thus, to achieve the appropriate fresh and hardened properties of an SCC mix, a reliable method should guarantee both its strength and its rheological properties, i.e. strength together with rheological properties need to be imposed as design criteria.

In addition to mix design, cement replacement materials (CRMs) are another important impact factor of fresh and hardened SCC. EFNARC (2005) explains that the cement type selection depends on the overall requirements for the concrete such as strength and durability. The most widely used CRMs are ground granulated blast furnace slag (ggbs), silica fume (SF) and fly ash (FA). More details of CRMs can be found in the following references (Dinakar et al., 2013a,b; Obla et al., 2003; Sonebi, 2004; Siddique and Khan, 2011).

The work of this thesis focusses on extending an existing systematic mix design procedure to SCCs with large proportions of CRMs. This work includes validating a micromechanical model for predicting the plastic viscosity for these mixes. In addition, the mix design procedure is linked for the first time to a hydration model, with new formulae for predicting the time dependent strength of these materials.

The main objectives of work described in this thesis are:

First: to study the rheological characteristics of SCC containing the CRM ggbs by considering two important parameters, the plastic viscosity and the yield stress.

Second: to present a new procedure for predicting the time-dependent strength development of concrete, including new formulae for 28 day and fully-hydrated strengths.

Third: to build a modified method for designing SCC mixes containing ggbs cement replacement levels of up to 80%, using a target plastic viscosity and a hardened compressive strength as design criteria.

Fourth: to include in the design procedure a new approach that considers strength requirements at multiple times after casting as way to maximise the long-term strength gain potential of SCC with high proportions of ggbs.

Fifth: to conduct an experimental validation of the proposed mix design method and to examine whether the produced SCC mixes meet the design criteria in both the fresh and hardened states.

Sixth: to emphasize the environmental benefits of using high proportions of ggbs in concrete, which include reductions in CO2 emissions and raw materials, as well as reductions in energy usage during production.

1.3 Research methodology

The above objectives were realised using the following methodology:

- **First**: collecting data available for concrete, mortar and cement paste containing ggbs as a partial replacement up to 80% of total cement weight, and processing these data to find a correlation between plastic viscosity of cement paste and ggbs percentage on one hand and with the water to binder ratio on the other hand, then relating the impact of increasing ggbs in mixes to the yield stress with the change in spreading time t_{stop}.
- **Second**: extending an existing rational hydration model to SCCs with up to 80% ggbs CRM, including developing new formulae for 28 day and full hydration strengths, and validating the model using new experimental data gathered in this programme of research.
- **Third:** adapting the formulae for estimating the plastic viscosity of an SCC mix based on micromechanical principles (Ghanbari and Karihaloo, 2009) and extending the method to mixes with ggbs levels of up to 80%.
- **Fourth:** proving the validity of the proposed mix design method by preparing a series of SCC mixes for a range of target plastic viscosities and compressive

strengths. Demonstrating that all of the designed mixes satisfy the relevant flow, compaction and hardened state criteria using the slump cone apparatus, J-ring assembly and compressive strength tests respectively.

- **Fifth:** Predicting and then validating a time-dependent compressive strength model for SCC with ggbs cement replacement levels from 0 to 80%, along with an associated strength gain potential factor (R) that quantifies the post 28-day strength gain potential of the mix.

1.4 Outline of the thesis

Chapter 1 highlights the scope of the research, presents the research objectives and methodology, outlines the structure of the thesis and presents the research output.

Chapter 2 reviews SCC literature, including SCC properties, mix design approaches, materials used in its production and their influence on its characteristics in the fresh and hardened states, the relative proportions of its constituents and standard tests employed for assessment of its properties. Also presented in this chapter is a brief review of the mechanical properties of SCC.

Chapter 3 describes the materials, mixes, experimental procedures and standards used in the work described in this thesis.

Chapter 4 considers SCC plastic properties, rheology parameters and associated measurement methods. The chapter also presents a method for calculating the plastic viscosity from the constituents and for estimating the yield stress of SCC mixes.

Chapter 5 presents a mathematical formulation for predicting the time-dependent compressive strength of hardened SCC, using w/b ratio and ggbs level as input parameters. The chapter also introduces a strength gain factor that quantities the difference between the compressive strength at full hydration and the strength at 28

days. In addition, the heat energy released from the hydration reaction is quantified at a range of times for the full range of SCC mixes considered in this programme of work.

Chapter 6 describes a systematic approach for designing SCC mixes with ggbs CRM levels from 0 to 80% (the quantity of ggbs in the total binder). The approach ensures that both plastic and hardened material criteria are satisfied. In contrast to previous design approaches, the method considers the strength required at multiple times after casting (not just 28-days). The approach also includes an evaluation of the heat of hydration.

Chapter 7 presents the experimental validation of the mix design procedure described in Chapter 6.

Chapter 8 draws the overall conclusions from this research and makes some recommendations for further study.

1.5 Some specific terms used in the thesis

For convenience, a number of abbreviations are used in the thesis, as follows;

- 'ggbs %' or the 'ggbs level' refers to the percentage (or proportion) of cement replaced by ggbs (the quantity of ggbs in the total binder);
- unless noted otherwise, 'strength' refers to the average compressive cube strength of hardened concrete and the 'ultimate strength' refers to the strength at full hydration, i.e. when the degree of hydration has reached its ultimate value.

Other abbreviations and the notation used in the thesis are provided in the notation section.

Chapter 2 Background to SCC and cement replacement materials

2.1 Introduction

This chapter provides an overview of the development of SCC, highlighting the constituent materials used in SCC and their influence on SCC mix characteristics in both the fresh and hardened states. It reviews mix design methods used for the development of SCC and testing methods for SCC in its fresh state, the use of granulated ground blast furnace slag (ggbs) in concrete and the rheological properties of SCC.

Additional literature review is provided in Chapters 4, 5 and 6 on plastic parameters, hydration models and SCC mix design procedures respectively.

2.2 Self-compacting concrete: definition

The British Standard (BS EN 206-9 2010) definition of SCC is "the concrete that is able to flow and compact under its own weight; fill the formwork with its reinforcement, ducts, box-outs etc., whilst maintaining homogeneity".

Other researchers Bartos and Marrs (1999) and Khayat (1999) have defined SCC in almost the same terms as a highly flow-able concrete that should meet the following requirements:

- Flow-ability: SCC should have the ability to flow (horizontally and vertically upwards, if necessary) and fill all spaces in formwork without any external compaction.
- Passing-ability: SCC should be able to pass around heavy reinforcing steel bars without any blockage or/ nesting.
- Segregation resistance: SCC should remain homogeneous and cohesive without any separation of its heavy components (aggregate particles or/and fibres), throughout the entire construction process (mixing, transporting, handling, placing, casting, etc.).

2.3 SCC development

The first prototype of SCC was developed in 1986 by Prof. Okamura and his students at the University of Tokyo (e.g. Ozawa and Maekawa (Ouchi et al., 1998) in Japan when skilled labour was in limited supply. This initial version of SCC has since been developed for specialized applications. Since these developments, Japan has undertaken intensive research, particularly within the research institutes of large construction companies, and consequently, SCC has been used in many applications (Billberg, 1999; Okamura and Ouchi, 1999). The successful use of SCC in Japan has drawn the attention of many European countries. Sweden was the first country in Europe to develop SCC, from where the technology spread to other Scandinavian countries at the end of the 1990s (Goodier, 2003).

Since its introduction in Japan in the late 1980s, the use of SCC in the building industry has become ubiquitous. The main benefits from using SCC in building structures include shortening the construction period and thus increasing productivity, and assuring compaction in the structure (particularly in confined zones) thus enhancing the construction quality and eliminating noise due to vibration. In addition, these factors have led to substantial improvements in the on-site working environment (Bartos and Cechura, 2001; Rwamamara and Simonsson, 2012).

2.4 Advantages and disadvantages of using SCC

2.4.1 The advantages of using SCC

SCC offers many advantages (Naik et al., 2012), such as:

- cost saving on machinery, energy, and labour related to concrete compaction:
- a high-level of quality control:

- a high-quality finish, which is critical in architectural concrete, precast construction, as well as for cast-in-place concrete construction:
- a reduction in the need for surface defect remedies (patching):
- an increase in the service life of moulds/formwork:
- improved coverage of reinforcement bars:
- a reduction in the construction time:
- an improvement in the quality, durability, and reliability of concrete structures due to better compaction and homogeneity of concrete:
- an ability to reach narrow areas such as thin-walled elements or elements with limited access:
- a reduction in noise and vibration and associated improvement in the working environment.

2.4.2 The disadvantages of using SCC

Some of the disadvantages of using SCC are outlined below.

- SCC requires more careful selection of the constituent materials compared with those needed for vibrated concrete.
- Extra control is needed for measurement and monitoring of the constituent materials. The rheological properties of SCC are much more sensitive to small changes in moisture content of the aggregate (e.g. 1%) than is the case for vibrated concrete.
- Traditionally, many trial batches need to be prepared in the laboratory as well as at ready-mixed concrete plants.
- Greater overall costs due to the cost of additional components (i.e. filler, admixtures) compared with normal concrete.

2.5 Characteristics of SCC in the fresh state

The design of SCC must meet three criteria as shown in Figure 2.1: high filling ability, high passing ability, and good stability (Khayat et al., 1999b). Stability comprises two aspects: static segregation, which is defined as the separation of coarse aggregate and paste when the concrete is at rest, and dynamic segregation which occurs during the transport and casting of the concrete, i.e. during flow (Esmaeilkhanian et al., 2014).

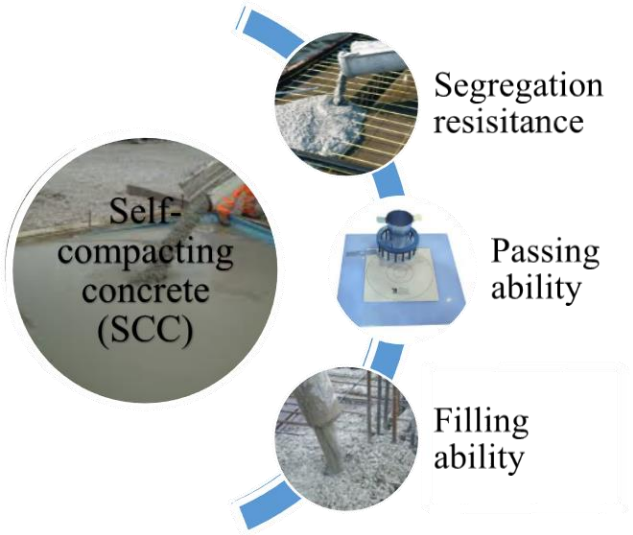

Figure 2.1 Fundamental elements of SCC

These three key requirements are related. A change in one property will lead to a change in one or both of the others. Both insufficient filling ability and segregation result in unsatisfactory passing ability. Segregation resistance increases as filling ability increases. When designing an SCC mix for a particular application there is a trade-off between these parameters (Pamnani, 2014).

2.5.1 Filling-ability

The filling ability of SCC (unconfined flowability) can be characterised as the ability of the concrete to move freely and with certain capacity into and to fill all spaces of the

formwork under its own weight (EFNARC, 2005). Filling-ability can be achieved by reducing friction between SCC solid particles (fine and coarse aggregates), accomplished by adding more lubrication as water and/or super-plasticiser (SP). Increasing the water content may decrease the particle friction and improve filling ability, but this can lead to segregation, and further consequential reduction in strength and durability. However, unlike an increase in water content, SP decreases the particle friction by dispersing cement particles and retains the deformability and homogeneity of SCC mix.

The required filling ability of an SCC mix is successfully obtained when sufficient paste covers the surface of the aggregate particles, and any excess paste minimizes the friction between them. Without a paste layer, excessive friction would be initiated between the aggregate particles, resulting in extremely limited workability. Figure 2.2 displays the formation of cement paste layers around aggregate particles.

A recent study, Al-rubaye (2017) and Alyhya et al. (2017) used a 3D model to simulate L-Box and V-funnel tests with the aim of establishing reliable flow and filling-ability criteria. They considered of the effects large aggregate particles and their orientations on the flow properties of the simulated mix.

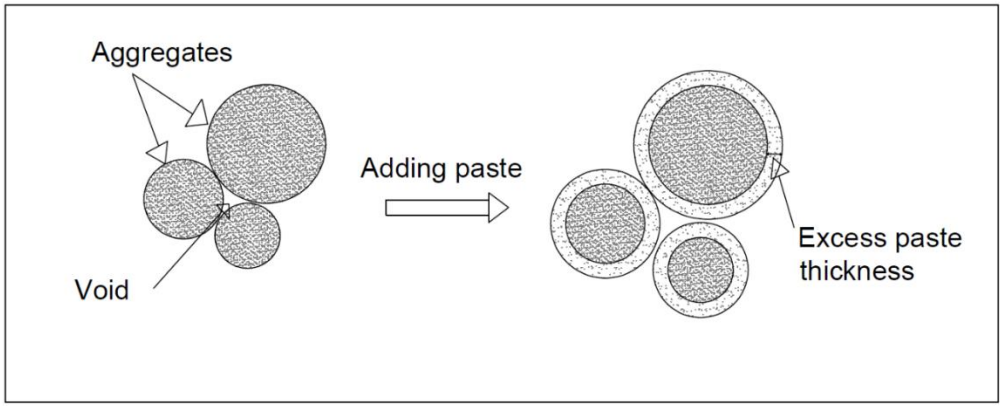

Figure 2.2 Excess paste layer around aggregates, after (Deeb, 2013)

2.5.2 Passing ability

Passing ability is the ability of an SCC mix to reshape and move through narrow spaces (e.g. between reinforcing bars) without blocking, while maintaining good homogeneity. This avoids coarse aggregate arching, blockage and segregation during flow. There is a potential risk of blocking when there is interaction between aggregate particles and between aggregate particles and boundaries (e.g. formwork in restricted spaces). When flowing SCC reaches a tight space, the different flow velocities of the aggregate and mortar can result in an excess of coarse aggregate particles in the restricted zone. Thus, some aggregate particles may bridge or arch at narrow openings preventing the rest of concrete from passing, as shown in Figure 2.3 (Tangtermsirkul and Khayat, 2000). Blocking action mainly depends on the size, shape, and content of coarse aggregate.

The irregular shape of particle clusters and the distribution of coarse aggregate particles play a crucial factor in determining the likelihood of blockages occurring. From multiple simulations, Cui et al. (2018) confidently concluded that blocking is fundamentally probabilistic, i.e. the probability of a blockage occurring when SCC crosses a flow constriction increases with the number of aggregate particles passing through the constriction. The J-ring and L-box tests are the most common methods used to assess the passing ability of an SCC mix. In some recent studies, Abo Dhaheer et al. (2016) and Al-rubaye (2017) used a 3D model to simulate the flow behaviour of SCC in J-Ring and L-Box tests and determine the final distribution of the coarse aggregate particles, the spread diameter and the t_{500} time parameter. Several other investigations (Sonebi et al., 2007; Safiuddin et al., 2011; Gesoğlu et al., 2014; Wang et al., 2020) have shown that plastic properties play a significant role in producing acceptable SCC mixes.

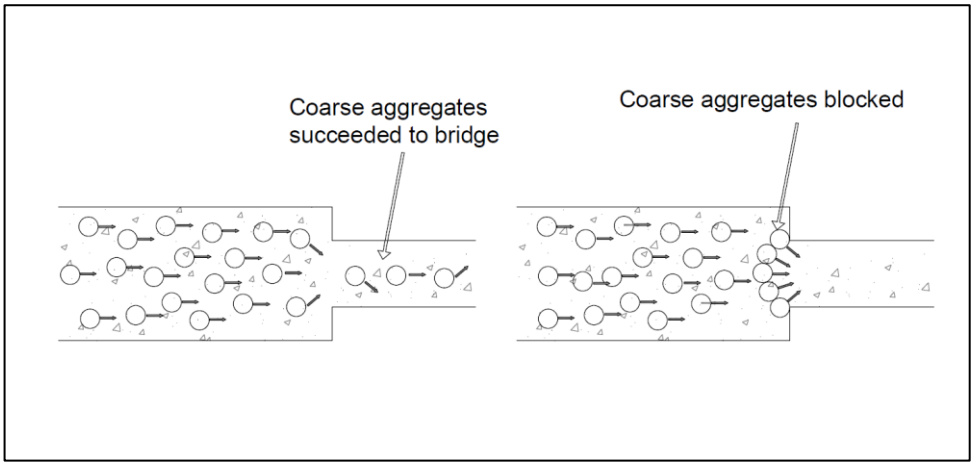

Figure 2.3 Blocking mechanism, after (Tangtermsirkul and Khayat, 2000)

The passing ability is a significant factor in any situation where aggregate particles in an SCC mix have to rearrange themselves to pass through a tight opening (Figure 2.4) (Daczko, 2012). Smaller particle sizes and reduced coarse aggregate content, as well as high paste volume, are very effective factors in preventing blocking (Billberg et al., 2004). Billberg et al. also concluded that the ability of SCC to pass through a tight opening depends primarily on the yield stress of the mix rather than its viscosity. However, a paste with sufficient viscosity can also prevent local accumulations of coarse aggregate particles and hence avoid blocking.

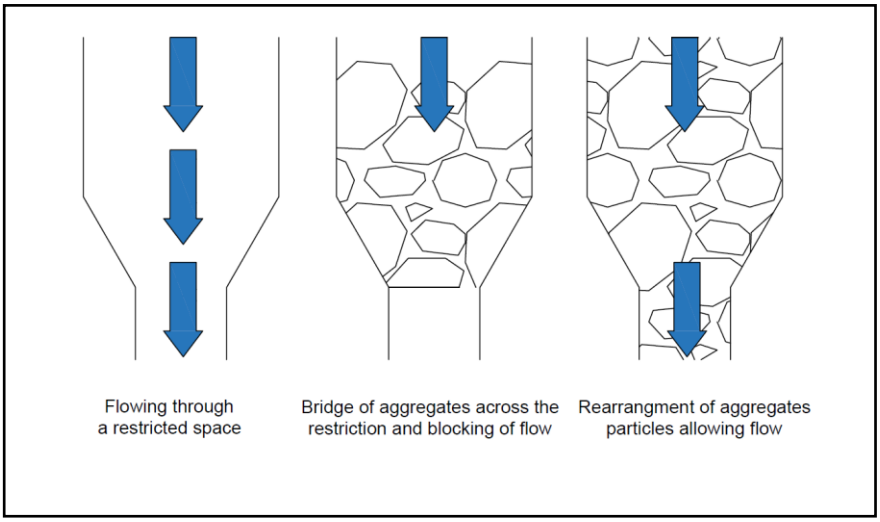

Figure 2.4 Aggregate blocking and flowing through a tight opening, After (Daczko, 2012)

2.5.3 Segregation resistance

Segregation resistance or stability is the ability of SCC to remain uniform and cohesive throughout the entire construction process (mixing, transporting, handling, placing, casting etc.). The coarse aggregate particles remain evenly distributed during flow as well as when at rest, until the concrete has set. Altering the powder content and/or using a viscosity modifying agent (VMA) enables a mix to be created with appropriate viscosity and thus stability. Limiting the size and content of coarse aggregate in a mix is also effective in preventing segregation (RILEM TC174, 2000).

The present investigation into the rheological characteristics of SCC containing the CRM ggbs in the higher range (25%-80%) considered two important parameters; the plastic viscosity (η) and the yield stress (τ_y). These parameters are used to assess whether a mix satisfies the plastic design criteria (i.e. flow-ability, passing-ability and segregation avoidance), as explained above. Their values are notably affected by the level of the ggbs when the percentage exceeds 25% (Abo Dhaheer (2016b). The trends are; the higher ggbs level the higher yield stress the lower plastic viscosity. Reliably establishing the rheological parameters for mixes with high ggbs levels is one of the main research gaps considered in this study. Further discussion on these issues will be presented in chapter 4 of this thesis.

2.6 Procedure for achieving viable SCC mixes

The method used to select the correct proportion of constituent materials is fundamental to achieving the required plastic and hardened properties of SCC (Sonebi and Yahia, 2020).

Five rules need to be followed in the selection of ingredients:

- Limit coarse aggregate content
- Use super-plasticiser
- Reduce water–powder ratio

- Increase paste content
- Sometimes use of a viscosity modifying agent

2.7 Forms of SCC

2.7.1 SCC based on increased powder content (Powder-type)

This type of mix is characterised by a low water–powder ratio (*w/p*) and a high powder content, which limits the free water content and increases the plastic viscosity. As a result of the high powder content, powder-type SCC mixes are sensitive to changes in constituent materials. Due to the low *w/p* ratio, such concretes have a high strength and low permeability but also have a high shrinkage potential (Kabagire et al., 2017; Pan et al., 2019).

2.7.2 SCC based on viscosity modifying agents (VMAs) (VMA-type)

This type of mix is characterized by a high VMA dosage, which is added primarily to increase the plastic viscosity (Piekarczyk, 2013; Zhang et al., 2020).

2.7.3 SCC based on both VMAs and powder (Combined–type)

This mix type has been developed to improve the robustness of powder-type SCC by adding small amounts of VMA. In these mixes, the VMA content is less than those in VMA-type SCC; the powder content and (*w/p*) ratio are less than those in the powder-type SCC. Viscosity is controlled by both the VMA and the powder. This type of SCC was reported to have high filling ability, high segregation resistance and improved robustness (Billberg, 2011; Li et al., 2020).

Partially replacing cement with ggbs, which has a specific gravity (SG) of 2.4, has implications when computing the volume of fines in a mix, since the cement it replaces has an SG of 2.95. The issue is addressed in this study.

2.8 Constituent materials of SCC mix

The effects of varying the type and proportions of SCC constituent materials are now outlined. The general composition of SCC is similar to that of conventional vibrated concrete. It consists of cement, coarse and fine aggregate, water and admixtures. However, the volume fractions of aggregate are different, with SCC having a lower coarse aggregate content and a greater content of fine materials than normal vibrated concrete (NVC). Figure 2.5 compares the volume fractions of ingredients in SCC and standard NVC (Okamura and Ouchi, 2003). The material properties and the proportion of the dense matrix of SCC allow the internal air bubbles to reach the concrete surface without any external vibration.

Increasingly, a wide range of waste materials are being used in the manufacture of concrete, due to concerns over climate change and sustainability in the construction sector. Nowadays, it is broadly accepted that the optimal behaviour of SCC produced with the addition of certain waste materials can rival the performance of SCC formed using conventional products (Granata, 2015; Guo et al., 2020; Revilla-Cuesta et al., 2020).

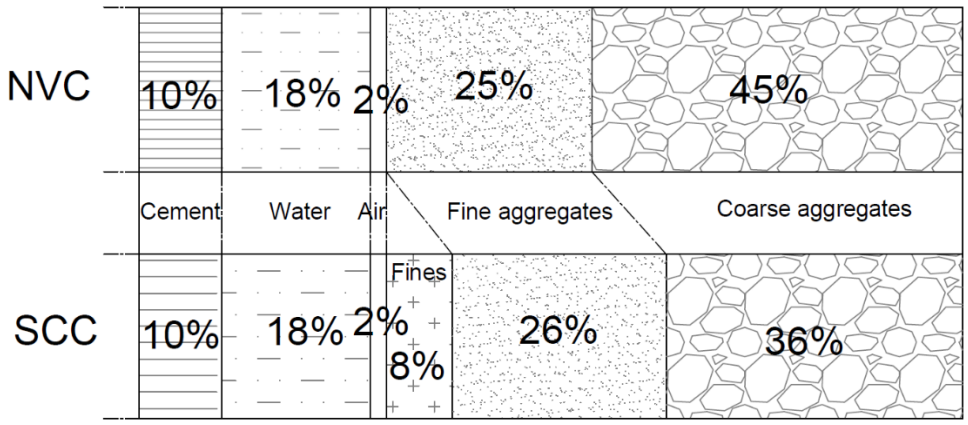

Figure 2.5 Comparison between NVC and SCC mix compositions, after (Alyhya, 2016)

Some SCC components, or proportions of those components, are classed as ‘powder’. This definition applies to material with particle sizes smaller than 0.125 mm. This applies

to all of the cement particles used in this study, the cement replacement material (i.e. ggbs) and the filler (limestone powder). Thus, the powder content used to compute the water /powder ratio is based on all of the material that meets this 0.125 mm criterion (i.e. cement + ggbs + limestone powder). By contrast, the quantity of 'binder' used to calculate the water binder ratio (*w/b* or *w/cm)* comprises the cement and ggbs.

The next section reviews the component materials in SCC and their influence on the fresh and hardened properties.

2.8.1 Cement

2.8.1.1 Portland cement

The correct choice of cement type plays a major role in producing SCC. Initially, researchers used CEM I in SCC mixes (See Chapter 6, Figure 3) but more recently new types of cement have become more widely available and are now recommended for producing SCC. The choice of cement for a particular application involves finding the right balance between the basic cement type and the cement replacement materials. As shown in Table 2.2, there are 19 types of CEM II varying from those with a low percentage of clinker (A) to those with a high percentage (C) (BS EN 179-1, 2011). Blended cement has dominated the construction demand in recent years. Moreover, the use of tertiary blends has the notable advantage of a binder system that has more than one cementitious replacement material (CRM), where one SCM compensates for the weakness of the other SCM, which in turn allows for a higher level of Portland cement replacement in concrete. These blends have been employed successfully to produce SCC with high strength at both early and later ages, and with increased quality and durability (Hooton et al., 2018). The typical powder content ranges (according to JSCE recommendations (Uomoto and Ozawa, 1999)) are shown in Table 2.1.

Table 2.1 Typical powder contents according to JSCE recommendations

SCC types	Powder content (%)	Mass* (kg/m^3)
• Powder Type	• 16-19	• 500-600
• Viscosity modifying agents (VMAs) Type	• 9.5-16	• 300-500
• Combined Type	• >13	• >410

*based on Portland cement only

Chemical admixtures are expensive and incorporating them into the mix may increase the cost of concrete. Achieving a high powder content by increasing the cement content is not feasible or desirable; it may lead to a significant rise in material cost and have a negative effect on the concrete's properties associated with the rise in temperature during hydration and higher drying shrinkage. In contrast, incorporating CRMs can lead to beneficial physical and chemical effects on the material packing and microstructure of the concrete (Hassan et al., 2000; Khatri and Sirivivatnanon, 1995; Mehta, 1994).

2.8.1.2 Blended cements

Blended cements are hydraulic cements that can be formed by mixing cementitious constituents. There are four types of blended cement, of which CEM II is the most common form (Table 2.2). The code A, B, and C refers to the level of clinker, which varies from high to low respectively. Available blended cements include Portland cement and ground granulated blast-furnace slag, Portland cement and silica fume, Portland cement and pozzolan, Portland cement and fly ash, Portland cement and burnt shale, Portland cement and limestone, and finally Portland composite.

Table 2.2 Cement types and compositions permitted by BS EN 197-1 (2011)

Cement type	Notation		Clinker %	Addition %
CEM I	Portland cement CEM I	CEM I	95-100	0-5
CEM II	Portland-slag cement	CEM II/A-s	80-94	6-20
		CEM II/B-s	65-79	21-35
	Portland-silica fume cement	CEM II/A-D	90-94	6-10
	Portland-pozzolana cement	CEM IIA-P	80-94	6-20
		CEM II/B-P	65-79	21-35
		CEM II/A-Q	80-94	6-20
		CEM II/B-Q	65-79	21-35
	Portland-fly ash cement	CEM II/A-V	80-94	6-20
		CEM II/B-V[a]	65-79	21-35
		CEM II/A-W	80-94	6-20
		CEM II/B-W	65-79	21-35
	Portland-burnt shale cement	CEM II/A-T	80-94	6-20
		CEM II/B-T	65-79	21-35
	Portland-limestone cement	CEM II/A-L[b]	80-94	6-20
		CEM II/A-L	65-79	21-35
		CEM II/A-LL	80-94	6-20
		CEM II/A-LL	65-79	21-35
	Portland-composite cement	CEM II/A-M	80-94	6-20
		CEM II/B-M	65-79	21-35
CEM III	Blast-furnace cement	CEM III/A	35-64	36-65
		CEM III/B	20-34	66-80
		CEM III/C	5-19	81-95
CEM IV	Pozzolanic cement	CEM IV/A	65-89	11-35
		CEM IV/B	45-64	36-55
CEM V	Composite cement	CEM V/A	40-64	36-60
		CEM V/B	20-38	61-80

[a] and [b] are the two type of cement have been used in current study.

Chemically, the basic reaction for CEM I results in one type of gel which gradually forms the microstructure of hardened cement in mortar concrete, but this is not the case for CEM II. In the current study, a combination of (ggbs and two types of blended cement)

were used; (i) Portland fly ash CEM II/B-V 32.5 clinker percent 65-79% and additions 21-35%; (ii) limestone cement CEM II A-L , clinker percent 80-94% and additions 6-20% according to the (BS EN 197-1, 2011). These are classified as combination cements. There are differences in the chemical hydration reactions of these two cements, due to the differences in the additions (column 4 Table 2.2) and clinker percentages.

2.8.1.3 Cement replacement materials (CRMs)

CRMs are materials with particle sizes finer than those of Portland cement. They are usually used as a partial replacement of Portland cement in SCC mixes and become involved in the hydration of cement reactions. These reactions are normally pozzolanic in nature. The most common CRMs used are ground granulated blast furnace slag (ggbs), silica fume (sf) and fly ash (FA).

These increase the workability of fresh normal concrete mixes and the beneficial effects of these materials, such as reduced PC content and lower heat of hydration, have been exploited in practical situations (Khayat et al., 2000). Ultra-fine particle binders such as condensed silica fume (CSF) have also been used in SCC, but these are associated with a reduction in the workability and slump; however, maintaining the desired workability can be achieved by increasing the super-plasticizer dosage or by using VMAs (Bernal et al., 2018). Fly ash (obtained from power station coal ash) has pozzolanic properties and can be used as a partial cement replacement in SCC. There are two classes of fly ash, i.e. class C fly ash and class F fly ash, which depend on the type of coal from which they are derived (Koehler et al. 2007).

In general CRMs are have lower costs than cement and give a positive impact on the environment by reducing the CO_2 emission indirectly by reducing the amount of cement used (Dunstan, 2011).

The next section demonstrates the properties, value and role of ggbs in SCC. Research on ggbs as a CRM is the main subject of this thesis.

2.8.1.4 Ground granulated blast furnace slag (ggbs)

Blast-furnace slag is a non-metallic product, consisting essentially of silicates and aluminosilicates of calcium, and of other bases that is created in a molten condition with iron in a blast furnace. Air-cooled blast-furnace slag is the material resulting from solidification of molten blast-furnace slag under atmospheric conditions; subsequent cooling may be accelerated by application of water to the solidified surface. Expanded blast-furnace slag is the lightweight, cellular material obtained by controlled processing of molten blast furnace slag with water, or water and other agents, such as steam or compressed air, or both. Granulated blast-furnace slag is the glassy granular material formed when molten blast-furnace slag is rapidly chilled, as by immersion in water.

Ground granulated blast-furnace slag (illustrated in Figure 2.6) is a by-product of iron production. It is classified by EN 15167-1 and EN 15167-2 (or BS 6699) according to its level of reactivity. Ggbs has been used as a cement replacement material in many countries. There are economic and environmental advantages of using this recycled material. Ggbs also has advantages in terms of the hardened concrete finish and durability (Uysal and Yilmaz, 2011; Boukendakdji et al., 2012; Dinakar et al., 2013b).

Figure 2.6 Physical appearance of ggbs used in current study 2021

The use of ggbs as a cementitious material dates back to 1774 when Loriot, a French engineer, made a mortar using ggbs in combination with slaked lime (Mather 1957). The use of ggbs in the production of blended cements accounts for between 6 and 35 % of Portland-Slag cement and 35 to 95 % of Blast furnace cement relative to the total amount of hydraulic cement produced in Europe (BS EN 197-1, 2011). The first recorded production of Portland blast-furnace slag cement was in Germany in 1892; the first United States production was in 1896. Until the 1950s, ggbs was used in the production of cement or as a cementitious material in two basic ways: as a raw material for the manufacture of Portland cement, and as a cementitious material combined with Portland cement, hydrated lime, gypsum, or anhydrite (ACI Committee, 2000). Since the late 1950s, the use of ggbs as a separate cementitious material added to the concrete mix with Portland cement has gained acceptance in South Africa, Australia, the United Kingdom, Japan, Canada, and the United States. According to a report by Curry (2020), domestic slag sales in the USA in 2019 were estimated at 17 million tons and valued at approximately 470 million USD. The composition of blast-furnace slag is determined by the ores, fluxing stone, and impurities in the coke put into the ggbs. Typically, silicon, calcium, aluminium, magnesium, and oxygen constitute at least 95% of the ggbs. Table 2.3 gives the chemical composition ranges for these elements (reported as oxides) in ggbs produced in the United States and Canada in 1988 (ACI Committee, 2000).

Table 2.3 Typical chemical composition of ggbs (ACI Committee, 2000)

Chemical constituents (as oxide)*	Range of composition percent by mass
SiO_2	32–42
Al_2O_3	7–16
CaO	32–45
MgO	5–15
S	0.7–2.2
Fe_2O_3	0.1–1.5
MnO	0.2–1.0

Except sulphate*

Regarding the hydraulic reactivity of ggbs, there is common agreement (Leung and Wong, 2011) that the basic hydration product formed when ggbs is mixed with Portland cement and water is essentially the same as the principal product formed when Portland cement hydrates, i.e. calcium–silicate hydrate (C-S-H). Slag hydrates are generally more gel-like than the products of Portland cement hydration, and so increase the density of the cement paste. When ggbs is mixed with water, the initial hydration rate is much slower than when Portland cement is mixed with water; therefore, Portland cement, alkali salts or lime are used to increase the reaction rate (ACI Committee, 2000; Özbay et al., 2016).

2.8.2 Aggregates

The aggregate used to form concrete is granulated mineral material from natural or artificial sources, or recycled from material previously used in construction. The shape, size, gradation, and volume fraction of the aggregate phases (coarse and fine) all influence the self-compaction properties of SCC (Koehler and Fowler, 2007; EFNARC, 2005). All standard sizes of coarse aggregate can be used to produce SCC. Domone (2006) reported in his study of sixty-eight applications of SCC that about 70% of cases used a maximum aggregate particle size in the range 16–20 mm, but that sizes larger than 20 mm could feasibly be used. Moreover, Domone reported that SCC would be more sensitive to segregation if a higher volume fraction or maximum size of coarse aggregate was used.

2.8.2.1 Fine aggregate

Fine aggregate (sand) comprises particles in the range 125 μm to 4 mm in size (BS EN 933-1, 2012 , BS EN 206-9, 2010, and BS EN 12620, 2013)The physical appearance and chemical composition of fine aggregate is highly variable, depending on the local rock sources and conditions. Sand with spherical particles (rather than angular crushed particles), a well-distributed grading and low absorption is preferable for forming SCC. It was reported by Alyhya (2016) that SCC performance varies with the moisture content of

the sand. It is important to control this moisture content when producing SCC as an error of 0.5% will cause a change in water content of 8kg/m^3 in concrete. This could cause a change in the slump spread of up to 45mm. Therefore, it is recommended to maintain the minimum moisture content of aggregate (FA and CA) above the SSD threshold. EFNARC (2005) states that "The influence of fine aggregates on the fresh properties of the SCC is significantly greater than that of coarse aggregate", particles size fractions of less than 0.125 mm should comprise the fines content of the paste and should also be considered in calculating the (*w/p*) ratio. Moreover, the proportion of fine particles (less than 125µm) in the fine aggregate has a greater influence on the properties of SCC than on those of NVC, since this proportion affects the amount of cohesion and segregation resistance (Topçu and Uğurlu, 2003; El-chabib and Nehdi, 2007; Yan et al., 2020).

2.8.2.2 Coarse aggregate

The coarse aggregate content of SCC should be kept to a defined upper limit (i.e. 36%) to reduce inter-particle friction and prevent blocking. The shape of the aggregate particles will affect performance, as will variations in the moisture content. The more spherical the aggregate particles the less likely they are to cause a blockage since they result in less frictional flow resistance (relative to angular particles) (EFNARC, 2005). Thus, naturally rounded aggregate is normally preferred over crushed angular aggregate for SCC.

2.8.3 Chemical admixtures

The production of SCC has been improved in recent years by the use of super-plasticisers (SP) or high-range water-reducing admixtures (HRWRs), and VMAs.

2.8.3.1 Super-plasticiser

Producing SCC with the required workability has become easier through the use of super-plasticisers and developments in admixture technology. There are four categories of SP:

sulfonated melamine formaldehyde condensates (plasticiser), sulfonated naphthalene formaldehyde condensates, modified lignosulfonates, and carboxylated acrylic ester co-polymers or poly-carboxylic ethers (Boukendakdji et al., 2012).

High-range water-reducers (HRWRs) or SPs contribute directly to the workability of SCC (Omran and Alkhyat, 2016). There are two benefits to incorporating SPs into SCC. SP controls the flow properties in SCC and allows the water to cement ratio to be minimised whilst maintaining workability and the required strength and durability. Flocculation and agglomeration of cement particles normally occur when they mix with water, due to Van der Waals and attractive electrostatic forces that are generated on the surface of the particles. This results in free water becoming trapped and a reduction in the consistency of the concrete (See Figure 2.7). Super-plasticisers or water-reducing agents produce a negative surface charge around cement particles, causing electrostatic dissonance, which in turn prevents the flocculation and agglomeration, and releases the trapped free water as shown in Figure 2.7. The HRWRs decrease the water content in concrete by up to 40% more than can be achieved by using conventional lignosulfonate-, melamine- or naphthalene-based superplasticisers (Alonso et al., 2013).

In recent study, Qian and De Schutter (2018) evaluated the differences and similarities of two types of superplasticizer in fresh cement paste; namely, Naphthalene Sulfonate Formaldehyde (NSF) and PolyCarboxylate Ester (PCE). They considered differences in the adsorption, dynamic yield stress, and thixotropic index. The results showed that NSF is less effective than PCE at decreasing the dynamic yield stress.

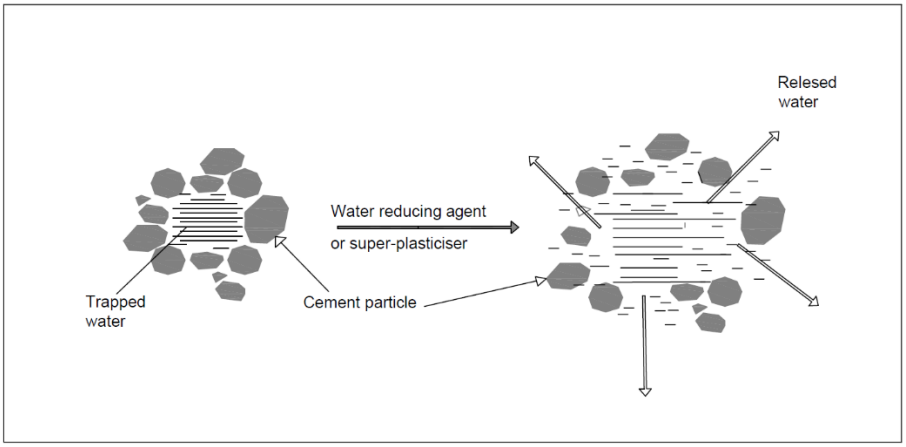

Figure 2.7 The effect of water-reducing agents or super-plasticisers on the flocculation of cement particles, including water entrapment and dispersion mechanisms

2.8.3.2 Viscosity modifying agents

VMA, also known as anti-washout admixtures, can be added to concrete mixes to improve segregation resistance, cohesiveness and reduce bleeding. In general, these admixtures increase yield stress and plastic viscosity. They may be also used as an alternative to increasing the powder content or reducing the water content of a concrete mixture (Koehler et al., 2007).

Acrylic- or cellulose-based water-soluble polymers or polysaccharides of microbial sources, such as welan gum are commonly used as viscosity-modifying agents in concrete. Water-soluble polymers can imbibe some of the free water in the system, the VMA works by increasing the viscosity of the cement paste which, in turn, enables the paste to hold aggregate particles in a stable suspension (Hisseine et al., 2018).

When using VMAs in SCC mixtures it is important to consider their compatibility with the super-plasticiser used. For instance, cellulose derivatives are incompatible with a naphthalene-based super-plasticiser, whereas welan gum is compatible (Khayat, 1995; Fantous and Yahia, 2020; Ma and Kawashima, 2020; Zhang et al., 2020).

Fantous and Yahia (2020a) reported that some VMAs affect the air content in SCC. For example, both synthetic copolymers and methylcellulose VMAs decrease the air content. Because of the shear thinning behaviour of VMA mixtures, even very small agitations can negatively influence the air content, spacing factor, and the specific surface in SCC.

2.8.3.3 Air-entraining admixtures

According to EFNARC, (2005), air-entraining admixtures should be used in the production of SCC to improve durability against freeze-thaw actions and to improve the finishing of flat slabs. Moreover, air-entrainment is particularly useful in stabilising low powder content, lower strength SCC.

2.8.4 Water

Water (*w*) is a important constituent of SCC. It is involved in the chemical reaction with Portland cement and profoundly influences both fresh and hardened properties of SCC. Rheologically, it can reduce the plastic viscosity and yield stress. The sensitivity of SCC to segregation tends to be greater when only water is used to improve filling ability. In fresh SCC, water retained by powder materials (cement and additions) and the free water controls the self-compactibility and performance of SCC (Alyhya, 2016). The water binder ratio (*w/b*) in SCC governs the strength of the hardened material and its durability, thus there is a balance between the amount of water required to achieve the plastic properties of the mix and that needed to achieve the hardened properties (Boukendakdji et al., 2012).

2.8.5 Mineral additions (Fillers)

Mineral additions can improve properties such as workability, strength, durability, and can control the rate of hydration, and thus produce variations in fluidity and stiffness (Hanehara and Yamada, 1999). According to Skarendahl and Petersson, (1999) and

EFNARC, (2005) a SCC must include total powder materials in the [(cementitious 10%) + (fillers 8%)] range 380-600 kg/m^3. They are classified in two groups, i.e. those with and without pozzolanic properties; those without pozzolanic properties are also termed fillers. One of the most commonly used fillers is ground limestone, otherwise known as limestone powder (LP). LP does not participate in cement hydration (Ye et al., 2007). It causes a change in the microstructure of the cement matrix; the small size of the particles increases the packing density of the powder, as well as enhancing the stability and the cohesiveness of fresh SCC. Excessive amounts of fine particles can result in a rise in the surface area of powder and an increase in inter-particle friction, due to solid–solid contact. In turn, this may affect the ability of the mixture to deform under its own weight, pass through obstacles and cause a rise in the viscosity (Pan et al., 2019; Anjos et al., 2020; Jain et al., 2020; Ostrowski et al., 2020; Vittalaiah et al., 2020).

Limestone powder plays a role in reducing the water absorption and can minimise drying shrinkage of SCC (Felekoğlu and Sarikahya, 2008). It has been reported that limestone powder has a marginal effect on viscosity but can raise the yield stress (Alyhya, 2016).

Although chalk powder is rarely used, SCCs containing 25 to 55% chalk were described by Türkel and Kandemir (2010). For, the same filling ability a higher volume of super-plasticiser is necessary to produce SCC mixes with chalk powder than those produced with limestone powder (Zhu and Gibbs, 2005).

The SSC mix composition needs to be selected carefully to satisfy the fresh and hardened mix design criteria, achieve the required quality and be economically viable.

2.9 Proportioning concrete containing ggbs

In most cases, ggbs has been used in proportions of 25–70% by mass of the total cementitious material. These proportions are in line with those established by (BS EN 197-1, 2011) for the production of Portland slag cement and blastfurnace cement. The proportion of ggbs incorporated will depend on the use of the concrete, the curing

temperature, the grade (activity) of ggbs and the Portland cement or other activator such as Na-based additives (Jeong et al., 2016). Where ggbs is combined with Portland cement, the combination of cementitious material will result in physical properties that are characteristic of the predominant material. Chidiac and Panesar (2008); Boukendakdji et al. (2012) and Dinakar et al. (2013b) reported that as the percentage of ggbs increases, a lower rate of strength gain should be expected, particularly at early ages, unless the water content is substantially reduced, or accelerators are used or accelerated curing is provided.

2.9.1 Effects of ggbs on properties of fresh concrete

Incorporating ggbs in self-compacting concrete has many advantages related to increasing its workability and durability, and increases its resistance to sulphate and chloride attack (Roussel, 2007). Ggbs powder has a lower density than Portland cement; therefore replacing a part of the cement by mass with ggbs will increase the paste volume, which in turn increases the cohesiveness, deformability and segregation resistance. The smoother surface texture of the slag particles and slow rate of hydration compared to cement tend to lower the water demand in blended cement and ggbs mixes more than cement-only mixes (Lewis et al., 2003). Ggbs blended concrete initially has a lower strength that cement-only concrete, but the strength increases during curing. Several factors, including chemical composition and glass content, affect the reactivity index of GGBS, which provides a measure of its cementitious performance. (BS EN 197-1, 2011) classifies slag by its reactivity level; e.g. Grade 80, Grade 100, or Grade 120, with Grade 120 having the highest reactivity index. Thus, given sufficient time for the activity level and the pozzolanic reaction and the formation of calcium hydroxide, the concrete made with a combination of ggbs and Portland cement will achieve a higher strength than cement-based concrete only (Oner and Akyuz, 2007).

2.9.2 Workability

Blast-furnace slag has good workability properties and improves the performance of self-compacting concrete in fresh state whilst avoiding the use of viscosity modifying admixtures (Ramanathan et al., 2013; Esmaeilkhanian et al., 2014). The results of extensive experimental work indicates that as ggbs content increases in SCC mixes, the water-to-binder ratio decreases for the same workability (Oner and Akyuz, 2007). A high volume fraction of ggbs may affect the stability of SCC and make it difficult to control the consistence, also, slower setting may increase the risk of segregation (EFNARC, 2005).

As discussed, high volume fractions of ggbs in SCC change the fresh properties of the mix. In this study, a mix design method is developed for SCC mixes with any ggbs cement replacement level up to 80%, which maintains the required workability and other plastic criteria. The achievement of this required a detailed study on plastic properties (see chapter 4).

2.10 Effects of ggbs on the properties of hardened concrete

2.10.1 Hydration of cement

The degree of hydration is a measure of the quantity of cement gel (hydration products) formed and is, therefore, linked to the heat of hydration. During the hydration process, the degree of hydration (α) is defined as the ratio between the quantity of hydrated cementitious material and the original quantity of cementitious material. The degree of hydration is a function of time, with α varying between 0.0, at the start of hydration, and 1.0 when hydration is fully completed. Not all of the cementitious material is likely to become hydrated, and an α of 1.0 may never be reached. After investigating the hydration of a range of different cementitious materials, Mills (1966) stated that, “In most, if not all, cement pastes hydration stops before the cement is totally consumed.” In Chapter 5, a model that evaluates the ultimate degree of hydration will be presented.

Hardening in cement is caused by chemical reactions between the cement clinker components and water. Tikalsky and Carrasquillo (1988) outlined the complex chemical reactions of Portland cement and fly ash (Reactions 1 and 2). When water is added to Portland cement, the first reaction to take place is one that forms the binding characteristics of concrete. As expressed in Reactions 1 and 2, the formation of calcium silicates hydrates (CSH) can form with the addition of water to either tricalcium silicate or dicalcium silicate. CSH accounts for about 50–60% of the volume of the hydrated paste and is strong, stable and durable under most conditions and controls the strength and durability of the hardened paste.

High levels of cement replacement by ggbs help in producing pumpable concrete for large pours and provide an economical way of suppressing the rate of heat release from the hydration reaction. For example, the access portal from Dunward Street forming part of the main access route to the Crossrail platforms at Whitechapel Station in London used 40 MPa SCC in which 70% of cement was replaced by ggbs in order that maximum temperature differential throughout the placement of large mass of concrete did not exceed 35^{o}C (NCE, 2014).

2.10.1.1 Compressive strength

SCC is usually designated by its compressive strength, because this is seen as the key parameter of the hardened material. Other mechanical properties provide an indication of the overall quality of the material (Khayat et al., 2019). Under standard curing conditions, the compressive strength of SCC is mostly determined by the water to binder (w/b) ratio. In addition to w/b ratio, various researchers (Voigt et al., 2006; Duran Atiş et al., 2007; Koehler and Fowler, 2007; Topçu et al., 2008; Daczko, 2012; Siddique, 2013; Adesina, 2020; Guo et al., 2020; Sonebi and Yahia, 2020) have pointed out that the type of cement and CRM have a notable impact on the compressive strength of SCC as do materials with pozzolanic properties, the type and size of aggregates, fibres, and the type and dosage of admixtures.

For a given w/b ratio, the compressive strength of SCC is generally higher than the comparable NVC because the former is more homogeneous and has a denser microstructure. The improved internal structure of SCC (relative to NVC) results from a suppression of segregation and bleeding, and a reduction in the w/b ratio and total porosity (Desnerck et al., 2014; Alyhya, 2016).

SCC designed with ggbs has a lower early age strength than cement-only concrete but the strength increases as the curing period is extended, so that ultimately ggbs blended concrete will attain a higher strength than cement-only concrete. This is because the slow pozzolanic reaction and the formation of calcium hydroxide requires time (Leung and Wong, 2011; Özbay et al., 2016; De Belie et al., 2018). Oner and Akyuz (2007) reported that the compressive strength of ggbs-containing concrete increases as the amount of ggbs increases, up to an optimum limit of around 55% of the total binder content. The same study showed that the compressive strengths at 360 days of mixes with high levels of ggbs surpassed those with lower ggbs levels.

An investigation to determine the efficiency of ggbs in SCC mixes (Dinakar et al., 2013a) showed that the compressive strength of their concrete exceeded 90 MPa at 28 days and 100 MPa at 90 days, as illustrated in Figure 2.8. Another study conducted on SCC-containing ggbs (Sethy et al., 2016) showed that concrete with lower compressive strengths (i.e. 20–30 MPa) can be produced with a slag replacement of about 80–90%, and that higher strengths, i.e. 60–100 MPa, can be developed with 30% and 60% slag replacement, respectively.

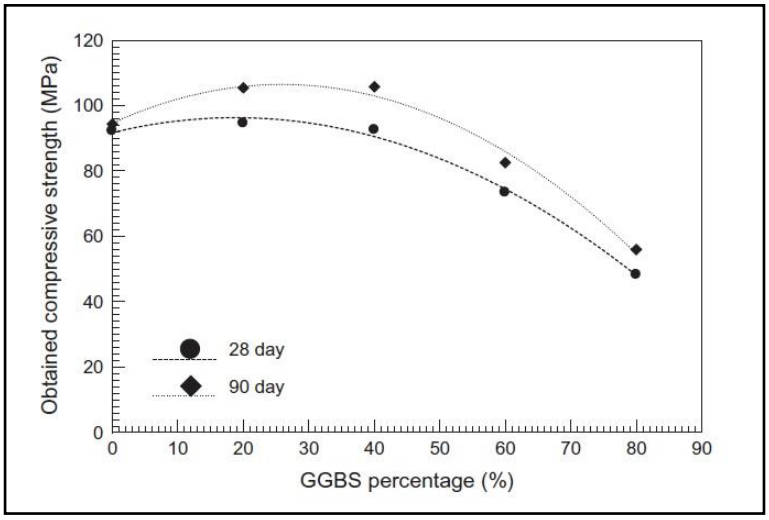

Figure 2.8 Compressive strength VS ggbs level %, after (Dinakar et al., 2013b)

2.10.2 Durability

De Schutter et al. (2008) suggested seven factors that should be considered when designing durable SCC mixes, namely: carbonation, chloride penetration, frost resistance, ASR, sulphate attack, thaumasite formation, and fire resistance. Normally, high performance concretes have good durability due to their higher compressive strength and dense (relatively impermeable) microstructure. A question remains of whether it is possible to produce highly durable concrete with medium or low performance. In this regard, Escadeillas and Waller (2007) investigated the 'potential' durability of medium strength self-compacting concretes and a reference NVC with similar compressive strengths and showed that the former achieved acceptable levels of durability.

Ggbs plays a significant physical-chemical role in improving SCC's long-term durability as a result of the long-term chemical (pozzolanic) reactions, which results in the formation of a gel that occupies the remaining spaces in the material matrix. From a chemical point of view, ggbs consumes the calcium hydroxide and makes for more resistant hydrated cement products. This results in a low permeability hardened cement paste with good resistance to sulphate and chloride attack etc. (Long et al., 2015; Owsiak and Grzmil,

2015; Dadsetan and Bai, 2017; Gholhaki et al., 2018; He et al., 2018; Saranya et al., 2018; Sharma and Khan, 2018; Awoyera et al., 2020; Huseien and Shah, 2020).

The durability of SCC is directly connected to the delayed hydration associated with the high ggbs replacement levels investigated in this study. This is a crucial matter because the presence of ggbs affects the rate of hydration, curing characteristics and associated strength development response over time of SCC.

2.11 Testing self-compacting concrete in the fresh state

Fresh state tests for SCC include the slump flow filling ability test and the J-ring passing ability test. These are discussed in Chapter 3. Other tests used to investigate the plastic properties of SCC are described here.

2.11.1 Filling ability and passing ability tests

The V-funnel test (BS EN 12350-9, 2010) is used to assess viscosity, filling ability and stability and the L-box test (BS EN 12350-10, 2010) is used to evaluate the passing-ability of SCC (EFNARC, 2005) (See Figure 2.9). The results of V-funnel tests categorise concrete into two classes based on viscosity; namely, viscosity class 1 (VF_1< 8.0s) and viscosity class 2 (8.0s≥VF_2>25.0s). The test is performed by measuring the time taken for concrete to flow out of the funnel under its own weight.

The L-box test (BS EN 12350-10, 2010) was developed in Japan to test underwater concrete, and is used to test highly flowable concretes. The L-box test is used to assess the passing ability of SCC in a confined space or, in other words, the ability of concrete to pass though narrow openings or reinforcing bars without blocking or segregation to fill a complex form.

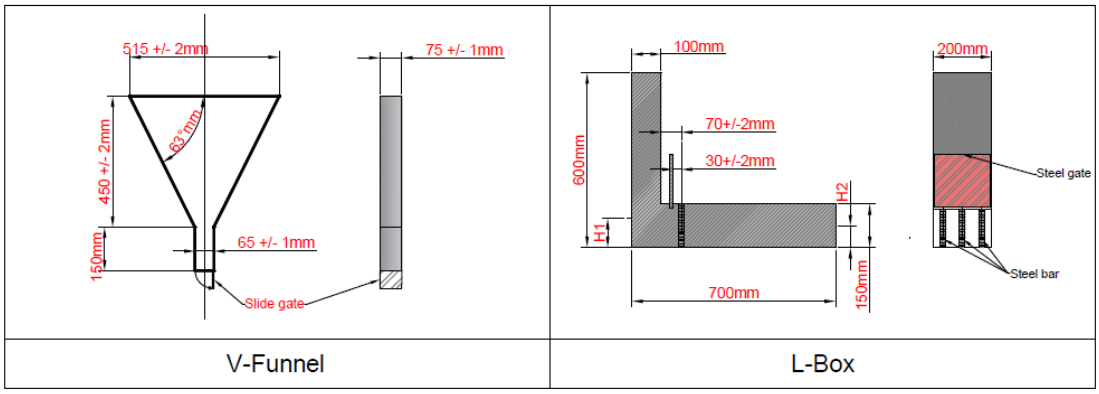

Figure 2.9 Set-up for V-funnel & L-Box tests

2.11.2 Segregation resistance and Sieve stability test

Since SCC components have particles of various sizes and densities and is susceptible to segregation; The stability of SCC can be controlled by, (i) incorporating high volumes of powder materials to bind additional free water (i.e reducing the water to powder ratio) and (ii) using viscosity modifying agents (VMAs). Minimising the proportion of coarse aggregate and the size of the coarse aggregate particles also helps prevent segregation.

Several empirical tests (PCI, 2003) have been reported to evaluate SCC segregation, these include the following approaches. (i) A visual inspection of the periphery of the concrete is carried out after measuring the slump flow spread and rating it from 0 to 3. This is an inadequate qualitative method that depends on the experience of the individual and fails to evaluate segregation quantitatively. (ii) The British standard (BS EN 12350-11, 2010) test for SCC involves the observation of fresh concrete for a period of 15 minutes, during which time the quantity of bleed water is qualitatively determined. After this period, a defined upper part of the sample is then poured onto a sieve with 5 mm^2 spaces. After a further 2 minutes, the weight of material that has passed through the sieve is recorded. The segregation ratio is defined as the mass of the material that has passed through the sieve relative to the mass of the sample placed on the sieve.

The applicability of existing standards (discussed above) for controlling segregation resistance and mix stability in our SCC mixes will be assessed in this study.

2.12 Existing mix design methods for SCC

This section briefly describes five published design principles of SCC mix design (Shi et al., 2015).

2.12.1 Empirical mix design method

In this method, initial mix proportions are based on empirical data including coarse and fine aggregate contents, water and cementitious material contents and super-plasticiser dosage (Shi et al., 2015). Numerous trial mixes and alterations are conducted to estimate the optimum proportion of constituents to produce the required properties. Based on observations, Okamura and Ouchi (1998) proposed a guide to mix proportions. This states that a fixed 50% of the solid volume should be coarse aggregate and a fixed 40% of the mortar volume should be fine aggregate. To ensure self-compactibility, trials vary the quantity of super-plasticiser dosage and the water/powder ratio within the range 0.9–1.0 by volume based on the powder properties. The empirical approach is simple but requires extensive and meticulous laboratory testing and it does not consider the properties of the aggregate (i.e. grading or maximum particle size). In a recent study (Gil et al., 2019), a new mix design procedure that can correlate the materials' composition and properties has been established based on the empirical method. Similar examples of mix design methods have been suggested by other authors (Edamatsu et al., 1998; Domone, 2010).

2.12.2 Compressive strength mix design method

In this category of SCC mix design, the quantity of cement, admixtures, water and aggregate are chosen to achieve the required compressive strength. Kheder and Al Jadiri (2010) developed a method that combines the requirements of the ACI 211.1 (1991) used

for proportioning normal vibrated concrete and EFNARC (2005) to increase the upper limit of the original compressive strength from 40MPa in ACI 211.1 to 75MPa. This method provides a simple and accurate procedure to calculate the specific quantities of components and reduces the need for trial mixes. The method of Dinakar et al., (2013b) is another mix proportioning method focused on compressive strength properties. This method includes ggbs as a CRM and allows for the associated potential reduction in the 28-day strength. The issues associated with time-dependent strength gain and the implications of having reduced relative 28 strengths (i.e. 28 day strength / ultimate strength), for concrete with high proportions of ggbs, are discussed in Chapters 5 and 6. Methods in this category consider the effects of relative proportions of fine and coarse aggregates and the contributions of CRMs on the properties of SCC.

2.12.3 Close aggregate packing mix design method

This method considers the relationships between paste and aggregate mix phases. It aims to find the mix components that achieve the least void space between aggregate particles (Shi et al., 2015). The main advantages are its simplicity in using a limited selection of binders, in contrast, the main disadvantage is that mix proportions calculated using this method tend to have segregation problems (Wang et al., 2014). There are many examples of this method: (Sedran and Larrard, 1999; Su et al., 2001; Sebaibi et al., (2013; Kanadasan and Razak, 2014).

2.12.4 Statistical factorial mix design method

The design mixes in this category are based on statistical measurements of the mix components and key parameters, such as the cement and CRM contents, water to powder ratio (w/p), the volume of coarse aggregate and the dosage of super-plasticiser on fresh and hardened properties of SCC. Based on a reference NVC mix design, the corresponding SCC mix proportions are calculated by determining the trend for each parameter (Shi et al., 2015). A clear example of this method is given by Khayat et al.

(1999). They considered five main mix parameters: coarse aggregate volume, cementitious materials content, water to cementitious materials ratio, VMA dosage, and super-plasticiser dosage in addition to different fine aggregate contents. In a statistically sound approach, all these parameters were assessed relative to the measured properties (slump flow, filling ability, V-funnel time and compressive strength). This mix design approach is suitable for a wide range of applications and provides an effective tool to determine the impact of key variables on SCC properties (Habibi and Ghomashi, 2018). The weakness of this approach is the establishment of statistical relationships, which require raw materials and considerable laboratory time. Similar approaches that use measurements of plastic properties have been suggested by a number of investigators (Sonebi et al., 2007; Safiuddin et al., 2011; Sonebi et al., 2020).

2.12.5 Rheology of paste mix design method

Methods in this category propose that the segregation resistance and workability of fresh concrete is dictated by the rheology of the cement paste matrix for a given particle size distribution and volume fraction of aggregate (Shi et al., 2015). Moreover, this approach requires a minimum yield stress and viscosity of paste that must be exceeded to avoid segregation under both static (rest) and dynamic (flow) conditions, respectively. Deeb and Karihaloo (2013) extended this rigorous mix proportioning approach (Karihaloo and Ghanbari, 2012) for proportioning high strength SCC mixes with and without steel fibres exploiting the plastic viscosity expression of Ghanbari and Karihaloo (2009). Their work increased the range of SCC mixes that could be designed using this method to include those formed with traditional coarse aggregate and extended the strength (28-day characteristic cube strength) range from 35 to 100MPa. This method did not provide any practical guidelines on how to select the most appropriate mix and the compressive strength was not explicitly imposed as a design criterion. The main advantage of these mix design methods is their ability to reduce laboratory testing and thus material consumption and to provide the basis for quality control and further development of new mineral and chemical admixtures. The methods proposed by Saak et al. (2001); Bui et al.

(2002); Ferrara et al. (2007); Abo Dhaheer et al (2016b) and Shi et al. (2018) are also based on similar concepts.

The earlier design method proposed by Abo Dhaheer (2016b) is limited mixes with up to 25% ggbs cement replacement. To allow for high proportions of ggbs (up to 80%) a revised approach is required for designing SCC mixes. This uses the target plastic viscosity and hardened compressive strengths at different ages as design criteria.

The growth in cement production has resulted in an increase in green house gases which are harmful to the environment. The best efficient way to reduce the CO2 emissions from cement production is to substitute a part of cement with other materials (CRM). One of the most important is ggbs since it is an industrial by-product associated with lower CO_2 levels than cement (Khokhar et al., 2010; Elchalakani et al., 2014; Jalal et al., 2015; Long et al., 2015; Omran and Alkhyat, 2016; De Belie et al., 2018; Saranya et al., 2018; Guo et al., 2020; Huseien and Shah, 2020.) DECC (2011) and CSMA (2021) reported that ggbs is one of the 'greenest' construction materials. Its only raw material is an exceptionally distinctive slag that is a by-product of iron production. Almost all of the slag from iron production can be used to form ggbs with no significant waste stream. Specifically, ggbs requires less than a fifth of the energy and produces less than a fifteenth of the CO_2 emissions of Portland cement production. Furthermore, ggbs does not require the quarrying of virgin materials, and if the slag was not used as cement it would have to be disposed of in a land fill or similar disposal site.

Each year, the UK uses up to two million tonnes of ggbs as cement replacement, which:

- reduces carbon dioxide emissions by some two million tonnes:
- reduces primary energy use by two thousand million kWhs:
- saves three million tonnes of quarrying:
- saves a potential landfill of two million tonnes.

The embodied CO_2 (ECO2) of cement is relatively, as illustrated in Table 2.10, which shows a comparison between Portland cement and various CRMs.

When Portland cement is considered on its own, it is understandable to see why some commentators suggest that one tonne of cement production leads to almost one tonne of CO2 emission.

Table 2.4 Embodied CO_2 Portland cement, ggbs, PFA and LP (UKQAA, 2010)

Materials	Embodied CO_2 kg/tonne
Portland cement CEM I	913
Ground Granulated Blast Furnace Slag (GGBS)	67
Pulverized Fly Ash (PFA)	4
Limestone (LP)	75

2.13 Some of SCC applications

The development of SCC concrete technology has given architectural and engineering designers the potential to create structural forms that would be difficult or impossible to produce using NVC. Figure 2.10 is an example of a recent SCC structure that houses a Holocaust memorial exhibition (OCCDC, 2021).

The benefits of including ggbs in concrete mixes are well established, as illustrated by the Severn crossing bridge Figure 2.11 in 1996 (Hanson, 1996), which used a concrete with a compressive strength of 70MPa and 70% ggbs CRM. Its use was driven by the need to have a very low heat of hydration rate and high sulphate and chloride ingress resistance, both of which were achieved.

In 2007, when massive concrete was required to construct the Landmark tower in Abu Dhabi in hot weather conditions, SCC was recommended (Unibeton, 2013). This project involved the largest quantity of self-compacting concrete in a single pour in the world, which was 16000 m^3 (See Figure 2.12). In practice, durability is based on the material selection, concrete composition, along with the degree of expertise during placing, compaction, finishing and curing.

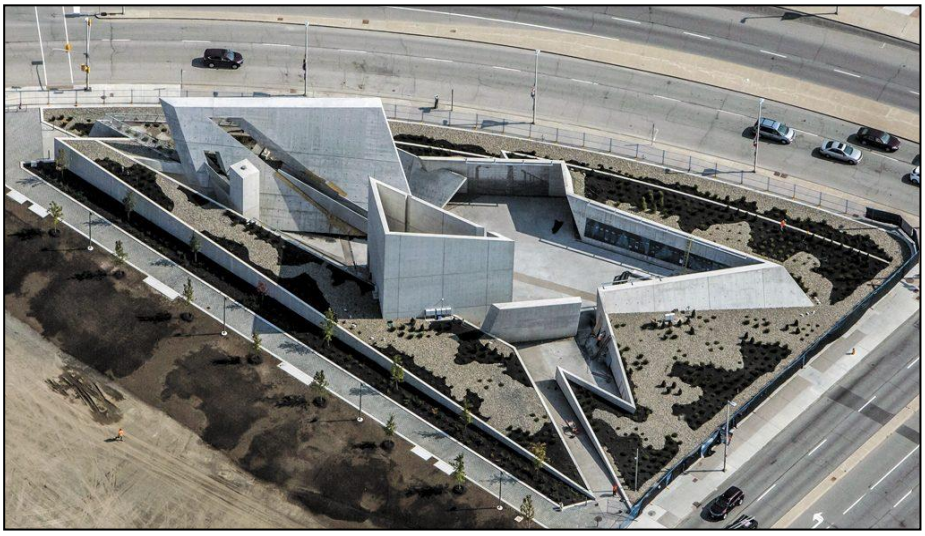

Figure 2.10 Winner of the Concrete Award for Architectural Hardscape, the National Holocaust Monument in Ottawa comprises six triangular concrete elements configured to create the points of a star October 2017. (OCCDC, 2021)

Figure 2.11 Bridge crossing point for the M4 motorway, over the Severn Estuary 1996 (Hanson, 1996)

Figure 2.12 The Landmark tower in Abu Dhabi 2007 (Unibeton, 2013)

2.14 Conclusions

This review chapter identified a number of areas in which data was lacking and research was required. In particular, the review showed that little research had been undertaken on SCC mixes with high levels of ggbs as a CRM. These 'research gaps' are listed below and provided the motivation for the current work.

- The prediction of the plastic and hardened properties of SCC mixes that contain significant quantities of ggbs as a CRM.
- A rational basis for designing SCC mixes with high percentages of ggbs.
- Methods for predicting the time dependent strength development of SCC with different percentages of ggbs.
- Data for concrete mixes (NVC and SCC) formed using cement CEM II and high percentages of ggbs since almost all of the previous work used CEM I cement.
- Mix design methods that simultaneously apply plastic and multiple hardened property criteria for SCC.

Chapter 3 Materials, experimental procedures and standards

3.1 Introduction

This chapter describes the materials, experimental procedures and standards used in the work described in chapters 4, 5, 6, and 7 of this thesis.

Additional details are provided in Appendices A, B, C, D, E, F and G.

3.2 Materials

In this study materials (cement, coarse and fine aggregates, additives, cement replacement materials ggbs) were used to develop SCC mixes according to the design procedure proposed in chapter 6. The specification for each of these component materials is given in Table 3.1.

Table 3.1 Materials detail under current study inclouding orginal sources

Material	Specification	Specific gravity*	Source
Cement	Portland fly ash type II/B-V 32.5 clinker percent 65-79% and additions 21-35% Limestone cement type II A-L , clinker percent 80-94% and additions 6-20% according to the (BS EN 197-1, 2011)	2.95	(TARMAC, 2021)
Ggbs	Local UK subside product can reference as x% in text of this thesis.	2.40	(Hanson, 2021)
Limestone	Crushed as a filler with maximum particle size 125 µm	2.40	
Fine aggregate	Blended crushed stone and river sand max. size 2mm	2.65	(Perkins, 2021)
Coarse aggregate	Crushed limestone coarse aggregate with a maximum size of 20 mm	2.80	
Superplasticiser	polycarboxylic ether-based type (MasterGlenium ACE 499)	1.07	(Solutions, 2021)

***Specific gravity values from (Abo Dhaheer,2016b), since the same materials are used in this study.**

A proportion of the river sand (See section 3.7) was replaced by an equivalent volume of the coarser fraction of limestone filler in the size range 125 µm–2 mm to maintain the required powder particle size limits (EN BS 206-9, 2010). The particle size distributions of the coarser fraction of limestone filler and river sand is shown in Figure 3.1

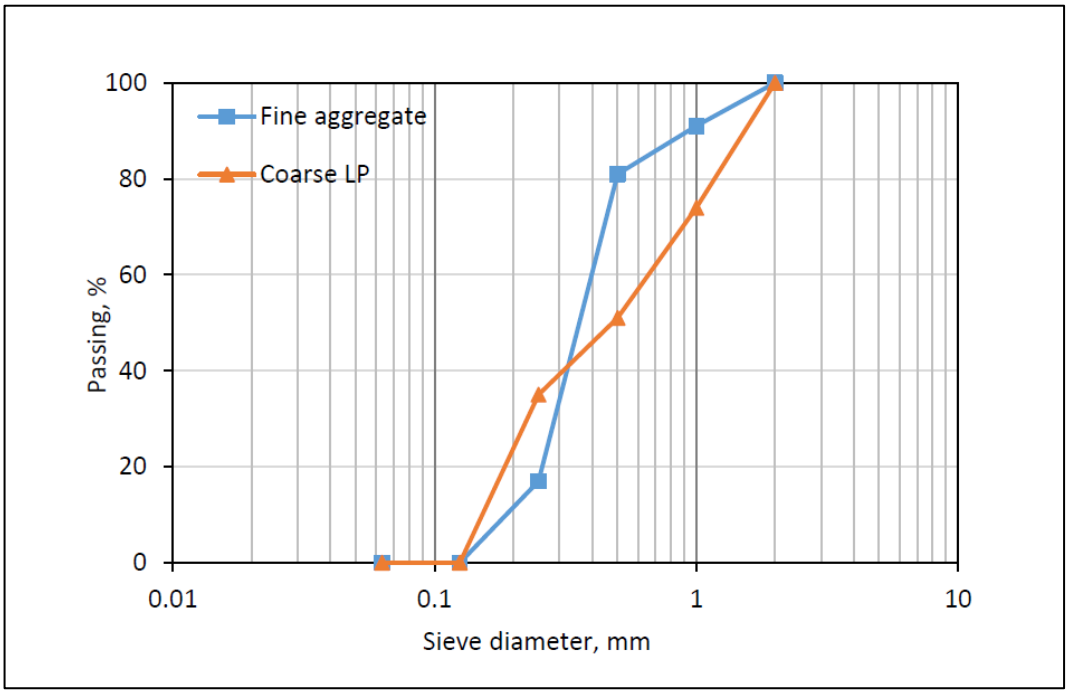

Figure 3.1 Particles size distribution curves for coarser fraction of limestone filler and fine aggregates

3.3 Mix preparation

A small planetary mixer was used to prepare the mixes in a sequential way. The constituents with the largest (coarse aggregate up to 20 mm) and the finest (Cement +GGBS) particle sizes were mixed together first; this was followed by the next coarsest (sand) and next finest constituent (limestone powder), and so on. Each mixing stage was undertaken for 2.5 minutes. The mix was fluidised in two stages; first by adding half of the water and half of the super-plasticiser (*SP*) to the dry mix and mixing for 2.5 minutes; and then by adding the remaining water and *SP*, and mixing for a further 2 minutes. The final mix was immediately transferred to a slump cone so that a flow test could be undertaken (see Section 3.5.1). The slump test for each mix was video-recorded from the time the

cone was lifted until the mix came to rest. The time taken for the fresh SCC mix to reach a 500mm diameter spread (t_{500}) and to come to rest (time t_{stop}, with spread diameter dimension *SF*) were determined from the time sequencing on the video recording, which had a recording rate of 1000 frames per second. Three frames from a representative video are shown in Figure 3.2.

Each mix in the trial mix process was assessed visually to check if any segregation or bleeding was detectable. The mix proportions were judiciously altered according to these observations. This trial mix process was continued until the mix met the flow-ability criterion in BS EN 206-9 (2010).

The moisture contained in the coarse and fine aggregates was measured and the associated quantity of water taken into account in the mix design. The reference moisture level is determined from the saturated surface dry (SSD) state of the aggregate.

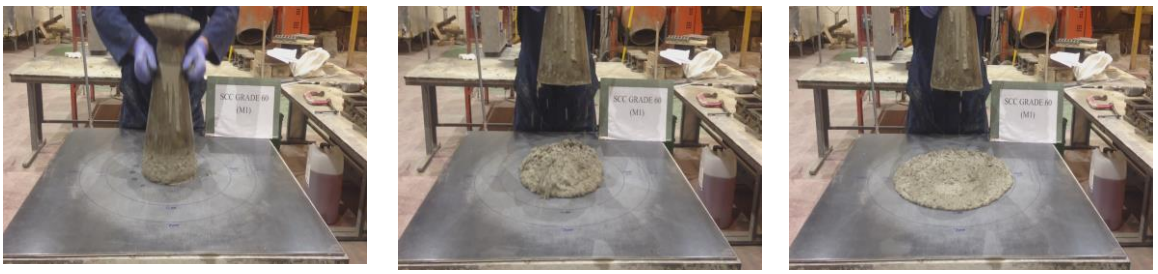

Figure 3.2 Video images of the slump cone test at three flow stages

3.4 Curing regime

A standard curing regime was used for all mixes. This involved the wet concrete being poured into a mould (cube) immediately after mixing, covered in wet hessian for 24 hours, demoulded and then cured under water at ambient temperature for the designated curing period, i.e. between 2 to 300 days (See section 3.7 for curing periods). Each sample was removed from the tank 24 hours before testing and allowed to dry in air.

3.5 Test of fresh state

3.5.1 Viscosity for cement paste

The viscosity of a representative sample of the cement pastes used in this study were measured using a type NDJ-8S viscometer (see Appendix A for details). The cement paste samples included the binder materials (i.e. cement and replacement ggbs), water and superplasticiser (for some of the tests).

Each individual sample had a volume of 400ml, which was placed in a 100×150 mm (diameter × height) glass container at room temperature (i.e. 17 ^{o}C). The duration of each test was between 3 and 5 minutes with the primary readings taken 2 minutes after the rotor was started. Rotor #2 was chosen for the tests with rotations rates of 1.5 to 60 rpm, which was in accordance with the user manual (see Appendix A). The cement used was CEM II (A-L)/32.5, and the ggbs replacement levels considered were 20%, 50% and 80%. Two series of tests were carried out, (i) Groups A-C without superplasticiser, and (ii) Groups A and B with superplasticiser. The results are shown in Tables 3.2 and 3.3 and illustrated and discussed in chapter 4. It is noted that, where necessary, the quantity of water was adjusted such that the mix proportions given in the tables produced one m^3 of concrete.

Table 3.2 Viscosity test on cement combination (CEM II A-L 32.5R +ggbs) without SP

Class	mix	CEM II%	ggbs%	Mass, kg/m³			w/b	Rotor No.	Speed (rpm)
				ggbs	cem	w			
Group A	V1	80	20	200	800	300	0.3	2	60
	V2	50	50	500	500	300	0.3	2	60
	V3	20	80	800	200	300	0.3	2	60
Group B	V4	80	20	200	800	500	0.5	2	60
	V5	50	50	500	500	500	0.5	2	60
	V6	20	80	800	200	500	0.5	2	60
Group C	V7	80	20	200	800	700	0.7	2	60
	V8	50	50	500	500	700	0.7	2	60
	V9	20	80	800	200	700	0.7	2	60

Table 3.3 Viscosity test on cement combination (CEM II A-L 32.5R +ggbs) with SP

Class	mix	CEM II%	ggbs%	Mass, kg/m³				w/b	SP%	Rotor No.	Speed (rpm)
				ggbs	cem	w	sp				
Group A	V1	80	20	200	800	300	3.5	0.3	0.35	2	60
	V2	50	50	500	500	300	3.5	0.3	0.35	2	60
	V3	20	80	800	200	300	3.5	0.3	0.35	2	60
Group B	V4	80	20	200	800	500	2	0.5	0.1	2	60
	V5	50	50	500	500	500	2	0.5	0.1	2	60
	V6	20	80	800	200	500	2	0.5	0.1	2	60
Group C	V7	80	20	200	800	700	0	0.7	0	2	60
	V8	50	50	500	500	700	0	0.7	0	2	60
	V9	20	80	800	200	700	0	0.7	0	2	60

3.5.2 Filling and flowability

The combined filling and flow-ability test is a modified version of the slump test (BS EN 12350-8, 2010) for which the apparatus is shown in Figure 3.3. The slump flow test is used to assess the horizontal flow-ability of SCC when there are no obstacles. The test measures three different aspects; the filling ability, measured from the final horizontal

flow diameter *SF*; the flow-ability, which is determined using t_{500}; and the segregation, which is assessed visually. The time when the flow stops, t_{stop}, is also recorded.

This relatively simple test, which uses an inverted or upright Abram's cone, is suitable for assessing the plastic properties of a mix on a construction site or in a laboratory.

The EFNARC (2005) specification for an SCC mix is an *SF* range of 650–750 mm, no visible segregation, and t_{500} [0.5s to 2.2s.] and t_{stop} [5s to 20s]. The testing apparatus and procedure are illustrated in Figures 3.3 and 3.4 where *SF* =0.5($d1+d2$)

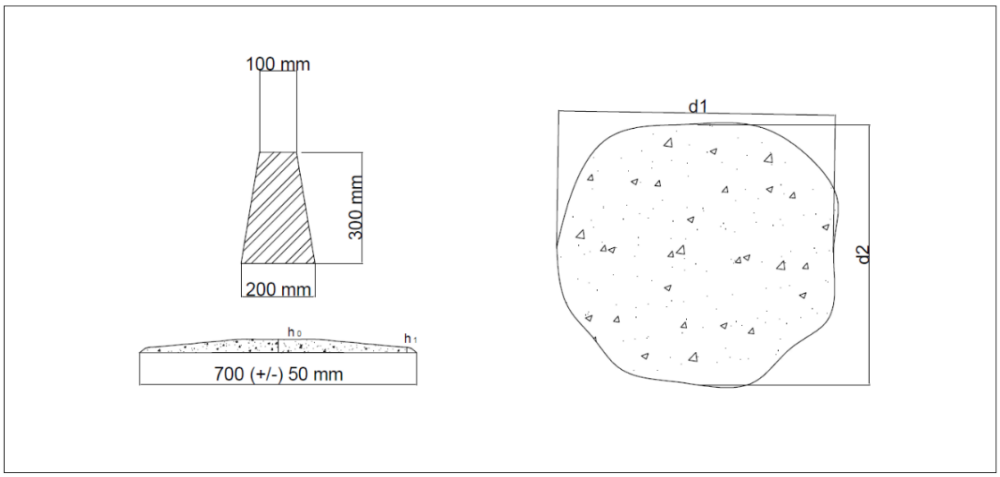

Figure 3.3 Slump test apparatus with hollow cone

Figure 3.4 Flow-ability test (cone)

3.6 Passing-ability test

The J-ring test is used in combination with the slump cone to assess the passing-ability of an SCC mix through gaps between obstacles, e.g. reinforcement. For this test, the slump test apparatus is used with an open steel ring (300±2mm) that is supported by twelve vertical steel rods (diameter = 18±0.5mm and height = 125mm), as shown in the Figures 3.5 and 3.6. The gap between the bars is (59±1mm) (BS EN 12350-12, 2010).

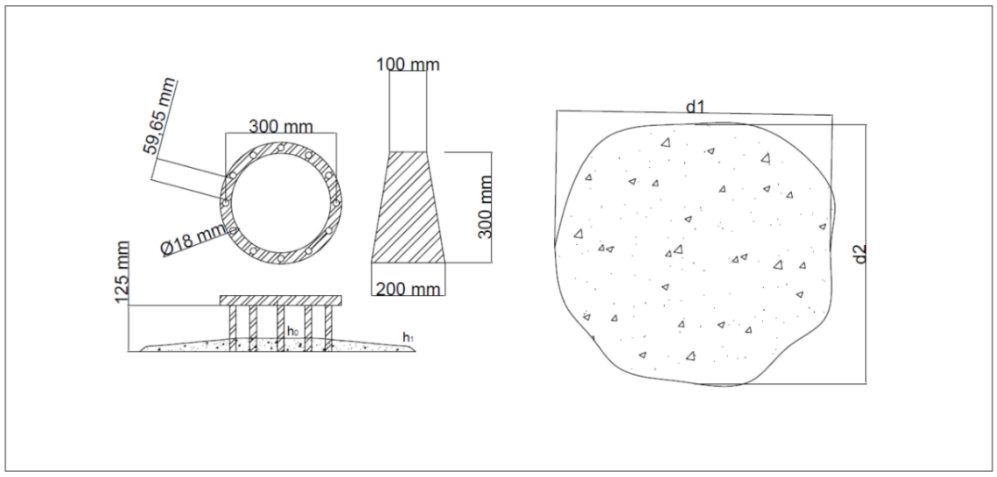

Figure 3.5 Standard J-Ring apparatus

Figure 3.6 Passing-ability test (J-ring)

After filling the cone with concrete without using any vibration or rodding, the cone is lifted perpendicular to the steel base plate allowing the concrete to flow freely. The time

needed for the flow to reach 500mm diameter is recorded as the J-Ring (t_{500j}). Once the flow has stopped, the spread dimension (SF_j)and stop time (t_{stop}) are recorded.

All mixes that satisfied the previously described flow-ability criterion and showed no signs of segregation (Section 3.5.1) were then subjected to the passing-ability test using the J-ring apparatus.

3.6.1 Spreading time t_{500} & t_{stop}

t_{500} is used to classify viscosity using the following EFNARC designations [(VS1≤ 2s) AND (VS2 > 2s)] (EFNARC, 2005). Prior to the work reported in this thesis there were no relationships or graphs that related t_{500} to the viscosity parameter η. This issue has been explored in the present work although, as may be seen in Chapter 7 (Figure 7.4), the relationship is highly nonlinear and varies with the percentage of cement replacement material.

Viscosity slump (VS1) describes a mix that has 'good filling-ability even with congested reinforcement'. It is capable of self-levelling and has a high quality surface finish. However, it is more likely to suffer from bleeding and segregation. Viscosity slump (VS2) has no upper class limit but by increasing the flow time of a mix it is more possible make it thixotropic, which may be helpful in limiting the fluid pressure on the formwork and improving segregation resistance. Negative consequences of using VS2 mixes include the potential for poor surface finishes (blow holes) and a greater sensitivity to stoppages or delays between successive lifts. The measured time until flow reach stops (t_{stopj}) only provides an indication of the yield stress; noting that the higher the yield stress, the greater the flow time. An estimation of the yield stress for a range of SCC mixes is given by Badry et al. (2016).

3.7 Mix sets

The following three sets of mixes were used in this programme of research:

Set 1 ($C1_1$, $C2_1$, $C3_1$ and $C4_1$). The proportions of these mixes are shown in Table 3.4. The binder refers to cement plus ggbs. These four mixes were used for the work on the hydration model described in chapter 6. The hydration study considered curing times of 2, 4, 7, 14, 28, 210, and 300 days. The powder content is the total weight of materials with particles sizes not exceeding 0.125 mm; this includes the cement, ggbs, limestone and a proportion of the fine aggregate.

Table 3.4 Mixes ingredients for SCC and ggbs (50%), (kg/m^3)

Mix ref.	Binder		b	w	w/b	SP	SP/b (%)	LP[a]	FA[b]		CA[c]
	cem	ggbs							FA*	FA**	
$C1_1$	108	108	216	147	0.68	1.10	0.51	187	310	593	930
C2	150	150	300	168	0.56	1.74	0.58	143	237	627	872
$C3_1$	192	192	384	184	0.48	2.80	0.73	146	242	515	847
C4	232	232	464	185	0.40	4.17	0.90	102	169	633	762

[a] Limestone powder <125 µm.

[b] Fine aggregate <2 mm (Note: a part of the fine aggregate FA* is the coarser fraction of the limestone powder, in the size range125 µm – 2 mm, whereas FA** refers to natural river sand <2 mm).

[c] Coarse aggregate <20 mm.

Set 2 (C30A-C80A & C40B-C60B). The twelve mixes used for developing and validating the mix design procedure (see Chapters 6 and 7) are given in Tables 3.5 and 3.6. In the CA series, the binder comprised 40% ggbs, whereas in the CB series the replacement level was 60% ggbs.

Table 3.5 Mix proportions of test SCC mixes, kg/m^3, ggbs 40%

Mix ref.	Binder		b	w	w/b	SP	SP/b (%)	LP[a]	FA[b]		CA[c]
	cem	ggbs							FA*	FA**	
C30A	190	127	317	216	0.68	1.4	0.44	195	292	481	773
C40A	233	155	388	217	0.56	1.8	0.46	153	230	528	758
C50A	272	181	453	218	0.48	2.7	0.59	148	223	516	738
C60A	286	190	476	190	0.40	3.7	0.77	116	174	615	789
C70A	305	203	508	173	0.34	4.6	0.91	118	177	626	803
C80A	348	232	580	168	0.29	5.8	1.00	120	180	602	782

[a] Limestone powder <125 µm.

[b] Fine aggregate <2 mm (Note: a part of the fine aggregate FA* is the coarser fraction of the limestone powder, in the size range125 µm – 2 mm, whereas FA** refers to natural river sand <2 mm).

[c] Coarse aggregate <20 mm.

Table 3.6 Mix proportions of test SCC mixes, kg/m^3, ggbs 60%

Mix ref.	Binder		b	w	w/b	SP	SP/b (%)	LP[a]	FA[b]		CA[c]
	cem	ggbs							FA*	FA**	
C40B	187	280	467	233	0.50	3.1	0.66	150	225	475	659
C50B	188	282	470	212	0.45	4.0	0.85	113	170	537	757
C60B	196	294	490	196	0.40	5.2	1.06	123	185	522	767

[a] Limestone powder <125 µm.

[b] Fine aggregate <2 mm (Note: a part of the fine aggregate FA* is the coarser fraction of the limestone powder, in the size range125 µm – 2 mm, whereas FA** refers to natural river sand <2 mm).

[c] Coarse aggregate <20 mm.

Set 3 ($C1_2$,$C3_2$,D1,F). The four mixes given in Table 3.7 were used to provide additional data to integrate the hydration model (Chapter 5) with the mix design procedure (Chapters 6 and 7). The ggbs replacement level considered in these mixes was 50%, 60%, and 80%. The study considered curing times of 7, 28, and 135 days.

The fresh and hardened properties of the set 2 and set 3 mixes are given in chapter 7.

Table 3.7 Mixes ingredients for SCC and ggbs [50% ($C1_2$ & $C3_2$), 60% (D1) and 80% (F)], kg/m^3

Mix ref.	Binder		b	w	w/b	SP	SP/b (%)	LP[a]	FA[b]		CA[c]
	cem	ggbs							FA*	FA**	
$C1_2$	173	173	346	215	0.62	2.1	0.60	147	200	558	800
$C3_2$	226	226	452	190	0.42	4.2	0.94	112	152	632	768
D1	135	203	406	196	0.58	3.4	1.00	212	288	443	804
F	70	282	564	176	0.50	4.2	1.20	151	205	586	838

[a] Limestone powder <125 µm.

[b] Fine aggregate <2 mm (Note: a part of the fine aggregate FA* is the coarser fraction of the limestone powder, in the size range125 µm – 2 mm, whereas FA** refers to natural river sand <2 mm).

[c] Coarse aggregate <20 mm.

3.8 Hardened state

3.8.1 Compressive strength of SCC test mixes

At least three 100 mm cubes from each variant of the test mixes were cast and cured in water at ambient temperature (20^{o}C) for the entire curing period. Each cube was air dried before testing according to the requirements of BS EN 12390-3:2019 The mean compressive strength and coefficient of variation was determined for each batch of cubes.

3.9 Data gathering and processing

The strengths obtained from 100mm cube tests may be related to uniaxial strengths (associated with cylinder strengths) using the standard dual strength classes of BS EN 206-1. These standard strength classes measured cube strengths (f_{cu}) and the equivalent cylinder strengths (f_c) are given in Table 3.8. These are based on the dual strength classes given in Table 3.1 of EN1992-1-1.

Table 3.8 Conversion from national standard specimens to 100 mm czubes (BS EN 206-1:2000, 2013+A1:2016)

Compressive strength class	*fc,* N/mm² Cylinder (Standard) (150*300)	*fcu*, N/mm² Cube (Standard) (150)	*fc*, N/mm² Cylinder (Equivalent) (100*200)	*fcu,* N/mm² Cube (Equivalent) (100)
C8/10	8	10	8.3	10.2
C12/15	12	15	12.5	15.3
C16/20	16	20	16.7	20.4
C20/25	20	25	20.8	25.5
C25/30	25	30	25.0	30.6
C30/37	30	37	30.8	37.7
C35/45	35	45	37.5	45.9
C40/50	40	50	41.7	51.0
C45/55	45	55	45.8	56.1
C50/60	50	60	50.0	61.2
C55/67	55	67	55.8	68.4
C60/75	60	75	62.5	76.5
C70/85	70	85	70.8	86.7
C80/95	80	95	79.2	96.9
C90/105	90	105	87.5	107.1
C100/115	100	115	95.8	117.4

3.10 Standards used in this programme of research

A list of the standards used in this PhD programme of research is given in Table 3.9.

Table 3.9 The main BS EN Standard applied in this study

Description	Code
➢ Testing fresh concrete Part 8: Self-compacting concrete - Slump-flow test	BS EN 12350-8:2010
➢ Testing fresh concrete Part 9: Self-compacting concrete – V-funnel test	BS EN 12350-9:2010
➢ Testing fresh concrete Part 10: Self-compacting concrete – L- Box test	BS EN 12350-10:2010
➢ Testing fresh concrete Part 11: Self-compacting concrete – sieve segregation test	BS EN 12350-11:2010
➢ Testing fresh concrete Part 12: Self-compacting concrete – J- ring test	BS EN 12350-12:2010
➢ Cement Part 1: Composition, specifications and conformity criteria for common cements	BS EN 197-1:2011
➢ Concrete Part 9: Additional Rules for Self-compacting Concrete (SCC)	BS EN 206-9:2010
➢ Concrete Part 1: Specifications, performance production and conformity	BS EN 206:2013+A1:2016
➢ Testing hardened concrete Part 3: Compressive strength of test specimen	BS EN 12390-3:2019
➢ Ground granulated blast furnace slag for use in concrete, mortar and grout ➢ Part 1: Definitions, specifications and conformity criteria	BS EN 15167-1:2006
➢ Ground granulated blast furnace slag for use in concrete, mortar and grout ➢ Part 2: Definitions, specifications and conformity evaluation	BS EN 15167-2:2006
➢ Ground granulated blast furnace slag for use with Portland cement	BS 6699:1992
➢ EFNARC The European Guidelines for Self-Compacting Concrete Specification, Production and Use	2005

3.11 Concluding remark

In this chapter, a description is given of the materials, test procedures and standards used for this research. This information is referenced in chapters 4 to 7.

Chapter 4 Plastic properties

4.1 Introduction

The ability to control the workability and self-compactibility of SCC is key to its effective production and use. Without this knowledge the design of an SCC mix for a particular application is an inefficient trial and error process. Tools to assess the plastic characteristics of SCC have been divided into three categories (Tattersall, 1991): qualitative assessment, quantitative empirical assessment and quantitative fundamental assessment. In the previous chapter, methods for the qualitative and quantitative assessment of SCC were presented; flow-ability, passing-ability and stability for the former; and slump flow and J-ring for the latter. In this chapter, methods for describing and predicting the workability of SCC will be reviewed in terms of its fundamental rheological properties.

4.2 Rheological properties

Rheology is a science of deformation and flow. It has been recognised as an crucial field of scientific study and by common consent is a difficult subject (Barnes et al., 1993). Innovative concretes have explicit properties, often gained by using additives, and these properties are substantially affected by rheological characteristics of the fresh cement paste. The first ideas of choosing materials having complementary resistance and rigidity was necessary at a time when the only available materials were obtained directly from soils (Cristescu, 2010). Workability is a way of describing the performance of concrete in the plastic state and for SCC it is often characterised using the following properties: flowing-ability, filling-ability, passing-ability, and stability (segregation resistance) (PCI, 2003).

Cement paste, mortar and concrete should be studied as systems; looking at these materials as systems represents a step forward, and the term “system properties (Rheology)” may be used as an alternative to “materials properties” when discussing mechanisms of plastic behaviour. Looking at cement paste, mortar and concrete as

systems puts our mind set in the right direction for investigating cement-based materials at different scales and in all subsequent stages of their lifetime. Rheology in the broad sense is the science of flow and deformation of matter under stress (Tattersall and Banfill, 1983). Fundamental rheological approaches make it possible to predict fresh properties, select materials and model processes to achieve the required performance. Knowing the rheological parameters (yield stress and plastic viscosity) of a fluid provides a quantitative and fundamental way of characterizing the flowing-ability, filling-ability, passing-ability and stability of SCC.

4.3 The rheological parameters of SCC

SCC in the plastic state behaves as a viscous non-Newtonian fluid, which can be described by a bi-linear Bingham-type rheological model (Heirman et al., 2009). This model uses two parameters, namely the plastic viscosity (η) and the yield stress (τ_y). Plastic viscosity is the measure of the resistance to flow due to internal friction. It can also be regarded as the ability of this fluid to resist shear or angular deformation, which is mainly due to the interaction between fluid particles. SCC should have a sufficiently high viscosity to ensure that aggregate particles are suspended in a homogenous manner within the concrete matrix without segregation, and to prevent excessive bleeding or paste separation. The yield stress is the measure of the minimum amount of energy required to initiate SCC flow. Flow starts once the shear stress becomes higher than the yield stress. However, when its value becomes equal to or lower than the yield stress, the flow stops. To be considered SCC, concrete must flow easily under its own weight, so its yield stress should be low as possible.

It is generally known that the slump property of a normal fresh cementitious mix is mainly governed by its yield stress (Kong et al., 2003). When the yield stress of a fresh concrete mix is greater than the stress caused by gravitational forces (termed the ‘gravitational stress’), the fresh mix is prevented from completely collapsing to the plate surface. As the yield stress becomes less than the gravitation stress, the final slump height decreases

meaning that the slump displacement increases. In this process, the contribution of the viscosity to the fresh properties is considered to be relatively small. Once the gravitational stress acting on the fresh mix is much greater than the yield stress, the fresh mix completely collapses onto the plate, followed by the spreading of the mix over the plate surface.

A number of investigations have shown that the role of viscosity is more important during spreading and that the yield stress of SCC mixes is very low (circa 200 Pa) (Dransfield, 2003; Badry et al., 2016) in comparison with normal concretes (thousands of Pa), and remains nearly constant over a large range of plastic viscosities as shown in Figure 4.1.

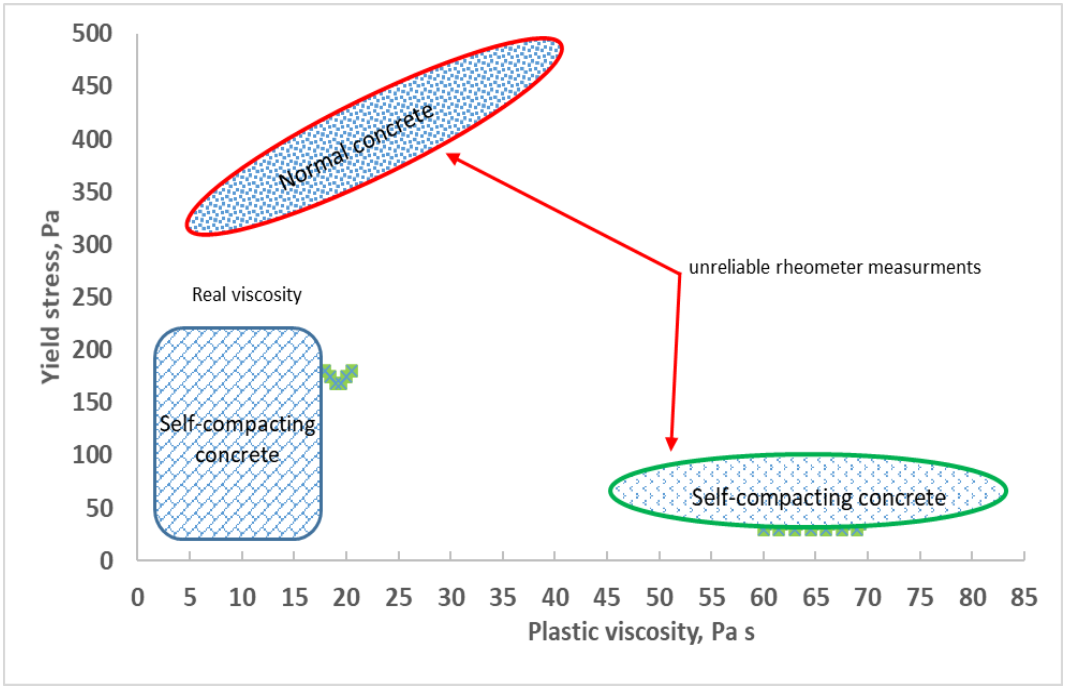

Figure 4.1 Rheological parameters for two types of concrete mix

4.4 Yield stress

Fresh concrete is a non-Newtonian fluid that may be described in terms of 'Bingham'-type models (See section 4.6). The yield stress τ_y in the Bingham fluid model is the minimum shear stress that an SCC mix has to overcome to start flowing.

4.5 Plastic viscosity

The resistance of SCC to flow due to internal friction is measured from the slope of the shear stress versus shear rate plot from rheometer flow curve measurements. Mixtures with high plastic viscosity are often described as “sticky” or “cohesive”. The plastic viscosity is closely related to t_{500} and the v-funnel time (the higher the plastic viscosity, the larger t_{500} and the v-funnel time).

SCC must have a sufficiently high plastic viscosity to suspend aggregate particles in a homogeneous manner within the concrete matrix without segregation and to prevent bleeding, excessive air migration, or paste separation.

4.6 Common rheological models

Fresh SCC is a suspension, and rheological equations typical for suspension flows are used to describe material flow behaviour mathematically. These equations give the evolution of stresses and deformations in the material. Fresh SCC exhibits complex non-Newtonian flow behaviour (Macosko, 1994). Most authors use the Bingham or Herschel-Bulkley models, which follow expressions 4.1-4.2 and 4.3-4.4 respectively. The Bingham equation is the most commonly used equation, which assumes the existance of a yield stress and linear behaviour when the shear stress exceeds the yield value. The reasons for the widespread acceptance of this model are mostly practical: the model parameters can be measured independently, and the flow of real SCC seems to follow this equation fairly well in most cases (Ferraris, 1999). An overview of different rheological equations that describe suspension flows can be found in (Macosko, 1994), and those used for cementitious materials are given in (Ferraris, 1999; Banfill, 2006).

4.6.1 Bingham plastic model

The basic Bingham model is written as;

$$\tau = \tau_y + \eta\dot{\gamma} \qquad \tau > \tau_y \qquad \textbf{(4. 1)}$$

$$\dot{\gamma} = 0 \qquad \tau \leq \tau_y \qquad \textbf{(4. 2)}$$

where τ_y = yield stress, η = plastic viscosity and $\dot{\gamma}$ = shear rate.

4.6.2 Herschel-Bulkley model

This model is a generalisation of the Bingham model in such a way that, upon deformation, the viscosity is affected by shear thinning (viscosity decreases with shear rate) or shear thickening (viscosity increases with the shear rate) (See Figure 4.2). The Herschel-Bulkley model is described by the follow equations;

$$\tau = \tau_y + \eta\dot{\gamma}^n \qquad \tau > \tau_y \qquad \textbf{(4. 3)}$$

$$\dot{\gamma} = 0 \qquad \tau \leq \tau_y \qquad \textbf{(4. 4)}$$

For n <1, the fluid exhibits shear thinning properties

n =1; the fluid shows Bingham behaviour

n >1, the fluid shows shear thickening behaviour

In expression (4.3), n is an empirical curve-fitting parameter identified as the flow behaviour index. For a shear thinning fluid, n has a value between 0 and 1. The greater degree of shear thinning the smaller value of n and vice versa. For a shear thickening fluid, n will be greater than unity.

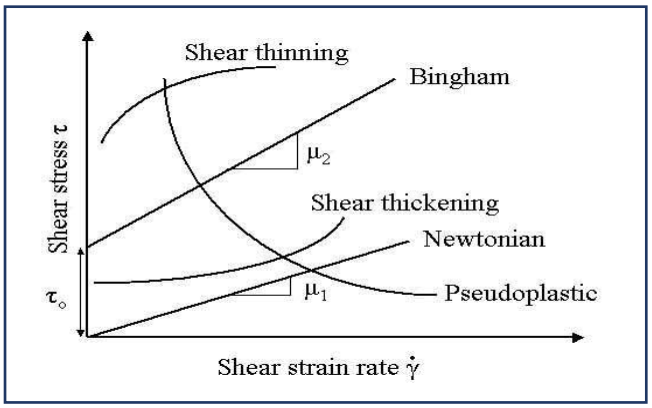

Figure 4.2 shear stress vs shear strain rate predictions with different models

4.6.3 Modified Bingham model

The Modified Bingham model is used when there is a non-linear relationship between τ and applied $\dot{\gamma}$, (see equation 4.5). It provides a closer match to the behaviour of many materials and predicts a lower level of shear-thinning (i.e. $n < 2$) than the Herschel-Bulkley model (Feys et al., 2013).

$$\tau = \tau_0 + \eta\dot{\gamma} + c\dot{\gamma}^2 \qquad \textbf{(4. 5)}$$

4.7 Assessment of rheological properties

A rheometer is commonly used to determine the Bingham parameters of general viscous liquids (such as cement pastes) and solid-liquid suspensions (such as SCC). When choosing rheometers, one should take into consideration the small size of aggregate used in SCC compared with conventional vibrated concrete, the presence of yield stress, moderate plastic viscosity, the potential for segregation and the high sensitivity to small changes in materials and their proportions. Basically, two types of rheometer can be used; namely, those that impose a controlled shear rate on SCC and measure its shear stress, and those that do the opposite (Domone, 2003).

Domone investigated several SCC mixes and found that different rheometers (see discussion of types below) give different values for the rheological parameters (see Figure

4.3). This confirmed the findings of Banfill et al. (2000) who used a set of comparative tests on SCC mixes using three different instruments. Both studies showed that the measured yield stress values were less affected by the type of rheometer than the plastic viscosity values. This suggests that there is still no reliable technique for measuring the plastic viscosity of SCC, and that there is a need for a universal tool for computing the plastic parameters (Vasilić, 2015).

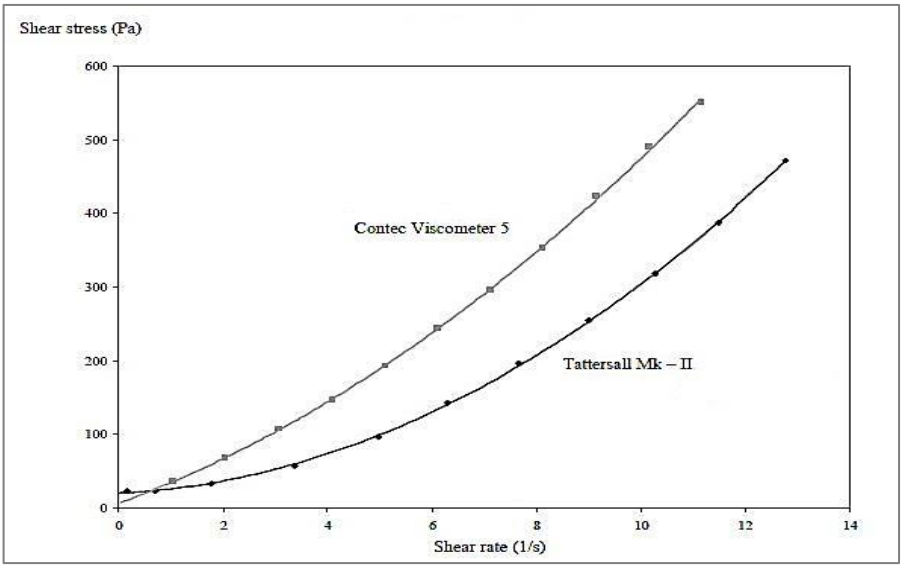

Figure 4.3 Two different responses for a single SCC mix tested with two rheometers (Feys et al., 2007)

There are various rheometers that can be used for determining the rheological properties of cementitious materials (Wallevik, 2009). Typically, the torque or force, and rotational or linear velocity are measured, then transformed to shear stress and shear strain values, which depend on the geometry of the instrument (Banfill et al., 2000). Four basic types of rheometer are listed in Table 4.1 along with some comments regarding the advantages and disadvantages of each type (Khayat et al., 2019).

Coaxial cylinder rheometers (ConTec and BML) are adequate to measure the rheological behaviour of mortars and cementitious composites because of the wide gap between the inner and outer cylinders, which allows for testing the mixtures with sand and fibres (Feys et al., 2013). Yield stress and viscosity can be estimated by using Reiner-Rivlin equation in fundamental units.

Table 4.1 Rheometers type for UHPC (Khayat et al., 2019)

Type	Apparatus	Advantage	Disadvantage
Parallel disc plate	BTRHEOM	(1) Small sample size (2) Can change temperature without reloading sample (3) Easy to load and clean	Shear rate is not uniform, which is fine for linear viscoelasticity fluids but not the case for nonlinear fluids
Concentric cylinders	Anton Paar MCR	(1) For large radii, the shear rate is nearly constant. (2) Ideally suited for pourable liquids; i.e. cement paste	(1) Difficult transformation for wide gap (2) Bottom effect (3) Risk of wall slip
Coaxial cylinders	ConTec, BML	(1) Suited for mortar and concrete containing coarse aggregate.	(1) Large sample volume (2) Risk of wall slip (3) Plug flow
Two-point test	MH system	(1) Suited for mortar and concrete containing coarse aggregate	(1) Large sample volume (2) Oil pressure needs to be monitored

4.8 Estimating plastic viscosity

From a mix design point of view, the most essential parameter is the plastic viscosity, which changes with the plastic viscosity of the paste and the mix composition. A method for calculating the plastic viscosity of SCC mixes is described in the remainder of this section.

The plastic viscosity of the homogeneous viscous binder paste (a mix of cement, ggbs, water, and super-plasticizer) can be measured fairly accurately with a viscometer. However, this is not possible for nonhomogeneous SCC, because there is a large scatter in the results when the plastic viscosity of the same SCC mix is measured with different rheometers (Banfill et al., 2000; Feys et al., 2007b; Wallevik and Wallevik, 2011). Feys et al. (2013) explain that the greatest error is obtained when using coaxial cylinder

rheometers. This is because a plug of material tends to form in the rheometer, as illustrated in Figure 4.4.

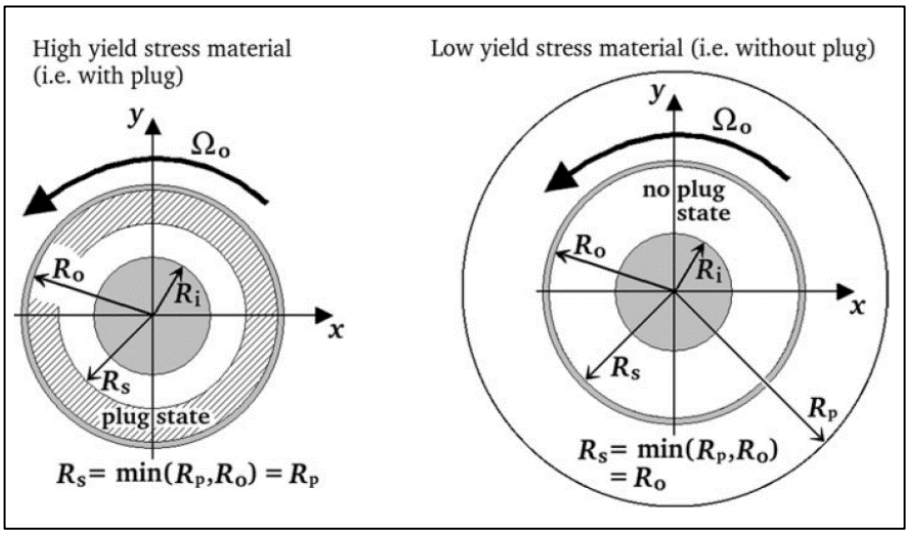

Figure 4.4 Schematic top view of a viscometer; left, illustrates a sample with sufficient yield stress to generate plug; right, a sample with insufficient yield stress to generate a plug (Feys et al., 2013)

Ghanbari and Karihaloo (Ghanbari and Karihaloo, 2009) therefore proposed a method (micromechanical procedure) for estimating the plastic viscosity of an SCC mix beginning with the plastic viscosity of the paste used in it. In this procedure, SCC is regarded as a two-phase suspension in which the solid phase is suspended in a viscous liquid phase. The increase in the plastic viscosity of the suspension resulting from the successive addition of the solid phases (filler, fine, and coarse aggregates) is estimated in a stepwise manner. In the first step, the solid phase is the finest solid material, e.g. the filler and the binder paste is the fluid phase. In the next step, the next solid phase, i.e. the fine aggregate is suspended in the viscous fluid phase now formed by the two-phase suspension from the first step. This procedure is continued until all the solid phases forming the mix have been added to the suspension. The plastic viscosity of the *i*-th liquid–solid suspension is estimated from the plastic viscosity of the preceding (i − 1)th phase

$$\boldsymbol{\eta_{ci} = \eta_{ci-1} \times f(\phi_i)} \quad \textbf{(4. 6)}$$

Here, η_{ci} is the plastic viscosity of the *i*-th liquid–solid suspension; η_{ci-1} = plastic viscosity of the preceding (*i* − 1)th phase. In the first step *i = 1,* η_{c0} is the known plastic viscosity of the paste; and $f_i(\phi_i)$ = a factor larger than unity that predicts the increase in the plastic viscosity induced by the solid phase with a volume fraction ϕ_i. Figure 4.5 shows the order of the successive two-phase suspensions used to compute the plastic viscosity of SCC.

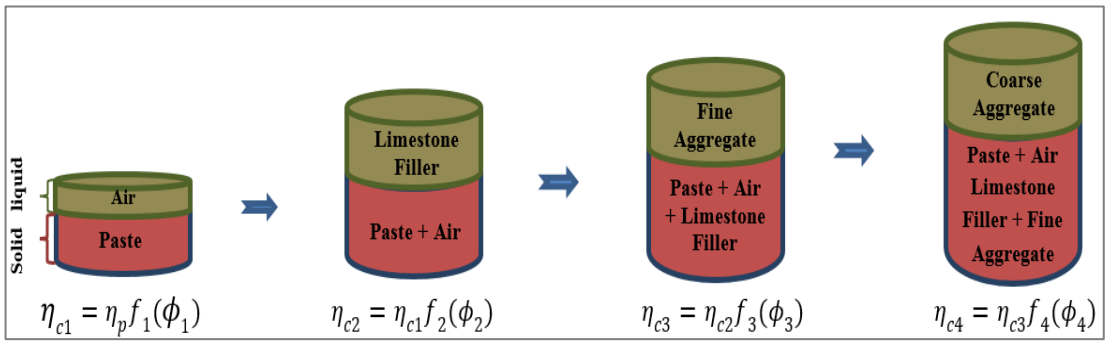

Figure 4.5 Two-phase liquid-solid suspensions hierarchy constituting an SCC mix (Ghanbari and Karihaloo, 2009)

According to this procedure, the plastic viscosity of an SCC mix is given by:

$$\boldsymbol{\eta_{ci} = \eta_{paste} \times f_1(\phi_1) \times f_2(\phi_2) \ldots\ldots \times f_n(\phi_n)} \quad \textbf{(4. 7)}$$

where *n* is the total number of solid phases in the mix. Besides the filler, fine, and coarse aggregates, air voids can be regarded as an additional phase. Einstein was the first to develop an expression $f_i(\phi_i)$ for dilute suspensions (second phase volume fraction less than 10%) containing randomly distributed rigid or hollow spheres with no hydrodynamic interactions:

$$\boldsymbol{f_i(\phi_i) = 1 + \check{H}\,\phi_i} \quad \textbf{(4. 8)}$$

The numerical factor $\check{H}$ is equal to 2.5 for rigid spherical particles and equal to 1 for spherical air bubbles that are packed randomly in a hexagonal arrangement. Subsequent

investigations have proved that the numerical factor 2.5 is quite accurate even for rigid ellipsoidal particles with an aspect ratio less than 3 (Struble and Sun, 1995).

However, when the concentration of the solid phase is increased (volume fraction >10% up to the maximum possible volume fraction, ϕ_m), the hydrodynamic interactions between the particles and the Brownian motions have to be taken into account. This was done by Krieger and Dougherty (Krieger, 1959) who proposed the formula 4.9

$$f_{(\phi_i)} = (1 - \frac{\phi_i}{\phi_m})^{-\psi\phi_m} \quad \textbf{(4. 9)}$$

The particle size distribution significantly affects ϕ_m. Its value is 0.74 for hexagonal close packing, 0.63 for random hexagonal packing, and 0.524 for cubic packing (Krieger and Dougherty, 1959). Furthermore, the numerical factor ψ and ϕ_m depend upon the shear rate; the former tends to decrease with increasing shear rate, whereas the latter shows the opposite trend. However, they change in such a way that a decrease in ψ leads to an increase in ϕ_m, but the product of the both changes remains nearly constant and on average equal to 1.9 (de Kruif et al., 1985). The volume fractions of the filler, fine, and coarse aggregates in most SCC mixes generally exceed 10%, so that their contribution to the increase in the known plastic viscosity of the paste can be calculated using Eq. 4.9. However, the volume fraction of the trapped air bubbles is low (around 2%) such that Eq. 4.8 can be used with the numerical factor $\check{H}$ equal to 1.0. For simplicity, the increase in the plastic viscosity of the SCC mix due to trapped air is included in the plastic viscosity of the paste in Eq. 4.10:

$$\eta_{mix} = \eta_{paste} \times (1 - \frac{\phi_{Filler}}{\phi_{mFiller}})^{-1.9} \times (1 - \frac{\phi_{Fine\ Agg.}}{\phi_{mFine\ Agg.}})^{-1.9} \times (1 - \frac{\phi_{Coarse\ Agg.}}{\phi_{mCoarse\ Agg.}})^{-1.9} \quad \textbf{(4. 10)}$$

It should be noted that the packing density (i.e. the maximum volume fraction, ϕ_m) increases with the addition of solid phases. When the first solid phase is added to the viscous paste, the packing is dense so that it can be approximated by hexagonal close packing with ϕ_m=0.74. However, when the last solid phase is added to the suspension, the packing is loose and it is appropriate to assume cubic packing with ϕ_m= 0.524.

where $\boldsymbol{\phi_{m\_filler}}$= 0.74, $\boldsymbol{\phi_{mFine\ Agg.}} = 0.63$, and $\boldsymbol{\phi_{mCoarse\ Agg.}} = 0.524$

In this study, an important amendment has been made to Abo Dhaheer et al.'s (2016b) parameter values. The maximum possible volume fraction parameters (ϕ_m ….) have been changed to allow for the effects of having higher proportions of ggbs and limestone powder (LP) in the mix. This ensures that the maximum packing volume criterion is not violated (see expression 4.11 and Table 4.2). The revised packing values are ϕ_m= 0.74 for the filler (the value for hexagonal close packing) and ϕ_m=0.524 (cubic packing) for the coarse aggregate.

$$\boldsymbol{Maximum\ possible\ volume} = \frac{N_{particle} * V_{particle}}{V_{unit\ cell}} \quad \textbf{(4. 11)}$$

where $N_{particle}$ is the number of the particles in the unit cell, $V_{particle}$ is the volume of each particle, and $V_{unit\ cell}$ is the total volume of available space. The proposed values also contrast with those used by Deeb and Karihaloo (2013) who used ϕ_m= 0.63 in all three phases.

Table 4.2 Maximum possible volume fraction

$\boldsymbol{\phi_m}$	Previous study (Abo Dhaheer,2016b)	Current study
$\boldsymbol{\phi_{m\_filler}}$	0.524	0.74
$\boldsymbol{\phi_{mFine\ Agg.}}$	0.63	0.63
$\boldsymbol{\phi_{mCoarse\ Agg.}}$	0.74	0.524

Regarding the rheological properties of cement paste; it is known (Nehdi and Rahman, 2004; Dinakar et al., 2013b; Abo Dhaheer et al., 2016b) that the replacement of 25% cement (*c*) by ggbs has little or no effect on the paste viscosity (η_{paste}). However, this is no longer true when 80% of cement is replaced by ggbs (Wang et al., 2002; Park et al., 2005; Hwang et al., 2009; Grzeszczyk and Janowska-Renkas, 2012; Tiwari et al., 2015), as illustrated by the data shown in Table 4.3

Table 4.3 Plastic viscosity for cement paste for different replacement fractions of cement by ggbs

Source	w/b	Plastic viscosity of cement paste, η (Pa s)						SP%
		ggbs						
		30%	40%	50%	60%	70%	80%	
(Tiwari et al., 2015)	**0.45**			0.16				0
(Grzeszczyk and Janowska-Renkas, 2012)	**0.45**		0.25		0.19		0.16	0
(Hwang et al., 2009)	**0.46**	0.32			0.15	0.13		0
(Wang et al., 2002)	**0.50**			0.08			0.12	0
(Tiwari et al., 2015)	**0.50**			0.09				0
(Tiwari et al., 2015)	**0.55**			0.06				0
(Tiwari et al., 2015)	**0.60**			0.04				0

The data presented in the aforementioned papers is insufficient to produce a reliable correlation between the plastic viscosity of cement paste, the ggbs replacement level and the w/b ratio (i.e. cement + ggbs) for the full range of ggbs percentages. However, by employing the above data and interpolating missing values, it is possible to see some trends in the plastic viscosity data for cement paste, as shown in Table 4.4. From the tabulated data it is clear that the paste viscosity decreases with increasing ggbs replacement level, and with the water and superplasticizer contents. This table will be referenced in the chapter 6 mix design procedure to choose the viscosity of the paste.

The method used to predict the values in Table 4.4 from Table 4.3 is now explained. The values in Table 4.3 proved insufficient to directly fit a two-variable function (w/b and ggbs) to the experimental data using regression methods. Rather, the following procedure used was;

1) Using the available values from Table 4.3, bounds were placed on the plastic viscosity values (given in brackets below) for each w/b ratio.
    - (0.38-0.17) for w/b=0.3
    - (0.28-0.14) for w/b=0.4
    - (0.16-0.03) for w/b=0.5

- (0.08-0.01) for w/b=0.6
- (0.04-0.005) for w/b=0.7

2) By inspection, approximate trends in ggbs and w/b were established and the most promising values selected for each w/b ggbs combination. In doing this, the differences between the values in each row (w/b ratio) were considered, and these are the values shown small font in Table 4.4.
3) Once the overall trends had been established, a fourth order function was fitted to the data for each ggbs level, as shown in Figure 4.6.
4) Steps 2 and 3 were then iterated until the coefficient of correlation between the available data and the 4^{th} order functions was a close as possible to one.
5) The final values were then determined and these are shown in Table 4.4.

Table 4.4 Predicted paste plastic viscosity Pa s

w/b	η (Pa s)					
	ggbs%					
	30%	**40%**	**50%**	**60%**	**70%**	**80%**
0.30	0.38	0.33	0.28	0.23	0.20	0.17
0.40	0.10	0.08	0.06	0.04	0.04	0.03
	0.28	0.25	0.22	0.18	0.16	0.14
0.50	0.12	0.13	0.14	0.13	0.12	0.11
	0.16	0.12	0.08	0.05	0.04	0.03
0.60	0.08	0.06	0.04	0.02	0.02	0.02
	0.08	0.06	0.04	0.03	0.02	0.01
0.70	0.04	0.025	0.01	0.01	0.01	0.005
	0.04	0.035	0.03	0.02	0.01	0.005

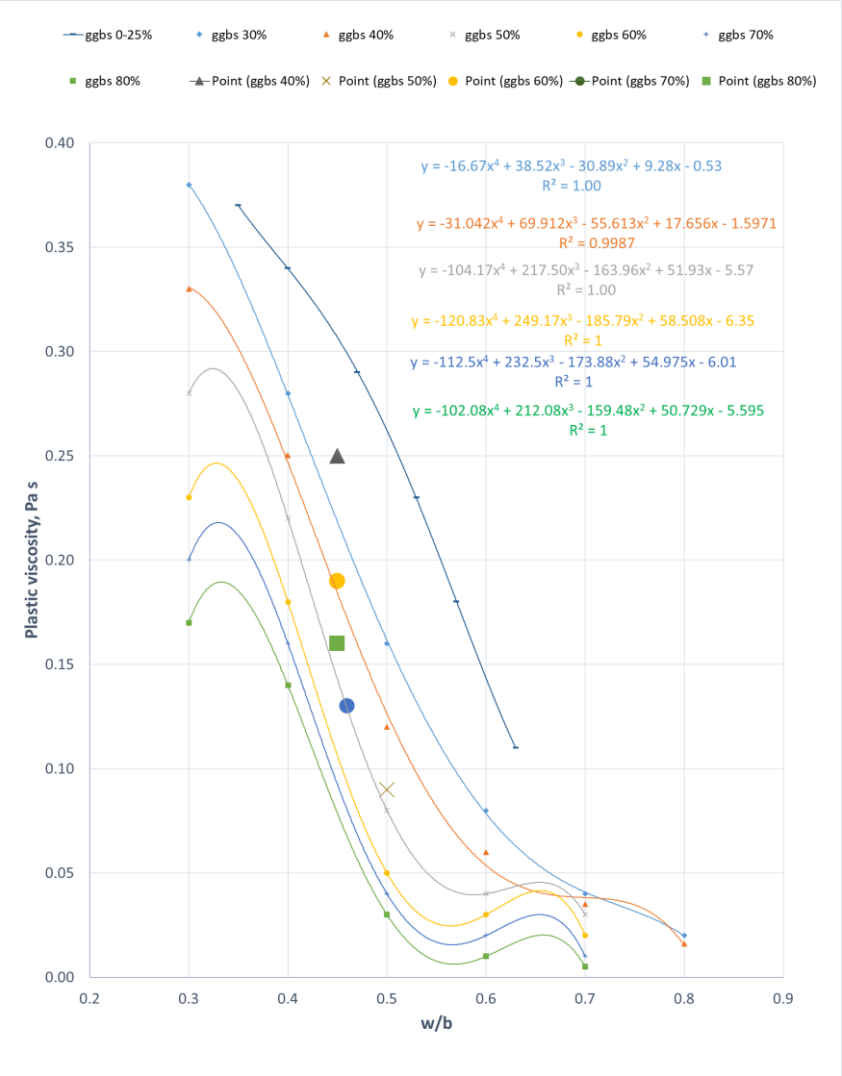

Figure 4.6 Plastic viscosity for cement paste of ggbs 0-80%

In the Figure 4.6 it can be seen that the trend in the plastic viscosity (w.r.t. f_{cu} for different ggbs levels) for cement paste with 25% ggbs 25 is not the same shape as in the higher range (i.e ggbs 30-80%). The reason of this because the viscosity does not change significantly with the ggbs level in the range 0-25%, as identified by Abo Dhaheer (2016b) and Nehdi and Rahman (2004).

4.9 Plastic viscosity of the cement paste

The experimental procedure for testing plastic viscosity of cement paste was described in (chapter 3 sec. 3.5.1). These tests used a non-Newtonian based viscometer and a summary of the pastes tested are given in Table 3.10. The results of the paste viscosity tests containing superplasticiser are presented in Table 4.5 and Figure 4.7.

Table 4.5 Viscosity test results on CEM II A-L 32.5R with superplasticiser SP

Class	mix	ggbs%	CEM II%	w/b	Rotor No.	Speed (rpm)	η (Pa s)	*SP/b%*
Group A	V1	20	80	0.3	2	60	0.278	0.35
	V2	50	50	0.3	2	60	0.112	0.35
	V3	80	20	0.3	2	60	0.181	0.35
Group B	V4	20	80	0.5	2	60	0.248	0.1
	V5	50	50	0.5	2	60	0.091	0.1
	V6	80	20	0.5	2	60	0.144	0.1
Group C	V7	20	80	0.7	2	60	0.205	0
	V8	50	50	0.7	2	60	0.061	0
	V9	80	20	0.7	2	60	0.120	0

The tests emphasise the need to use superplasticiser for mixes with low cement-binder ratios, which is consistent with the findings of other investigators (Park et al., 2005; Grzeszczyk and Janowska-Renkas, 2012). Furthermore, the same mixes were tried without using superplasticiser as listed in Table 4.6.

Table 4.6 Viscosity test results on CEM II A-L 32.5R without superplasticiser SP

Class	mix	ggbs%	cem%	w/b	Rotor No.	Speed	η (Pa s)
Group A	V1	20	80	0.3	2	1.5	10.023
	V2	50	50	0.3	2	1.5	9.535
	V3	80	20	0.3	2	1.5	8.640
Group B	V4	20	80	0.5	2	3	8.221
	V5	50	50	0.5	2	3	7.309
	V6	80	20	0.5	2	3	7.047
Group C	V7	20	80	0.7	2	60	0.181
	V8	50	50	0.7	2	60	0.144
	V9	80	20	0.7	2	60	0.120

Figure 4.7 shows the experimental results from the viscometer tests and Figure 4.8 gives the predicted values using the values in Table 4.4. It is evident from these figures that the experimental results for the cement paste plastic viscosity for ggbs 80% are noticeably different from the predicted values. The probable reason of this is that the viscometer gives inaccurate readings for fluids with high yield stresses; this phenomenon was also reported by Wang (2002). Furthermore, there may be variation in the results from the interpolation technique used.

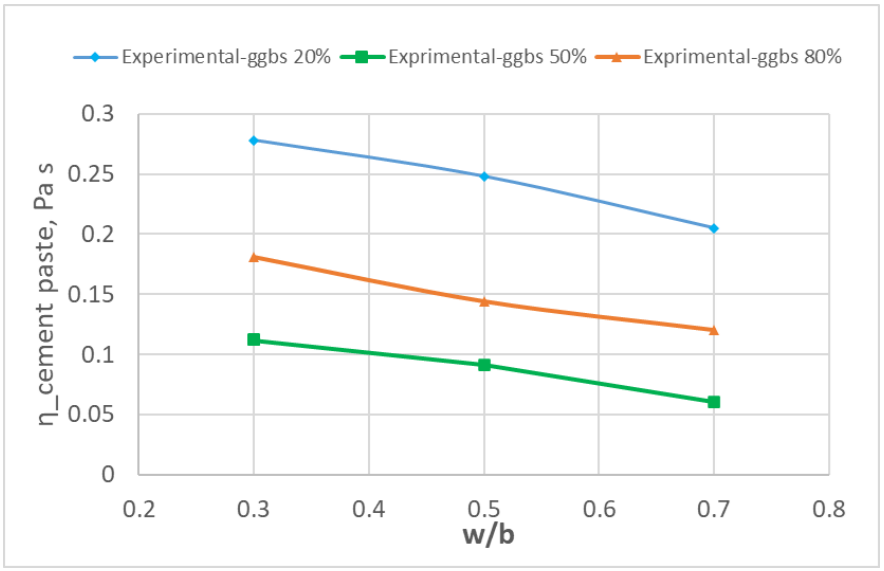

Figure 4.7 Plastic viscosity results of cement paste for current study, ggbs 20%, 50% and 80%

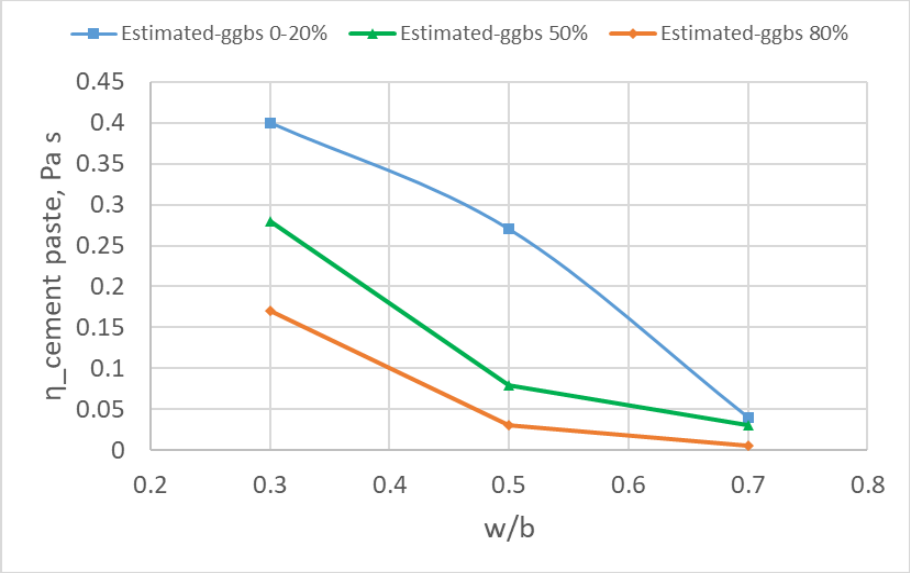

Figure 4.8 Predicted plastic viscosity of cement paste for ggbs 20%, 50% and 80%

4.10 Conclusions

The primary objective of this chapter was to present the micromechanical procedure (sec. 4.8) used in this work for calculating the plastic viscosity of SCC. The model is needed because rheometers are unable to reliably measure the plastic viscosity for reasons related to the heterogeneity of the mix.

Both the plasticity viscosity and yield strength parameters are required because SCC behaves as a non-Newtonian fluid.

The plastic viscosity prediction method is an essential component of the procedure described and verified in chapters 6 and 7 of this thesis.

The viscosity tests have clarified that the cement pastes used in this study have plastic viscosities in the range required for the SCC mix designs.

Previous work has not quantified the influence of ggbs percentage and w/b ratio on the plastic viscosity of cement paste for a full range of ggbs or w/b ratios. The use of existing data and careful interpolation allowed the dependence of the plastic viscosity to be determined for a wide range of these parameters.

Chapter 5 Hydration & strength development processes

5.1 Introduction:

Portland cement hydration is an exothermic process, and the cumulative amount of heat produced can affect the in-situ performance of structures (Schindler and Folliard, 2005). The total heat released and heat release rate during hydration depends on the composition and amount of cementitious material, as well as on the water-binder ratio of the mix (Schindler and Folliard, 2005). Cement components and their chemical composition not only govern the amount of heat released during hydration but also the rate at which the strength and stiffness of the hardened material develop. Schindler and Folliard (2005) suggest that the relative amount of heat released at a particular time after casting -relative to the total heat potential- provides a good measure of the degree of hydration. In turn, the degree of hydration may be related directly to the relative strength development of the hardened material.

In this chapter a procedure is described to predict the time-dependent concrete strength. The model builds on the work of Schindler and Folliard (2005) and DeSchutter and Taerwe (1996). The first of these two models defines the degree of hydration in terms of the relative heat release and the latter uses a relationship between the degree of hydration and the compressive strength.

In order to provide data for extending these approaches to SCC mixes with high proportions of ggbs, a series of experiments was undertaken. This involved the preparation and testing of four mixes (see set 1, Section 3.7). These all had Portland cement to ggbs ratios of 1:1 (i.e. 50% ggbs cement replacement) and included the following compressive strength classes; C20, C30, C40, and C50, with the mixes being denoted $C1_1$ to $C4_1$ respectively (see Table 3.4).

The layout of the remainder of this chapter is as follows;

section 5.2 presents the hydration and strength development models;

section 5.3 presents the results from some experiments undertaken to calibrate and subsequently validate the hydration, strength development and strength prediction models;

section 5.4 presents new formulae for predicting the 28-day and ultimate compressive strengths (i.e. the strength at full hydration);

section 5.5 describes the steps for computing the time-dependent compressive strength;

section 5.6 presents a validation of the time-dependent compressive strength calculation procedure;

section 5.7 assesses the consistency of the strength predictions;

section 5.8 defines a post 28 day compressive strength gain factor and discusses its potential in a new mix design procedure;

section 5.9 explains how the time-dependent heat of hydration is computed and gives values for the concretes considered in this study;

section 5.10 draws some conclusions from the work of the chapter.

5.2 Hydration and strength development model

The degree of hydration may be defined as the proportion of heat released by the hydration process at time t ($H(t)$) relative to the total heat released by the reaction (H_T). Many mathematical formulations to predict the degree of hydration have been proposed in the past (Knudsen, 1982; Freiesleben and Pedersen, 1985; Jonasson, 1988) and a comparison between these approaches is given in Figure 5.1. Most of these models are able to predict the degree of hydration curve for standard concrete with reasonable accuracy.

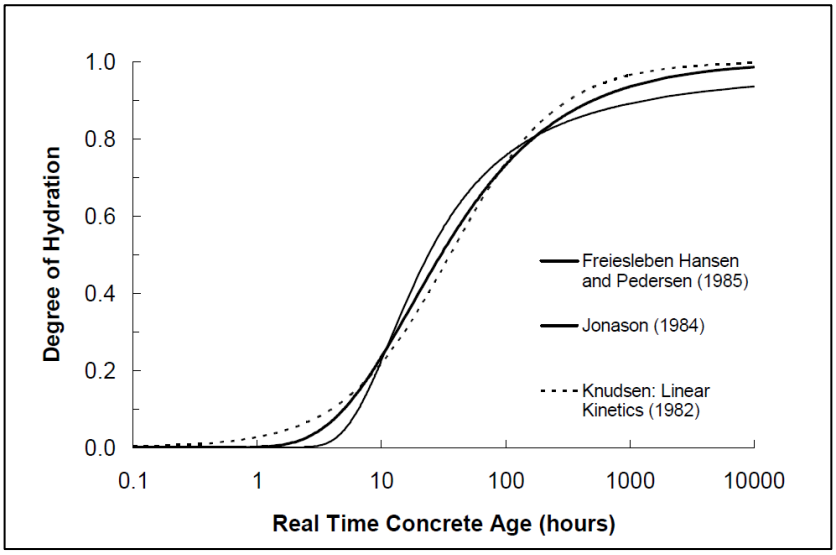

Figure 5.1 Comparing different hydration-maturity functions

Schindler (2002) (see also Schindler and Folliard, 2005) suggested a modification to Freiesleben and Pedersen's (1985) hydration function and introduced the ultimate degree of hydration parameter (α_u). The resulting relationship is given in equation 5.1.

$$\alpha(t_e) = \frac{H(t_e)}{H_T} = \alpha_u exp\left[-\left[\frac{\tau}{t_e}\right]\right]^{\beta} \quad \textbf{(5. 1)}$$

$\alpha(t_e)$ = the degree of hydration at equivalent age,

t_e = the effective time(hours),

τ = hydration time parameter (hours),

β = hydration shape parameter,

α_u = ultimate degree of hydration.

An expression for the total heat of hydration (H_T) is given in Section 5.9.

The effect of changing the hydration parameters (τ, β, and α_u) on the rate and ultimate degree of hydration is shown in Figure 5.2.

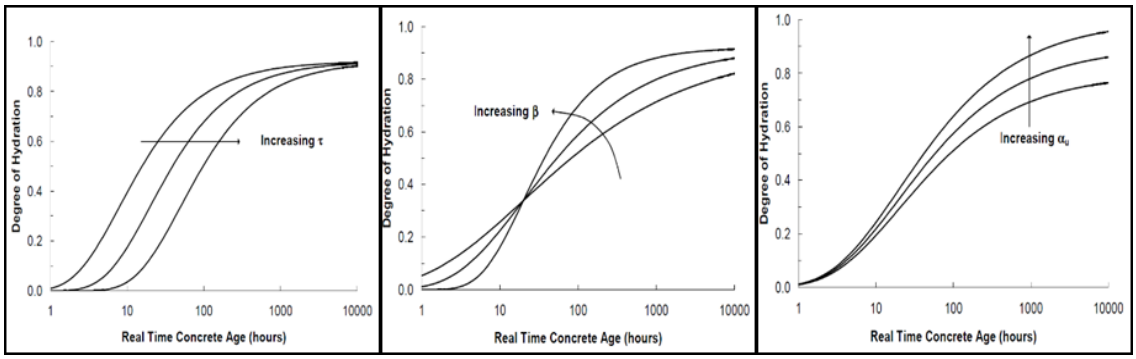

Figure 5.2 The effects of changing the hydration parameters (τ, β, and α_u) on the degree of hydration development.

Equation 5.1 includes the parameter (α_u) to characterize the ultimate extent of the hydration reaction. The effect of the water-binder ratio on the degree of hydration and heat evolution can be seen in Figure 5.3.

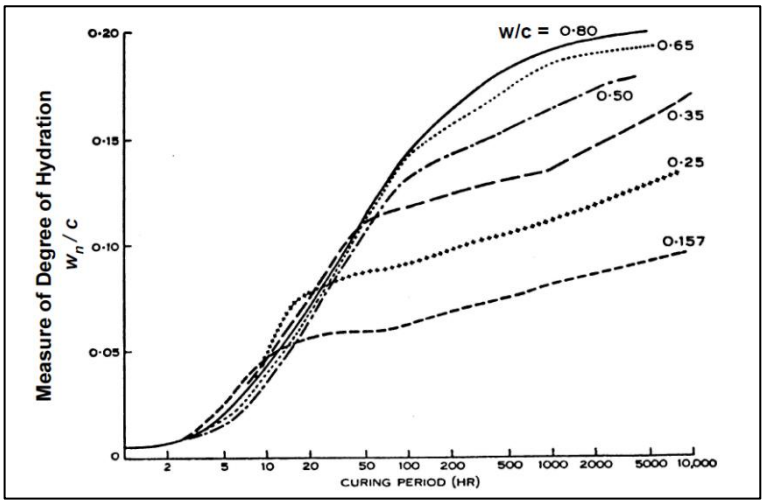

Figure 5.3 Ratio of chemically bound water per gram of cement versus log curing age (Taplin, 1959)

After investigating the hydration of a range of different cementitious materials, Mills (1966) stated that, "In most, if not all, cement pastes, hydration stops before the cement is totally consumed." The explanation of why the maximum degree of hydration is less than unity relates to the fact that hydration can only continue to develop if specific conditions are reached. The main two conditions (i and ii) are summarised below.

(i) Sufficient space is available for all hydration products. During hydration, the hydration products progressively fill the voids initially occupied by the mixing water. When no more capillary space is available, the hydration reaction ceases. From this requirement, it may be concluded that the lower the water cement (or water-binder) ratio, the less water per unit volume, and the lower the ultimate degree of hydration. This requirement can be quantified as follows (Hansen, 1986):

$$\alpha_u = \frac{w/c}{0.36} \leq 1 \qquad \textbf{(5. 2)}$$

(ii) Sufficient free water is available for the hydration reaction to progress. Free capillary water is required for the hydration process to continue. Based on properties of typical Portland cements, Hansen (1986) recommended the following formula for α_u:

$$\alpha_u = \frac{w/c}{0.42} \leq 1 \qquad \textbf{(5. 3)}$$

In order to measure the influence of the factors discussed above, Mills (1966) performed several tests to determine the maximum degree of hydration by determining the amount of chemically bound water after hydration is completed. Schindler (2002) used the findings of Mills, along with the results and the various physical limitations determined by Powers (1958), to derive the following expression for the ultimate degree of hydration for saturated concrete:

$$\alpha_u = \frac{0.262 \cdot w/c}{(w_n)_{max}(0.194 + w/c)} \qquad \textbf{(5. 4)}$$

where, $(w_n/c)_{max}$ = maximum mass ratio of (w_n/c) at complete hydration (g/g).

Mills recommended the use of the following:

- Cement: $(w_n/c)_{max}$ = 0.253, Powers and Brownyard (1946) also suggested a value of 0.253
- Cement with 50% Ggbs: $(w_n/c)_{max}$ = 0.261

w_n is defined as the mass of water that has chemically reacted with the cement i.e. chemical bound (non-evaporable) water. It can be quantified as the amount of water

emitted from a dried (105°C) specimen when it is subjected to ignition, which occurs at about 1050°C (Byfors and Betong, 1980). If the recommended $(w_n/c)_{max}$ of 0.253 is used, Equation 5.4 can be simplified to equation 5.5, which is recommended for use by Van Breugel (1997) and Cervera (1999). When 50% ggbs is used, Equation 5.6 presents the form recommended by Mills. The effect of varying the water-cement ratio on the ultimate degree of hydration as determined by equations 5.3, 5.5 and 5.6 is shown in Figure 5.4. This figure indicates that there is a large difference in the calculated ultimate degree of hydration from these three relationships.

For Cement:

$$\alpha_u = \frac{1.031 \cdot w/c}{0.194 + w/c} \quad \textbf{(5. 5)}$$

For Cement and 50% ggbs

$$\alpha_u = \frac{w/c}{0.194 + w/c} \quad \textbf{(5. 6)}$$

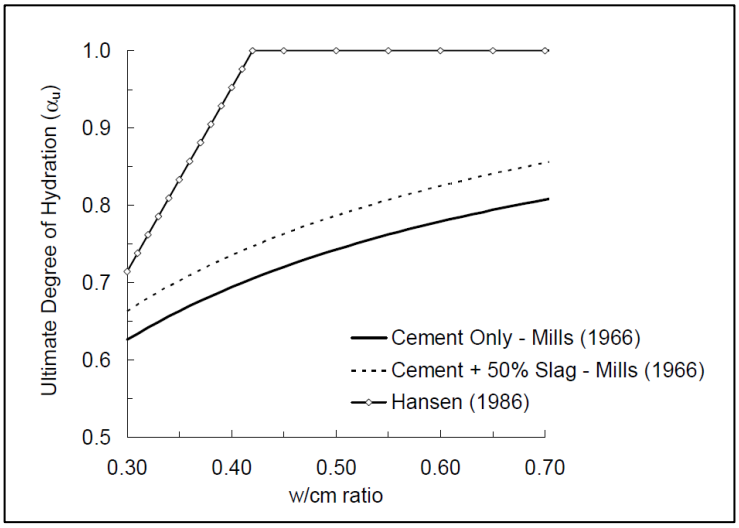

Figure 5.4 Comparing the effect of water-binder ratio on the ultimate degree of hydration predicted by equations 5.3, 5.5 and 5.6

Schindler and Folliard (2005) developed a relationship for α_u based on the above work and the results of 352 of their own experiments. The latter included mixes with CEM I cement and two types of fly ash (class C and F) as a CRM in the range 15% to 45%, and

mixes of CEM I cement and (30% and 50%) ggbs as a CRM . Accordingly, they proposed Equation 5.7 for α_u for a concrete that contains any percentage of slag (ggbs) and fly ash (FA).

$$\boldsymbol{\alpha_u = \frac{1.031.w/c}{0.194+w/c} + 0.50p_{FA} + 0.30p_{SLAG} \leq 1} \quad \textbf{(5. 7)}$$

where p_n represents the proportion of the cement formed of component *n.*

The two other parameters in Schindler and Folliard's hydration model (equation. 5.1) are τ and β. These depend on the fineness of the cement and its composition, including the amount of ggbs and FA, as follows;

$$\boldsymbol{\tau = 66.78 \,.\, p_{C_3A}{}^{-0.154} . p_{C_3S}{}^{-0.401} . Blaine^{-0.804} p_{SO_3}{}^{-0.758} . \exp(2.187 p_{SLAG} + 9.50 p_{FA} . p_{FA-C_aO})} \quad \textbf{(5.8)}$$

$$\boldsymbol{\beta = 181.4 \,.\, p_{C_3A}{}^{0.146} . p_{C_3S}{}^{0.227} . Blaine^{-0.535} p_{SO_3}{}^{0.558} . \exp(-0.647 p_{SLAG})} \quad \textbf{(5.9)}$$

where Blaine = Blaine value, specific surface area of cement (cm^2/g)

Changing the cement type will affect the C_3A, C_3S, SO_3 and Blaine values in the above equations. The cement component proportions for standard type Portland cement of CEM I 42.4N and CEM II A-L 32.5R are given in Table 5.1 (Mrema, 2010).

Table 5.1 Fraction by weight of total cement content for CEM I 42.5N and CEM II A-L 32.5R (Mrema, 2010).

Cement type	Chemical composition							Blaine cm^2/g
	C_3S	C_2S	C_3A	C_4AF	Free CaO	SO_3	MgO	
A-CEM I	0.529	0.218	0.075	0.085	0.666	0.027	0.012	367
B-CEM II	0.531	0.205	0.084	0.082	0.663	0.026	0.010	378

Table 5.2 and Figure 5.5 show the variation of the parameters τ and β with the percentage of ggbs for CEM II cement. It is evident that the characteristic time (τ) grows with the proportion of ggbs while the hydration shape parameter (β) decreases.

Table 5.2 Estimation of τ and β by using Eqs. (5.8 & 5.9)

Cement type	C_3A	C_3S	Blaine	SO_3	τ(hrs)	β
CEM II	0.084	0.531	378	0.026	17.071	0.578
CEM II + 20% GGBS	0.084	0.531	378	0.026	26.44	0.508
CEM II + 30% GGBS	0.084	0.531	378	0.026	32.90	0.476
CEM II + 40% GGBS	0.084	0.531	378	0.026	40.94	0.446
CEM II + 50% GGBS	0.084	0.531	378	0.026	50.95	0.418
CEM II + 60% GGBS	0.084	0.531	378	0.026	63.41	0.392
CEM II + 70% GGBS	0.084	0.531	378	0.026	78.91	0.368
CEM II + 80% GGBS	0.084	0.531	378	0.026	98.20	0.345

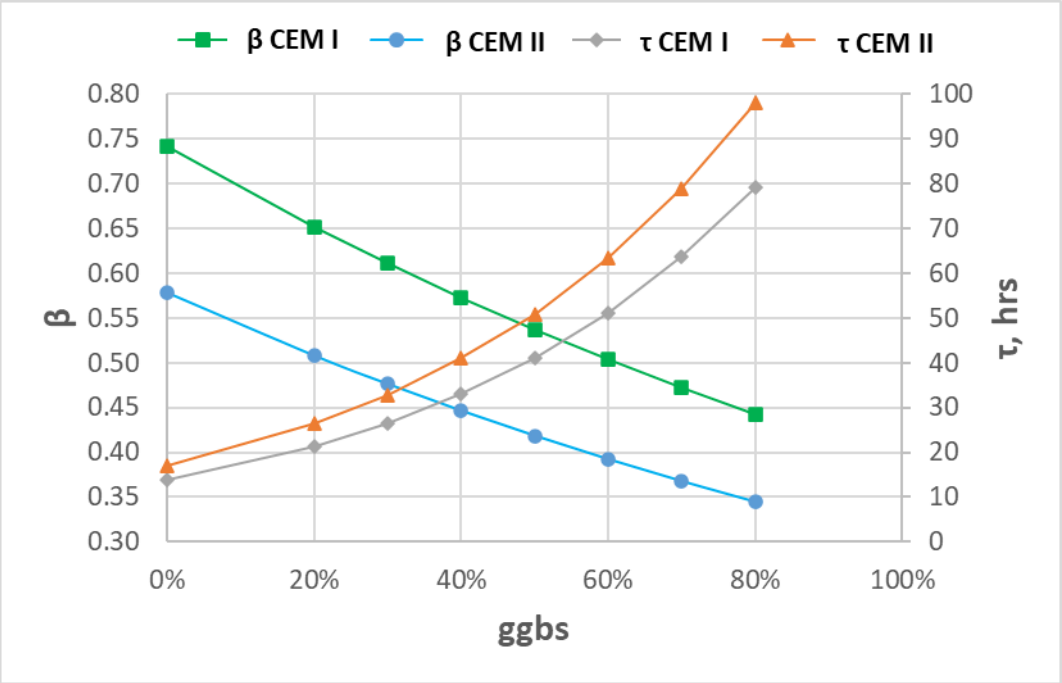

Figure 5.5 Variation of parameters τ and *β* with ggbs replacement level

The degree of hydration computed using equation 1 is now used to evaluate the time-dependent compressive strength. Using a model proposed by De Schutter and Taerwe (1996), the compressive strength is given by;

$$\frac{f_c(\alpha)}{f_c(\alpha=1)} = \left(\frac{\alpha-\alpha_o}{1-\alpha_o}\right)^a \quad \textbf{(5. 10)}$$

where $\alpha_0$and a are parameters that depend on the concrete composition and w/b ratio.

The original form suggests that the ultimate degree of hydration is unity (i.e. α_u=1), whereas (as discussed above) this is not normally the case and the limit for α is α_u equation 5.7. To allow for this, equation 5.11 will be used in place of 5.10. Also, the uniaxial compressive strength (f_c) has been replaced with the compressive cube strength (f_{cu}) used in the present study.

$$\boldsymbol{f_{cu}(\alpha_{t_e}) = f_{cu\_ult} \cdot \left(\frac{\alpha_{t_e}-\alpha_o}{\alpha_u-\alpha_o}\right)^a} \quad \textbf{(5. 11)}$$

where:

$\boldsymbol{\alpha_{t_e}}$= the degree of hydration at time $\boldsymbol{t_e}$ equation 5.1.

$\boldsymbol{\alpha_u}$= the ultimate degree of hydration equation 5.7.

$f_{cu}(\alpha)$= compressive strength at degree of hydration α.

f_{cu_ult}= compressive strength at the ultimate degree of hydration.

5.3 Experimental investigation and results

A set of experiments were undertaken to validate the hydration model for the SCC mixes considered in the present work and to provide data for a new method for predicting the ultimate and 28-day compressive strengths. Details of the materials and mix compositions used for these experiments are given in Chapter 3 (see set 1 in Section 3.7). The study considered curing times of 2, 4, 7, 14, 28, 210, and 300 days. The results are presented in Figure 5.6. It is noted that all of these mixes had a ggbs replacement level of 50%.

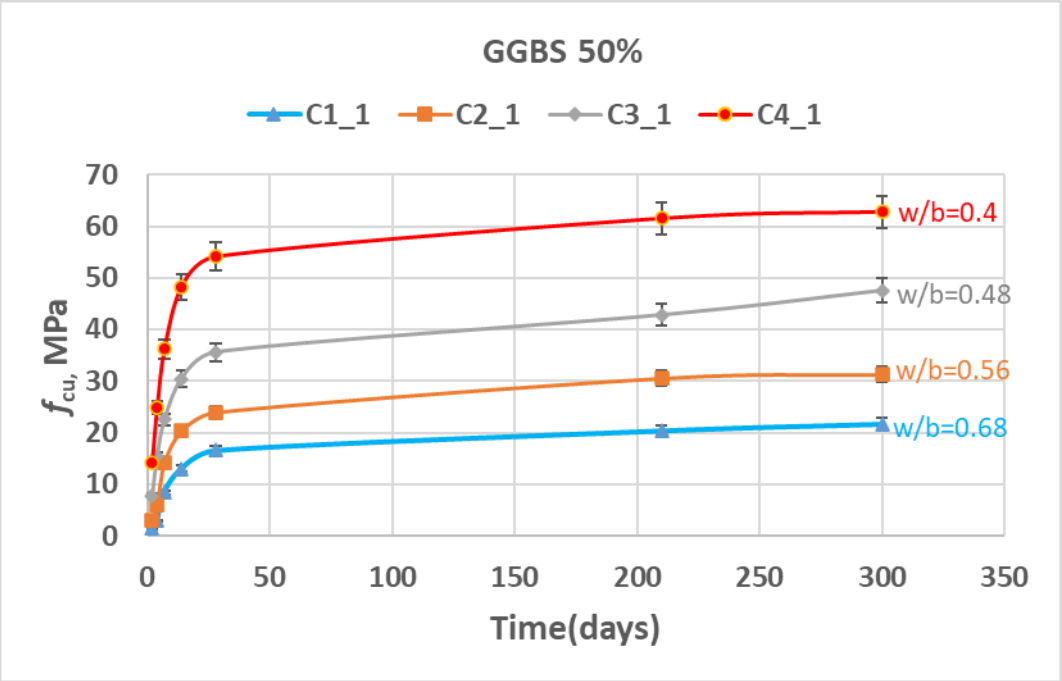

Figure 5.6 Compressive strength results for mixes set 1 (C1_1 to C4_1), ggbs 50% in times 2, 4, 7, 14, 28, 210 and 300 days

5.4 Predicting the ultimate and 28-day compressive strengths

The mix design procedure to be presented in chapter 6 requires the prediction of either the 28 day compressive strength and/or the compressive strength at the ultimate degree of hydration. These two values (i.e. f_{cu28} and f_{cu_ult}) may be determined (semi) independently or linked via the hydration model described in section 5.2. It may seem logical to use the latter approach in which f_{cu28} is computed from a predicted f_{cu_ult} ; however, most previous work on strength predictions have been based on 28 day strength values. Therefore, in order to relate this previous work to the present investigation, an expression will first be developed for the 28 day strength, then a related expression will be presented for the ultimate strength and finally the consistency between these two expressions will be assessed using the degree of hydration relationship.

5.4.1 Compressive strength at 28 days hydration

The compressive cube strength (f_{cu}) of a concrete mix is primarily determined by the ratio of water to binder (*w/b*) under given curing conditions.

Abo Dhaheer *et al.* (2016b) proposed the following equation for predicting the 28-day compressive cube strength (in MPa) from the w/b ratio for mixes containing 25% ggbs for concrete grades C30 to C80;

$$f_{cu} = \frac{195}{12.65^{\left(\frac{w}{b}\right)}} \quad \textbf{(5. 12)}$$

Noting that from this point forward f_{cu} denotes the 28-day compressive cube strength unless noted otherwise.

Abo Dhaheer *et al.* (2016b) determined this equation using regression analysis from a large amount of published data, as illustrated in Figure 5.7:

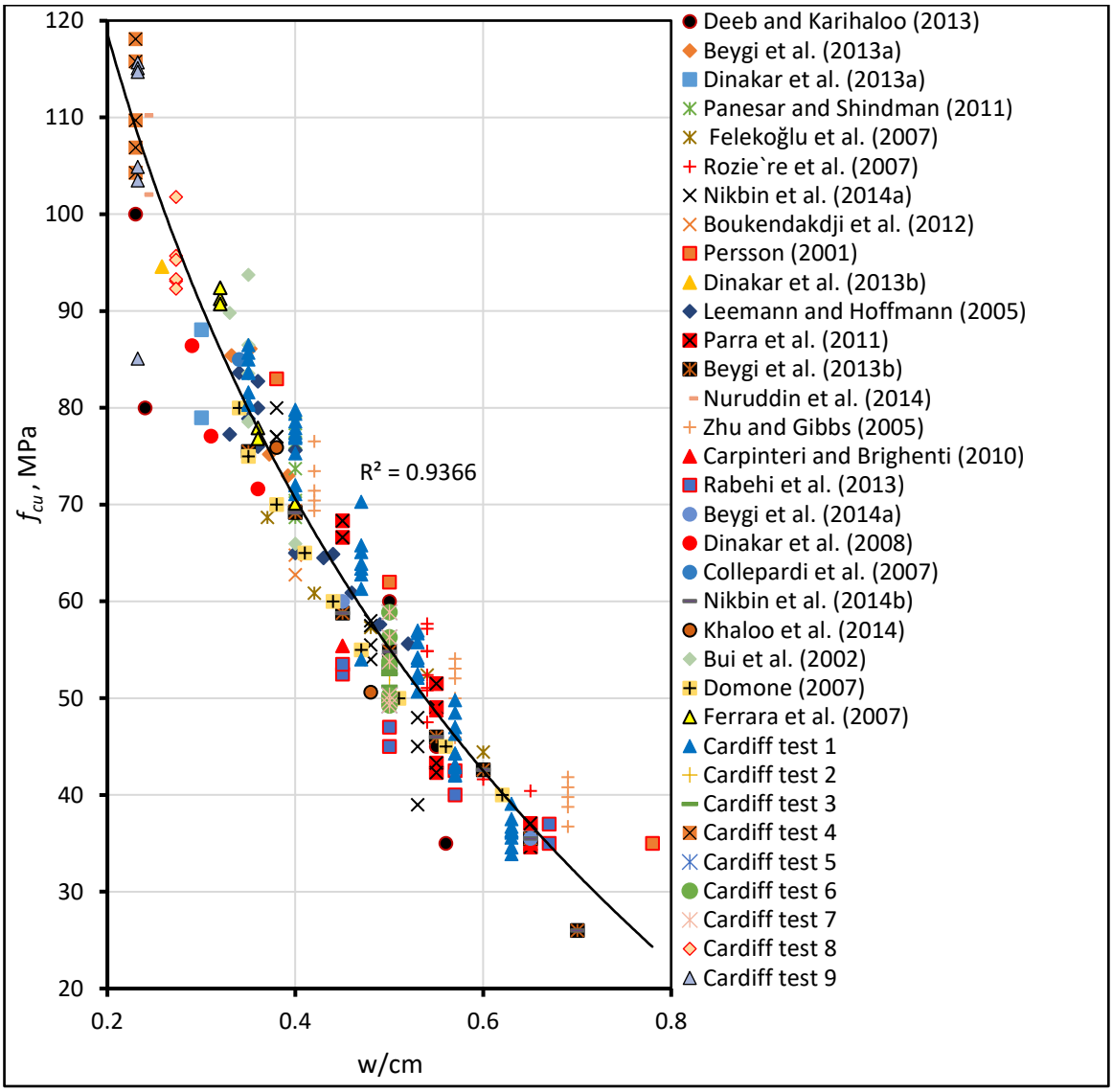

Figure 5.7 Relationship between compressive strength and water to binder ratio for 0-25% ggbs (Abo Dhaheer et al., 2016b)

Whilst equation 5.12 provides an adequate strength prediction for SCC concretes with up to 25% ggbs, it was found to be inaccurate for higher ggbs replacements levels up to 80%. This issue has been explored by a number of investigators (Bharatkumar et al., 2001; Khatib and Hibbert, 2005; Duran Atiş and Bilim, 2007; Oner and Akyuz, 2007; Chidiac and Panesar, 2008; Shi et al., 2009; Elahi et al., 2010; Topcu and Boga, 2010; Becknell and Hale, 2011; Güneyisi and Gesoğlu, 2011; Kou et al., 2011; Leung and Wong, 2011; Megat Johari et al., 2011; Li et al., 2012; Deeb and Karihaloo, 2013; Elchalakani et al., 2014), the

data have been presented in appendix B. In order to develop a compressive strength prediction formula that covered the full range of ggbs replacement (0-80%), data from these articles were extracted (see Figures 5.10-5.15 and Appendix B for the raw data) (section 5.3). Where the data were given in terms of f_c, the values were converted to equivalent f_{cu} values using the (BS EN 206, 2013) equivalence relationships for 100 mm cubes. There is considerable scatter in the surveyed data, which no doubt reflects differences in the curing conditions, cement type, superplasticiser dose, coarse aggregate content, and the maximum size of coarse aggregate. Furthermore, most of the data were for NVC. It is clear from these data and the observations of the investigators that, (i) the degree of hydration at 28 days decreases with the % of ggbs, and (ii) the % of ggbs has a moderate effect on the ultimate strength. Collating the data and accounting for these observations, the following equation was developed, which is illustrated in Figure 5.8.

$$\boldsymbol{f_{cu1} = \chi_1 \cdot (2 - ggbs\%) \cdot 10^{(2-\chi_2 \cdot \frac{w}{b})}} \quad \textbf{(5. 13)}$$

where f_{cu1} is the 28-day cube strength predicted using equation 5.13, and χ_1 and χ_2, are factors depending on cement type and mix materials. For the materials used in this study, χ_1=1, and χ_2=1, these factors have no units and were included in the function to accommodate future cements and mixes.

The method used to determine equation 5.13 is explained below.

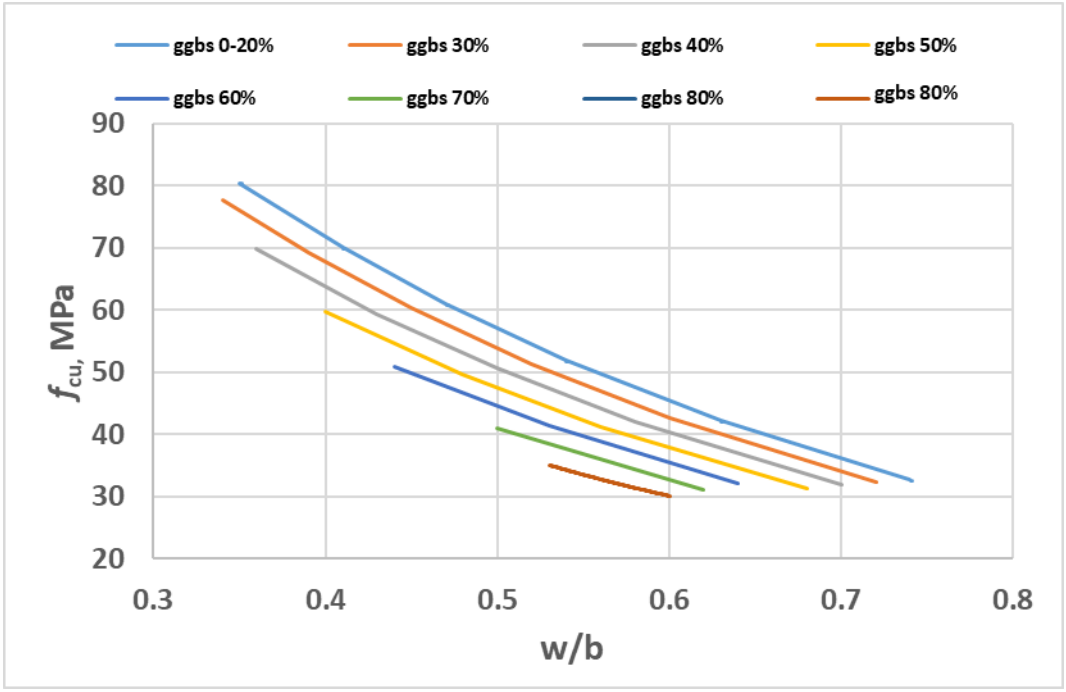

Figure 5.8 Relationship between w/b, ggbs%, and f_{cu}

A comparison between the f_{cu} values predicted using equations 5.12 and 5.13, for concrete with 25% ggbs, is shown in Figure 5.9. The graphs show that for this ggbs level, the predictions from the two equations are close to one another.

A comparison between the experimental data gathered from the previously mentioned references and equations 5.13 are given in Figures 5.10 & 5.11. This covers concretes with ggbs replacement levels of 30 to 80%. These graphs show the increasing inaccuracy of Abo Dhaheer *et al.'s* expression as the percentage of ggbs increases. The plots also illustrate that the new proposed equation 5.13 provides an acceptable fit to the experimental data, particularly when the variations in the experimental data (discussed above) are taken into account. The steps used to develop equation 5.13 are given below in 5.4.2.

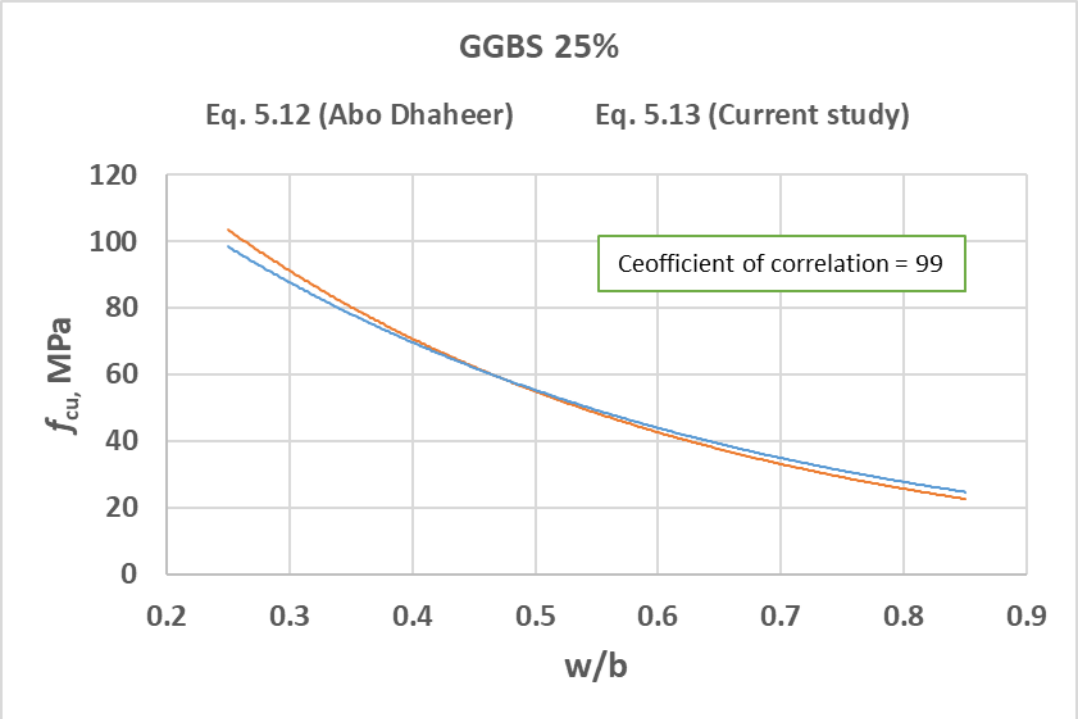

Figure 5.9 Relationship between compressive strength and water to binder ratio for 0.25 ggbs

5.4.2 Steps used to develop a general formula for predicting the 28-day compressive strength.

1) Existing data (see Appendix B) were collected, as shown in Figure 5.10 and Table 5.3. These data are given in terms of f_{cu} vs w/b for a range a ggbs percentages.
2) New data was then gathered (i.e. mix sets A-ggbs40% and B-ggbs60%), as shown in Table 5.4.
3) A combined data set was then produced and missing values interpolated / extrapolated where necessary. The combined data set is shown in Table 5.5. Whilst an attempt was made to use mathematical interpolation to fill in the missing values, a degree of judgement was applied in producing Table 5.5.
4) Regression was then applied to the f_{cu} vs w/b data for each ggbs percentage shown in Table 5.5, with the 'best fit' being judged from the R^2 correlation coefficient.

5) A range of function forms were explored to determine a single function that could reproduce the experimentally observed trends for the full range of data (Table 5.5). This started with the form of best fit lines, but it was found that these varied considerably with ggbs level. Then other equations types were tried until the form shown in equation 5.13 was arrived at. This was a trial and error process that used the author's knowledge of various function types and how they behaved.
6) Finally, the coefficients of correlation between equation 5.13 and the data shown in Table 5.5 were determined (using EXCEL) for each ggbs level, and the coefficients of the equation altered until the best fit to the full data set was obtained. A comparison between equation 5.13 and the full data set, along with the R^2 values, are shown in Figure 5.11.

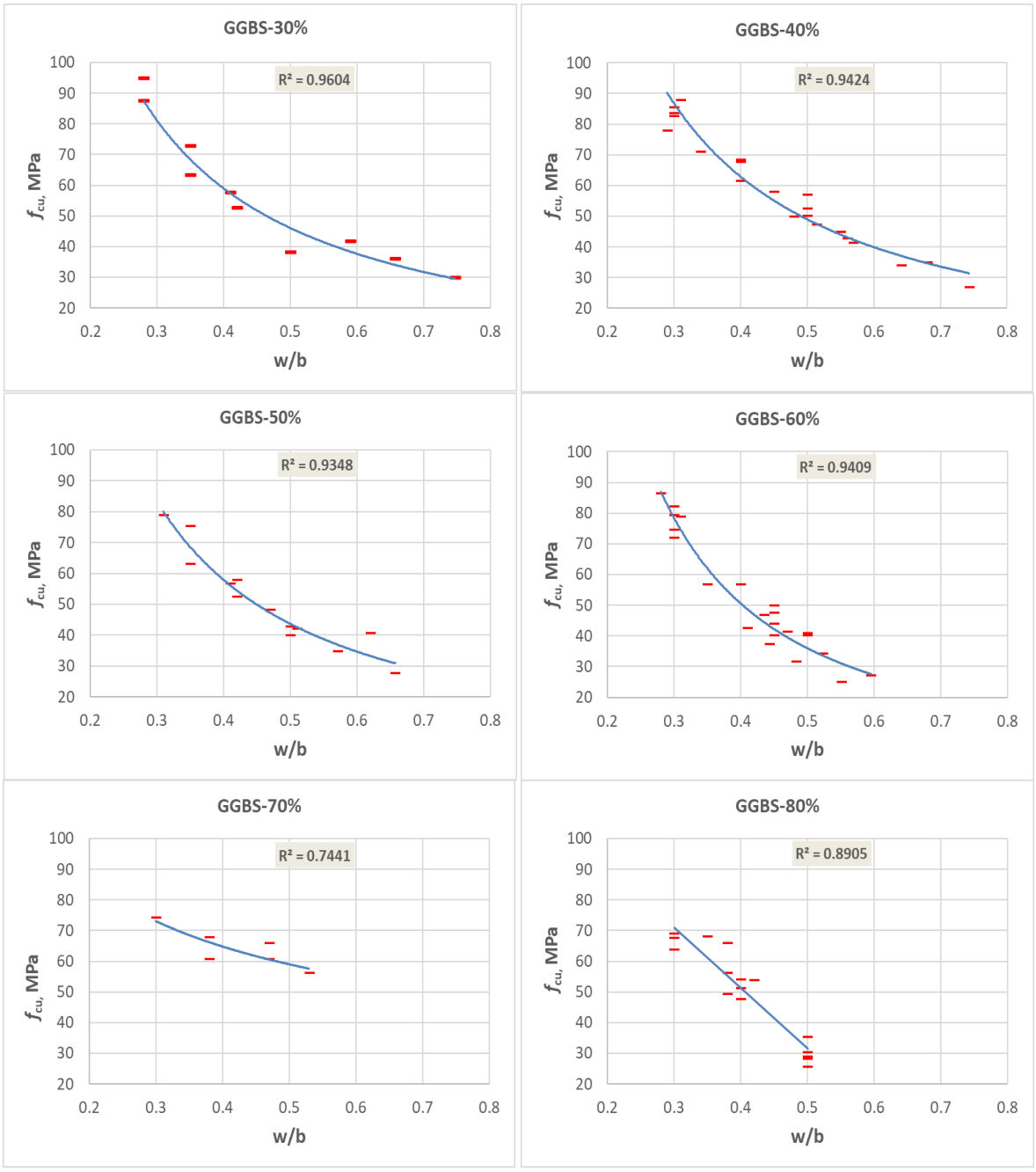

Figure 5.10 Correlation between w/b ratio and compressive strength from gathered data for ggbs (30%-80%)

Table 5.3 f_{cu} (MPa) vs w/b for ggbs 30%-80% using data from Figure 5.10

ggbs %	Compressive strength Grade, MPa					
	30	40	50	60	70	80
30%	0.74	0.57	0.46	0.39	0.34	0.30
40%	0.75	0.60	0.49	0.42	0.36	
50%	0.67	0.53	0.45	0.38		
60%	0.56	0.46	0.40			
70%	N/A	N/A				
80%	0.50					

Table 5.4 Experimental results: f_{cu} (MPa) vs w/b for ggbs 40% and 60%

Ggbs 40%	f_{cu}	35	43	50	61	71	78
	w/b	0.68	0.56	0.48	0.40	0.34	0.29
Ggbs 60%	f_{cu}		48	52	57		
	w/b		0.5	0.45	0.4		

Table 5.5 Combined f_{cu} vs w/b data for ggbs 30%-80% including interpolated values

ggbs %	Compressive strength Grade, MPa					
	30	40	50	60	70	80
30%	0.72	0.60	0.52	0.45	0.39	0.34
40%	0.70	0.58	0.50	0.43	0.36	
50%	0.68	0.56	0.48	0.40		
60%	0.64	0.53	0.44			
70%	0.62	0.50				
80%	0.57					

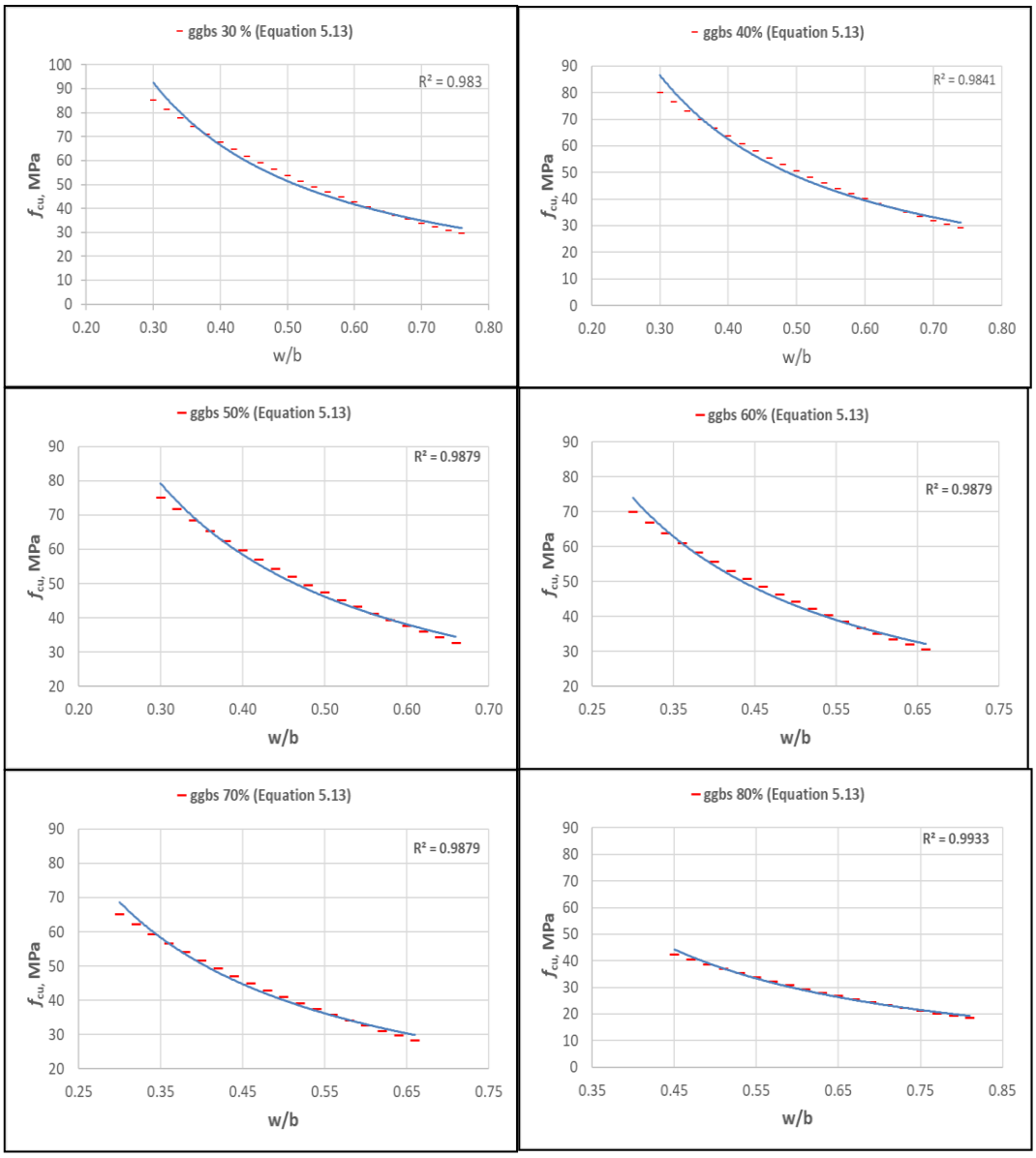

Figure 5.11 Correlation between w/b ratio and compressive strength from single equation 5.13 for ggbs (30%-80%)

5.4.3 Compressive strength at ultimate hydration

The same basic form of equation can be used to predict the ultimate compressive strength for the whole range of ggbs replacement levels. As mentioned above, the effect

of the ggbs on f_{cu_ult} is much less than on the 28 day strength, and f_{cu_ult} is greater than f_{cu} at 28 days. Allowing for these two factors, gave the following expression for f_{cu_ult}:

$$f_{cu1\_ult} = \chi_3(2 - 0.2\text{ggbs}\%) \cdot 10.4^{(2-\chi_4 \cdot \frac{w}{b})} \quad \textbf{(5. 14)}$$

The values for the material factors χ_3 and χ_4 used in this study are given in Table 5.8.

Equation 5.10 can be used to determine the ultimate strength from the 28 strength and vice versa; however, it was felt beneficial to have a separate equation for the ultimate strength, as shown in equation 5.14. This was determined using equations 5.13 and 5.10, along with the experimental data for the strength development beyond 28 days. The function determined has a similar form to equation 5.13, but with different coefficients that reflect the reduced influence on final strength of the ggbs level.

It is interesting to plot f_{cu1_ult} from equation 5.14 against the w/b ratio for different ggbs percentages (See Figure 5.12). This shows that the final strength is relatively insensitive to the ggbs level.

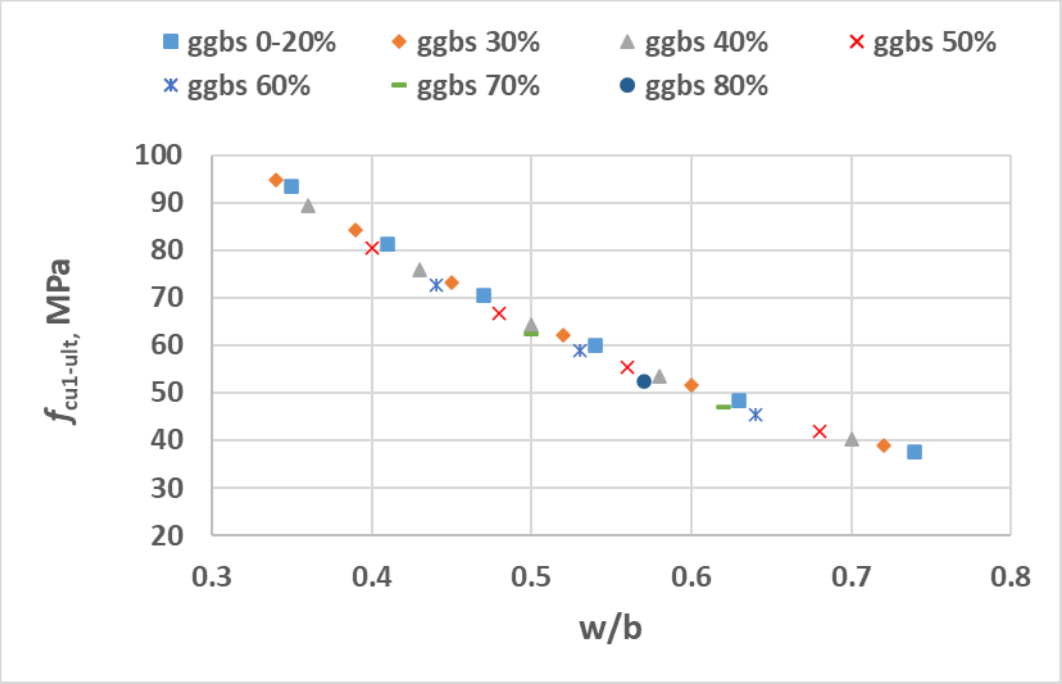

Figure 5.12 Correlation between ultimate compressive strength (equation 5.13) $f_{cu1\text{-}ult}$, and w/b ratio for the entire ggbs range

5.5 Computing the time-dependent compressive strength

The application of equations 5.1, 5.7, 5.11 and 5.14 to the calculation of the compressive strength at a given time is explained in Figure 5.13. The parameters α_0 and a are obtained from De Shutter and Taerwe (1996) and take the values $\alpha_0 = 0.25$ and a = 0.6. The parameters τ and β are obtain from equations 5.8 and 5.9 respectively, using the chemical composition data in Table 5.1 for the relevant cement type.

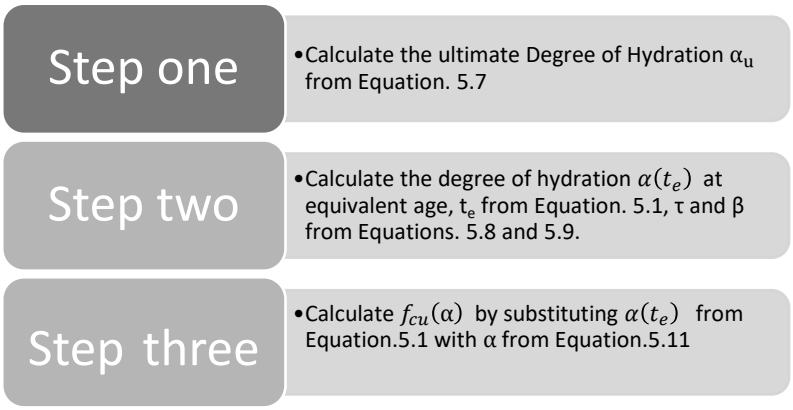

Figure 5.13 Flow chart for compressive strength estimation procedure

5.6 Validation of the time-dependent compressive strength calculation procedure

The accuracy of the combined hydration-strength development model is now assessed by comparing the predicted compressive strengths at different times with those measured in the tests described in the section 5.3. The α_u values computed from equation 5.7 are given in Table 5.6.

Table 5.6 Calculated αu values for the set 1 mixes, ggbs 50%

Designation	w/c	α_u
$C1_1$	0.68	0.95
$C2_1$	0.56	0.92
$C3_1$	0.48	0.88
$C4_1$	0.40	0.84

The computed cube strength values are compared with the experimental results in Figures 5.14 to 5.17 for mixes $C1_1$ to $C4_1$ respectively. In addition, the specific calculated values and coefficients are given in Table 5.7 for mix $C3_1$. The full results for the other mixes are presented in Appendix C.

As may be seen from Figures 5.14 to 5.17, the combined hydration strength-development model is able to predict the characteristics of the strength development curve with good accuracy with.

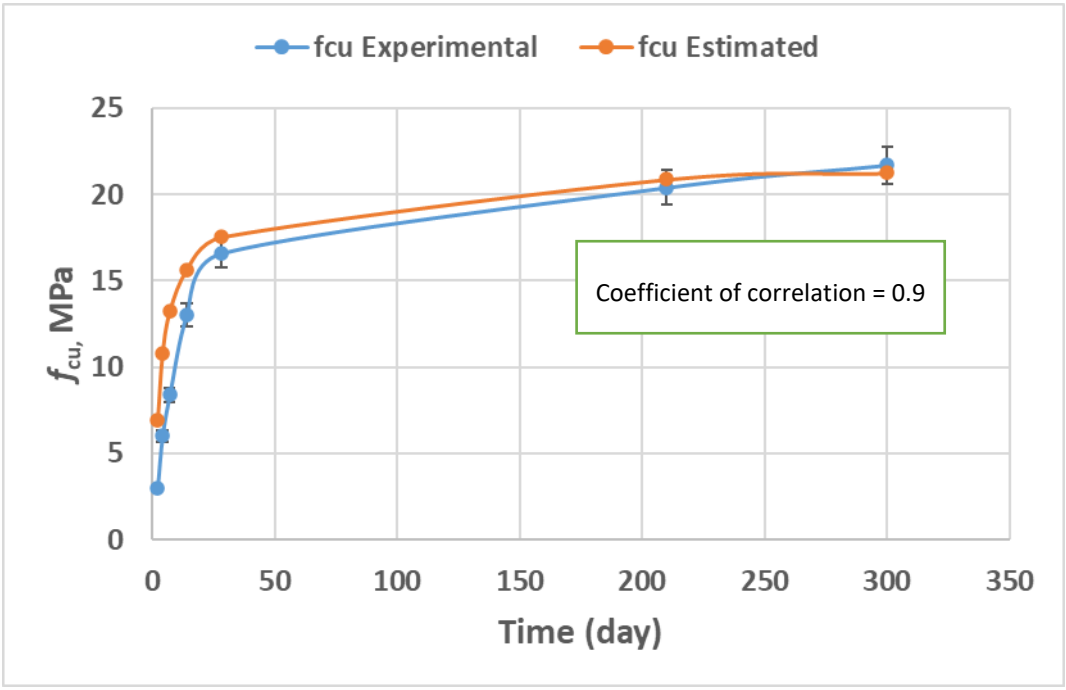

Figure 5.14 Calculated compressive strength $C1_1$ including f_{cu}(300) days

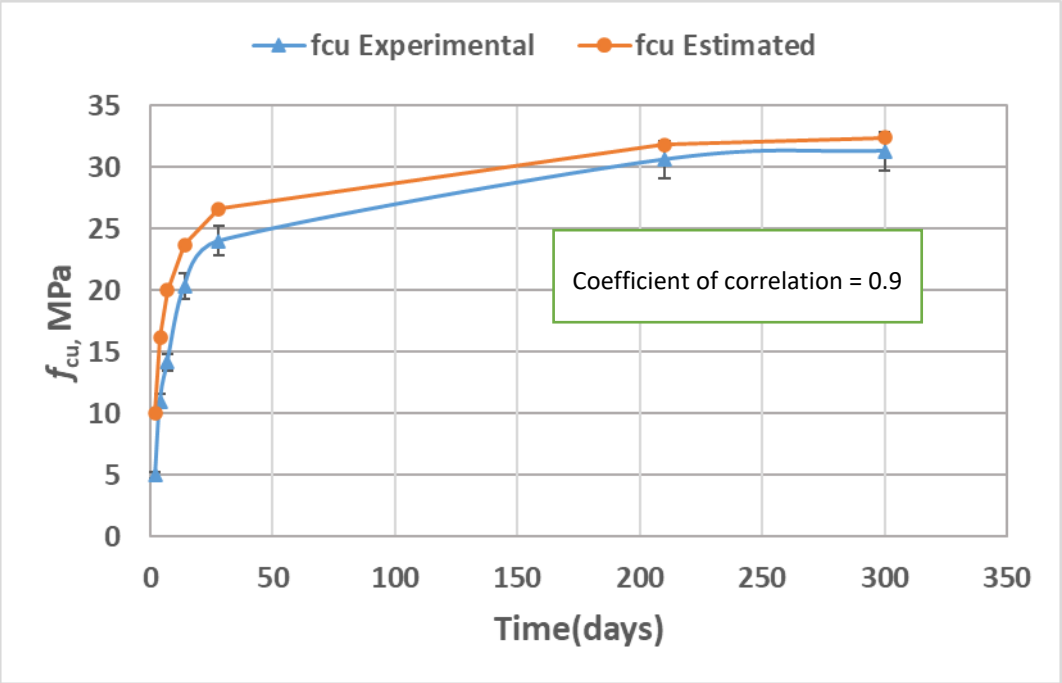

Figure 5.15 Calculated compressive strength $C2_1$ including f_{cu}(300) days

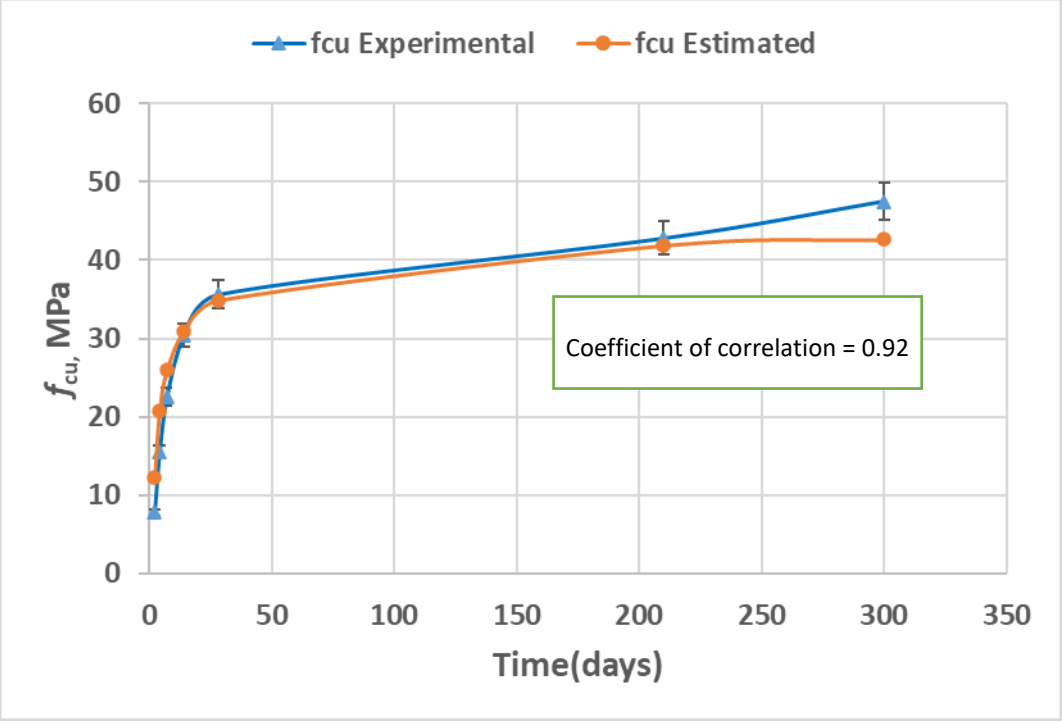

Figure 5.16 Calculated compressive strength $C3_1$ including f_{cu} (300) days

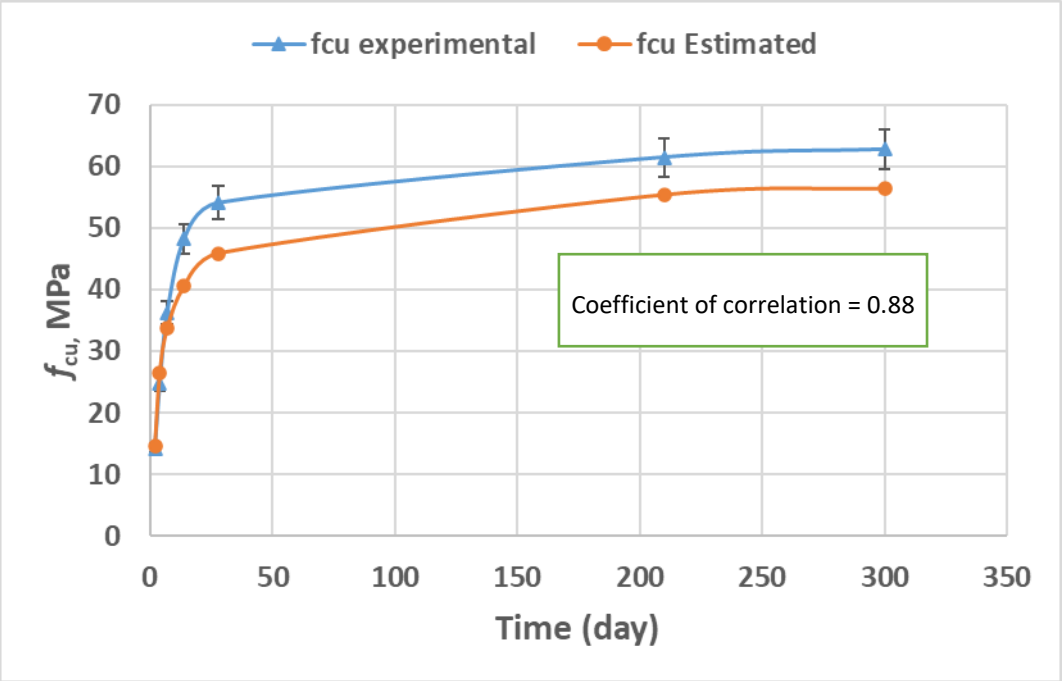

Figure 5.17 Calculated compressive strength $C4_1$ including f_{cu} (300) days

In the graph 5.17 it can be seen there is inadequate matching between the experimental results and the calculated values for mix $C4_1$ for low w/b ratios. Further research and more experimental data would be required to improve the accuracy of the prediction in this range.

Table 5.7 Estimated $\alpha(te)$ for Mix $C3_1$,

α_u	τ	β	t_e(days)	t_e(hrs)	$\alpha(t_e)$	$f_{cu}(t)$ Experimental	$f_{cu}(\alpha)$ Calculated
0.88	38.22	0.554	2	48	0.364	7.8	9.4
0.88	38.22	0.554	4	96	0.483	15.5	17.9
0.88	38.22	0.554	7	168	0.567	22.6	23.6
0.88	38.22	0.554	14	336	0.652	30.4	29.2
0.88	38.22	0.554	28	672	0.717	35.6	33.5
0.88	38.22	0.554	210	5040	0.823	42.8	40.2
0.88	38.22	0.554	300	6480	0.830	43.80	40.7

t_e is assumed to be equal to real time (t) since the concrete cubes remained very close to the laboratory ambient temperature of 20°C

The time dependent compressive strength calculation is now extended to the full range of ggbs proportions considered in this study (i.e. cement replacement levels of 20% to 80%). The C30 mix has been selected to illustrate the computation. Table 5.8 gives the hydration parameters, as well as the computed 28 day and ultimate compressive strengths. Table 5.9 presents the computed strength results at different curing times. Computed results relating to the other mixes are given in Appendix D.

Table 5.8 Calculated f_{cu} at 28 days from the ultimate strength for design mix C30

ggbs%	α_u	τ	β	t_e(days)	t_e(hrs)	α(te)	f_{cu1_ult}	f_{cu1}
20%	0.88	26.44	0.51	28	672	0.723	37.5	31.6
30%	0.90	32.90	0.48	28	672	0.711	38.9	31.6
40%	0.93	40.94	0.45	28	672	0.696	40.3	31.4
50%	0.95	50.95	0.42	28	672	0.678	41.8	31.1
60%	0.97	63.41	0.39	28	672	0.653	45.4	32.1
70%	1.00	78.91	0.37	28	672	0.631	47.1	31.5
80%	1.01	98.20	0.34	28	672	0.603	52.4	33.1

Table 5.9 Compressive strength at different times for C30 mixes with different %ggbs

ggbs %	Compressive strength, MPa				
	variable time (days)				
	7	28	90	180	360
20%	26.1	31.6	34.2	35.1	35.8
30%	25.3	31.6	34.6	35.8	36.6
40%	24.5	31.4	34.9	36.3	37.3
50%	23.5	31.1	35.0	36.7	37.9
60%	23.5	32.1	36.7	38.7	40.3
70%	22.4	31.5	36.6	38.9	40.6
80%	22.8	33.1	39.0	41.7	43.9

As discussed earlier, the difference between the 28 day and ultimate strengths grows with the proportion of ggbs. This phenomenon was observed by Oner and Akyuz (2007) and Megat Johari *et al.* (2011) but the difference has not previously been quantified for a full range of strengths and ggbs replacement percentages. This post 28-day strength development value could be used to determine the self-healing potential of a concrete mix (see section 5.8).

5.7 Assessing the consistency of the strength predictions

As discussed in section 5.4, f_{cu} at 28 days can be calculated in two ways i.e. from equation 5.13 and from equation 5.15

$$\boldsymbol{f_{cu2-28} = \left(\frac{\alpha_{28}-\alpha_o}{\alpha_u-\alpha_o}\right)^a \cdot f_{cu1\_ult}} \qquad \textbf{(5. 15)}$$

Where . $\boldsymbol{f_{cu1\_ult}}$ (equation 5.14)

α_{28} is the degree of hydration at 28 days

A comparison between the values predicted using these two approaches is shown in Figure 5.18. This shows that predictions using the two methods are very close to each other. The exact differences are given in Figure 5.18 and these show that they a larger for the lowest w/b (5% and 7%), with all other w/b ratios having differences of 3% or less.

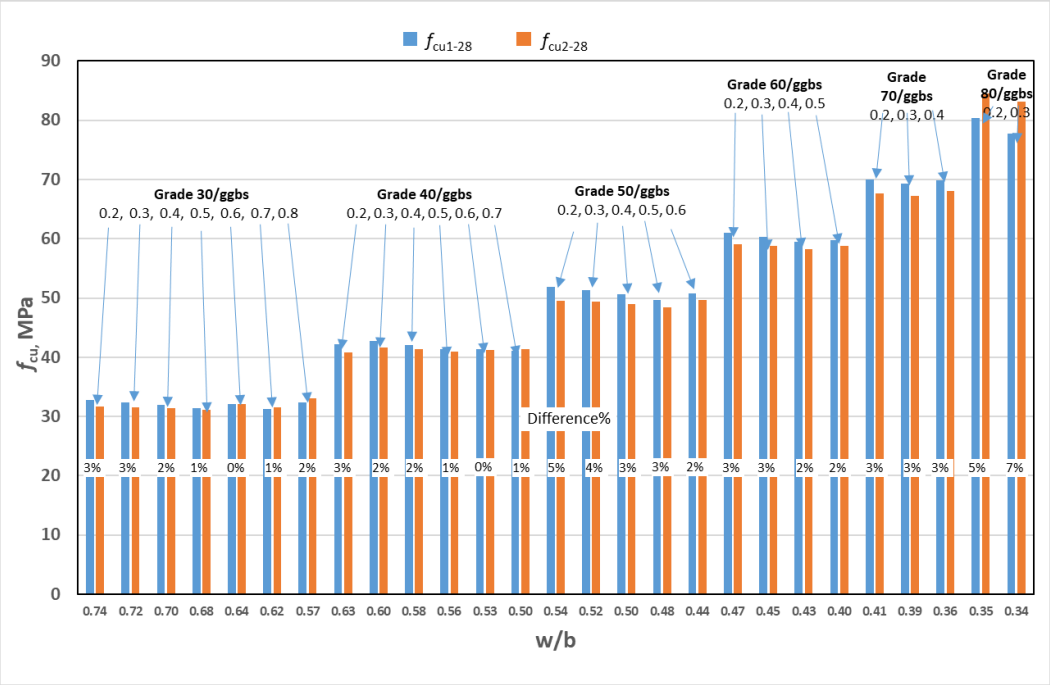

Figure 5.18 Predicted compressive strength at 28 days from equations 5.13 and 5.15

Alternatively, f_{cu1} from equation 5.13 and the degree of hydration at 28 days can be used to predict the final strength, as follows;

$$f_{cu2-ult} = \left(\frac{\alpha_{28}-\alpha_o}{\alpha_u-\alpha_o}\right)^{-a} \cdot f_{cu1\_28} \qquad \textbf{(5. 16)}$$

For completeness, a comparison between the two predictions for f_{cu_ult} is shown in Figure 5.19. As may be expected, the values predicted using equations 5.14 and 5.16 are close to one another.

The full set of Tables for both f_{cu_ult} and f_{cu_28} for equations 5.13, 5.14, 5.15 and 5.16 is listed in Appendix E.

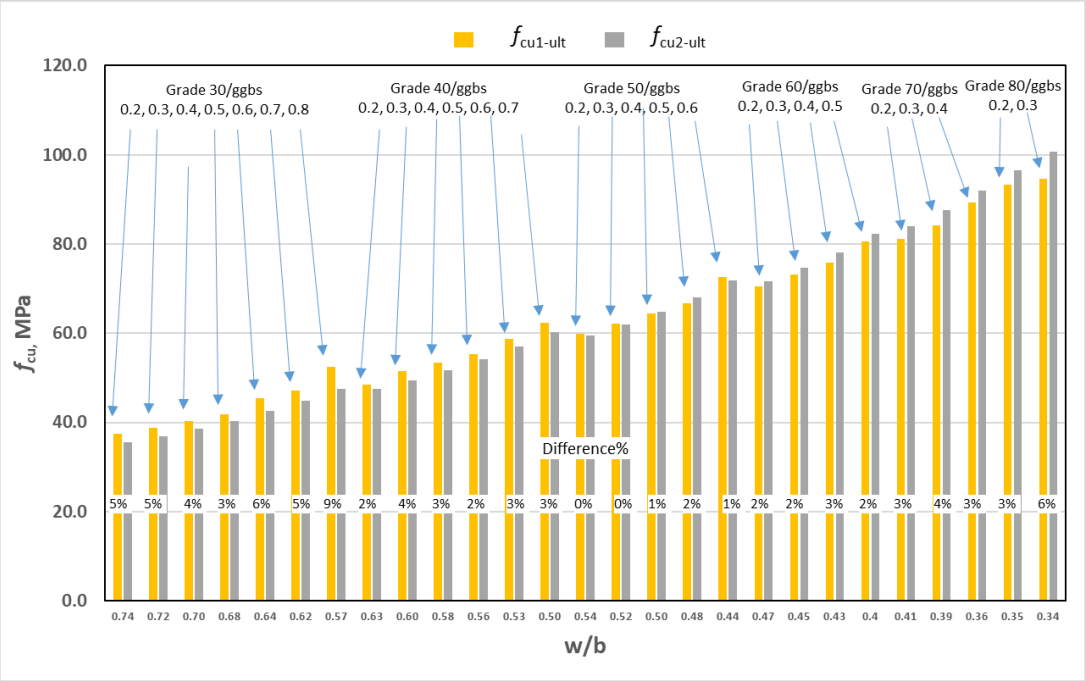

Figure 5.19 Predicted ultimate compressive strength from equations 5.14 and 5.16

A comparison between predicted strength using equation 5.16 and the experimental data is presented in Figure 5.20 for specimens with an age of 300 days.

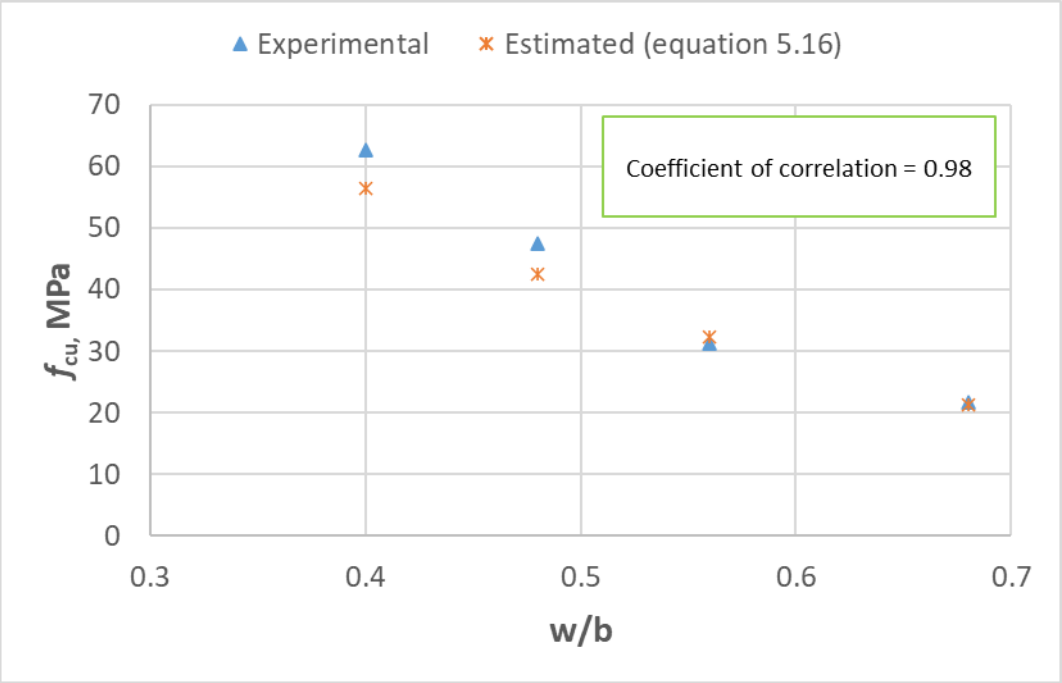

Figure 5.20 Comparison between experimental results and equation 5.16 for mixes $C1_1$-$C4_1$ at 300 days

It may be seen in Figure 5.20 that there is a slight deviation between the experimental data and the calculated values in the lower w/b range. It is likely that, in this range, there is insufficient space for the hydration products. As soon as the space is restricted in this way, the trend in the w/b vs strength data is likely to change. This is not fully reflected in the predictive formula.

The values of χ_3 and χ_4 for the mixes considered in this study are given in Tables 5.8 and 5.9, and strength predictions obtained using these values in equation 5.14, along with equation 5.16, are given in Figures 5.21-5.23.

Table 5.10 calculation details to find the factors χ_3 and χ_4

Mix type	f_{cu},target	ggbs%
Set 1	30	50%
	30	50%
	40	50%
	50	50%
Set 3	30	50%
	50	50%
	30	60%
	30	80%

Table 5.11 Further details for the calculation of factors χ_3 and χ_4

χ_3	χ_4	w/b	f_{cu} _28 exp	f_{cu} _tef exp	f_{cu1} _ult calc	f_{cu2}_tef calc	f_{cu1} _28 calc
1.3	1.5	0.68	16.6	21.7	23.6	22.6	18.6
1.3	1.5	0.56	24.0	31.3	36.0	34.4	28.2
1.3	1.5	0.48	35.6	47.5	47.6	45.4	37.2
1.3	1.5	0.4	54.1	62.8	63.0	60.0	49.0
0.8	0.75	0.62	40.9	48.9	53.1	49.0	41.1
0.8	0.75	0.42	58.1	63.9	75.3	69.3	58.1
0.8	0.75	0.58	47	54.5	56.0	50.5	41.1
0.8	0.75	0.50	35.50	39.6	62.3	53.0	40.5

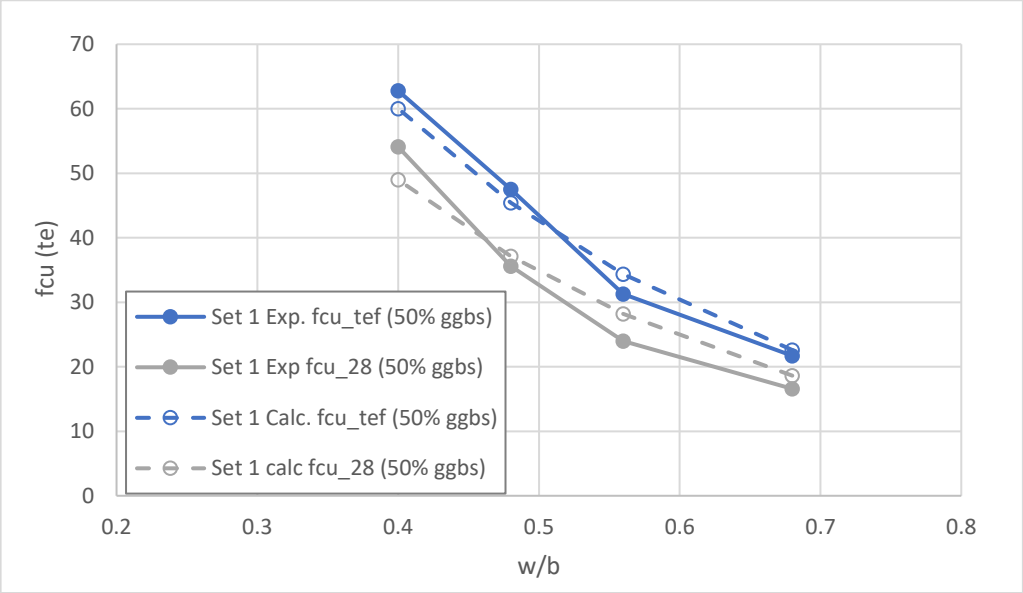

Figure 5.21 Compressive strength after applying χ_3=1.3 and χ_4=1.5 for mix set 1 for t_{ef}=300

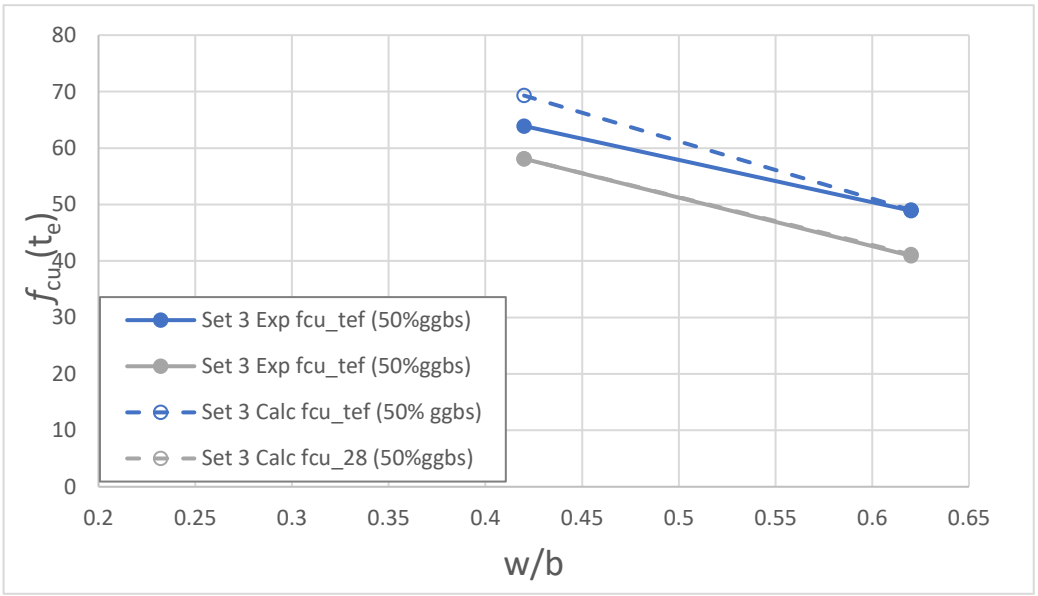

Figure 5.22 Compressive strength after applying χ_3=0.8 and χ_4=0.75 for mix set 3 for t_{ef}=150

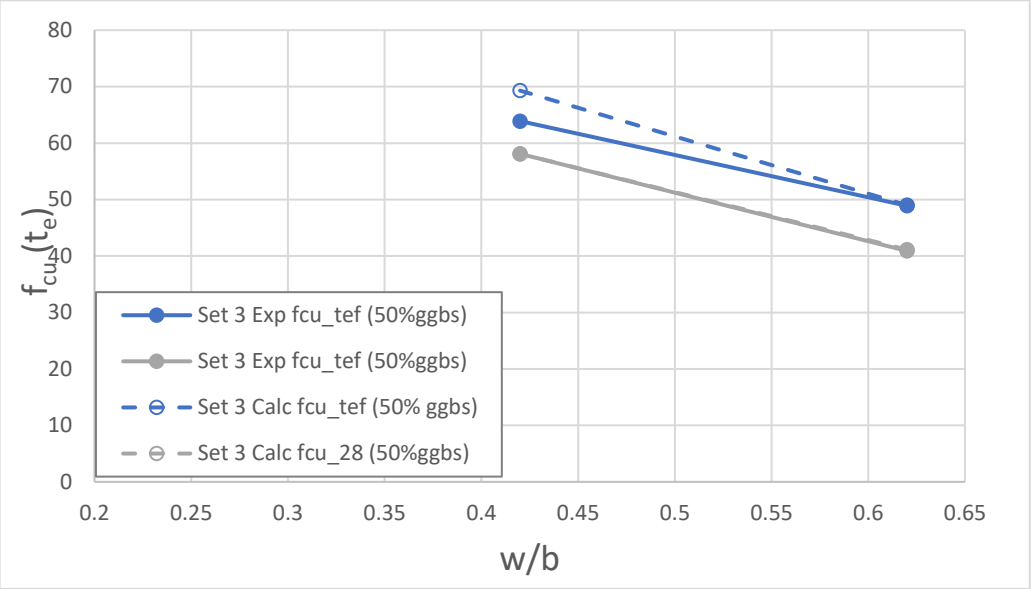

Figure 5.23 Compressive strength after applying χ_3=0.8 and χ_4=0.75 mix set 3 for t_{ef}=150

5.8 Post 28 day compressive strength gain factor (R)

Traditionally concrete mixes are designed for a 28 day strength, but as seen in the data presented in this chapter, the degree of hydration at 28 days varies greatly with the percentage of ggbs. This means that the strength gain after 28 days also varies with the ggbs level. To quantify this, a strength gain factor (R) is introduced, as follows;

$$\boldsymbol{R} = \frac{f_{cu\_ult} - f_{cu\_28}}{f_{cu\_28}} \qquad (5.\ 17)$$

Using the hydration model, R has been computed for a range of strengths and ggbs replacement levels. The results are given in Figure 5.24. These data illustrate that mixes with high ggbs replacement levels have high (post 28 day) strength gain potentials.

Also, the greater R, the greater the associated self-healing potential. This means that mixes could be designed on the basis of a 28 day strength and a strength gain potential

or, alternatively, designed based on an ultimate strength (f_{cu_ult}) with a check made to see if the strength at 28 days (or any other time) is adequate. This opens the door to a more flexible procedure for designing SCC mixes that is not so restrained by the 28 day strength. This new procedure is explained in Chapter 6.

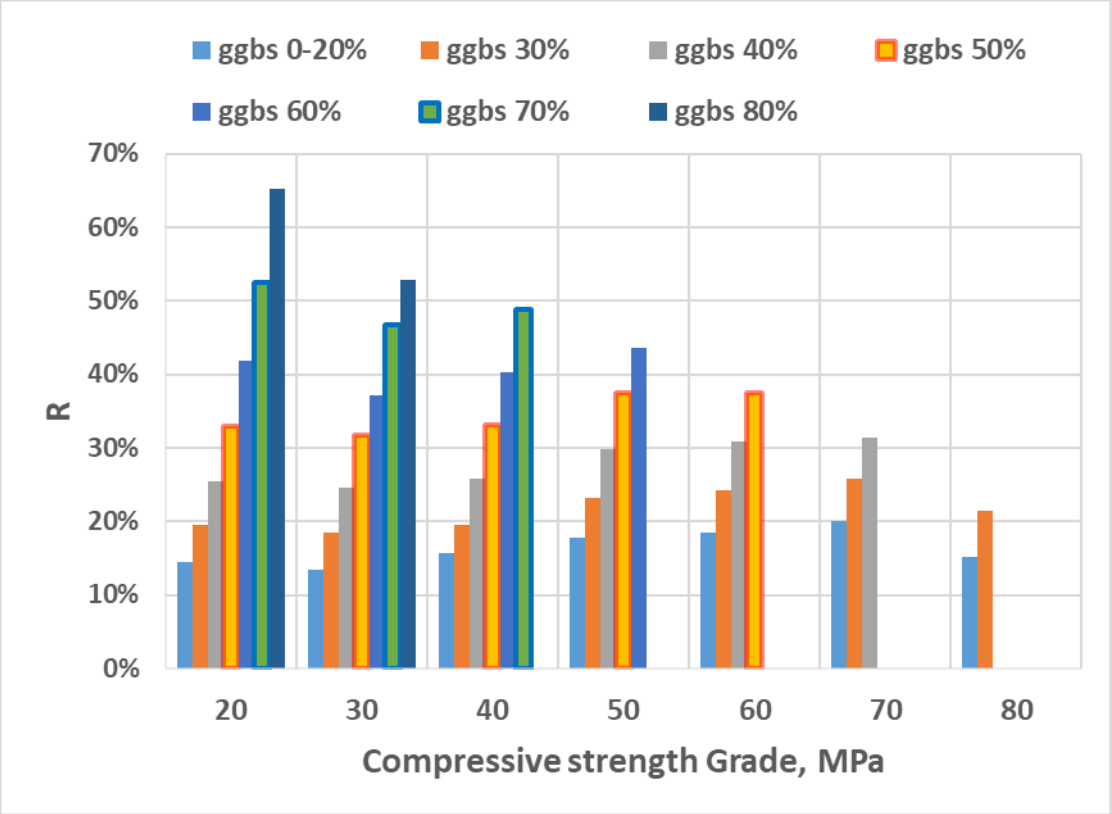

Figure 5.24 Compressive strength gain R for C30-80 concretes with a ggbs range of 20-80%

5.9 Quantifying the heat of hydration

As shown in equation (1), the degree of hydration may be defined in terms of the relative release of heat from the hydration process. To evaluate the quantity of heat released at a given time (t), a prediction of the total heat of hydration (H_T) is required. This can be calculated using Equation 5.18 (Schindler and Folliard, 2005).

$$H_{total} = H_{cem} \cdot p_{cem} + 461 . p_{slag} \quad \textbf{(5. 18)}$$

where;

p_{cem} = cement weight ratio in terms of total cementitious content,

p_{slag} = slag weight ratio in terms of total cementitious content,

$$\boldsymbol{H_{cem}} = 500p_{C_3S} + 260p_{C_2S} + 866p_{C_3A} + 420p_{C4AF} + 624p_{SO_3} + 1186p_{Free\ C_aO} + 850p_{M_gO}$$

Using equation 5.1, the data from Tables 5.1, 5.2 and 5.5 for a C30 target mix, the heat of hydration released at different times for mixes with only 50% ggbs Figure 5.25 and different ggbs percentages are shown in Figures 5.26 and 5.27. Values for the full strength range (30, 40, 50, 60, 70, and 80) are given in Appendix F.

The time dependent heat of hydration was estimated by calculating the degree of hydration from equation 5.1 and then multiplying it by the total heat of hydration from equation 5.18, as shown below in equation 5.19. The estimated heat is based on the semi-adiabatic test data of Schindler (2002).

$$\boldsymbol{H(t_e) = H_{total} \times \alpha(t_e)} \quad \textbf{(5.19)}$$

The calculation of the heat released is integrated into the mix design procedure described in Chapter 6.

The model adopted here is considered reasonable for the present work, because the focus of this work is not on the heat of hydration, but a refinement to the model, which is more accurate for cements with high ggbs replacement levels, has been given by Paine et al. 2005.

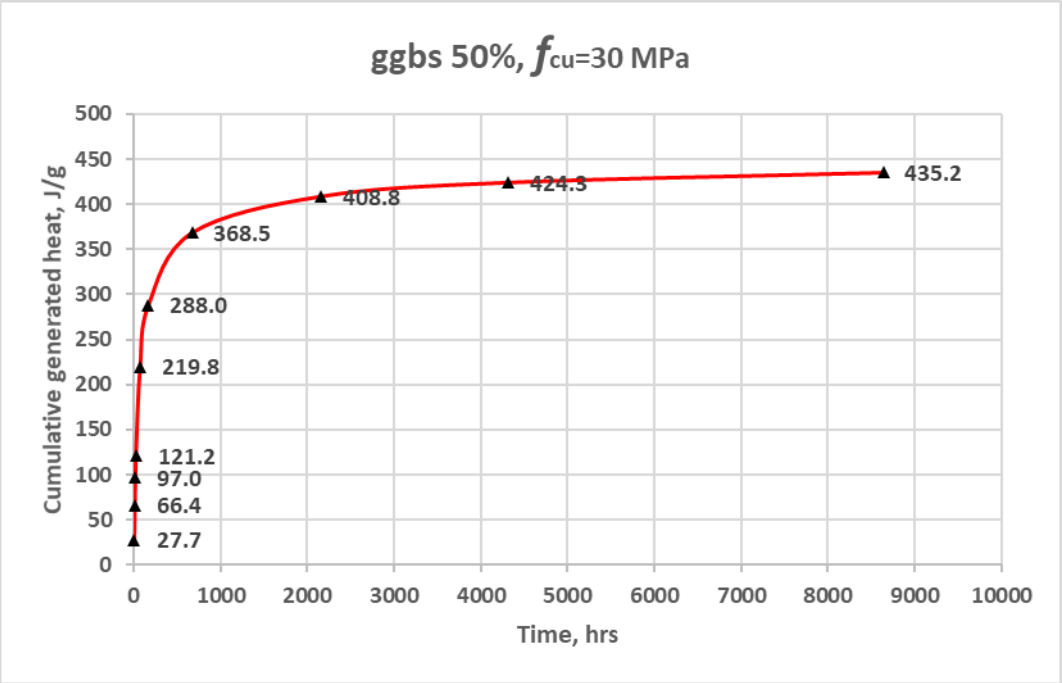

Figure 5.25 Predicted heat of hydration (semi-adiabatic) vs ggbs 50% at various times for C30

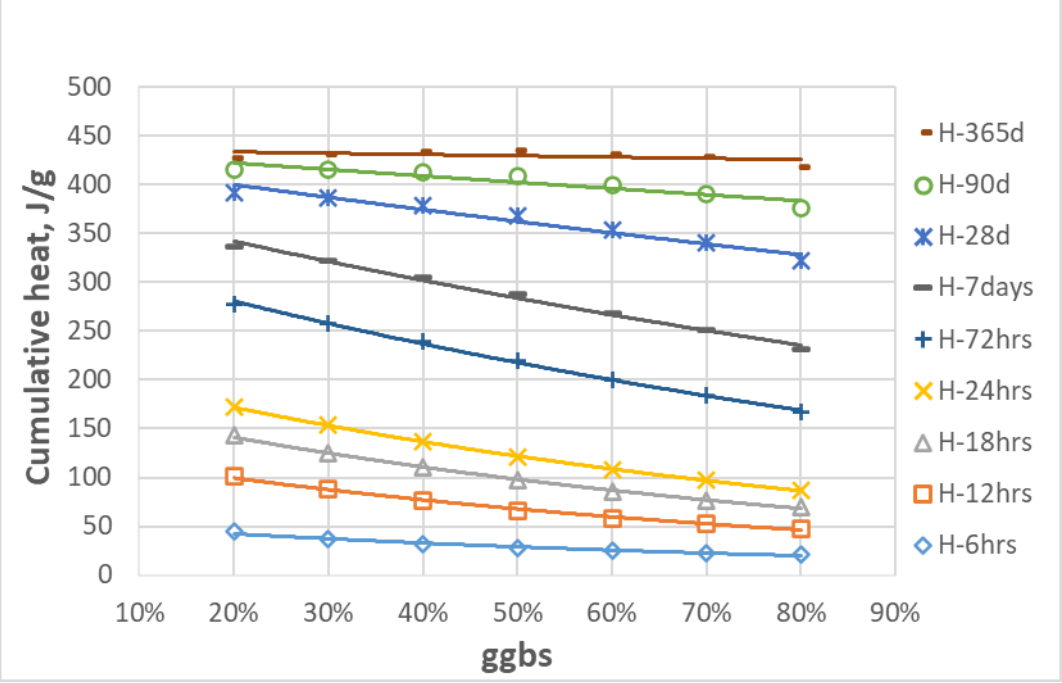

Figure 5.26 Predicted cumulative heat of hydration (semi-adiabatic) vs ggbs percent at various times for C30

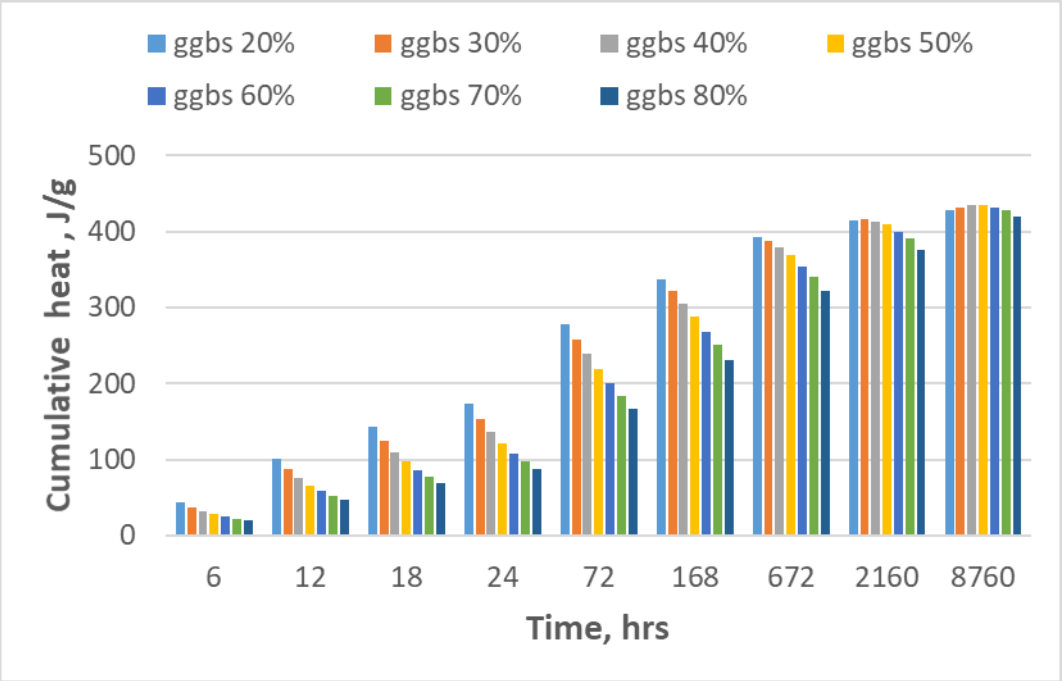

Figure 5.27 Predicted cumulative heat of hydration (semi-adiabatic) for various times for C30 MPa

5.10 Conclusions

New formulae for predicting the 28 day and ultimate compressive strengths of SCC concrete provide accurate estimates of these values.

The new experimental strength development data for SCC mixes with high ggbs cement replacement levels are useful for validating hydration and strength development models for SCC.

The extended hydration and strength development models of Schlinder and Folliard (2005) and De Schutter and Taerwe (1996)) provide an effective method for predicting the time dependent compressive strength of SCC mixes with high levels of ggbs cement replacement.

The difference between the 28 and ultimate compressive strengths of SCC concrete grows with the proportion of ggbs. This difference could be used as a measure of self-healing potential, which can be built into a new mix design procedure.

A prediction of the time-dependent heat of hydration is provided for the full range of SCC mixes considered in this programme of work. These calculations are integrated with the mix design procedure described in Chapter 6.

Chapter 6 Mix design procedure

6.1 Introduction

The required performance of self-compacting concrete (SCC) can be achieved by proportioning mixes that balance the competing requirements of flow and passing/filling ability with the resistance to segregation of the mix ingredients, and -at the same time- achieve the required hardened properties (Domone and Jin, 1999; Edamatsu et al., 1999; Hiromi Fujiwara, 1999; Khayat et al., 1999a; Okamura and Ouchi, 1999; Domone, 2000; Alami et al., 2016; Cepuritis et al., 2016; Ferraris et al., 2016). The early mix proportioning method proposed by Okamura et al.(Okamura and Ouchi, 1999; Domone, 2000; Okamura and Ouchi, 2003), and later developed by others (Ouchi et al., 1998), were all heuristic in nature, requiring many trial mixes. Later, investigations carried out on the rheological properties of SCC led to improvements in mix design procedures (Örjan Petersson, 1999; Saak et al., 2001b; Roussel, 2006; Chidiac and Mahmoodzadeh, 2009; Li and Kwan, 2011; Li and Kwan, 2013; Figueiras et al., 2014). These methods are also discussed in Shi et al. (2015).

The aforementioned work of the 1980s, 90s and early 2000s led to the development of The European Federation of National Trade Associations guidelines (EFNARC, 2005), which provide typical ranges for the primary mix ingredients (see Table 6.1) that depend on the desired strength and other performance attributes. The ENFARC approach, and the more recent methods discussed above, still require a considerable degree of trial and error testing.

A more rational mix design method for proportioning normal strength SCC mixes with up to 25% ggbs was presented in a recent study by Abo Dhaheer et al. (2016b) (See also Abo Dhaheer et al. ,2016a). Their study improved upon the method for proportioning the same grade of SCC mixes based on their plastic viscosity by Karihaloo and Ghanbari (2012) and Deeb and Karihaloo (2013). The improvement included the explicit imposition of the target cube compressive strength of the mix as a design requirement and the provision of practical guidelines on how to choose the most appropriate mix proportions.

Table 6.1 Typical range of SCC mix compositions according to (EFNARC, 2005)

Constituent	Typical range by mass **(kg/m^3)**	Typical range by volume **(l/m^3)**
Powder (cementitious materials + filler)	380 – 600	
water	150 – 210	150 – 210
Coarse aggregate	750 – 1000	270 – 360
Fine aggregate	Typically 48 – 55% of total aggregate mass.	
Water to powder ratio by Vol	0.85 – 1.10	

In this study, the rational mix design method proposed in Abo Dhaheer et al. (2016a,b) is extended to mixes in which up to 80% of cement is replaced by ggbs. The extension is by no means trivial because the higher level of ggbs affects both the the plastic properties of the mix (viscosity, yield stress and stability) and the target characteristic cube strength. A qualitative illustration of the interaction between w/b and the required plastic and hardened properties of SCC mixes containing at least 30% ggbs is given in Figure 6.1 (Park et al., 2005).

A particular challenge of designing mixes with high levels of ggbs is that the lower limit of plastic viscosity that can be achieved is highly sensitive to the level of this cement replacement material. As in Abo Dhaheer et al. (2016b), design charts are provided for choosing the mix proportions that reach the target plastic viscosity in the range 1 or 2 to 14 Pa s, and the target cube compressive strength in the range of 30–80 MPa. The lower limit of target plastic viscosity depends on the replacement level, i.e. 1 Pa s for ggbs levels in the range 60% to 80%, and 2 Pa s in the range 30% to 50%. The viscosity is achieved by adjusting the superplasticiser dose (typically 0.2 to 1.2% of the mass of binder).

In addition, the ultimate strength and remaining hydration potential at 28 days have been introduced into the new mix design procedure.

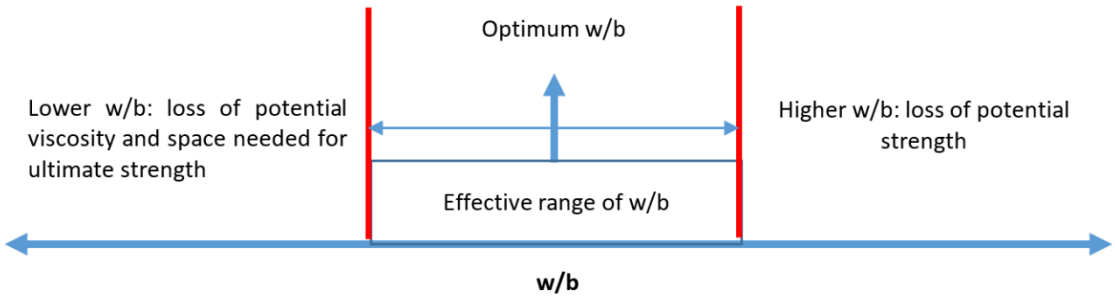

Figure 6.1 Qualitative effects of varying w/b for SCC containing ggbs >30%

6.2 Design criteria and parameters

The criteria and parameters used in the mix design process, and in the subsequent validation, are set out in the Table 6.2 and Figure 6.2. In Figure 6.2, x-time refers the age of the concrete for which the compressive strength is designed.

Table 6.2 Limitation of design criteria

Parameters/Criteria	Limits	Commentary
Viscosity class	Class 1 t_{500} ≤ 2 Sec.	VS1 has good filling-ability even with congested reinforcement.
	Class 2 t_{500} > 2 Sec.	VS2 has no upper-class limit but with increasing flow time it is more likely to exhibit thixotropic effects, which may be helpful in limiting the formwork pressure or improving segregation resistance.
Yield stress	Measuring t_{stop}	the longer t_{stop} the higher ggbs level
Spreading diameter	700±50 mm	For assessment of material after spreading must visually show no segregation in this limit to pass the test.
Heat of hydration	Between 87 and 173 J/g for ggbs 0.8 to ggbs 0.2 at 24hrs period	Determined by type of application.
Ultimate compressive strength	37 to 97 MPa	Depending on time when application structure unloaded.
Compressive strength at 28 days	30 to 80 MPa	
Varied time compressive strength	56, 90, 180, 270, and 365 days	Depending on the desirable time
Compressive strength gain (R)	10-15 % for 20% ggbs and 40-60 % for ggbs 80%	See Figure 5.24

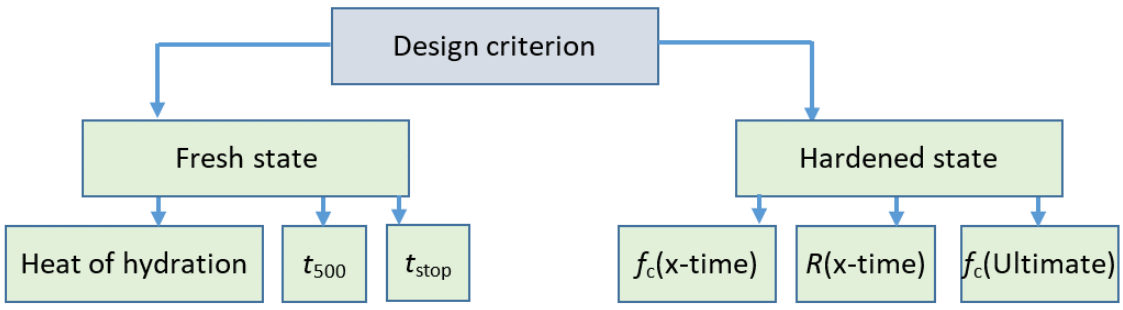

Figure 6.2 SCC mix design criteria

6.2.1 Plastic viscosity

As explained in chapter 4, the plastic viscosity of the mix is computed using the following equation;

$$\boldsymbol{\eta_{mix} = \eta_{paste} \times (1 - \frac{\phi_{Filler}}{\phi_{m\_Filler}})^{-1.9} \times (1 - \frac{\phi_{Fine\ Agg}}{\phi_{m\_FineAgg}})^{-1.9} \times (1 - \frac{\phi_{Coarse\ Agg}}{\phi_{m\_CoarseAgg}})^{-1.9}} \quad \textbf{(6. 1)}$$

where ϕ_{m_Filler}= 0.74, $\phi_{m\_FineAgg}$= 0.63, and $\phi_{m\_CoarseAgg}$= 0.524

It is known (Nehdi and Rahman, 2004; Dinakar et al., 2013; Abo Dhaheer et al., 2016b) that the replacement of 25% cement (*c*) by ggbs has little or no effect on the paste viscosity (η_{paste}). However, this is not the case when up to 80% of cement is replaced by ggbs, as shown by a number of investigators (Wang et al., 2002; Park et al., 2005; Hwang et al., 2009; Grzeszczyk and Janowska-Renkas, 2012; Tiwari et al., 2015). The strong dependency of the plastic viscosity on the proportion of ggbs (once the percentage exceeds 25%) is shown Figure (4.6, page 88) which is a representation of the data presented in chapter 4 (Table 4.4)

6.3 Superplasticizer

The superplasticizer dose required to produce an effective SCC needs to be carefully chosen to achieve a target plastic viscosity (for the mix) in the range 1-14 Pa s, with the actual target value depending on the concrete grade and cement type (see Table 6.3, and Figures 6.3 and 6.4). The manufacturer of the SP used in this study (MasterGlenium) recommends that the effective dosage is between 0.2–1.2 kg per 100 kg of mass binder. This range (also expressed as 0.2-1.2%) by mass of binder was used in this study.

From a series of trial mixes, and from data from the literature (see Chapter 4), it was found that the SP dose required to maintain the required plastic viscosity increases with the percentage of ggbs. This is reflected in the data presented in Table 6.3 that were

obtained from the experimental work described in chapter 7. Figures 6.3 and 6.4 provide a visual representation of the Table 6.3 data for mixes with 30% and 50% ggbs.

Table 6.3 Superplasticizer range dosage

ggbs	f_{cu} (MPa)	w/b	η_{mix} (Pa s)	(SP/b)%
0-25%	30	0.74	3--15	0.2-0.6
	40	0.63	4--15	0.2-0.6
	50	0.54	5--15	0.3-0.8
	60	0.47	6--15	0.4-1.0
	70	0.41	7--15	0.8 -1.2
	80	0.35	8--15	1.0-1.2
30%	30	0.72	2--10	0.2-0.6
	40	0.60	2--10	0.2-0.6
	50	0.52	3--12	0.4-1.0
	60	0.45	4--12	0.4-1.0
	70	0.40	8--14	0.8 -1.2
	80	0.36	9--14	1.0-1.2
40%	30	0.70	2--12	0.3-0.6
	40	0.58	2--12	0.4-1.0
	50	0.50	4--12	0.6-1.0
	60	0.43	6--13	0.8 -1.2
	70	0.38	7--13	1.0-1.2
50%	30	0.68	2--8	0.6-1.0
	40	0.56	2--8	0.6-1.0
	50	0.48	4--10	0.8 -1.2
	60	0.40	7--11	1.0-1.2
60%	30	0.64	1--6	0.6-1.0
	40	0.53	1--7	0.8 -1.2
	50	0.44	2--8	1.0-1.2
70%	30	0.6	1--6	0.8 -1.2
	40	0.48	1--6	1.0-1.2
80%	30	0.55	1--4	1.0-1.2

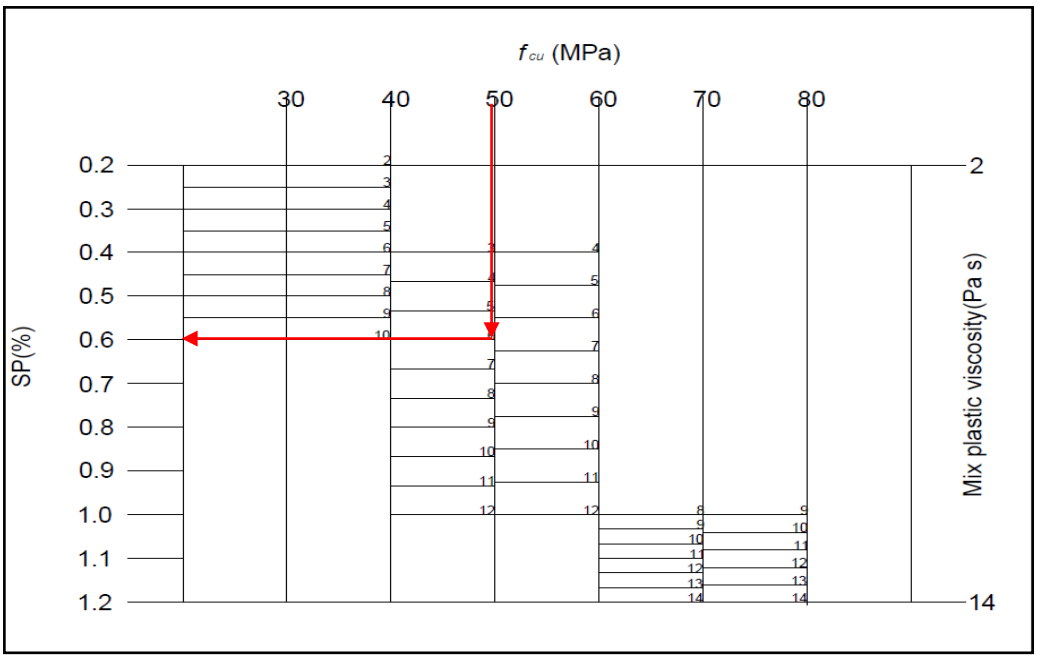

Figure 6.3 Super-Plasticiser (SP) dose as f_c and η_{mix} for ggbs 30%

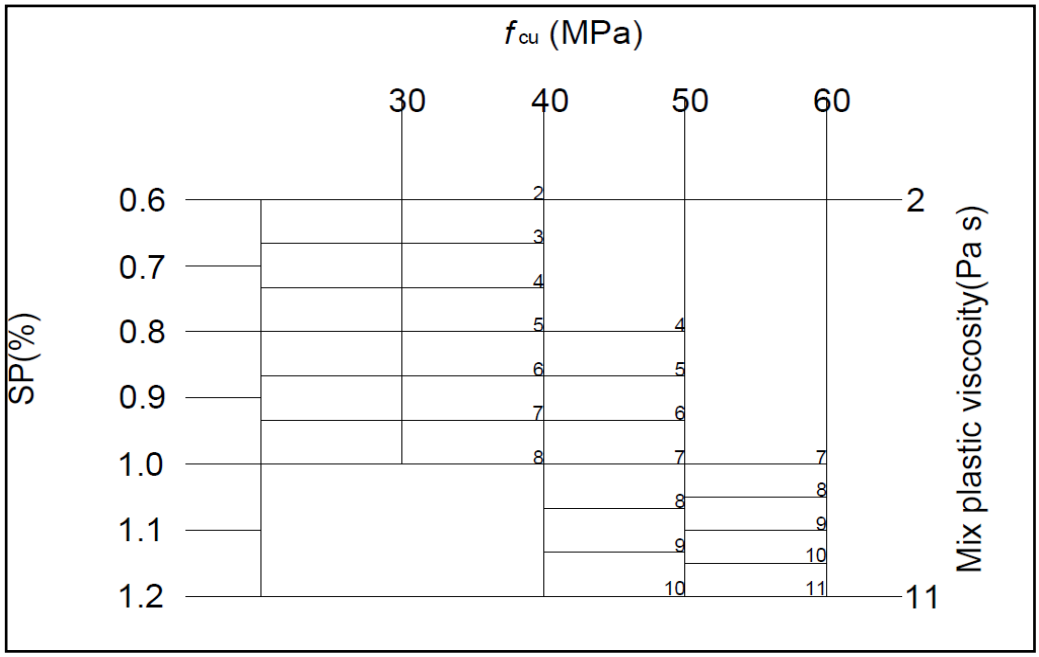

Figure 6.4 Super-Plasticiser (SP) dose as f_c and η_{mix} for ggbs 50%

6.4 Compressive strength

The compressive strength of a concrete mix is primarily determined by the ratio of water to binder (*w/b*) under given curing conditions. Formulae for predicting the 28-day cube strength (f_{cu}) and the strength at the ultimate degree of hydration (f_{cu_ult}) were presented in chapter 5. For convenience these are reproduced below.

$$f_{cu} = \chi_1.(2 - ggbs\%) \cdot 10^{(2-\chi_2 .\frac{w}{b})} \quad \textbf{(6. 2)}$$

$$f_{cu\_ult} = \chi_3.(2 - 0.2ggbs\%) \cdot 10.4^{(2-\chi_4\frac{w}{b})} \quad \textbf{(6. 3)}$$

Figures (5.8, p108) and (5.12, p114), which represent equations 6.2 and 6.3 respectively, will be used in the mix design procedure described in section 6.5 to determine the w/b ratio for a selected target compressive strength.

In chapter 5, R was defined as the post 28 day compressive strength gain factor (see equation 5.18). This is represented for the range of SCC mixes considered in this programme of work in Figure (5.24, p128). The fact that R varies considerably with the percentage of ggbs in the mix creates the possibility of designing mixes for multiple strength criteria, rather than the traditional approach of focussing on the 28 day strength. This could have considerable economic and environmental benefits.

To explore these issues, the required concrete strength at different ages after casting is considered. Most concrete structures (e.g. bridges and buildings) are not subject to their full design loads until many months after the concrete is first cast. Also, various parts of a structure (e.g. foundations, superstructure) are cast at different times and are subject to different percentages of their full design loads at a given point in time. This could mean, for example, that a concrete that achieves a strength of 30MPa at 28 days would be adequate to accommodate the construction loads at that age but a strength of 50MPa would be required at (say) 200 days to support the full design load. The traditional approach would use a material with a characteristic strength of 50MPa at 28 days,

irrespective of its strength gain potential after this time. This issue is also important because a 30MPa / 80% ggbs concrete would have far less embodied energy than a standard concrete that had a strength of 50MPa at 28 days.

Designing in this way would require more effort but the potential savings are considerable. In a period when there is a need to save energy and reduce CO2 emissions from concrete production, the additional design effort is worthwhile. The proposed new design procedure allows for this type of multiple strength criteria design.

6.5 Heat of hydration

The heat generated due to the chemical hydration reaction between the water and the binder (cement +ggbs) is an important consideration in the mix design process. The total amount of heat released and the rate at which the heat is released can be particularly important in large concrete pours, in which the differential temperature distributions can lead to the formation of early age cracks (Bamforth, 2007). Standard design guides would not cover the type of specialist SCC mix considered in this PhD research programme and therefore the heat of hydration at different times has been evaluated for these mixes using the method described in Chapter 5. This is illustrated for a set of C30 mixes in Figure (5.26, p130). The figures for other concrete grades are given in Appendix F.

6.6 Basic steps of the proposed mix design method

The basic steps of the mix design method are summarised below, and Figure 6.5

1) Select the mix design criteria from Table 6.2

2) Either:

(i) Calculate the w/b ratio (noting the binder includes cement and ggbs) for a target 28 day strength from equation 6.2 (or use Figure 6.6) and, if required, check that strength development factor (R) meets the required value.

Or

(ii) Calculate the w/b ratio that produces the cube characteristic strength at the required age (t_{age}) from Eq. 6.3 (or uses Figure 6.7) depending on the ggbs replacement level, and check that the required strengths at other ages are satisfied.

3) Calculate the plastic viscosity of the paste from Figure 4.6 depending on the ggbs fraction for w/b determined in step 2.

4) Choose the water content in the range of 150–210 kg/m^3, following EFNARC and calculate the mass of the binder (b) in kg/m^3. Then, calculate the mass of cement (kg/m^3) depending on the ggbs replacement level.

It is important to highlight that Eqs. 6.2 and 6.3 are more applicable for cement type I or type II/B-V 32.5 R, or type II/A-L 32.5 R. In the latter type of blended cement, it is known that the addition of fly ash in this blended cement does not affect plastic viscosity of paste (Manawadu et al., 2015).

5) Select the super-plasticizer (SP) dosage from Table 6.3 as a percent of the binder mass (or equivalently use Figure 6.3 for 30% ggbs or Figure 6.4 for 50% ggbs)

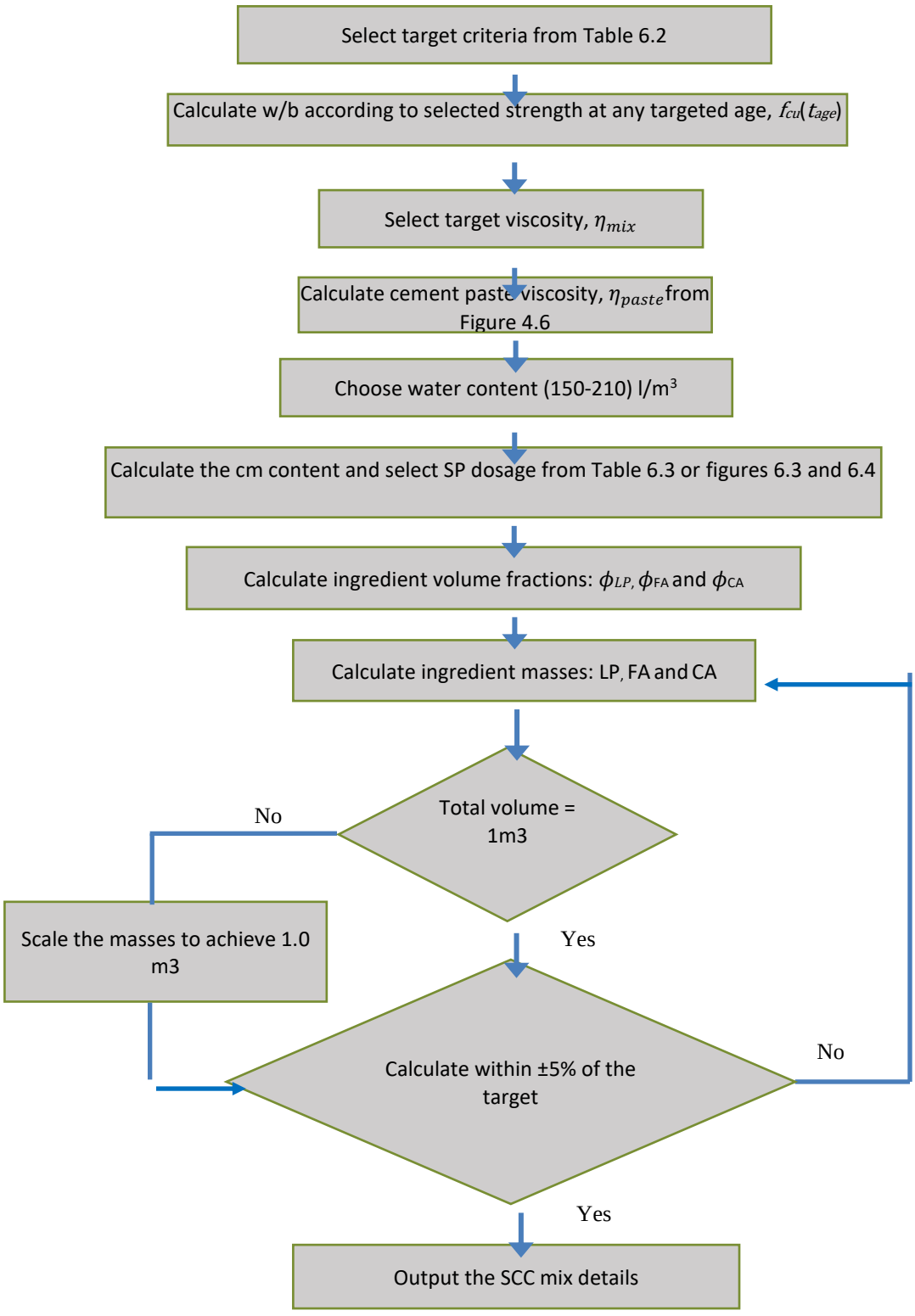

Figure 6.5 Flow chart of the mix design procedure

6.7 Design charts for mix proportioning of normal and high strength SCC mixes

In this section design charts for proportioning SCC mixes are presented, with one set for each of ggbs replacement level and compressive strength considered. The characteristic cube compressive strength of the mixes at 28 days can range from 30 to 80 MPa, and at the ultimate degree of hydration from 37 to 97 MPa. The target plastic viscosity of the mix can range from 1 to 14 Pa s. The lower limit of target plastic viscosity of the mix depends on the replacement level, with 1 Pa s for the replacement level range 60% to 80% and 2 Pa s in the range 30% to 50%. The procedure used to build these charts was reported in Abo Dhaheer et al. (2016a). This was achieved using a Matlab code written by the author. This considered the limits shown in Table 6.1, and used w/b and the plastic viscosity as the main variables.

Selected charts are shown in Figures 6.6 and 6.7, while the full set can be seen in Appendix G. In all these figures, the term *cm* refers to binder or cementitious material, *LP* to limestone powder filler (particle size ≤ 125 μm), *FA* to fine aggregate (particle size in the range from 125 μm to 2 mm), and *CA* to coarse aggregate (particle size range from 2 to 20 mm). The viscosity of the mix (η) in the denominator of the line labels in Figures 6.6 and 6.7 is the target plastic viscosity of the mix (η_{mix}) and the denominator applies to all of the terms i.e. CM+LP+FA+CA/η means (CM+LP+FA+CA)/ $\eta_{mix.}$

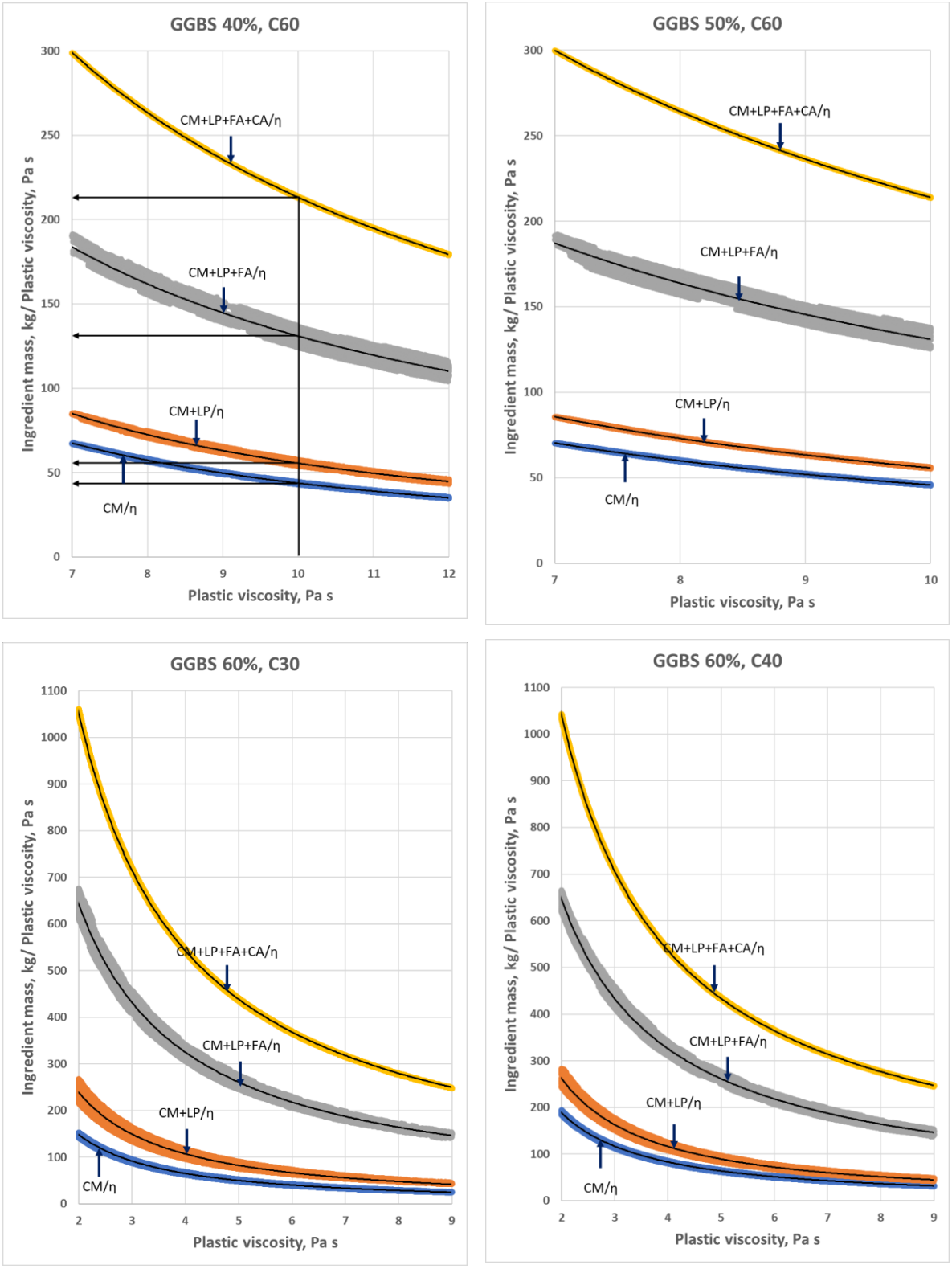

Figure 6.6 Ingredient mass (kg) normalised by mix plastic viscosity vs. plastic viscosity of the mix

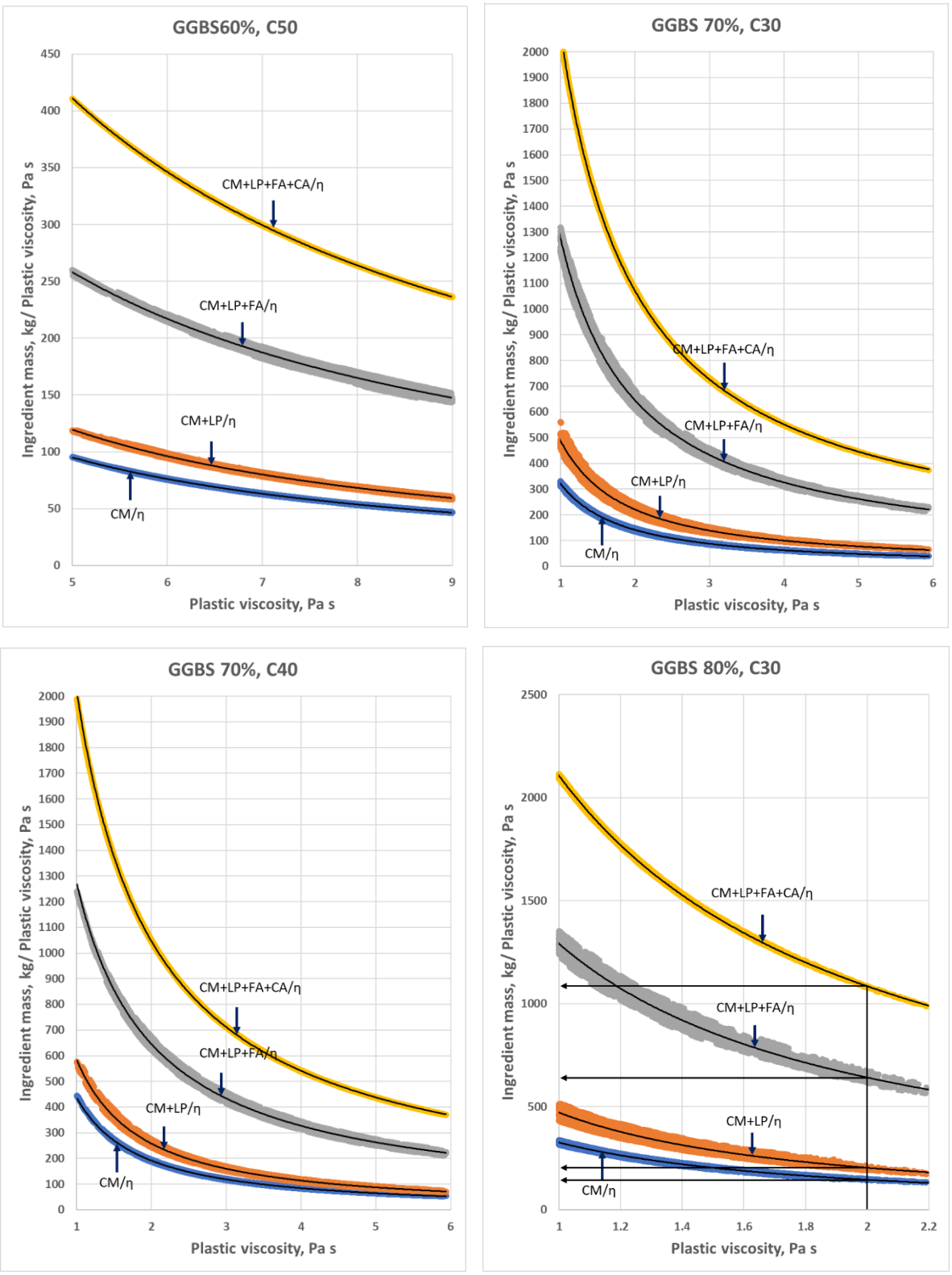

Figure 6.7 Ingredient mass (kg) normalised by mix plastic viscosity vs. plastic viscosity of the mix

6.8 Examples of the use of design charts

The process of using the design charts for proportioning SCC mixes will be demonstrated using two examples.

6.8.1 Example 1

As the first example, suppose that an SCC mix with the target ultimate compressive strength of 70 MPa and a 28 day minimum strength of 60 MPa is needed for a non-pumping large pour application. As it is a non-pumping application, the SCC can have a reasonably high plastic viscosity of the mix, say 10 Pa s. However, as it is a large pour there is need to suppress the heat of hydration by replacing, say 40% of the cement with ggbs. The specified limits for the allowable heat generated ($H(t)$) at times (6,12,18 and 24 Hrs) are (60, 140, 200, and 280 J/g) respectively. For this example, the design charts in Figure 6.6 are used.

- **Part I**/ Check general parameters

(1) For the desired target ultimate strength of 75 MPa, a 28 day strength of 60MPa and ggbs replacement level of 0.4 (40%), the *w/b*=0.43 for f_{cu}=60MPa is obtained from Figure 5.8.

(2) The binder content by mass (b) is read off the bottom curve in Figure 6.11 corresponding to η_{mix} = 10 Pa s. This gives $\frac{cm}{\eta} = 44$, whence cm= 10×44 = 440 kg/m^3

(3) Thus, the mass of cement is c= 0.6 × 440 = 264 kg/m^3, and that of ggbs = 0.4 × 440 =176 kg/m^3. Finally, from step (1), the mass of water is w = 0.43× 440 = 189.2 kg/m^3.

(4) select a trial super-plasticizer (SP) dosage from Table 6.3 as a percentage of the mass of binder to be 0.6 % or 2.64 kg/m^3;

(5) Calculate the plastic viscosity of the paste from Figure 4.6 corresponding to w/b = 0.43. It works out to be = 0.211 Pa s;

(6) The masses of the three solid phases (LP, FA and CA) can now be read off the design charts corresponding to η_{mix} = 10 Pa s, in Figure 6.6 beginning with the second curve from bottom. This gives $\frac{cm+LP}{10} = 55$, whence (cm+LP) = 10×55 = 550, so that LP = 550 – 440 = 110 kg/m^3.

(7) Next, from the third curve from bottom, $\frac{cm+LP+FA}{10} = 125$, whence (cm+LP+FA) = 1250, so that FA = 1250 – 550 = 700 kg/m^3.

(8) Finally, from the top curve, $\frac{cm+LP+FA+CA}{10} = 212$, whence (cm+LP+FA+CA) = 2120, so that CA = 2120 – 1250 = 870 kg/m^3;

(9) The total volume of the mix using the above mix component masses and densities is

$$\text{Vol} = \frac{c}{\rho c} + \frac{ggbs}{\rho ggbs} + \frac{W}{\rho w} + \frac{SP}{\rho sp} + \frac{LP}{\rho lp} + \frac{FA}{\rho fa} + \frac{CA}{\rho ca} + 0.02 \text{ (air bubbles)}$$

$$= \frac{264}{2950} + \frac{176}{2400} + \frac{189.2}{1000} + \frac{2.64}{1070} + \frac{110}{2400} + \frac{700}{2650} + \frac{870}{2800} + 0.02 \quad = 0.995 \text{ m}^3$$

$$= \frac{265.3}{2950} + \frac{176.9}{2400} + \frac{190.2}{1000} + \frac{2.7}{1070} + \frac{110.6}{2400} + \frac{703.5}{2650} + \frac{874.4}{2800} + 0.02 \quad = 1.000 \text{ m}^3$$

(10) The plastic viscosity of the mix so proportioned is calculated using Eq. 6.1

$$\eta_{mix} = 0.211 \times \left(1 - \frac{0.109}{0.74}\right)^{-1.9} \times \left(1 - \frac{0.386}{0.63}\right)^{-1.9} \times \left(1 - \frac{0.312}{0.524}\right)^{-1.9} = 9.69 \text{ Pa s}$$

$$Error = \frac{(Calculated\ \eta_{mix} - Target\ \eta_{mix})}{Target\ \eta_{mix}} \times 100$$

$$Error = \frac{9.69 - 10}{10} \times 100 = -3.14\%$$

If it is assumed that the acceptable error in the target plastic viscosity of the mix is ±5%, then the mix proportioning of the first example SCC mix is complete.

- **Part II**/ Check heat of hydration

From Figure F4 (Appendix F) the heat generated at (6,12,18 and 24 Hrs) are (30, 70, 100, and 120 J/g) respectively, which is below the mix recommended limits.

From the design results, all preferable parameters have been achieved.

6.8.2 Example 2

As the second example, suppose that an SCC mix with 28 days target compressive strength of 30 MPa is needed for a pumped large pour application. As it is a pumped application, the SCC must have a reasonably low plastic viscosity of the mix, say 2.0 Pa s. However, as it is a large pour there is need to suppress the heat of hydration by replacing, say 80% of cement by ggbs and the recommended heat of hydration at 3 days should not exceed 270 J/g. Furthermore, a post 28-days strength potential is evaluated.

For this example, the design charts in Figure 6.7 are used.

Part I/ Check general parameters

1. For the desired target strength of 30 MPa and ggbs replacement level of 0.8 the *w/b*= 0.57 is obtained from Figure 5.8 (approximately).

2. The binder content by mass (*cm*) is read off the bottom curve in Figure 6.7 corresponding to η_{mix} = 2.0 Pa s. This gives $\frac{cm}{\eta} = 151$, whence *cm*= 2.0×150 = 300 kg/m^3.

3. Thus, the mass of cement is *c*= 0.2 × 300 = 60 kg/m^3, and that of ggbs is ggbs = 0.8 × 300 = 240 kg/m^3. Finally, from step (1), the mass of water is *w* = 0.57 × 300 = 171 kg/m^3.

4. Select a trial super-plasticizer dosage (SP) dosage from Table 6.4 as a percentage of the mass of binder to be 1.1 % or 3.3 kg/m^3.

5. Calculate the plastic viscosity of the paste from Figure 4.6 corresponding to *w/b* = 0.57. It works out to be = 0.0145 Pa s.

6. The masses of the three solid phases (LP, FA and CA) can now be read off the design charts corresponding to η_{mix} = 2.0 Pa s, in Figure 6.7, beginning with the second curve from bottom. This gives $\frac{\boldsymbol{cm+LP}}{\mathbf{2.0}} = \mathbf{191}$, whence (cm+LP) = 2.0×191 = 382, so that LP = 382 – 300 = 82 kg/m^3.

7. Next, from the third curve from bottom, $\frac{\boldsymbol{cm+LP+FA}}{\mathbf{2.0}} = \mathbf{635}$,whence (cm+LP+FA) = 1270, so that FA = 1270 – 382 = 888 kg/m^3.

8. Finally, from the top curve, $\frac{\boldsymbol{cm+LP+FA+CA}}{\mathbf{2.0}} = \mathbf{1075}$, whence (cm+LP+FA+CA) = 2150, so that CA = 2150– 1270 = 880 kg/m^3.

9. The total volume of the mix using the above mix component masses and densities is

$$\text{Vol} = \frac{c}{\rho c} + \frac{ggbs}{\rho ggbs} + \frac{W}{\rho w} + \frac{SP}{\rho sp} + \frac{LP}{\rho lp} + \frac{FA}{\rho fa} + \frac{CA}{\rho ca} + 0.02 \text{ (air-bubbles)}$$

$$= \frac{60}{2950} + \frac{240}{2400} + \frac{171}{1000} + \frac{3.3}{1070} + \frac{82}{2400} + \frac{888}{2650} + \frac{880}{2800} + 0.02 \quad = 0.998 \text{ m}^3.$$

$$= \frac{60.1}{2950} + \frac{240.5}{2400} + \frac{171.3}{1000} + \frac{3.3}{1070} + \frac{82.2}{2400} + \frac{888.9}{2650} + \frac{881.8}{2800} + 0.02 \quad = 1.000 \text{ m}^3.$$

10. The plastic viscosity of the mix so proportioned is calculated using Eq. 6.1.

$$\eta_{mix} = 0.0145 \times \left(1 - \frac{0.098}{0.74}\right)^{-1.9} \times \left(1 - \frac{0.490}{0.63}\right)^{-1.9} \times \left(1 - \frac{0.315}{0.524}\right)^{-1.9} = 1.9 \text{ Pa s}$$

$$Error = \frac{(Calculated\ \eta_{mix} - Target\ \eta_{mix})}{Target\ \eta_{mix}} \times 100$$

$$Error = \frac{1.9-2}{2} \times 100 = -4.97\ \%$$

The error is within the acceptable limits ±5%, so the proportioning of the example SCC mix is complete.

- **Part II** /Checking the heat generated and R value

From the Figure F1 Appendix F it can be obtained the recommended values of heat generated at (72 Hrs) is 170 J/g.

Finding (R) value as below

$$\boldsymbol{R} = \frac{f_{cu\_ult} - f_{cu}(28)}{f_{cu}(28)} * 100$$

$= \frac{45-30}{30} * 100 = 50\%$

The mix design outputs for the example are satisfied the input parameters.

6.8.3 Example 3

As the third example, suppose that an SCC mix with an ultimate 200 day target compressive strength of 45 MPa and minimum strength at 28 days of 40 MPa is needed for multistorey building with floors that will not be loaded until 8 months. As it is a pumped application, the SCC must have a reasonably low plastic viscosity of the mix, say 2.0 Pa s , replacement ggbs level say 60%.

For this example, the design charts in Figure 6.6 are used.

Part I/ Check general parameters

1. For the desired 200 day target strength of 45 MPa and ggbs replacement level 0.6, *w/b*= 0.53 (Figure 5.8) and 28-day strength of 40 MPa.

2. The binder content by mass (*cm*) is read off the bottom curve in Figure 6.6 corresponding to η_{mix} = 2.0 Pa s. This gives $\frac{cm}{\eta} = 190$, whence *cm*= 2.0×190 = <u>380</u> kg/m^3.

3. Thus, the mass of cement is c= 0.4 × 380 = 152 kg/m^3, and that of ggbs is ggbs = 0.6 × 380 = 228 kg/m^3. Finally, from step (1), the mass of water is w = 0.53 × 380 = 201.4 kg/m^3.

4. Select a trial super-plasticizer dosage (SP) dosage from Table 6.4 as a percentage of the mass of binder to be 0.9 % or 3.42 kg/m^3.

5. Calculate the plastic viscosity of the paste from Figure 4.6 corresponding to w/b = 0.53. It works out to be = 0.047 Pa s.

6. The masses of the three solid phases (LP, FA and CA) can now be read off the design charts corresponding to η_{mix} = 2.0 Pa s, in Figure 6.6, beginning with the second curve from bottom. This gives $\frac{cm+LP}{2.0} = \mathbf{275}$, whence (cm+LP) = 2.0×275 = 550, so that LP = 550 – 380 = 170 kg/m^3.

7. Next, from the third curve from bottom, $\frac{cm+LP+FA}{2.0} = \mathbf{645}$,whence (cm+LP+FA) = 1300, so that FA = 1290 – 550 = 740 kg/m^3.

8. Finally, from the top curve, $\frac{cm+LP+FA+CA}{2.0} = \mathbf{1045}$, whence (cm+LP+FA+CA) = 2150, so that CA = 2090– 1290 = 800 kg/m^3.

9. The total volume of the mix using the above mix component masses and densities is

$$\text{Vol} = \frac{c}{\rho c} + \frac{ggbs}{\rho ggbs} + \frac{W}{\rho w} + \frac{SP}{\rho sp} + \frac{LP}{\rho lp} + \frac{FA}{\rho fa} + \frac{CA}{\rho ca} + 0.02 \text{ (air-bubbles)}$$

$$= \frac{152}{2950} + \frac{228}{2400} + \frac{201.4}{1000} + \frac{3.42}{1070} + \frac{170}{2400} + \frac{740}{2650} + \frac{800}{2800} + 0.02 \quad = 1.007 \text{ m}^3.$$

$$= \frac{150.9}{2950} + \frac{226.4}{2400} + \frac{200}{1000} + \frac{3.4}{1070} + \frac{168.8}{2400} + \frac{734.8}{2650} + \frac{749.4}{2800} + 0.02 \quad = 1.000 \text{ m}^3.$$

10. The plastic viscosity of the mix so proportioned is calculated using Eq. 6.1.

$$\eta_{mix} = 0.047 \times \left(1 - \frac{0.16}{0.74}\right)^{-1.9} \times \left(1 - \frac{0.387}{0.63}\right)^{-1.9} \times \left(1 - \frac{0.284}{0.524}\right)^{-1.9} = 2.01 \text{ Pa s}$$

$$Error = \frac{(Calculated\ \eta_{mix} - Target\ \eta_{mix})}{Target\ \eta_{mix}} \times 100$$

$$Error = \frac{2.01 - 2.0}{2.0} \times 100 = 0.52\%$$

The error is within the acceptable limit of ±5%, so the proportioning of the example SCC mix is complete.

The estimated compressive strength for this example can be shown in Table 6.4 below, see estimation of the compressive strength in chapter 5.

Table 6.4 Calculation of estimated compressive strength at 200 days

ggbs	α_u	τ	β	t_e*(day)*	t_e*(hours)*	$\alpha(t_e)$	f_{cu} -28 MPa	f_{cu}-200 MPa
0.6	0.93	63.41	0.39	200	4800	0.778	40.0	46.7

6.9 Discussion and conclusions

An effective mix proportioning method has been developed for designing SCC with a mid to high range of ggbs (30-80) based on the rheological characteristics represented by plastic viscosity of the mix and the target compressive strength. Guidelines have been provided by way of design charts for choosing the mix proportions. Several examples have been given to demonstrate the simplicity of the use of mix design charts. The effect of choosing the mix proportions on, above, and below the best-fit lines in the design charts on the plastic viscosity of the mix has been revealed.

The design procedure also allows mixes to be designed for multiple hardened strength criteria. This could result in significant energy savings and reductions in CO2 emissions from concrete production.

Chapter 7 Experimental validation of the mix design procedure

7.1 Introduction

The mix design procedure was described in the previous chapter, including several examples on the use of the design charts. In this chapter, an experimental validation of the procedure is provided that assesses whether the mixes designed with various ggbs levels meet the criteria required of SCC mixes. Details of the mix materials (water, cement, coarse and fine aggregates, additives and cement replacement material ggbs), and mixing procedure were given in chapter 3.

The mixes used for the validation experiments are given in Tables 7.1 and 7.2. These cover a strength range from 30 to 80 MPa and ggbs levels from 40 to 80%. As may be seen from the Table, the mixes are divided into two sets (2 and 3) with set 2 having a different cement type from set 3 (see chapter 3). The reason for the change in cement type related to the first cement being unavailable in the second half of 2020.

Table 7.1 Mix proportions of test SCC mixes, kg/m³

Mix ref.	Binder		b	w	w/b	SP	SP/b (%)	LP[a]	FA[b]		CA[c]
	cem	ggbs							FA*	FA**	
C30A	190	127	317	216	0.68	1.4	0.44	195	292	481	773
C40A	233	155	388	217	0.56	1.8	0.46	153	230	528	758
C50A	272	181	453	218	0.48	2.7	0.59	148	223	516	738
C60A	286	190	476	190	0.40	3.7	0.77	116	174	615	789
C70A	305	203	508	173	0.34	4.6	0.91	118	177	626	803
C80A	348	232	580	168	0.29	5.8	1.00	120	180	602	782
C40B	187	280	467	233	0.50	3.1	0.66	150	225	475	659
C50B	188	282	470	212	0.45	4.0	0.85	113	170	537	757
C60B	196	294	490	196	0.40	5.2	1.06	123	185	522	767
$C1_2$	173	173	346	215	0.62	2.1	0.60	147	200	558	800
$C3_2$	226	226	452	190	0.42	4.2	0.94	112	152	632	768
D1	135	203	406	196	0.58	3.4	1.00	212	288	443	804
F	70	282	564	176	0.50	4.2	1.20	151	205	586	838

[a] Limestone powder <125 µm.

[b] Fine aggregate <2 mm (Note: a part of the fine aggregate FA* is the coarser fraction of the limestone powder, in the size range125 µm – 2 mm, whereas FA** refers to natural river sand <2 mm).

[c] Coarse aggregate <20 mm.

Table 7.2 Further SCC mixes details

Mixes	Reference	ggbs	Nominal η, Pa s	Actual η, Pa s	Nominal f_{cu} MPa	Cement type
Set 2A	C30A	40%	2	1.91	30	CEM II fly ash (V-B), 32,5R
	C40A		3	2.92	40	
	C50A		4	3.89	50	
	C60A		8	7.78	60	
	C70A		12	11.95	70	
	C80A		12	12.40	80	
Set 2B	C40B	60%	1	1.00	40	CEM II fly ash (V-B), 32,5R
	C50B		2	1.91	50	
	C60B		3	2.92	60	
Set 3	$C1_2$	50%	2	2.00	40	CEM II Limestone (A-L), 32,5R
	$C3_2$	50%	6	6.01	60	
	D1	60%	2	2.00	50	
	F	80%	2	1.99	30	

The mixes were designed using the design charts and calculation steps described in Chapter 6.

The steps of the experimental validation procedure described in this chapter are summarised in the flow chart presented in Figure 7.1. The plastic mix must satisfy the flowability and passability criteria described in Chapter 6, which are summarised for convenience in Table 7.3.

Table 7.3 Limitation of design criteria

Parameters/Criteria	Limits	Commentary
❖ Viscosity class	Class 1 $t_{500} \leq 2$ Sec.	VS1 has good filling-ability even with congested reinforcement.
	Class 2 $t_{500} > 2$ Sec.	VS2 has no upper-class limit but with increasing flow time it is more likely to exhibit thixotropic effects, which may be helpful in limiting the formwork pressure or improving segregation resistance.
❖ Yield stress	Measuring t_{stop}	the longer t_{stop} the higher ggbs level
❖ Spreading diameter	700±50 mm	For assessment of material after spreading must visually show no segregation in this limit to pass the test.
❖ Heat of hydration	Between 87 and 173 J/g for ggbs 0.8 to ggbs 0.2 at 24hrs period	Determined by type of application.
❖ Ultimate compressive strength	37 to 97 MPa	Depending on time when application structure unloaded.
❖ Compressive strength at 28 days	30 to 80 MPa	
❖ Varied time compressive strength	56, 90, 180, 270, and 365 days	Depending on the desirable time
❖ Compressive strength gain (R)	10-15 % for 20% ggbs and 40-60 % for ggbs 80%	See Figure 5.24

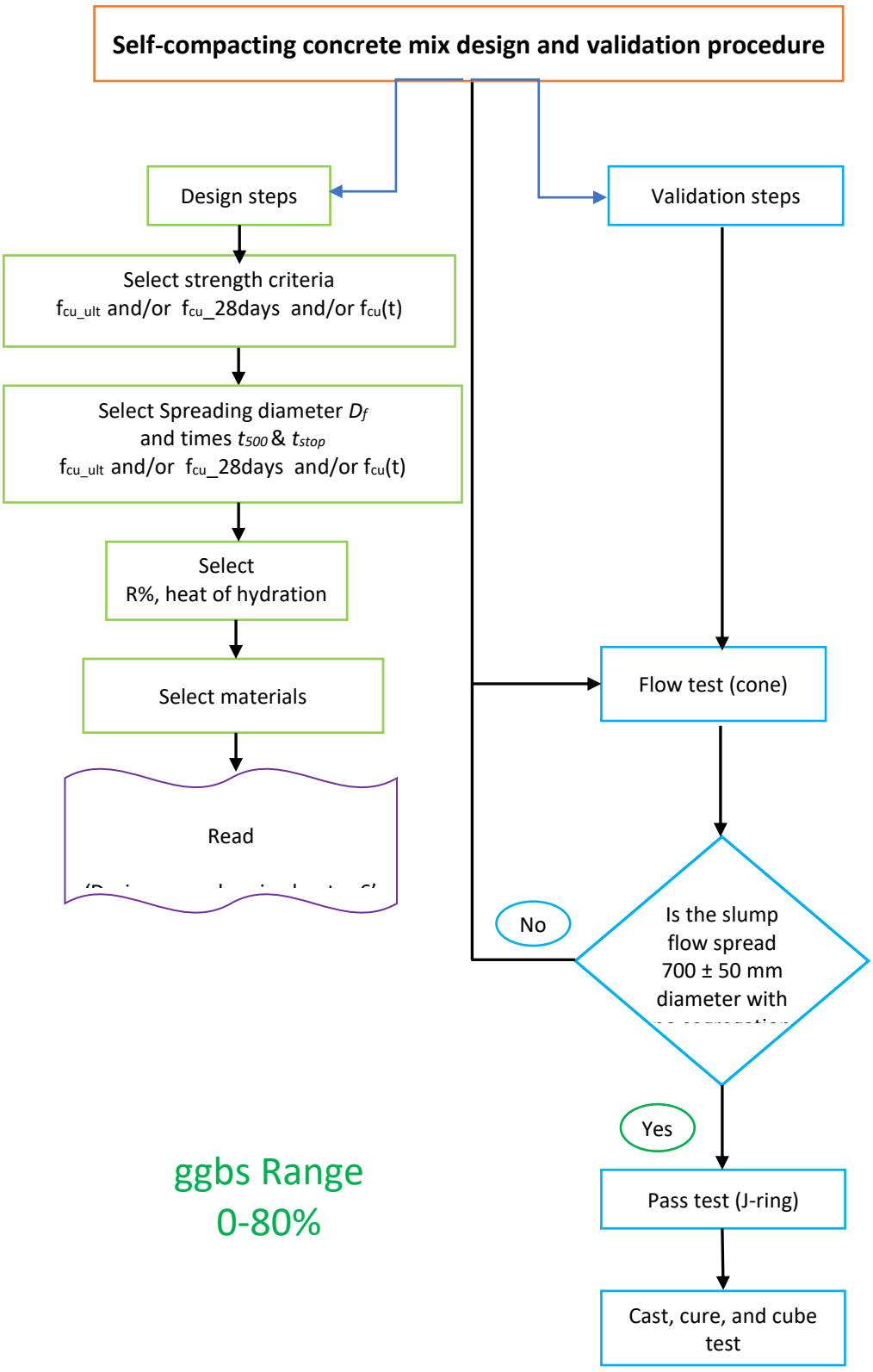

Figure 7.1 Flow chart for the design and validation procedure

7.2 Tests results on fresh SCC

The slump flow and J-ring pass-ability tests were described in chapter 3. A separate video-recorded slump-flow and J-ring test was carried out for every mix. The results from all of the slump and J-ring validation tests are given in Table 7.4.

Table 7.4 (Set 2 and 3) Flow and Passing-ability test results

Mix Ref.	ggbs	η (Pa s)	Slump flow		J-ring pass		D_f-D_j(mm)	η Class
			t_{500} (s)	D_f (mm)	t_{500J} (s)	D_{fj} (mm)		
C30A	40%	1.91	0.5	650	0.6	650	20	VS1
C40A	40%	2.92	0.5	680	0.6	670	10	VS1
C50A	40%	3.89	0.5	700	0.7	690	10	VS1
C60A	40%	7.78	1.6	750	1.7	730	20	VS1
C70A	40%	11.95	1.6	750	1.9	730	20	VS1
C80A	40%	12.40	1.8	750	2.0	730	20	VS1
C30B	60%	1.00	0.4	700	0.5	690	10	VS1
C40B	60%	1.91	0.7	750	0.8	730	20	VS1
C50B	60%	2.92	1.4	750	1.6	725	25	VS1
$C1_2$	50%	2.00	0.8	710	1.2	710	0	VS1
$C3_2$	50%	6.01	1.8	750	2.4	740	20	VS1
D1	60%	2.00	1.6	660	2.6	650	10	VS1
F	80%	1.99	2.2	730	2.7	705	25	VS2

The final position of the plastic SCC for a selection of set 2 tests, taken from the videos, are shown in Figures 7.2 & 7.3 for the slump tests and 7.4 & 7.5 for the J-ring tests, and those for set 3 (both slump and J-ring) are given in Figures 7.6 to 7.9.

All mixes met the slump test spread-range criterion (650–750 mm) and showed no signs of segregation or bleeding, the latter being judged according to BS EN 12350-8 (2010).

Figure 7.2 Horizontal spread of SCC mix when it stopped to flow

Figure 7.3 Horizontal spread of SCC mix when it stopped to flow

All the above mixes also satisfied the J-ring pass-ability criterion (EFNARC, 2005b; EN BS 206-9, 2010) with no nesting of the larger aggregate particles in the gaps between the rods and no signs of segregation.

A criterion set out in BS EN 12350-12 (2010) is that the difference between the spread in the standard slump flow test and the spread in the J-ring test should not exceed 25mm. This criterion was satisfied by all mixes. The corresponding spreads from four set 3 mixes are shown in Figures 7.6 to 7.9.

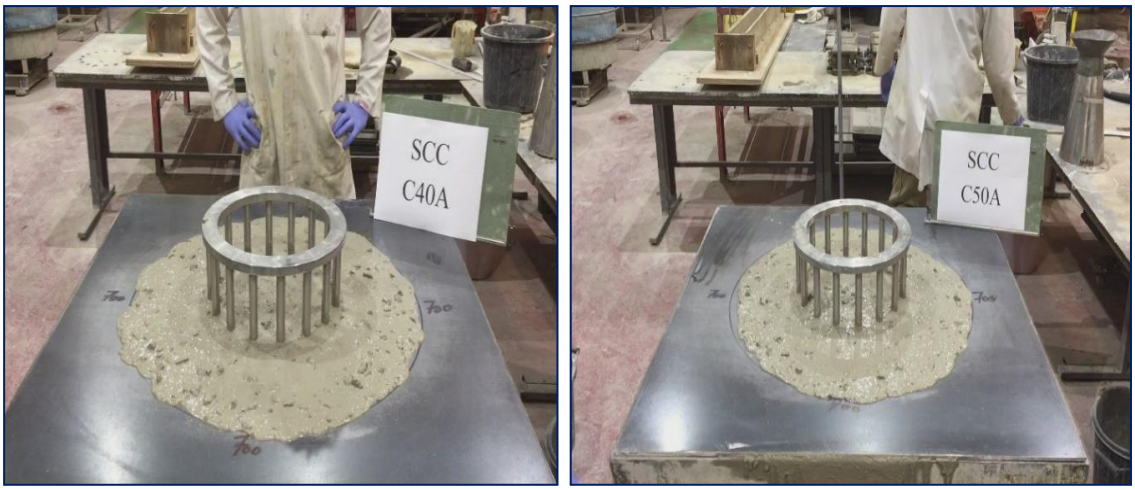

Figure 7.4 J-Ring final horizontal spread of SCC mix

Figure 7.5 J-Ring final horizontal spread of SCC mix

Figure 7.6 Slump and J-Ring final horizontal spreads for mix $C1_2$

Figure 7.7 Slump and J-Ring final horizontal spreads for mix $C3_2$

Figure 7.8 Slump and J-Ring final horizontal spreads for mix D1

Figure 7.9 Slump and J-Ring final horizontal spreads for mix F

SCC has a mix design requirement that the dynamic viscosity meets certain criteria (see Tables 7.1 and 7.2). However, the tests (slump flow and J-ring) used to judge whether a mix meets these plastic criteria do not directly measure the dynamic viscosity. This is understandable because, for the reasons explained in Chapter 4, the dynamic viscosity of a concrete mix is very difficult to measure directly. It is also known, as discussed in Chapter 4, that the plastic behaviour of the mix is influenced by the fluid's yield stress, although there is no specific criteria used in either the mix design or mix validation

procedures related to the yield stress. It would be useful to have a way of linking the slump flow parameters (t_{500} , t_{stop} and D_f) and the dynamic viscosity, and to have some indication of the effect of changing the yield stress on these flow parameters. The data collected in the validation exercise (Table 7.3) provides a means of exploring these relationships. This has been accomplished by plotting the t_{500} , t_{stop} and D_f against η for the set 2 and set 3 mixes. These plots, given in Figures 7.10 to 7.12, show a number of trends. As expected, Figure 7.10 shows that t_{500} increases with increasing plastic viscosity for the same target flow spread. Also, t_{500} increases significantly with increasing ggbs level for ggbs levels greater than 25% .

Badry, Kulasegaram and Karihaloo (2016) showed conclusively that t_{500}, t_{stop} and D_f depend on both the yield stress and the dynamic viscosity. Using the graphs presented by Badry et al., and the trends shown in Figures 7.11 and 7.12, is is clear that the ggbs level has a significant effect on the yield stress. Furthermore, it is evident that mixes with replacement levels up to 50%, and a consistent plastic viscosity (2.0 Pa s), spread more quickly (i.e. have a shorter t_{500}) than mixes of the same plastic viscosity but with replacement levels exceeding this value (see Figure 7.12). Thus, it is clear that the ggbs level has an effect on the yield stress of the mix and therefore its flow-ability.

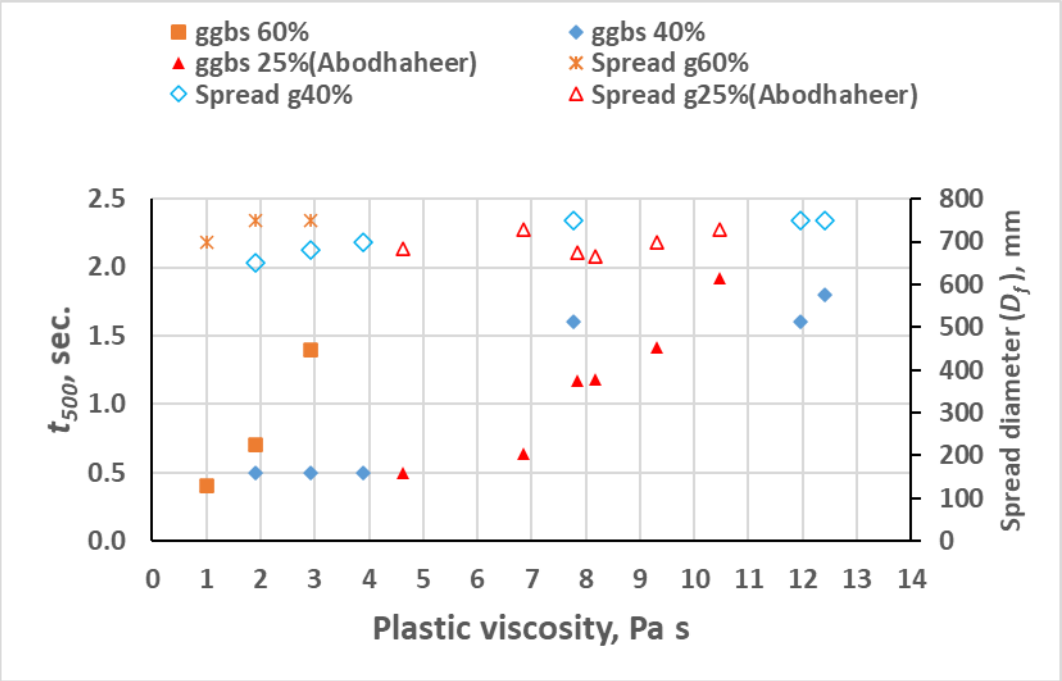

Figure 7.10 Variation of t_{500} and D_f with plastic viscosity

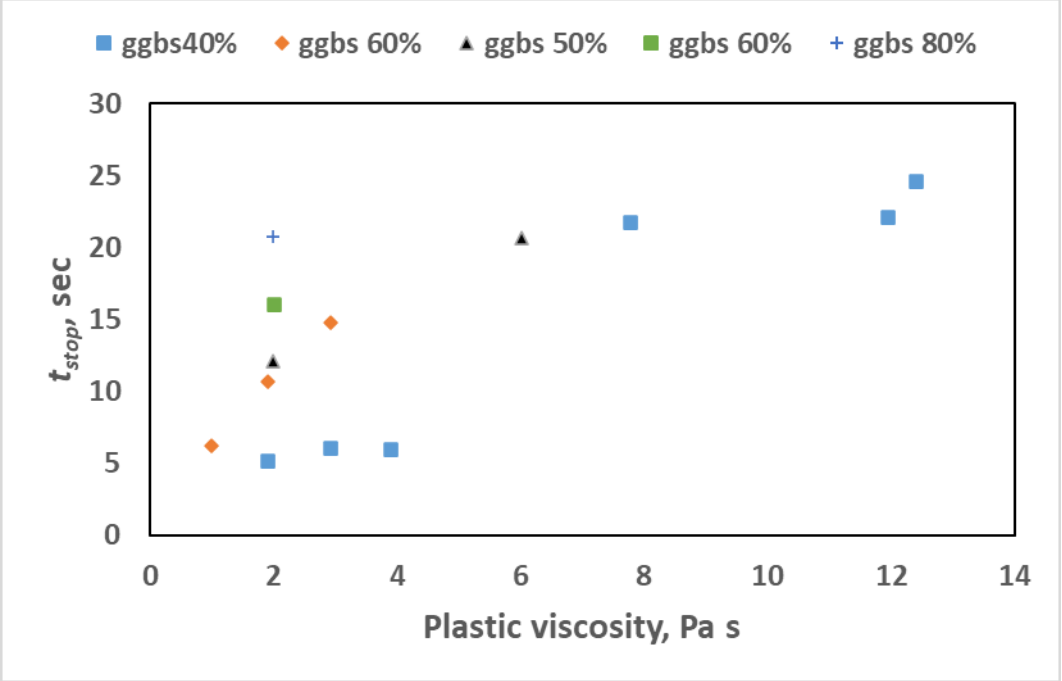

Figure 7.11 Relationship between t_{stop} and the plastic viscosity for various ggbs levels (set 2 and 3)

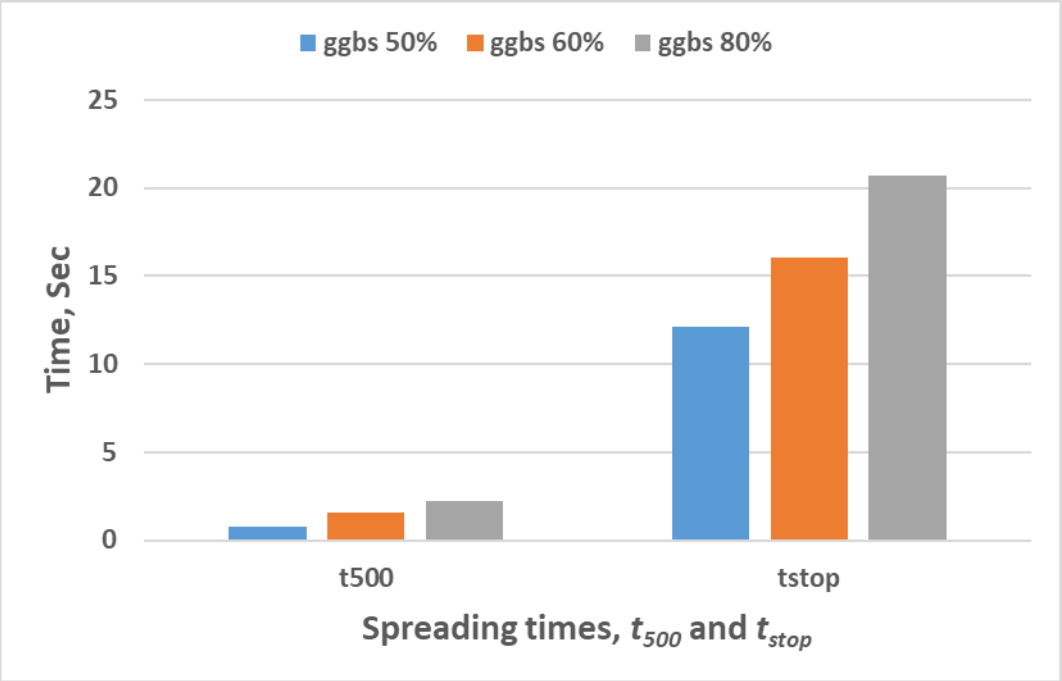

Figure 7.12 Relation between spreading times, t_{500} and t_{stop} and ggbs level (Set 3)

7.3 Compressive strength of SCC test results

At least three 100 mm cubes from each variant of the test mixes were cast, cured and tested in accordance with the procedure described in Chapter 3. The mean values of the 28 day compressive cube strength for mix sets 2 and 3 are given in Table 7.4, along with the coefficients of variation (CoV) and associated 95% confidence characteristic values. The mean and predicted strengths are also plotted against the w/b ratio in Figure 7.13 and.

The results given in Table 7.5 show that the compressive strengths of all cubes were within (or just above) the specified limits. This provides confidence in the mix design procedure and in the equations used within the procedure.

The change from CEMII (V-B) to CEMII (A-L) cement did not affect the applicability of the prediction equations. However, as noted earlier in chapters 3 and 5, the equation for the

28 day strength would vary with cement type (I,II,III) and(N, R, S), and both the 28 day strength and strength at ultimate hydration would vary with the cement strength rating (32.5,42.5,52.5).

Table 7.5 Compressive strength results of SCC mixes, Sets 2 and 3

Mix Ref.	ggbs%	w/b	f_{cu_Mean} (MPa)	CoV %	$f_{cu\_Estimated}$ (MPa)	Allowable limits (MPa)	$f_{cu\_char.}$ (MPa)
C30A	40%	0.68	35.0	3.8	33	27-33	31.78
C40A	40%	0.56	43.0	4.3	44	37-43	36.44
C50A	40%	0.48	50.0	4.3	53	47-53	46.85
C60A	40%	0.40	61.0	4.7	64	57-63	55.97
C70A	40%	0.34	71.0	3.0	73	67-73	67.10
C80A	40%	0.29	78.0	2.4	82	77-83	75.15
C40B	60%	0.50	48.0	1.7	44	37-43	46.32
C50B	60%	0.45	52.0	3.8	50	47-53	48.84
C60B	60%	0.40	57.0	3.9	56	57-63	53.72
$C1_2$	50%	0.62	41.0	2.4	36	37-43	38.94
$C3_2$	50%	0.42	58.0	0.9	57	57-63	56.98
D1	60%	0.58	47.0	2.5	37	47-53	44.67
F	80%	0.50	36.0	2.6	38	27-33	33.99

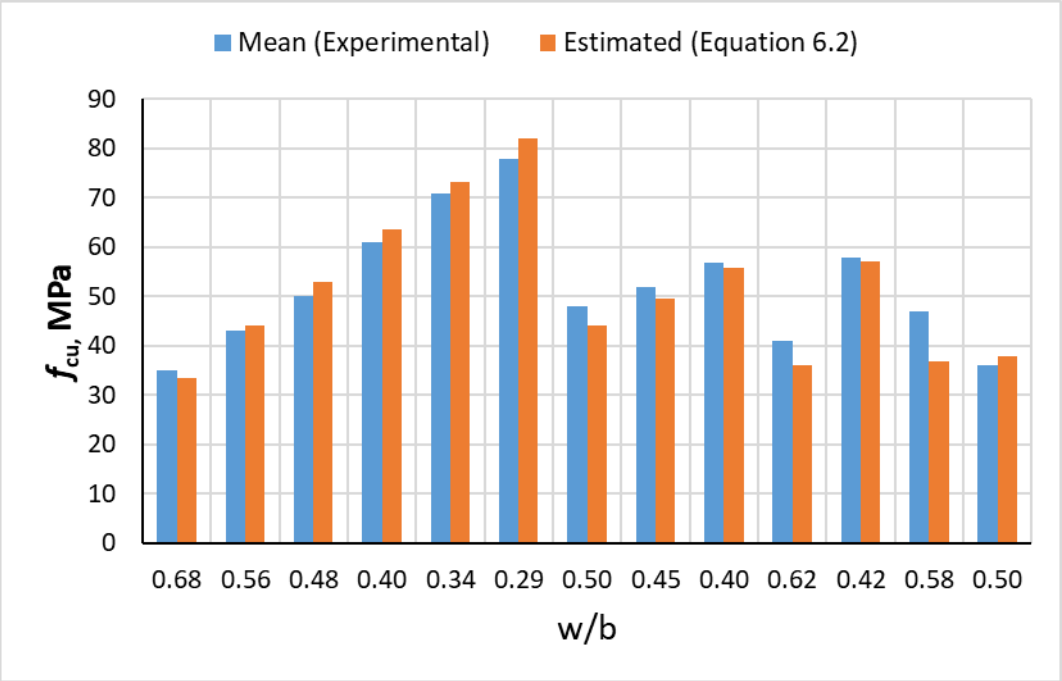

Figure 7.13 Compressive strength comparison between mean and predicted

For mix set 3, the compressive strength of the hardened concrete was measured at a range of times after casting up to 135 days. These results are presented in Figures 7.14 and 7.15. As may be seen, the strength gains over time are consistent with the combined hydration and strength development model presented in Chapter 5. The associated post-28 day strength gain factors (R_{135}) (see section 5.8) are shown in Figure 7.15. It is noted that the R_{135} values computed here are the 135 day strengths rather than the values at full hydration. It is clear from comparing Figure 7.15 with the plots for R at full hydration (Figure 5.24) that the gap between R_{135} and R increases with the level of ggbs. The adjusted values for full hydration are shown in Table 7.6.

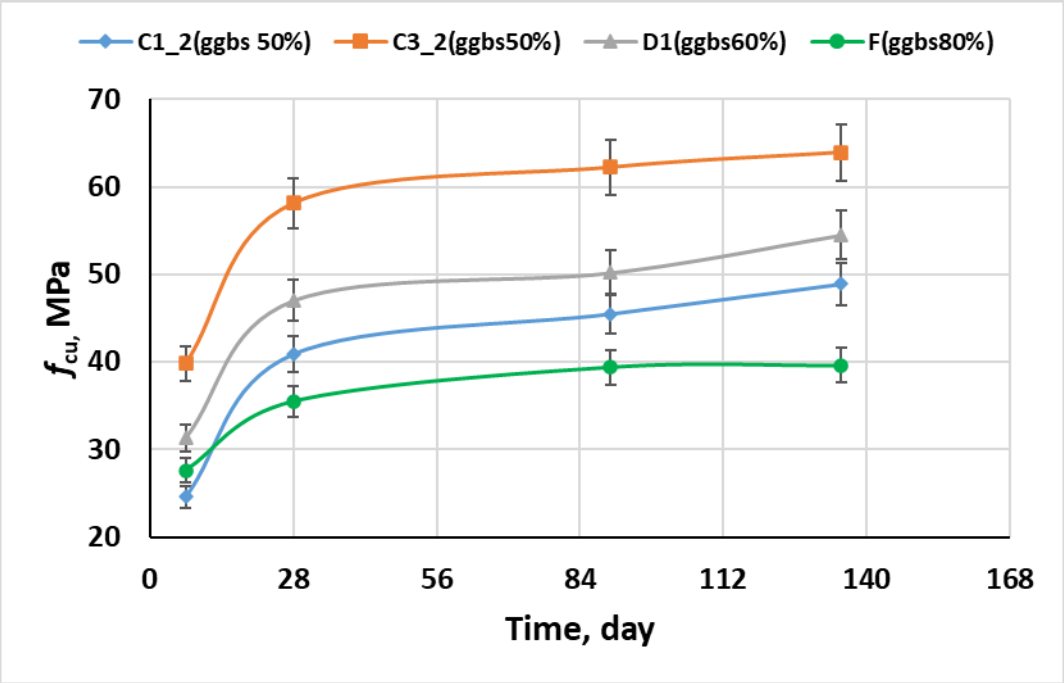

Figure 7.14 Compressive strength results up to 135 days

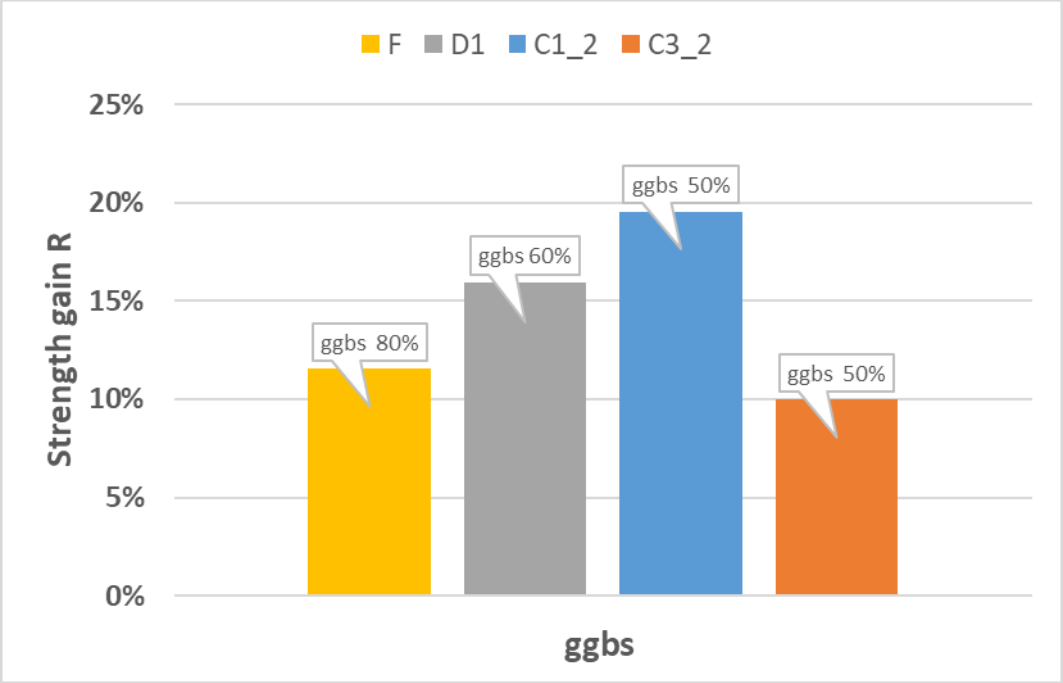

Figure 7.15 post-28 day strength gain factor (R_{135}) at 135 days

Table 7.6 Extrapolated R values at full hydration.

ggbs	w/b	f_{cu} (28day)	f_{cu} (ultimate)	R%
0.4	0.68	35	40	15
0.4	0.56	43	53	23
0.4	0.48	50	64	27
0.4	0.4	61	76	25
0.4	0.34	71	88	24
0.4	0.29	78	98	26
0.6	0.50	48	59	24
0.6	0.45	52	67	28
0.6	0.40	57	75	31
0.5	0.62	41	46	11
0.5	0.42	58	72	25
0.6	0.58	47	49	5
0.8	0.50	36	58	62

7.4 Discussion

The measured plastic properties of the mixes met the design criteria for all mixes.

The influence of the proportion of ggbs on flow parameters (t_{500}, t_{stop} and D_f) is significant, which means that it is insufficient to rely only on the plastic viscosity to determine if an SCC mix will meet the plastic criteria. This justifies the need for different charts for each ggbs level (see Figures 6.6 and 6.7). Also, the influence of ggbs on the the flow parameters governs the range of viscosity classes that can be achieved for each ggbs level. From the results, it can be observed that most mixes are class VS1 and only mix F is

class VS2, even with the minimum value of plastic viscosity. This is attributed to the higher yield stress of this high ggbs % mix.

A more general point, that is highlighted by the present results, is that the maximum 28 day strength that can be achieved with an SCC mix decreases with the increasing ggbs level. This is because the range of w/b ratios required to satisfy the plastic mix criteria limits the maximum achievable 28-day strength. This is different from NVC, for which the plastic criteria are easier to achieve. For instance, a w/b=0.4 with 80% ggbs is acceptable for NVC but not for the SCC. The 28 day limiting values are highlighted in Figure 7.16. However, as discussed in Chapters 5 and 6, the strength at full hydration relative to the 28-day strength increases greatly with the ggbs% and therefore significantly higher strengths, than those shown in Figure 7.16, are achievable with high ggbs% mixes.

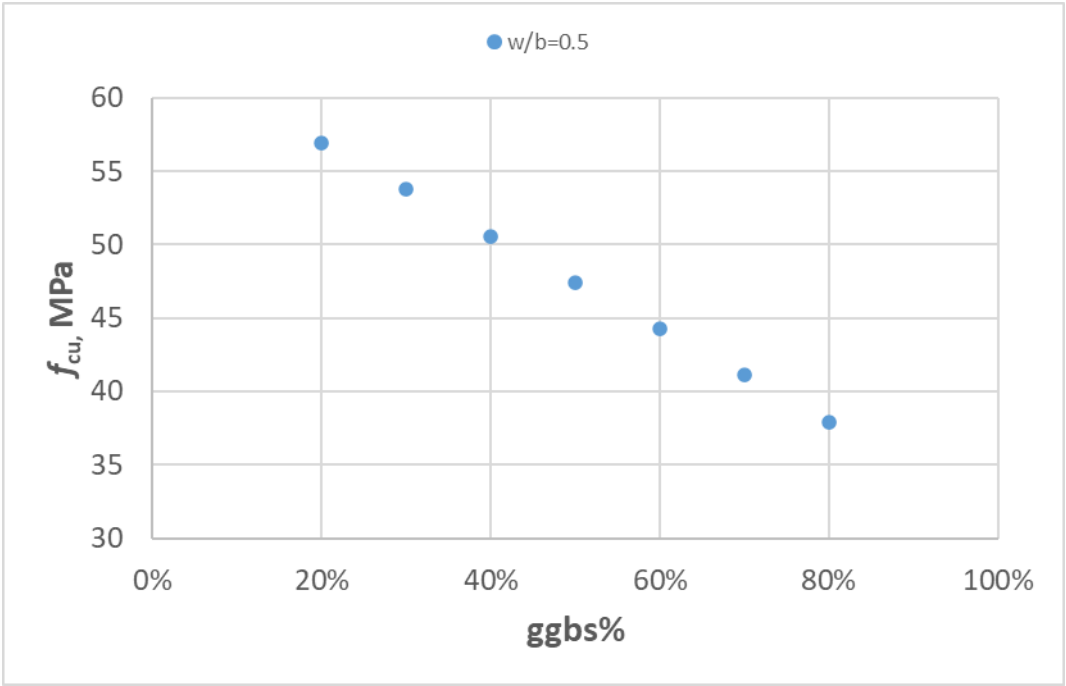

Figure 7.16 Effect of ggbs level on compressive strength for only SCC

7.5 Conclusions

This chapter presented an experimental validation of the mix design method. In addition, the results from the experiments quantify the influence of the ggbs level on the plastic parameters and compressive strengths.

The main conclusions from the work of this chapter are given below.

- The mix design procedure provides a reliable and systematic method for designing SCC mixes with a range of ggbs levels from 0 to 80%.
- The procedure leads to mixes that satisfy both plastic and hardened deign criteria.
- The ggbs level affects both the dynamic viscosity and yield stress of SSC in the plastic state. This means that it is insufficient to a use a single plastic parameter (i.e. viscosity) to characterise a mix. Therefore different plastic design curves are required for mixes with different ggbs replacement levels.
- The ggbs level limits the range of plastic properties and compressive strengths achievable for SCC mixes with ggbs levels greater than 25% when compared to those for mixes with ggbs levels $\leq$25%.

Chapter 8 Conclusions and recommendations for further study

8.1 Conclusions

The individual conclusions from the work of this thesis were given in Chapters 4 to 7. These conclusions are now brought together to provide the overall conclusions from this PhD programme of research that has developed a new design procedure for self-compacting concrete mixes. This new procedure covers mixes with ggbs cement replacement levels from 0 to 80%.

- SCC is a non-Newtonian fluid that can be described with a Bingham-type flow model that has dynamic viscosity and yield stress as its primary parameters.
- The dynamic viscosity is a key parameter in the design and behaviour of SCC in the plastic state but it is a parameter that is very difficult, and unreliable, to measure directly due to effects of the inclusions (filler, fine and coarse aggregate) on the plastic behaviour of the inhomogeneous fluid.
- The dynamic viscosity of SCC can be calculated accurately using the micro-mechanical hierarchical suspensions model originally suggested by Ghanbari and Karihaloo (2009) with the dynamic viscosity of the paste as a primary input. Different parameters, from those of previous investigators, are required to simulate the plastic properties of SCC mixes with high percentages of ggbs.
- The micro-mechanical model for predicting the viscosity of SCC mixes can be used to produce design charts for this type of concrete.
- A new table that relates the ggbs percentage and w/b ratio to the dynamic viscosity of cement paste provides a convenient method for predicting its viscosity.
- The 28 day and ultimate (i.e. at full hydration) compressive strengths of SCC concrete with ggbs levels of 0 to 80% can be predicted reliably with new formulae that have the w/b ratio and ggbs level and the primary inputs.
- When rearranged, the above formulae provide a convenient method of determining the w/b ratio required to achieve a target 28 day and/or ultimate strength.

- The combined hydration and strength development models of Schlinder and Folliard (2005) and De Schutter and Taerwe (1996) provides an effective method for predicting the time dependent compressive strength of SCC mixes with high ggbs levels.
- New experimental data for SCC mixes with a range of ggbs cement replacement levels was useful for calibrating and validating the above strength development model.
- The difference between the 28 day and fully-hydrated compressive strengths of SCC concrete grows with the proportion of ggbs. This difference is quantified in a new factor (R) that provides a measure of the post-28 day strength development potential.
- The 28 day and ultimate strength prediction formulae, combined with the strength development model, led to the development of a new mix design procedure that allows strengths at multiple times to be considered.
- A new chart presented in this thesis can be used for predicting the time-dependent heat of hydration for the full range of SCC mixes considered in the present research.
- The new mix design procedure, which uses design charts for predicting the plastic and hardened properties of a mix, is an effective and convenient way to design SCC mixes. The method eliminates the need for extensive trial mixes.
- A number of mix design worked examples demonstrate the convenience and simplicity of the design procedure.
- The new design procedure also allows mixes to be designed for multiple strengths at different times after casting. The new method can used to save energy and reduce CO2 emissions of SCC by maximising the potential of the low energy waste material ggbs.
- Experimental validation shows that the mix design procedure works well for SCC mixes with the full range of ggbs levels (0 to 80%). The procedure results in mixes that satisfy all of the necessary plastic and hardened design criteria.

- Including significant levels of ggbs in a mix can limit the range of plastic properties and compressive strengths achievable when compared to those for mixes with ggbs levels $\leq$25%.
- Mixes with high percentages of ggbs have higher post-28-day strength development potentials and are significantly more environmentally friendly than concrete that has lower levels of cement replacement material.

8.2 Recommendations for further study

Several areas are recommended for future study:

- Extend the design procedure to SCCs formed with different cements by undertaking further experiments on plastic and hardened properties;
- Extend the strength range of the hardened material to include higher strength concretes, with 28 day compressive strengths in the range 90 to 120MPa;
- Extend the procedure to include fibre-reinforced SCC mixes with high levels of ggbs, exploring steel, polymer and organic fibres;
- Explore the possibility of including permeability as a factor in the mix design procedure;
- Considering the degree of durability as a specific factor in the SCC mix design procedure along with the associated minimum and maximum cement contents and w/b ratios.
- Investigate the formwork pressure applied by the SCC mixes considered in this work.

9 References;

Abo Dhaheer, M.., Al-Rubaye, M.M., Alyhya, W.S., Karihaloo, B.L. and Kulasegaram, S. (2016a). Proportioning of self-compacting concrete mixes based on target plastic viscosity and compressive strength: Part II - experimental validation. *Journal of Sustainable Cement-Based Materials* 5(4), pp. 217–232.

Abo Dhaheer, M.S., Al-Rubaye, M.M., Alyhya, W.S., Karihaloo, B.L. and Kulasegaram, S. (2016b). Proportioning of self–compacting concrete mixes based on target plastic viscosity and compressive strength: Part I - mix design procedure. *Journal of Sustainable Cement-Based Materials* 5(4), pp. 199–216.

ACI Committee (2000). Ground Granulated Blast-Furnace Slag as a Cementitious Constituent in Concrete. *ACI 233R-95* 95(Reapproved), pp. 1–18.

ACI Committee 211 (1991). Standard practice for selecting proportions for normal, heavyweight, and mass concrete. (Reapproved 2002), pp. 1–38.

Adesina, A. (2020). Performance and sustainability overview of alkali-activated self-compacting concrete. *Waste Disposal & Sustainable Energy* 2(3), pp. 165–175. doi: 10.1007/s42768-020-00045-w.

Alami, M.M., Erdem, T.K. and Khayat, K.H. (2016). Development of a new test method to evaluate dynamic stability of self-consolidating concrete. In: Khayat, K. H. ed. *8th International RILEM Symposium on Self-Compacting Concrete*. Washington DC: RILEM Publications SARL, pp. 113–122.

Alonso, M.M., Palacios, M. and Puertas, F. (2013). Compatibility between polycarboxylate-based admixtures and blended-cement pastes. *Cement and Concrete Composites* 35(1), pp. 151–162.

Alyhya, W.S. (2016). *Self-Compacting Concrete : Mix Proportioning , Properties and Its Flow Simulation in the V-Funnel*. UK: Cardiff University.

Anjos, M.A.S., Camões, A., Campos, P., Azeredo, G.A. and Ferreira, R.L.S. (2020). Effect of

high volume fly ash and metakaolin with and without hydrated lime on the properties of self-compacting concrete. *Journal of Building Engineering* 27(April 2019)

Awoyera, P.O., Akinwumi, I.I., Karthika, V., Gobinath, R., Gunasekaran, R., Lokesh, N., Manikandan, M. and Narmatha, T. (2020). Lightweight Self-Compacting Concrete Incorporating Industrial Rejects and Mineral Admixtures: Strength and Durability Assessment. *Silicon* 12(8), pp. 1779–1785.

Badry, F.F., Kulasegaram, S. and Karihaloo, B.L. (2016). Estimation of the yield stress and distribution of large aggregates from slump flow test of self- compacting concrete mixes using smooth particle hydrodynamics simulation. *Journal of Sustainable Cement-Based Materials* 5(3), pp. 117–134.

Bamforth, P. (2007). *Early-Age thermal crack control in concrete*. 1st ed. London, UK: Construction Industry Research and Information Association(CIRIA) C660.

Banfill, P., Beaupré, D., Chapdelaine, F., de Larrard, F., Domone, P., Nachbaur, L., Sedran, T., Wallevik, O. and Wallevik, J.E. (2000). *Comparison of concrete rheometers: international tests at LCPC (Nantes, France) in October 2000, NISTIR 6819*. Nantes, France.

Banfill, P.F.G. (2006). Rheology of Fresh Cement and Concrete. *Rheology Reviews 2006* 2006, pp. 61–130.

Barnes, H.A., Hutton, J.F. and Walters, K. (1993). An Introduction to Rheology. In: Walters, K. ed. *Rheology of materials and engineering structures*. Sobotka: Elsevier, pp. 119–128.

Bartos, P.J.M. and Marrs, D.L. (1999). 15 DEVELOPMENT AND TESTING OF SELF-COMPACTING GROUT FOR THE PRODUCTION OF SIFCON. In: *PRO 6: 3rd International RILEM Workshop on High Performance Fiber Reinforced Cement Composites (HPFRCC 3)*., p. 171.

Becknell, N.P. and Hale, W.M. (2011). Effect of Slag Grade and Cement Source on the Properties of Concrete. *International Journal of Concrete Structures and Materials* 5(2),

pp. 119–123.

De Belie, N., Soutsos, M. and Gruyaert, E. (2018). *Properties of Fresh and Hardened Concrete Containing Supplementary Cementitious Materials: State-of-the-Art Report of the RILEM Technical Committee 238-SCM, Working Group 4*.

Benaicha, M., Roguiez, X., Jalbaud, O., Burtschell, Y. and Alaoui, A.H. (2015). Influence of silica fume and viscosity modifying agent on the mechanical and rheological behavior of self compacting concrete. *Construction and Building Materials* 84, pp. 103–110.

Bernal, J., Reyes, E., Massana, J., León, N. and Sánchez, E. (2018). Fresh and mechanical behavior of a self-compacting concrete with additions of nano-silica, silica fume and ternary mixtures. *Construction and Building Materials* 160, pp. 196–210.

Bharatkumar, B.H., Narayanan, R., Raghuprasad, B.K. and Ramachandramurthy, D.S. (2001). Mix proportioning of high performance concrete. *Cement and Concrete Composites* 23(1), pp. 71–80.

Billberg, P. (1999). *Self-compacting concrete for civil engineering structures: The Swedish experience*. Swedish Cement and Concrete Research Institute.

Billberg, P. (2011). Influence of powder type and VMA combination on certain key fresh properties of SCC. In: 9th International Symposium on High Performance Concrete — Design, Verification and Utilisation, Rotorua, New Zealand. *pci* , p. 2011.

Billberg, P.H., Petersson, Ö., Westerholm, M., Wüstholz, T. and Reinhardt, H. (2004). Summary report on work package 3.2: Test methods for passing ability. *Cement and Concrete Research Institute , CBI Universität Stuttgart , IWB .*

Boukendakdji, O., Kadri, E.-H. and Kenai, S. (2012). Effects of granulated blast furnace slag and superplasticizer type on the fresh properties and compressive strength of self-compacting concrete. *Cement and Concrete Composites* 34(4), pp. 583–590.

Van Breugel, K. (1997). Simulation of Hydration and Formation of Structure in Hardening Cement-Based Materials-HYMOSTRUC.

BS EN 12350-10 (2010). BSI Standards Publication Testing fresh concrete Part 10 : Self-compacting concrete — L box test. *BSI Standards Publication* PART 10

BS EN 12350-11 (2010). Testing fresh concrete Part 11 : Self-compacting concrete — Sieve segregation test. *BSI Standards Publication*

BS EN 12350-12 (2010). Testing fresh concrete Part 12: Self-compacting concrete -- J ring test. *BSI Standards Publication*

BS EN 12350-8 (2010). Testing fresh concrete: Self-compacting concrete-Slump-flow test. *BSI Standards Publication*

BS EN 12350-9 (2010). BSI Standards Publication Testing fresh concrete V-funnel test. *BSI Standards Publication*

BS EN 12390-3:2009 (2011). Testing hardened concrete: Compressive strength of test specimens. BSI, London, uk. *BSI Standards Publication*

BS EN 12620 (2013). BSI Standards Publication Aggregates for concrete. *British Standard*

BS EN 197-1 (2011). Cement. Composition, specifications and conformity criteria for common cements. *BSI Standards Publication*

BS EN 206-9 (2010). Concrete, Part 9: Additional Rules for Self- compacting Concrete (SCC). London: BSI.

BS EN 206+A1:2016 (2013). Concrete — Specification , performance , production and conformity. *BSI Standards Publication*

BS EN 206 (2013). Concrete — Specification , performance , production and conformity. *BSI Standards Publication*

BS EN 933-1 (2012). Tests for geometrical properties of aggregates Part 1 : Determination of particle size distribution — Sieving method. *British Standards Institution, London, UK*

Bui, V.K., Akkaya, Y. and Shah, S.P. (2002). Rheological model for self-consolidating concrete. *ACI Materials Journal* 99(6), pp. 549–559.

Byfors, J. and Betong, S. forskningsinstitutet för cement och (1980). *Plain Concrete at Early Ages*. Stockholm, Sweden: Swedish Cement and Concrete Research Institute.

Cepuritis, R., Jacobsen, S., Smeplass, S., Mørtsell, E. and Wigum, B.J. (2016). Micro-Proportioning of SCC with Crushed aggregate : Rheology of Filler Modified Cement Pastes. In: Khayat, K. H. ed. *8th International RILEM Symposium on Self-Compacting Concrete*. Washington DC: RILEM Publications SARL, pp. 3–13.

Cervera, M., Oliver, J. and Prato, T. (1999). Thermo-Chemo-Mechanical Model for Concrete. I: Hydration and Aging. *Journal of Engineering Mechanics* 125(9), pp. 1018–1027.

Chidiac, S.E. and Mahmoodzadeh, F. (2009). Plastic viscosity of fresh concrete - A critical review of predictions methods. *Cement and Concrete Composites* 31(8), pp. 535–544.

Chidiac, S.E. and Panesar, D.K. (2008). Evolution of mechanical properties of concrete containing ground granulated blast furnace slag and effects on the scaling resistance test at 28 days. *Cement and Concrete Composites* 30(2), pp. 63–71.

Cristescu, C. (2010). *Materials with rhelogical properties/calculation of structures*. 1st ed. New Jersey,: Wiley.

CSMA (2021). The CSMA (Cementitious Slag Makers Association).pdf.

Curry, K. c. (2020). *Iron and steel slag statitics*. Available at: http://www.slg.jp/pdf/Amounts of steel Slag 2017FY.pdf.

Daczko, J.A. (2012). *Self-consolidating concrete: Applying what we know*. USA: Spon Press.

Dadsetan, S. and Bai, J. (2017). Mechanical and microstructural properties of self-compacting concrete blended with metakaolin, ground granulated blast-furnace slag and fly ash. *Construction and Building Materials* 146, pp. 658–667.

DECC (2011). Guidelines to Defra/DECC's GHG Conversion Factors for Company Reporting. *Department of Energy and Climate Change and Department for Environment Food and Rural Affairs* , p. 50.

Deeb, R. and Karihaloo, B.L. (2013). Mix proportioning of self-compacting normal and high-strength concretes. *Magazine of Concrete Research* 65(9), pp. 546–556.

DeSchutter, G., Ye, G., Audenaert, K., Bager, D., Baroghel-Bouny, V., Bellmann, F., Boel, V., Bonen, D., Boström, L., Corradi, M., Gartner, E., Hama, Y., Jacobsen, S., Jansson, R., Justnes, H., Khayat, K., Khrapko, M., Leemann, A., Luco, L.F., Magarotto, R., Nowak, A.S., Persson, B., Poppe, A.M., Qian, C., Setzer, M.J., Sideris, K., Skarendahl, A., Sonebi, M., Stark, J., Tang, L., Trägardh, J., Wallevik, O., Zhu, W. and Zverev, I. (2008). Final report of RILEM TC 205-DSC: Durability of self-compacting concrete. *Materials and Structures/Materiaux et Constructions* 41(2), pp. 225–233. doi: 10.1617/s11527-007-9319-9.

DeSchutter, G. and Taerwe, L. (1996). Degree of hydration-based description of mechanical properties of early age concrete. *Materials and Structures* 29, pp. 335–344.

Desnerck, P., Boel, V., Craeye, B. and Itterbeeck, P.. (2014). *Mechanical properties of self-compacting concrete*. Mechanical. Khayat, K. H. and Schutter, G. De eds.

Dinakar, P., Kartik Reddy, M. and Sharma, M. (2013a). Behaviour of self compacting concrete using Portland pozzolana cement with different levels of fly ash. *Materials and Design* 46, pp. 609–616.

Dinakar, P., Sethy, K.P. and Sahoo, U.C. (2013b). Design of self-compacting concrete with ground granulated blast furnace slag. *Materials and Design* 43, pp. 161–169.

Domone, P.L. (2000). Self-Compacting Concrete - State-of-the-Art Report of RILEM TC 174-SCC: Mix design: part VI. In: Skarendahl, A. and Petersson, O. eds. *RILEM State-of-the-Art Reports*. Cachan, France: RILEM Publications SARL, p. pp 168.

Domone, P.L. (2003). Fresh concrete. In: Newman, J. and Choo, B. eds. *Advanced concrete technology*. UK: Elsevier Ltd

Domone, P.L. (2006). Self-compacting concrete : An analysis of 11 years of case studies. *Cement and Concrete Composites* 28, pp. 197–208.

Domone, P.L. (2010). *Proportioning of self-compacting concrete – the UCL method*. Department of Civil , Environmental and Geomatic Engineering, University College of London, UK.

Domone, P.L. and Jin, J. (1999). Properties of mortar for self- compacting concrete. In: Skarendah, A. and Petersson, Ö. eds. *1st International RILEM symposium on self-compacting concrete*. Stockholm, Sweden: RILEM Publications SARL, pp. 109–120.

Doug Hooton, R., Zhutovsky, S. and Kamali-Bernard, S. (2018). Ternary blends. *RILEM State-of-the-Art Reports* 25, pp. 303–315.

Dransfield, J. (2003). Admixtures for concrete, mortar and grout. In: Newman, J. and Choo, B. S. eds. *Advanced Concrete Technolog Constituent Materials*. 1st Editio. Oxford, UK: Elsevier, p. Chapter 4.

Dunstan, E.R. (2011). How does pozzolanic reaction make concrete green. In: *2011 World of Coal Ash (WOCA) Conference*. Ash Library, Denver, CO, USA, pp. 1–14.

Duran Atiş, C., Bilim, C., Atis, C.D., Bilim, C., Duran Atiş, C. and Bilim, C. (2007). Wet and dry cured compressive strength of concrete containing ground granulated blast-furnace slag. *Building and Environment* 42(8), pp. 3060–3065.

Duran Atiş, C. and Bilim, C. (2007). Wet and dry cured compressive strength of concrete

containing ground granulated blast-furnace slag. *Building and Environment* 42(8), pp. 3060–3065.

Edamatsu, Y., Nishida, N. and Ouchi, M. (1998). A rational mix-design method for selfcompacting concrete considering interaction between coarse aggregate and mortar particles. In: Å. Skarendahl and Ö. Pettersson ed. *1st International RILEM Symposium on Self-Compacting Concrete*. RILEM Publications SARL, Stockholm, Sweden: RILEM Publications SARL, pp. 1307–12.

Edamatsu, Y., Nishida, N. and Ouchi, M. (1999). A rational mix-design method for selfcompacting concrete considering interaction between coarse aggregate and mortar particles. In: Skarendah, A. and Petersson, Ö. eds. *1st International RILEM Symposium on Self-Compacting Concrete*. Stockholm, Sweden: RILEM Publications SARL, pp. 309–320.

EFNARC (2005a). The European guidelines for self-compacting concrete; specification, production and use. (May), pp. 1–63.

EFNARC (2005b). The European guidelines for self-compacting concrete; Specification, Production and Use. [Online] 2005 Available from: www.efnafrc.org. (May), pp. 1–63.

El-chabib, H. and Nehdi, M. (2007). Effect of Mixture Design Parameters on Segregation of Self-Consolidating Concrete. *ACI Materials Journal* (103), pp. 374–383.

Elahi, A., Basheer, P.A.M., Nanukuttan, S. V. and Khan, Q.U.Z. (2010). Mechanical and durability properties of high performance concretes containing supplementary cementitious materials. *Construction and Building Materials* 24(3), pp. 292–299.

Elchalakani, M., Aly, T. and Abu-Aisheh, E. (2014). Sustainable concrete with high volume GGBFS to build Masdar City in the UAE. *Case Studies in Construction Materials* 1, pp. 10–24.

EN BS 206-9 (2010). Concrete, additional Rules for Self- compacting Concrete (SCC). *BSI Standards Publication*

Escadeillas, G. and Waller, V. (2007). Estimates of self-compacting concrete ‘ potential ’ durability. *Construction and Building Materials* 21, pp. 1909–1917.

Esmaeilkhanian, B., Khayat, K.H., Yahia, A. and Feys, D. (2014). Effects of mix design parameters and rheological properties on dynamic stability of self-consolidating concrete. *Cement and Concrete Composites* 54, pp. 21–28.

Fantous, T. and Yahia, A. (2020a). Effect of HRWR-VMA-AEA combinations and shear on air-void characteristics in self-consolidating concrete. *Construction and Building Materials* 253, p. 119192. doi: 10.1016/j.conbuildmat.2020.119192.

Fantous, T. and Yahia, A. (2020b). Effect of viscosity and shear regime on stability of the air-void system in self-consolidating concrete using Taguchi method. *Cement and Concrete Composites* 112(April), p. 103653.

Felekoğlu, B. and Sarikahya, H. (2008). Effect of chemical structure of polycarboxylate-based superplasticizers on workability retention of self-compacting concrete. *Construction and Building Materials* 22(9), pp. 1972–1980.

Ferrara, L., Park, Y.D. and Shah, S.P. (2007). A method for mix design of fiber-reinforced self-compacting concrete. *Cement and Concrete Research* 37(6), pp. 957–971.

Ferraris, C.F. (1999). Measurement of the rheological properties of high performance concrete: State of the art report. *Journal of Research of the National Institute of Standards and Technology* 104(5), p. 461.

Ferraris, C.F., Martys, N.S., Olivas, A. and George, W.L. (2016). Calibration of Rheometers for Cementitious Materials. In: Khayat, K. H. ed. *8th International RILEM Symposium on Self-Compacting Concrete*. Washington DC: RILEM Publications SARL, pp. 147–157.

Feys, D., Heirman, G., Schutter, G. De, Verhoeven, R., Vandewalle, L. and Gemert, D. Van (2007a). Comparison of two concrete rheometers for shear thickening behaviour of SCC. In: Schutter, G. De and Boel, V. eds. *5th Int. RILEM Symposium on Self-Compacting*

Concrete. Ghent, Belgium: RILEM Publications SARL, pp. 365–370.

Feys, D., Heirman, G., De Schutter, G., Verhoeven, R., Vandewalle, L. and Van Gemert, D. (2007b). Comparison of two concrete rheometers for shear thickening behaviour of SCC. In: Schutter, G. De and Boel, V. eds. *5th Int. RILEM Symposium on Self-Compacting Concrete*. RILEM Publications SARL, pp. 1–6.

Feys, D., Wallevik, J.E., Yahia, A., Khayat, K.H. and Wallevik, O.H. (2013). Extension of the Reiner-Riwlin equation to determine modified Bingham parameters measured in coaxial cylinders rheometers. *Materials and Structures/Materiaux et Constructions* 46(1–2), pp. 289–311.

Figueiras, H., Nunes, S., Coutinho, J.S. and Andrade, C. (2014). Linking fresh and durability properties of paste to SCC mortar. *Cement and Concrete Composites* 45, pp. 209–226.

Freiesleben, H.P. and Pedersen, E.J. (1985). *Curing of Concrete Structures Freiesleben Draft DEB- Guide to Durable Concrete Structures, Appendix 1, Comité Euro-International du Béton, Lausanne, Switzerland, 1985*.

Ghanbari, A. and Karihaloo, B.L. (2009). Prediction of the plastic viscosity of self-compacting steel fibre reinforced concrete. *Cement and Concrete Research* 39(12), pp. 1209–1216.

Gholhaki, M., Kheyroddin, A., Hajforoush, M. and Kazemi, M. (2018). An investigation on the fresh and hardened properties of self-compacting concrete incorporating magnetic water with various pozzolanic materials. *Construction and Building Materials* 158, pp. 173–180.

Gil, A.M., Khayat, K.H. and Tutikian, B.F. (2019). An experimental approach to design self-consolidating concrete. *Construction and Building Materials* 229, p. 116939.

Goodier, C.I. (2003). Development of self-compacting concrete. *structures and buildings* 156(SB4), pp. 405–414.

Granata, M.F. (2015). Pumice powder as filler of self-compacting concrete. *Construction and Building Materials* 96, pp. 581–590.

Grzeszczyk, S. and Janowska-Renkas, E. (2012). The influence of small particle on the fluidity of blast furnace slag cement paste containing superplasticizers. *Construction and Building Materials* 26(1), pp. 411–415.

Güneyisi, E. and Gesoğlu, M. (2011). Properties of self-compacting portland pozzolana and limestone blended cement concretes containing different replacement levels of slag. *Materials and Structures* 44(8), pp. 1399–1410.

Guo, Z., Jiang, T., Zhang, J., Kong, X., Chen, C. and Lehman, D.E. (2020). Mechanical and durability properties of sustainable self-compacting concrete with recycled concrete aggregate and fly ash, slag and silica fume. *Construction and Building Materials* 231, p. 117115.

Hanehara, S. and Yamada, K. (1999). Interaction between cement and chemical admixture from the point of cement hydration , absorption behaviour of admixture , and paste rheology. 29, pp. 1159–1165.

Hansen, T.C. (1986). Physical structure of hardened cement paste. A classical approach. *Materials and Structures* 19(6), pp. 423–436.

Hanson (2021). Ground granulated blastfurnance slag. *HEIDELBRGCEMENTGROUP* . Available at: https://www.hanson.co.uk.

Hanson, U. (1996). Prince of wales bridge. Available at: https://www.hanson.co.uk/en/case-study/second-severn-crossing.

Hassan, K.E., Cabrera, J.G. and Maliehe, R.S. (2000). The effect of mineral admixtures on the properties of high-performance concrete. *Cement and Concrete Composites* 22(4), pp. 267–271.

He, X., Ma, M., Su, Y., Lan, M., Zheng, Z., Wang, T., Strnadel, B. and Zeng, S. (2018). The effect of ultrahigh volume ultrafine blast furnace slag on the properties of cement pastes. *Construction and Building Materials* 189, pp. 438–447.

Heirman, G., Hendrickx, R., Vandewalle, L., Van Gemert, D., Feys, D., De Schutter, G., Desmet, B. and Vantomme, J. (2009). Integration approach of the Couette inverse problem of powder type self-compacting concrete in a wide-gap concentric cylinder rheometer. Part II. Influence of mineral additions and chemical admixtures on the shear thickening flow behaviour. *Cement and Concrete Research* 39(3), pp. 171–181.

Hiromi Fujiwara, S.N. (1999). Study on self compactability of high fluidity concrete. In: Skarendah, A. and Petersson, Ö. eds. *1st International RILEM Symposium on Self-Compacting Concrete*. Stockholm, Sweden: RILEM Publications SARL

Hisseine, O.A., Basic, N., Omran, A.F. and Tagnit-Hamou, A. (2018). Feasibility of using cellulose filaments as a viscosity modifying agent in self-consolidating concrete. *Cement and Concrete Composites* 94(September), pp. 327–340. Available at: https://doi.org/10.1016/j.cemconcomp.2018.09.009.

Huseien, G.F. and Shah, K.W. (2020). Durability and life cycle evaluation of self-compacting concrete containing fly ash as GBFS replacement with alkali activation. *Construction and Building Materials* 235, p. 117458. Available at: https://doi.org/10.1016/j.conbuildmat.2019.117458.

Hwang, H., Lee, S. and Sakai, E. (2009). Rheological behavior of a slag cement paste prepared by adjusting the particle size distribution. *JOURNAL OF CERAMIC PROCESSING RESEARCH* 10(4), pp. 409–413.

Jain, A., Gupta, R. and Chaudhary, S. (2020). Sustainable development of self-compacting concrete by using granite waste and fly ash. *Construction and Building Materials* 262, p. 120516.

Jalal, M., Pouladkhan, A., Harandi, O.F. and Jafari, D. (2015). Comparative study on effects of Class F fly ash, nano silica and silica fume on properties of high performance self compacting concrete. *Construction and Building Materials* 94, pp. 90–104.

Jeong, Y., Eun, J., Jun, Y., Park, J. and Ha, J. (2016). In fl uence of four additional activators on hydrated-lime [Ca (OH) 2] activated ground granulated blast-furnace slag. *Cement and Concrete Composites* 65, pp. 1–10.

Jonasson, J.E. (1988). Hett—A computer program for the calculationof strength, equivalent hydration period and temperature. *Swedish Cement and Concrete Research Institute, Stockholm, Sweden (in Swedish)*

Kabagire, K.D., Diederich, P., Yahia, A. and Chekired, M. (2017). Experimental assessment of the effect of particle characteristics on rheological properties of model mortar. *Construction and Building Materials* 151, pp. 615–624.

Karihaloo, B.L. and Ghanbari, A. (2012). Mix proportioning of self-compacting high and ultra high performance concretes with and without steel fibres. *Magazine of Concrete Research* 64(12), pp. 1089–1100.

Khatib, J.M. and Hibbert, J.J. (2005). Selected engineering properties of concrete incorporating slag and metakaolin. *Construction and Building Materials* 19(6), pp. 460–472.

Khatri, R.P. and Sirivivatnanon, V. (1995). Effect of different supplementary cementitious materials on mechanical properties of high performance concrete. *Cement and Concrete Research* 25(1), pp. 209–220.

Khayat, K.H. (1995). Effects of Antiwashout Admixtures on Fresh Concrete Properties. *ACI Materials Journal* 92, pp. 164–171.

Khayat, K.H., Ghezal, A. and Hadriche, M.S. (1999a). Factorial design models for proportioning self- consolidating concrete. *Materials and Structures* 32(November), pp.

679–686.

Khayat, K.H., Hu, C. and Monty, H. (1999b). *Stability of self-consolidating concrete, Advantages, and Potential Applications*. Skarendah, A. and Petersson, Ö. eds. Paris, France: RILEM Publications SARL.

Khayat, K.H. (1999). Workability, testing, and performance of self-consolidating concrete. *ACI Materials Journal* 96(3), pp. 346–353.

Khayat, K.H., Ghezal, A. and Hadriche, M.S. (2000). Utility of statistical models in proportioning self- consolidating concrete. *Materials and Structures* 33(June), pp. 338–344.

Khayat, K.H., Meng, W., Vallurupalli, K. and Teng, L. (2019). Rheological properties of ultra-high-performance concrete — An overview. *Cement and Concrete Research* 124(March), p. 105828.

Kheder, G.F. and Al Jadiri, R.S. (2010). New method for proportioning self-consolidating concrete based on compressive strength requirements. *ACI Materials Journal* 107(5), pp. 490–497.

Khokhar, M.I.A., Roziere, E., Turcry, P., Grondin, F. and Loukili, A. (2010). Mix design of concrete with high content of mineral additions: Optimisation to improve early age strength. *Cement and Concrete Composites* 32(5), pp. 377–385.

Knudsen, T. (1982). Modeling hydration of Portland cement—the effect of particle size distribution. In: *Proceedings of the engineering foundation conference on characterization and performance prediction of cement and concrete*.

Koehler, E.P., Fowler, D.W., Folet, E.H., Rogers, G.J., Watanachet, S. and Jung, M.J. (2007). *Self-Consolidating Concrete for Precast Structural Applications :Mixture Proportions, Workability, and Early-Age Hardened Properties, Aggregates Foundation for Technology: Research and Education*. University of Texas, Austin, CTR Technical Report: 0-5134-1, pp.

372.

Koehler, E.P. and Fowler, D.W. (2007). *Aggregates in self-consolidating concrete. International Center for Aggregates Research (ICAR)*. The University of Texas at Austin, USA.

Kou, S.C., Poon, C.S. and Agrela, F. (2011). Comparisons of natural and recycled aggregate concretes prepared with the addition of different mineral admixtures. *Cement and Concrete Composites* 33(8), pp. 788–795.

Krieger, I.M. (1959). A mechanism for Non-Newtonian flow in suspensions of rigid spheres. *Journal of Rheology.* 3(1), pp. 137–152.

Krieger, I.M. and Dougherty, T.J. (1959). A mechanism for Non-Newtonian flow in suspensions of rigid spheres. *Journal of Rheology.* 3(1), pp. 137–152.

de Kruif, C.G., Iersel, E.M.F. and Vrij, A. (1985). Hard sphere colloidal dispersions: Viscosity as a function of shear rate and volume fraction. *The Journal of chemical physics* 83(9), pp. 4717–4725.

Lachemi, M., Hossain, K.M. a, Lambros, V. and Bouzoubaâ, N. (2003). Development of Cost-Effective Self-Consolidating Concrete Incorporating Fly Ash, Slag Cement, or Viscosity-Modifying Admixtures. *ACI Materials Journal* 100(100), pp. 419–425.

Lachemi, M., Hossain, K.M. a, Lambros, V., Nkinamubanzi, P.C. and Bouzoubaâ, N. (2004). Self-consolidating concrete incorporating new viscosity modifying admixtures. *Cement and Concrete Research* 34(6), pp. 917–926.

Leemann, A. and Winnefeld, F. (2007). The effect of viscosity modifying agents on mortar and concrete. *Cement and Concrete Composites* 29(5), pp. 341–349.

Leung, P.W.C. and Wong, H.D. (2011). *Final Report on Durability and Strength Development of Ground Granulated Blastfurnace Slag Concrete*. Hong Kong.

Li, H., Huang, F., Yi, Z., Wang, Z., Zhang, Y. and Yang, Z. (2020). Investigations of mixing technique on the rheological properties of self-compacting concrete. *Applied Sciences (Switzerland)* 10(15). doi: 10.3390/app10155189.

Li, L.G. and Kwan, A.K.H. (2011). Mortar design based on water film thickness. *Construction and Building Materials* 25(5), pp. 2381–2390.

Li, L.G. and Kwan, A.K.H. (2013). Concrete mix design based on water film thickness and paste film thickness. *Cement and Concrete Composites* 39, pp. 33–42.

Li, Q., Li, Z. and Yuan, G. (2012). Effects of elevated temperatures on properties of concrete containing ground granulated blast furnace slag as cementitious material. *Construction and Building Materials* 35, pp. 687–692.

Long, G., Gao, Y. and Xie, Y. (2015). Designing more sustainable and greener self-compacting concrete. *Construction and Building Materials* 84, pp. 301–306. doi: 10.1016/j.conbuildmat.2015.02.072.

Ma, S. and Kawashima, S. (2020). Investigating the Working Mechanisms of Viscosity-Modifying Admixtures through Rheological and Water Transport Properties. *Journal of Materials in Civil Engineering* 32(2), p. 04019357. doi: 10.1061/(asce)mt.1943-5533.0003018.

Macosko, C.W. (1994). *Rheology: Principles, measurements and applications*. USA: Wiley-VCH.

Manawadu, A.K., Wijesinghe, W.M.K.B. and Abeyruwan, H. (2015). Rheological Behaviour of Cement Paste with Fly Ash in the Formulation of Self- Compacting Concrete (SCC). Sri Lanka

Megat Johari, M.A., Brooks, J.J., Kabir, S. and Rivard, P. (2011). Influence of supplementary cementitious materials on engineering properties of high strength concrete. *Construction and Building Materials* 25(5), pp. 2639–2648.

Mehta, P.K. (1994). Mineral admixtures for concrete-an overview of recent developments. Advances in Cement and Concrete. In: Grutzeck, M. W. and Sarkar, S. L. eds. *Proceedings of Engineering Foundation Conference*. New yourk, USA: American Society of Civil Engineers, pp. 243–256.

Mills, R.H. (1966). Factors Influencing Cessation of Hydration in Water Cured Cement Pastes. *Highway Research Board Special Report* (90)

Mrema, A.L. (2010). Comparison of the properties of portland cement and portland-limestone cement. *Advances and Trends in Structural Engineering, Mechanics and Computation - Proceedings of the 4th International Conference on Structural Engineering, Mechanics and Computation, SEMC 2010* (Cem I), pp. 951–954.

Naik, T.R., Kumar, R., Ramme, B.W. and Canpolat, F. (2012). Development of high-strength, economical self-consolidating concrete. *Construction and Building Materials* 30, pp. 463–469.

NCE (2014). Concrete: Cool customer. Available at: http://www.newcivilengineer.com/technical-excellence/concrete-cool-customer/8670399.article.

Nehdi, M. and Rahman, M.-A.A. (2004). Estimating rheological properties of cement pastes using various rheological models for different test geometry, gap and surface friction. *Cement and Concrete Research* 34(11), pp. 1993–2007.

Neville, A.M. (1995). *Properties of concrete*. Longman London.

OCCDC (2021). *Reinforced concrete reference guide*. Available at: https://rebar.org/wp-content/uploads/2017/03/OCCDC-Reference-Guide-V3.pdf.

Okamura, H. and Ouchi, M. (1998). Self-compacting high performance concrete. *Progress in Structural Engineering and Materials* 1(4), pp. 378–383.

Okamura, H. and Ouchi, M. (1999). Self-compacting concrete, present use and future. In: Skarendah, A. and Petersson, Ö. eds. *1st International RILEM Symposium on Self-Compacting Concrete*. Stockholm, Sweden: RILEM Publications SARL, pp. 3–14.

Okamura, H. and Ouchi, M. (2003). Self-Compacting Concrete. *Advanced Concrete Technology* 1(1), pp. 5–15.

Omran, A. and Alkhyat, K. (2016). Models to predict form pressure exerted by SCC – results of six field campaignsity. In: *SCC 2016 8 th International RILEM Symposium on Self-Compacting Concrete- Flowing toward Sustainability*., p. 1196.

Oner, A. and Akyuz, S. (2007). An experimental study on optimum usage of GGBS for the compressive strength of concrete. *Cement and Concrete Composites* 29(6), pp. 505–514.

Örjan Petersson, P.B. (1999). Investegation of blocking of self compacting concrete.pdf. In: Skarendah, A. and Petersson, Ö. eds. *1st International RILEM Symposium on Self-Compacting Concrete*. Stockholm, Sweden: RILEM Publications SARL

Ostrowski, K., Stefaniuk, D., Sadowski, Ł., Krzywiński, K., Gicala, M. and Różańska, M. (2020). Potential use of granite waste sourced from rock processing for the application as coarse aggregate in high-performance self-compacting concrete. *Construction and Building Materials* 238, pp. 1–14. doi: 4.

Ouchi, M., Hibino, M., Ozawa, K. and Okamura, H. (1998). A rational mix-design method for mortar in self-compacting concrete. *Structural Engineering & Construction: Tradition, Present and Future.* 2, pp. 1307–1312.

Owsiak, Z. and Grzmil, W. (2015). The evaluation of the influence of mineral additives on the durability of self-compacting concretes. *KSCE Journal of Civil Engineering* 19(4), pp. 1002–1008. doi: 10.1007/s12205-013-0336-7.

Özbay, E., Erdemir, M. and Durmuş, H.İ. (2016). Utilization and efficiency of ground granulated blast furnace slag on concrete properties – A review. *Construction and*

Building Materials 105, pp. 423–434.

Paine, K.A., Zheng, L. and Dhir, R.K. (2005). Experimental study and modelling of heat evolution of blended cements. *Advances in Cement Research* 17(3), pp. 121–132.

Pan, Z., Zhou, J., Jiang, X., Xu, Y., Jin, R., Ma, J., Zhuang, Y., Diao, Z., Zhang, S., Si, Q. and Chen, W. (2019). Investigating the effects of steel slag powder on the properties of self-compacting concrete with recycled aggregates. *Construction and Building Materials* 200, pp. 570–577.

Park, C.K., Noh, M.H. and Park, T.H. (2005). Rheological properties of cementitious materials containing mineral admixtures. *Cement and Concrete Research* 35, pp. 842–849.

PCI (2003). *Interim Guidelines for the Use of Self-Consolidating Concrete in Precast/Prestressed Concrete Institute Member Plants*.

Perkins, T. (2021). Building materials. Available at: https://www.travisperkins.co.uk.

Piekarczyk, B.Ł.- (2013). Effect of viscosity type modifying admixture on porosity , compressive strength and water penetration of high performance self-compacting concrete. *Construction and Building Materials* 48, pp. 1035–1044.

Powers, T.C. (1958). Structure and physical properties of hardened Portland cement paste. *JJournal of the American Ceramic Society* 41(1), pp. 1–6.

Qian, Y. and De Schutter, G. (2018). Different effects of NSF and PCE superplasticizer on adsorption, dynamic yield stress and thixotropy of cement pastes. *Materials* 11(5)

Ramanathan, P., Baskar, I., Muthupriya, P. and Venkatasubramani, R. (2013). Performance of self-compacting concrete containing different mineral admixtures. *KSCE Journal of Civil Engineering* 17(2), pp. 465–472.

Revilla-Cuesta, V., Skaf, M., Faleschini, F., Manso, J.M. and Ortega-López, V. (2020). Self-compacting concrete manufactured with recycled concrete aggregate: An overview.

Journal of Cleaner Production 262

RILEM TC174 (2000). *Self-compacting concrete*. Skarendahl, Å. and Petersson, Ö. eds. Stockholm, Sweden: RILEM Publications S.A.R.L.

Roussel, N. (2006). A Theoretical Frame to Study Stability of Fresh Concrete. *Materials and Structures* 39(1), pp. 81–91.

Roussel, N. (2007). Rheology of fresh concrete: from measurements to predictions of casting processes. *Materials and Structures* 40(10), pp. 1001–1012.

Saak, A.W., Jennings, H.M. and Shah, S.P. (2001a). New methodology for designing self-compacting concrete. *ACI Materials Journal* 98(6), pp. 429–439.

Saak, A.W., Jennings, H.M. and Shah, S.P. (2001b). New methodology for designing self-compacting concrete. *ACI Materials Journal* 98(6), pp. 429–439.

Saranya, P., Nagarajan, P. and Shashikala, A.P. (2018). Eco-friendly GGBS Concrete: A State-of-The-Art Review. *IOP Conference Series: Materials Science and Engineering* 330(1)

Schindler, A.K. (2002). *Concrete Hydration , Temperature Development , and Setting at Early-Ages*.

Schindler, A.K. and Folliard, K.J. (2005). Heat of hydration models of cementitious materials. *Advances in Cement Research* 102(1)

Sharma, R. and Khan, R.A. (2018). Influence of copper slag and metakaolin on the durability of self compacting concrete. *Journal of Cleaner Production* 171, pp. 1171–1186. Available at: https://doi.org/10.1016/j.jclepro.2017.10.029.

Shi, C., Wu, Z., Lv, K. and Wu, L. (2015). A review on mixture design methods for self-compacting concrete. *Construction and Building Materials* 84, pp. 387–398.

Shi, C., Jiao, D. and Yuan, Q. (2018). Mixture design of concrete based on rheology. In:

Zhang, C. S. & Z. and Khayat, K. H. K. H. eds. *4th International Symposium on Design, Performance and Use ofSelf-Consolidating Concrete SCC'*. Changsha, China, pp. 3–15.

Shi, H., Xu, B. and Zhou, X. (2009). Influence of mineral admixtures on compressive strength, gas permeability and carbonation of high performance concrete. *Construction and Building Materials* 23(5), pp. 1980–1985.

Siddique, R. (2013). Compressive strength, water absorption, sorptivity, abrasion resistance and permeability of self-compacting concrete containing coal bottom ash. *Construction and Building Materials* 47, pp. 1444–1450.

Skarendahl, A. and Petersson, Ö. (1999). Self-Compacting Concrete. In: *PRO 7: 1st International RILEM Symposium*. Stockholm, Sweden: RILEM publications, p. 768.

Solutions, M. builder (2021). Master Gelenium ACE 499. *High-Range Water Reducing Admixture for Concrete*

Sonebi, M., Abdalqader, A., Fayyad, T., Perrot, A. and Bai, Y. (2020). Optimisation of rheological parameters, induced bleeding, permeability and mechanical properties of supersulfated cement grouts. *Construction and Building Materials* 262, p. 120078.

Sonebi, M. and Yahia, A. (2020). Mix design procedure, tests, and standards. In: Siddique, R. ed. *Self-Compacting Concrete: Materials, Properties and Applications*. Cambidge: Elsevier Inc., pp. 1–30.

Struble, L. and Sun, G.K. (1995). Viscosity of Portland cement paste as a function of concentration. *Advanced Cement Based Materials* 2(2), pp. 62–69.

Sun, Z., Voigt, T. and Shah, S.P. (2006). Rheometric and ultrasonic investigations of viscoelastic properties of fresh Portland cement pastes. *Cement and Concrete Research* 36(2), pp. 278–287.

Tangtermsirkul, S. and Khayat, K.H. (2000). Fresh concrete: properties and tests: part III.,

pp. 17–22.

Taplin, J.H. (1959). A Method for Following the Hydration Reaction in Portland Cement Paste. *Australian Journal of Applied Science* 10, pp. 329–345.

TARMAC (2021). Tarmac, cement and lime. Available at: http://www.tarmac.com/dop.

Tattersall, G.H. and Banfill, P.F.G. (1983). *The rheology of fresh concrete*. Pitman Advanced Pub. Program.

Tattersall, H. (1991). *Workability and quality control of concrete.* First Edit. London: Taylor & Francis Publication.

Tiwari, A.K., Panseriya, M.M., Mathur, P.C. and Chowdhury, S. (2015). Effect of supplementary cementitious materials on the rheology of blended cements. *Journal of Materials in Civil Engineering* 303, pp. 205–216.

Topçu, I.B., Karakurt, C. and Saridemir, M. (2008). Predicting the strength development of cements produced with different pozzolans by neural network and fuzzy logic. *Materials and Design* 29(10), pp. 1986–1991.

Topcu, I.B. and Boga, A.R. (2010). Effect of ground granulate blast-furnace slag on corrosion performance of steel embedded in concrete. *Materials and Design* 31(7), pp. 3358–3365.

Topçu, I.B. and Uğurlu, A. (2003). Effect of the use of mineral filler on the properties of concrete. *Cement and Concrete Research* 33(7), pp. 1071–1075. doi: 10.1016/S0008-8846(03)00015-2.

Türkel, S. and Kandemir, A. (2010). Fresh and Hardened Properties of SCC Made with Different Aggregate and Mineral Admixtures. *Journal of Materials in Civil Engineering* 22(10), pp. 1025–1032.

UKQAA (2010). Technical datasheet: embodied CO2e of UK cement, additions and

cementitious material. 44(0), pp. 1–11.

Unibeton (2013). Landmark Abu Dhabi 2007. Available at: http://www.unibetonrm.com/en-gl/news/largest-quantity-of-self-compacting-concrete-in-the-world.

Uomoto, T. and Ozawa, K. (1999). Recommendation for self-compacting concrete. *JSCE* , p. 1999.

Uysal, M. and Yilmaz, K. (2011). Effect of mineral admixtures on properties of self-compacting concrete. *Cement and Concrete Composites* 33(7), pp. 771–776.

Valcuende, M., Parra, C., Marco, E., Garrido, A., Martínez, E. and Cánoves, J. (2012). Influence of limestone filler and viscosity-modifying admixture on the porous structure of self-compacting concrete. *Construction and Building Materials* 28(1), pp. 122–128.

Vasilić, K. (2015). *A Numerical Model for Self-Compacting Concrete Flow through Reinforced Sections : a Porous Medium Analogy*. PhD thesis, Faculty of Civil Engineering, The Technical University of Dresden, Berlin, Germany.

Vittalaiah, A., Ravinder, R. and Vivek Kumar, C. (2020). Study on effect of strength and durability parameters and performance of Self Compacting Concrete replacement with GGBS at different dosages. *E3S Web of Conferences* 184, pp. 2–6.

Voigt, T., Malonn, T. and Shah, S.P. (2006). Green and early age compressive strength of extruded cement mortar monitored with compression tests and ultrasonic techniques. *Cement and Concrete Research* 36(5), pp. 858–867.

Wallevik, J.E. (2009). Rheological properties of cement paste: Thixotropic behavior and structural breakdown. *Cement and Concrete Research* 39(1), pp. 14–29.

Wallevik, O.H. and Wallevik, J.E. (2011). Rheology as a tool in concrete science : The use of rheographs and workability boxes. *Cement and Concrete Research* 41(12), pp. 1279–

1288.

Wang, K., Konsta-gdoutos, M.S. and Shah, S.P. (2002). Hydration , rheology , and strength of ordinary Portland cement (OPC) -cement kiln dust (CKD) -slag binders. *ACI Materials Journal* (99), pp. 173–179.

Yan, W., Cui, W. and Qi, L. (2020). Effect of aggregate gradation and mortar rheology on static segregation of self-compacting concrete. *Construction and Building Materials* 259, p. 119816.

Ye, G., Liu, X., De Schutter, G., Poppe, A.-M. and Taerwe, L. (2007). Influence of limestone powder used as filler in SCC on hydration and microstructure of cement pastes. *Cement and Concrete Composites* 29, pp. 94–102.

Zhang, J., Gao, X. and Yu, L. (2020). Improvement of viscosity-modifying agents on air-void system of vibrated concrete. *Construction and Building Materials* 239, p. 117843. Available at: https://doi.org/10.1016/j.conbuildmat.2019.117843.

Zhu, W. and Gibbs, J.C. (2005). Use of different limestone and chalk powders in self-compacting concrete. *Cement and Concrete Research* 35(July 2004), pp. 1457–1462.

Appendixes

Appendix A The instructions of using viscometer type NDJ-8S

Table A1 Viscometer type (NDJ-8S) specification and measurements details

Specification	Description
• Measuring range	1mPa s ~ 2000,000mPa s (Below 15 cp requires ULR ultra-low viscosity adapter)
• Displaying resolution	0.01mPa s
• Measurement accuracy	±2% (full measuring range)
• Rotor spec.	Rotor #1, #2, #3, and #4 (Rotor #0 is optional)
• Rotating speed	0.3, 0.6, 1.5, 3, 6, 12, 30, and 60 rpm
• Sample volume	300mL – 400mL

Figure A1 Viscometer type NDJ-8S

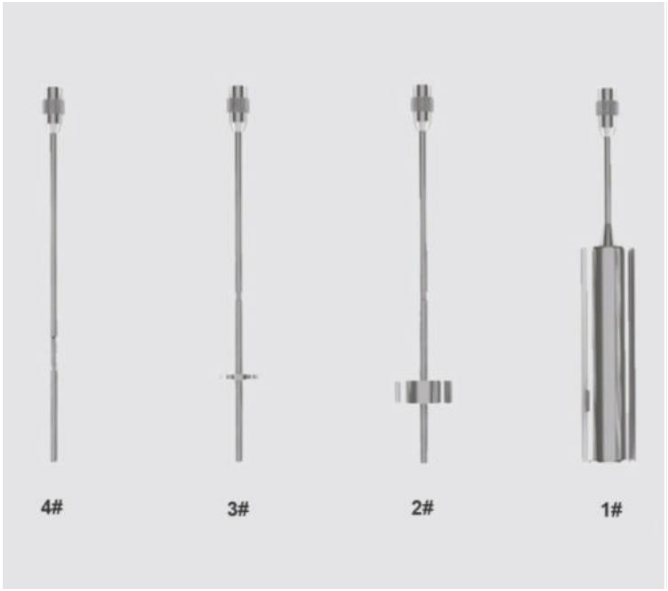

Figure A2 Rotor number and shape for viscometer NDJ-8S

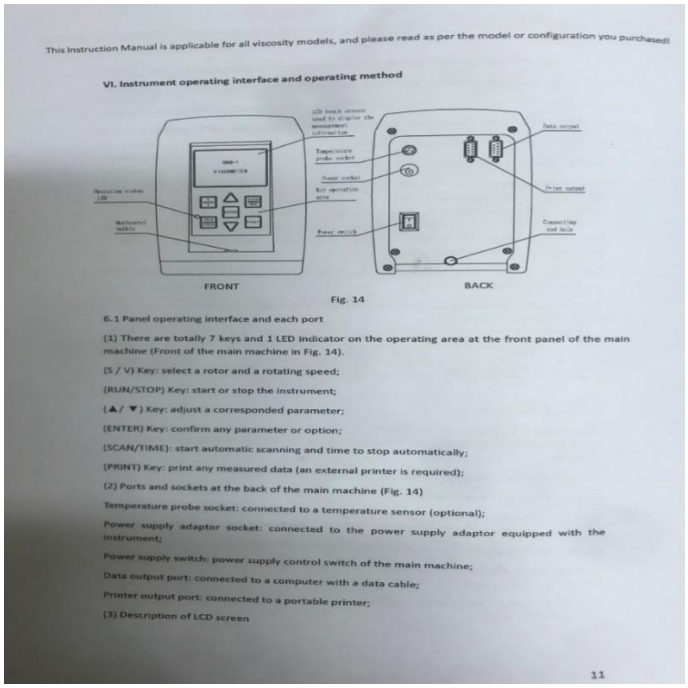

This Instruction Manual is applicable for all viscosity models, and please read as per the model or configuration you purchased!

VI. Instrument operating interface and operating method

FRONT BACK

Fig. 14

6.1 Panel operating interface and each port

(1) There are totally 7 keys and 1 LED indicator on the operating area at the front panel of the main machine (Front of the main machine in Fig. 14).

(S / V) Key: select a rotor and a rotating speed;

(RUN/STOP) Key: start or stop the instrument;

(▲/ ▼) Key: adjust a corresponded parameter;

(ENTER) Key: confirm any parameter or option;

(SCAN/TIME): start automatic scanning and time to stop automatically;

(PRINT) Key: print any measured data (an external printer is required);

(2) Ports and sockets at the back of the main machine (Fig. 14)

Temperature probe socket: connected to a temperature sensor (optional);

Power supply adaptor socket: connected to the power supply adaptor equipped with the instrument;

Power supply switch: power supply control switch of the main machine;

Data output port: connected to a computer with a data cable;

Printer output port: connected to a portable printer;

(3) Description of LCD screen

11

Figure A3 Instruction from user manual

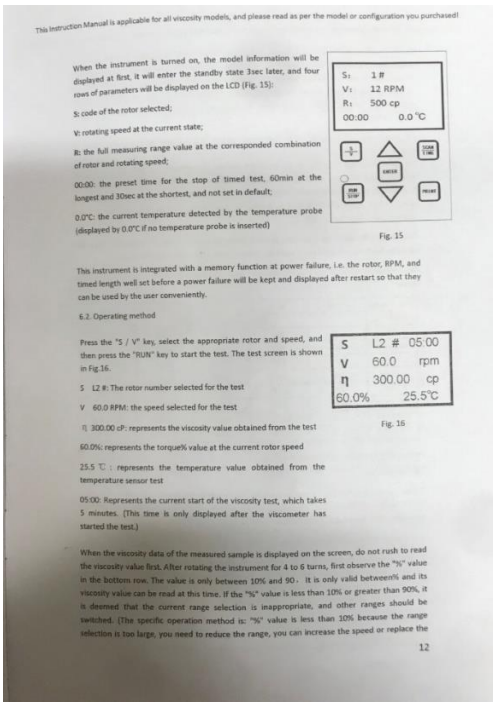

This Instruction Manual is applicable for all viscosity models, and please read as per the model or configuration you purchased!

When the instrument is turned on, the model information will be displayed at first. It will enter the standby state 3sec later, and four rows of parameters will be displayed on the LCD (Fig. 15):

S: code of the rotor selected;

V: rotating speed at the current state;

R: the full measuring range value at the corresponded combination of rotor and rotating speed;

00:00: the preset time for the stop of timed test, 60min at the longest and 30sec at the shortest, and not set in default;

0.0℃: the current temperature detected by the temperature probe (displayed by 0.0℃ if no temperature probe is inserted)

S: 1 #
V: 12 RPM
R: 500 cp
00:00 0.0 ℃

Fig. 15

This instrument is integrated with a memory function at power failure, i.e. the rotor, RPM, and timed length well set before a power failure will be kept and displayed after restart so that they can be used by the user conveniently.

6.2. Operating method

Press the "S / V" key, select the appropriate rotor and speed, and then press the "RUN" key to start the test. The test screen is shown in Fig.16.

S L2 #: The rotor number selected for the test

V 60.0 RPM: the speed selected for the test

η 300.00 cP: represents the viscosity value obtained from the test

60.0%: represents the torque% value at the current rotor speed

25.5 ℃ : represents the temperature value obtained from the temperature sensor test

05:00: Represents the current start of the viscosity test, which takes 5 minutes. (This time is only displayed after the viscometer has started the test.)

S L2 # 05:00
V 60.0 rpm
η 300.00 cp
60.0% 25.5℃

Fig. 16

When the viscosity data of the measured sample is displayed on the screen, do not rush to read the viscosity value first. After rotating the instrument for 4 to 6 turns, first observe the "%" value in the bottom row. The value is only between 10% and 90 - It is only valid between% and its viscosity value can be read at this time. If the "%" value is less than 10% or greater than 90%, it is deemed that the current range selection is inappropriate, and other ranges should be switched. (The specific operation method is: "%" value is less than 10% because the range selection is too large, you need to reduce the range, you can increase the speed or replace the

12

Figure A4 Instruction from user manual

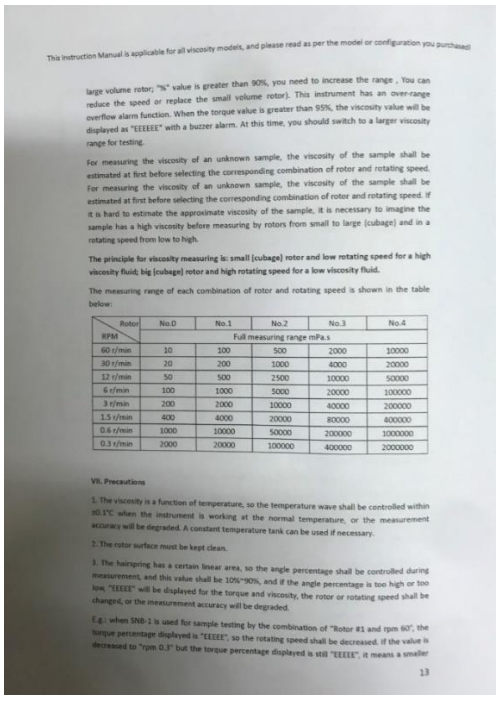

This Instruction Manual is applicable for all viscosity models, and please read as per the model or configuration you purchased!

large volume rotor; "%" value is greater than 90%, you need to increase the range , You can reduce the speed or replace the small volume rotor). This instrument has an over-range overflow alarm function. When the torque value is greater than 95%, the viscosity value will be displayed as "EEEEEE" with a buzzer alarm. At this time, you should switch to a larger viscosity range for testing.

For measuring the viscosity of an unknown sample, the viscosity of the sample shall be estimated at first before selecting the corresponding combination of rotor and rotating speed. For measuring the viscosity of an unknown sample, the viscosity of the sample shall be estimated at first before selecting the corresponding combination of rotor and rotating speed. If it is hard to estimate the approximate viscosity of the sample, it is necessary to imagine the sample has a high viscosity before measuring by rotors from small to large (cubage) and in a rotating speed from low to high.

The principle for viscosity measuring is: small (cubage) rotor and low rotating speed for a high viscosity fluid; big (cubage) rotor and high rotating speed for a low viscosity fluid.

The measuring range of each combination of rotor and rotating speed is shown in the table below:

Rotor / RPM	No.0	No.1	No.2	No.3	No.4
	Full measuring range mPa.s				
60 r/min	10	100	500	2000	10000
30 r/min	20	200	1000	4000	20000
12 r/min	50	500	2500	10000	50000
6 r/min	100	1000	5000	20000	100000
3 r/min	200	2000	10000	40000	200000
1.5 r/min	400	4000	20000	80000	400000
0.6 r/min	1000	10000	50000	200000	1000000
0.3 r/min	2000	20000	100000	400000	2000000

VII. Precautions

1. The viscosity is a function of temperature, so the temperature wave shall be controlled within ±0.1℃ when the instrument is working at the normal temperature, or the measurement accuracy will be degraded. A constant temperature tank can be used if necessary.

2. The rotor surface must be kept clean.

3. The hairspring has a certain linear area, so the angle percentage shall be controlled during measurement, and this value shall be 10%~90%, and if the angle percentage is too high or too low, "EEEEE" will be displayed for the torque and viscosity, the rotor or rotating speed shall be changed, or the measurement accuracy will be degraded.

E.g.: when SNB-1 is used for sample testing by the combination of "Rotor #1 and rpm 60", the torque percentage displayed is "EEEEE", so the rotating speed shall be decreased. If the value is decreased to "rpm 0.3" but the torque percentage displayed is still "EEEEE", it means a smaller

13

Figure A5 Instruction from user manual

Appendix B Processed row data from literature justified to 100 mm cube

Table B1 Compressive strength data for ggbs 30 % gathered from references

Ref.	ggbs	w/b	fcu
(Oner and Akyuz, 2007)	0.30	0.87	23.5
(Oner and Akyuz, 2007)	0.30	0.75	30.0
(Oner and Akyuz, 2007)	0.30	0.66	36.1
(Oner and Akyuz, 2007)	0.30	0.59	41.8
(Güneyisi and Gesoğlu, 2011)	0.30	0.35	63.6
(Bharatkumar et al., 2001)	0.35	0.30	72.9
(Li et al., 2012)	0.30	0.41	57.7
(Shi et al., 2009)	0.30	0.28	95.0
(Shi et al., 2009)	0.30	0.28	87.6

Table B2 Compressive strength data for ggbs 40 % gathered from references

Ref.	ggbs	w/b	fcu
(Deeb and Karihaloo, 2013)	0.40	0.56	35.0
(Deeb and Karihaloo, 2013)	0.40	0.55	45.0
(Oner and Akyuz, 2007)	0.40	0.74	27.0
(Oner and Akyuz, 2007)	0.40	0.64	34.0
(Oner and Akyuz, 2007)	0.40	0.57	41.4
(Oner and Akyuz, 2007)	0.40	0.51	47.5
(Chidiac and Panesar, 2008)	0.40	0.31	88.0
(Duran Atiş and Bilim, 2007)	0.40	0.30	82.7
(Duran Atiş and Bilim, 2007)	0.40	0.30	85.5
(Duran Atiş and Bilim, 2007)	0.40	0.30	83.7
(Duran Atiş and Bilim, 2007)	0.40	0.40	68.6
(Duran Atiş and Bilim, 2007)	0.40	0.40	68.2
(Duran Atiş and Bilim, 2007)	0.40	0.40	67.8
(Duran Atiş and Bilim, 2007)	0.40	0.50	57.0

(Duran Atiş and Bilim, 2007)	0.40	0.50	52.7
(Duran Atiş and Bilim, 2007)	0.40	0.50	50.3
Current study	0.40	0.68	35.0
Current study	0.40	0.56	43.0
Current study	0.40	0.48	50.0
Current study	0.40	0.40	61.7
Current study	0.40	0.34	71.0
Current study	0.40	0.29	78.0

Table B3 Compressive strength data for ggbs 50 % gathered from references

Ref.	ggbs	w/b	fcu
(Oner and Akyuz, 2007)	0.50	0.66	27.8
(Oner and Akyuz, 2007)	0.50	0.57	34.9
(Oner and Akyuz, 2007)	0.50	0.51	42.3
(Oner and Akyuz, 2007)	0.50	0.47	48.4
(Güneyisi and Gesoğlu, 2011)	0.50	0.50	40.0
(Bharatkumar et al., 2001)	0.50	0.50	42.9
(Chidiac and Panesar, 2008)	0.50	0.31	79.0
(Li et al., 2012)	0.50	0.41	56.8
Current study	0.50	0.42	58.1

Table B4 Compressive strength data for ggbs 60 % gathered from references

Ref.	ggbs	w/b	fcu
(Oner and Akyuz, 2007)	0.56	0.60	27.2
(Oner and Akyuz, 2007)	0.56	0.52	34.5
(Oner and Akyuz, 2007)	0.56	0.47	41.5
(Oner and Akyuz, 2007)	0.56	0.43	47.0
(Oner and Akyuz, 2007)	0.61	0.55	25.1
(Oner and Akyuz, 2007)	0.61	0.48	31.8
(Oner and Akyuz, 2007)	0.61	0.44	37.5
(Oner and Akyuz, 2007)	0.61	0.41	42.7
(Chidiac and Panesar, 2008)	0.60	0.31	79.0
(Becknell and Hale, 2011)	0.60	0.45	50.1

(Becknell and Hale, 2011)	0.60	0.45	47.6
(Becknell and Hale, 2011)	0.60	0.45	40.2
(Becknell and Hale, 2011)	0.60	0.45	44.1
(Shi et al., 2009)	0.60	0.30	72.0
(Shi et al., 2009)	0.60	0.35	57.0
(Duran Atiş and Bilim, 2007)	0.60	0.30	74.8
(Duran Atiş and Bilim, 2007)	0.60	0.30	79.4
(Duran Atiş and Bilim, 2007)	0.60	0.30	82.2
(Duran Atiş and Bilim, 2007)	0.60	0.50	40.9
(Duran Atiş and Bilim, 2007)	0.60	0.50	40.3
(Megat Johari et al., 2011)	0.60	0.28	86.7
Current study	0.60	0.40	57.0

Table B5 Compressive strength data for ggbs 70 % gathered from references

ref	ggbs	w/c	fc
(Elahi et al., 2010)	0.70	0.30	74.3
(Leung and Wong, 2011)	0.70	0.53	56.3
(Leung and Wong, 2011)	0.70	0.53	56.3
(Leung and Wong, 2011)	0.70	0.47	60.8
(Leung and Wong, 2011)	0.70	0.47	66.0
(Elchalakani et al., 2014)	0.70	0.38	68.0
(Elchalakani et al., 2014)	0.70	0.38	60.8

Table B6 Compressive strength data for ggbs 80 % gathered from references

ref	ggbs	w/c	fc
(Duran Atiş and Bilim, 2007)	0.80	0.30	64.0
(Duran Atiş and Bilim, 2007)	0.80	0.30	69.1
(Duran Atiş and Bilim, 2007)	0.80	0.30	67.7

(Duran Atiş and Bilim, 2007)	0.80	0.40	51.4
(Duran Atiş and Bilim, 2007)	0.80	0.40	54.2
(Duran Atiş and Bilim, 2007)	0.80	0.40	47.8
(Duran Atiş and Bilim, 2007)	0.80	0.50	30.5
(Duran Atiş and Bilim, 2007)	0.80	0.50	25.8
(Duran Atiş and Bilim, 2007)	0.80	0.50	28.3
(Elchalakani et al., 2014)	0.80	0.38	66.0
(Elchalakani et al., 2014)	0.80	0.35	68.3
(Elchalakani et al., 2014)	0.80	0.42	54.0
(Elchalakani et al., 2014)	0.80	0.38	56.3
(Elchalakani et al., 2014)	0.80	0.38	49.5
(Khatib and Hibbert, 2005)	0.80	0.50	29.0
Current study	0.80	0.50	35.5

Appendix C Tables of compressive strength at interval times; Experimental and Estimated

Figure C1 Experimental results of compressive strength, GGBS 50%

Curing time (days)	Compressive strength, MPa			
	C1	C2	C3	C4
2	1.5	3.0	7.8	14.3
4	3.0	6.0	15.5	24.8
7	8.4	14.2	22.6	36.2
14	13.0	20.4	30.4	48.3
28	16.6	24.0	35.6	54.1
210	20.4	30.6	42.8	61.5
300	21.7	31.30	47.5	62.8

Figure C2 Exprimental and Estimated compressive strength for Mix $C1_1$

αu	τ	β	te(day)	te(hrs)	α(te)	fcu Exp.	fcu Est.
0.95	50.95	0.418	2	48	0.341	3.0	6.9
0.95	50.95	0.418	4	96	0.441	6.0	10.8
0.95	50.95	0.418	7	168	0.518	8.4	13.3
0.95	50.95	0.418	14	336	0.603	13.0	15.7
0.95	50.95	0.418	28	672	0.676	16.6	17.5
0.95	50.95	0.418	210	5040	0.821	20.4	20.9
0.95	50.95	0.418	300	7200	0.838	21.7	21.2

Figure C3 Exprimental and Estimated compressive strength for Mix $C2_1$,

αu	τ	β	te(day)	te(hrs)	α(te)	fcu Exp.	fcu Est.
0.92	50.95	0.418	2	48	0.330	5.0	10.1
0.92	50.95	0.418	4	96	0.427	11.0	16.2
0.92	50.95	0.418	7	168	0.501	14.2	20.0
0.92	50.95	0.418	14	336	0.584	20.4	23.7
0.92	50.95	0.418	28	672	0.655	24.0	26.6
0.92	50.95	0.418	210	5040	0.795	30.6	31.8
0.92	50.95	0.418	300	7200	0.811	31.30	32.4

Figure C4 Exprimental and Estimated compressive strength for Mix $C3_1$,

αu	τ	β	te(day)	te(hrs)	α(te)	fcu Exp.	fcu Est.
0.88	50.95	0.418	2	48	0.316	7.8	12.2
0.88	50.95	0.418	4	96	0.409	15.5	20.8
0.88	50.95	0.418	7	168	0.480	22.6	25.9
0.88	50.95	0.418	14	336	0.559	30.4	31.0
0.88	50.95	0.418	28	672	0.626	35.6	34.9
0.88	50.95	0.418	210	5040	0.760	42.8	41.9
0.88	50.95	0.418	300	7200	0.776	47.50	42.6

Figure C5 Exprimental and Estimated compressive strength $C4_1$,

αu	τ	β	te(day)	te(hrs)	α(te)	Fc Exp.	fc Est.
0.84	50.95	0.418	2	48	0.301	14.3	14.6
0.84	50.95	0.418	4	96	0.390	24.8	26.6
0.84	50.95	0.418	7	168	0.458	36.2	33.7
0.84	50.95	0.418	14	336	0.533	48.3	40.6
0.84	50.95	0.418	28	672	0.598	54.1	45.9
0.84	50.95	0.418	210	5040	0.726	61.5	55.4
0.84	50.95	0.418	300	7200	0.741	62.80	56.4

Appendix D Tables of estimated compressive strength at 28 days and ultimate

Figure D1 Estimated fc at 28 days from the ultimate strength for C30 target

ggbs	αu	τ	β	te(day)	te(hrs)	α(te)	fcu1(ult)	fcu1(28)
0.2	0.88	26.44	0.51	28	672	0.723	37.5	31.6
0.3	0.90	32.90	0.48	28	672	0.711	38.9	31.6
0.4	0.93	40.94	0.45	28	672	0.696	40.3	31.4
0.5	0.95	50.95	0.42	28	672	0.678	41.8	31.1
0.6	0.97	63.41	0.39	28	672	0.653	45.4	32.1
0.7	1.00	78.91	0.37	28	672	0.631	47.1	31.5
0.8	1.01	98.20	0.34	28	672	0.603	52.4	33.1

Figure D2 Estimated fc at 28 days from the ultimate strength for C40 target

ggbs	αu	τ	β	te(day)	te(hrs)	α(te)	fcu1(ult)	fcu1(28)
0.2	0.85	26.44	0.51	28	672	0.699	48.5	40.8
0.3	0.87	32.90	0.48	28	672	0.685	51.5	41.7
0.4	0.89	40.94	0.45	28	672	0.670	53.4	41.4
0.5	0.92	50.95	0.42	28	672	0.652	55.4	40.9
0.6	0.93	63.41	0.39	28	672	0.629	58.8	41.2
0.7	0.95	78.91	0.37	28	672	0.604	62.4	41.4

Figure D3 Estimated fc at 28 days from the ultimate strength for C50 target

ggbs	αu	τ	β	te(day)	te(hrs)	α(te)	fcu1(ult)	fcu1(28)
0.2	0.82	26.44	0.51	28	672	0.675	59.0	49.5
0.3	0.84	32.90	0.48	28	672	0.663	61.2	49.4
0.4	0.86	40.94	0.45	28	672	0.648	63.5	49.0
0.5	0.88	50.95	0.42	28	672	0.629	65.8	48.3
0.6	0.90	63.41	0.39	28	672	0.603	71.5	49.7

Figure D4 Estimated fc at 28 from the ultimate strength for C60 target

ggbs	αu	τ	β	te(day)	te(hrs)	α(te)	fcu1(ult)	fcu1(28)
0.2	0.79	26.44	0.51	28	672	0.651	70.5	59.0
0.3	0.81	32.90	0.48	28	672	0.639	73.1	58.7
0.4	0.83	40.94	0.45	28	672	0.623	75.9	58.2
0.5	0.84	50.95	0.42	28	672	0.601	80.5	58.7

Figure D5 Estimated fc at 28 from the ultimate strength for C70 target

ggbs	αu	τ	β	te(day)	te(hrs)	α(te)	fcu1(ult)	fcu1(28)
0.2	0.76	26.44	0.51	28	672	0.626	81.2	67.6
0.3	0.78	32.90	0.48	28	672	0.614	84.2	67.3
0.4	0.79	40.94	0.45	28	672	0.593	89.4	68.1

Figure D6 Estimated from the ultimate strength for C80 target

ggbs	αu	τ	β	te(day)	te(hrs)	α(te)	fcu1(ult)	fcu1(28)
0.2	0.72	21.32	0.65	28	672	0.651	93.4	84.6
0.3	0.75	26.53	0.61	28	672	0.650	94.6	83.1

Appendix E Compressive strength comparison; Ultimate [f_{cu2}(ult) , f_{cu1}(ult)] and [f_{cu1}(28) , f_{cu2}(28)]

Table D1 (28-days) Compressive strength comparison between Equations 5.13 and 5.16

fcu Grade	ggbs	w/b	fcu1(28)	fcu2(28)
C30	0.2	0.74	32.8	31.6
	0.3	0.72	32.4	31.6
	0.4	0.70	31.9	31.4
	0.5	0.68	31.3	31.1
	0.6	0.64	32.1	32.1
	0.7	0.62	31.2	31.5
	0.8	0.57	32.3	33.1
C40	0.2	0.63	42.2	40.8
	0.3	0.60	42.7	41.7
	0.4	0.58	42.1	41.4
	0.5	0.56	41.3	40.9
	0.6	0.53	41.3	41.2
	0.7	0.50	41.1	41.4
C50	0.2	0.54	51.9	49.5
	0.3	0.52	51.3	49.4
	0.4	0.50	50.6	49.0
	0.5	0.48	49.7	48.3
	0.6	0.44	50.8	49.7
fcu Grade	ggbs	w/b	61.0	59.0
C60	0.2	0.47	60.3	58.7
	0.3	0.45	59.4	58.2
	0.4	0.43	59.7	58.7
	0.5	0.40	70.0	67.6
C70	0.2	0.41	69.3	67.3
	0.3	0.39	69.8	68.1
	0.4	0.36	80.4	84.6
C80	0.2	0.35	77.7	83.1

	0.3	0.34	32.8	31.6

Table D2 Ultimate compressive strength MPa comparison between Equations 5.14 and 5.17

fcu Grade	ggbs	w/b	fcu1(ult)	fcu2(ult)
C30	0.2	0.74	37.5	35.5
	0.3	0.72	38.9	36.9
	0.4	0.70	40.3	38.5
	0.5	0.68	41.8	40.4
	0.6	0.64	45.4	42.5
	0.7	0.62	47.1	44.8
	0.8	0.57	52.4	47.5
C40	0.2	0.63	48.5	47.5
	0.3	0.60	51.5	49.4
	0.4	0.58	53.4	51.6
	0.5	0.56	55.4	54.2
	0.6	0.53	58.8	57.0
	0.7	0.50	62.4	60.3
C50	0.2	0.54	59.9	59.6
	0.3	0.52	62.1	62.0
	0.4	0.50	64.4	64.8
	0.5	0.48	66.8	68.1
	0.6	0.44	72.6	71.9
C60	0.2	0.47	70.5	71.7
	0.3	0.45	73.1	74.7
	0.4	0.43	75.9	78.2
	0.5	0.4	80.5	82.3
C70	0.2	0.41	81.2	84.0
	0.3	0.39	84.2	87.6
	0.4	0.36	89.4	91.9
C80	0.2	0.35	93.4	96.5
	0.3	0.34	94.6	100.7

Appendix F Heat of hydration for rang of ggbs (0-80%) and range of compressive strength (30-80) MPa

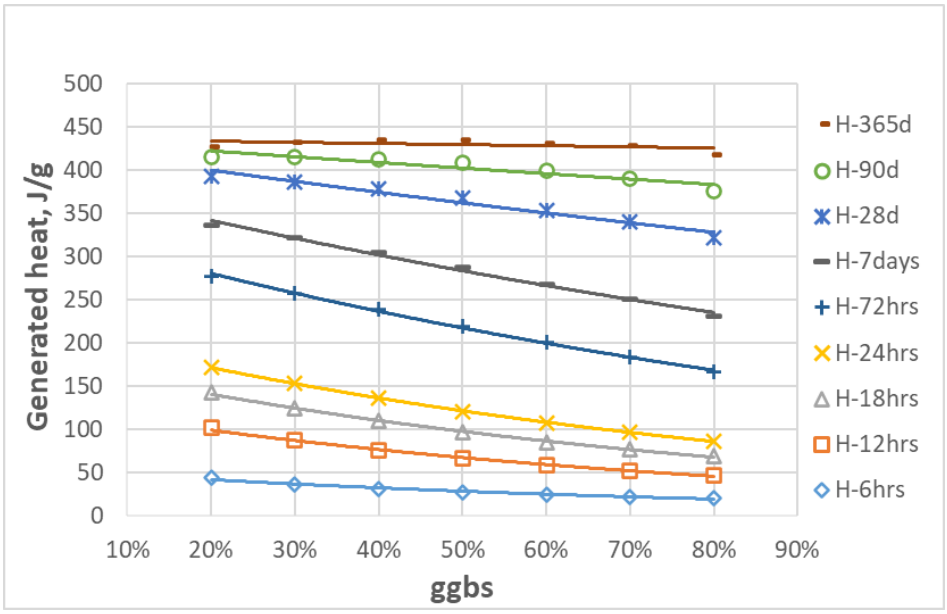

Figure F1 Heat of hydration C30 MPa

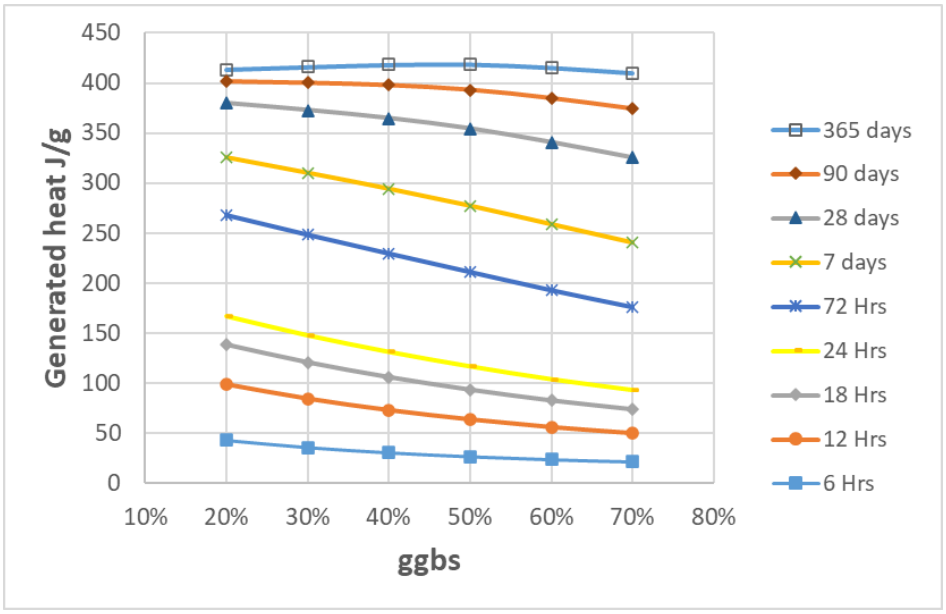

Figure F2 Heat of hydration C40 MPa

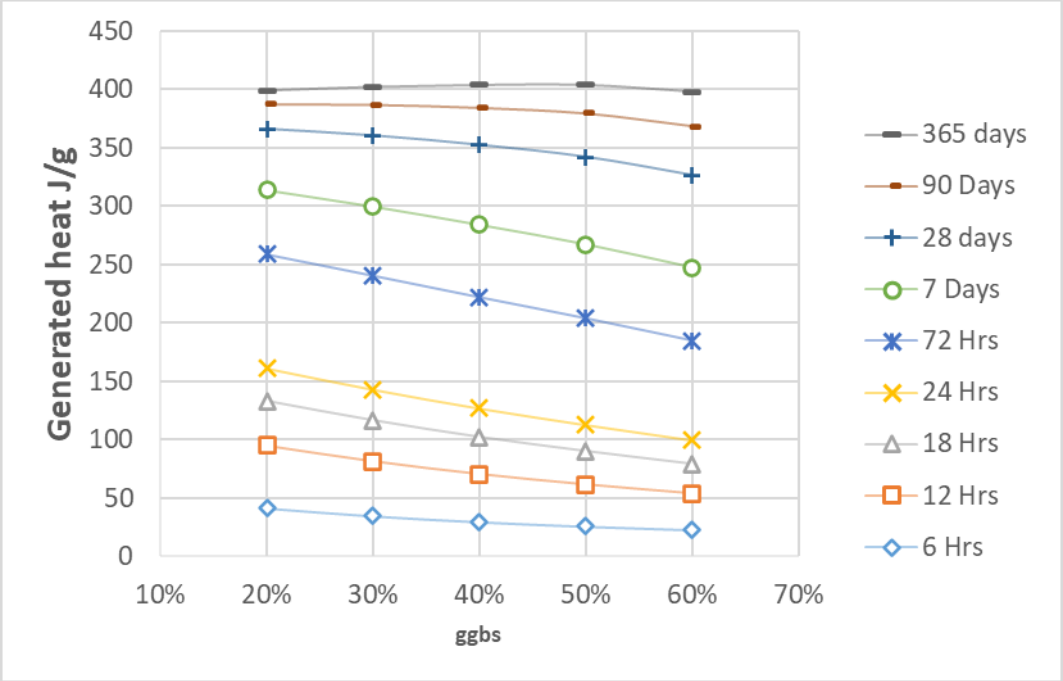

Figure F3 Heat of hydration C50 MPa

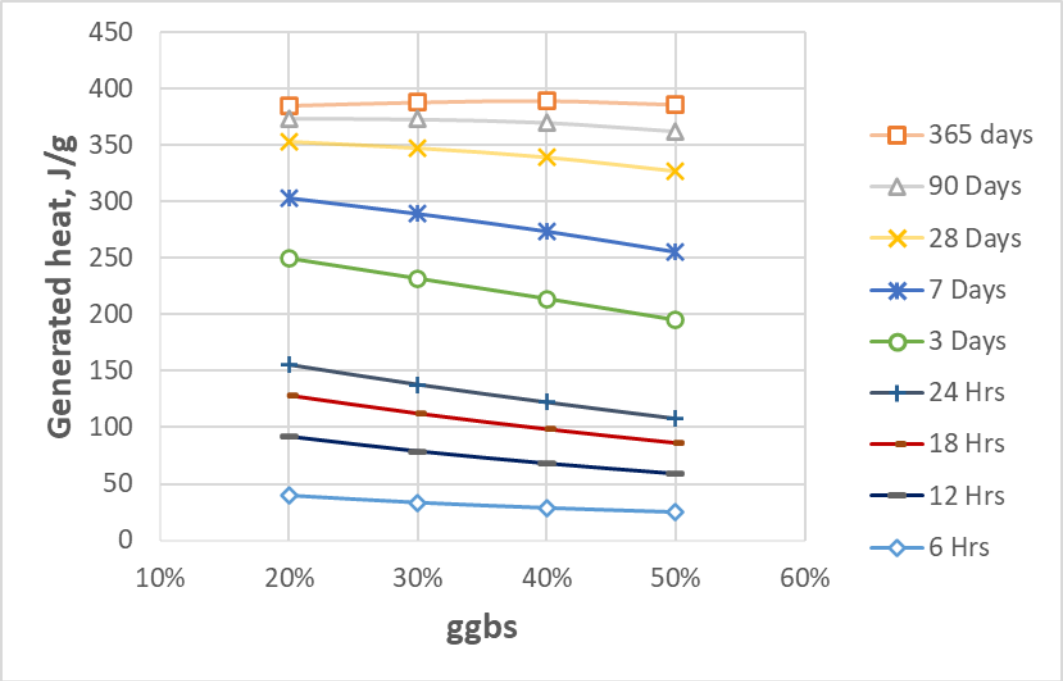

Figure F4 Heat of hydration C60 MPa

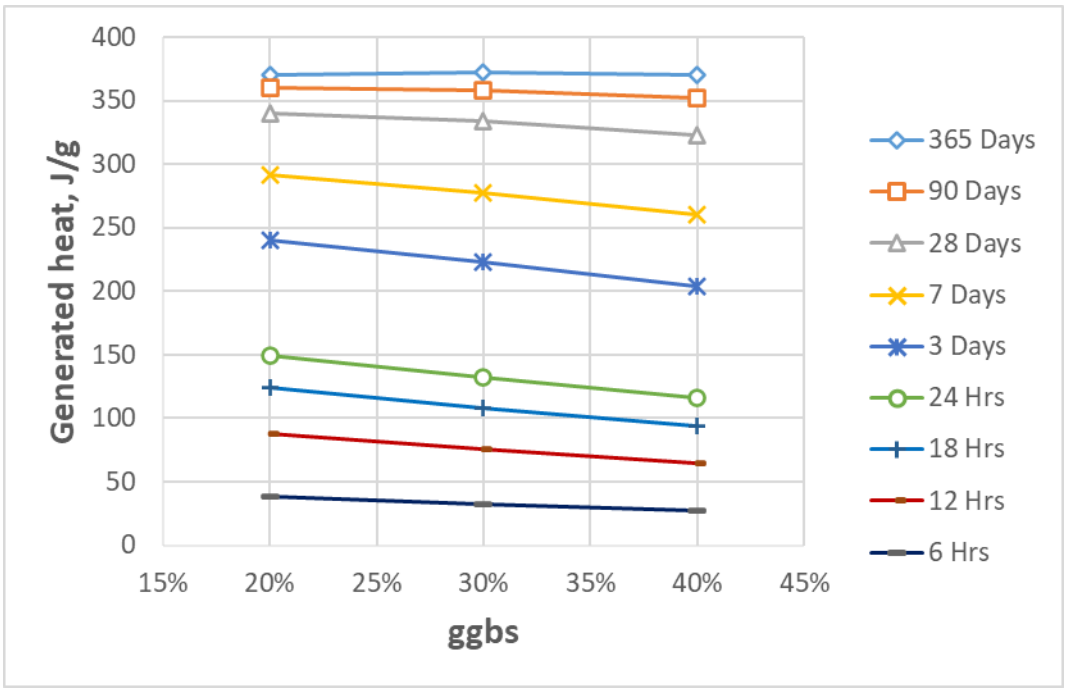

Figure F5 Heat of hydration C70 MPa

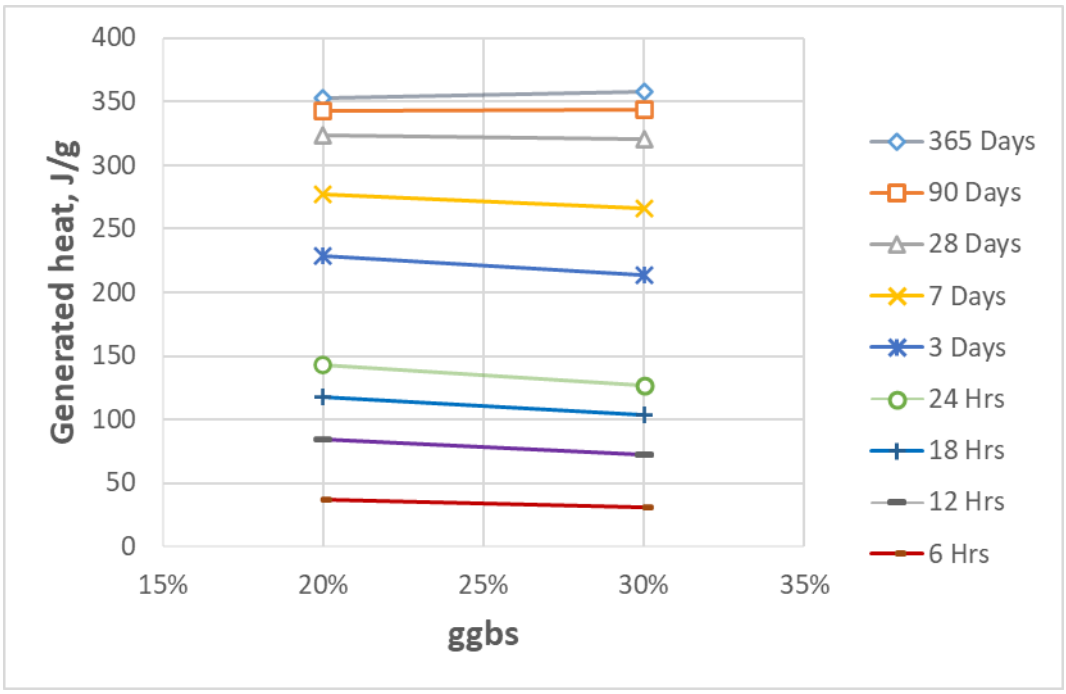

Figure F6 Heat of hydration C80 MPa

Appendix G Design charts for mix design procedure for ggbs (30-80%) and targeted compressive strength 30-80 MPa.

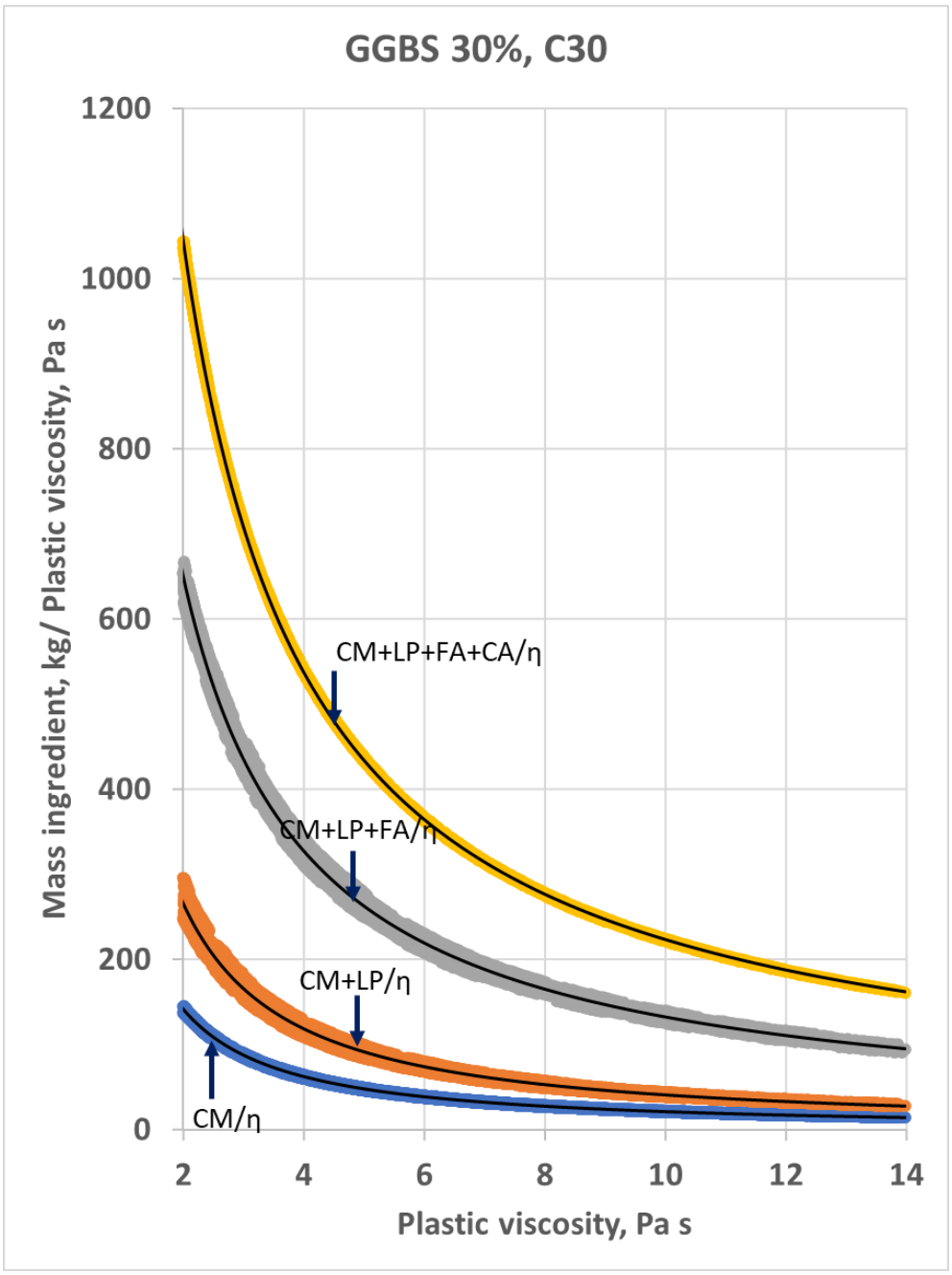

Figure G1 Ingredient mass (kg) normalised by mix plastic viscosity vs. plastic viscosity for ggbs 30% and compressive strength 30MPa mix

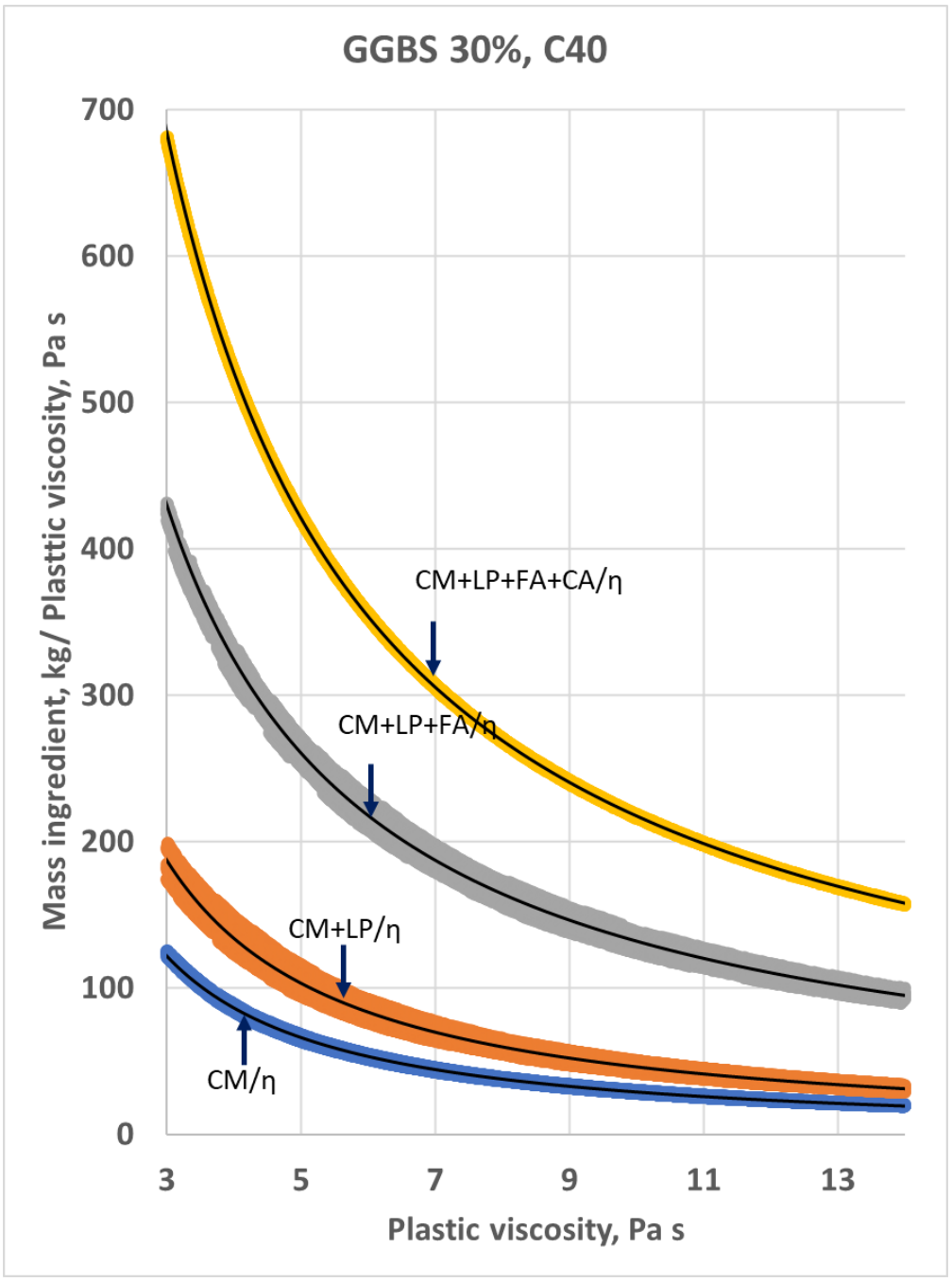

Figure G2 Ingredient mass (kg) normalised by mix plastic viscosity vs. plastic viscosity for ggbs 30% and compressive strength 40MPa mix

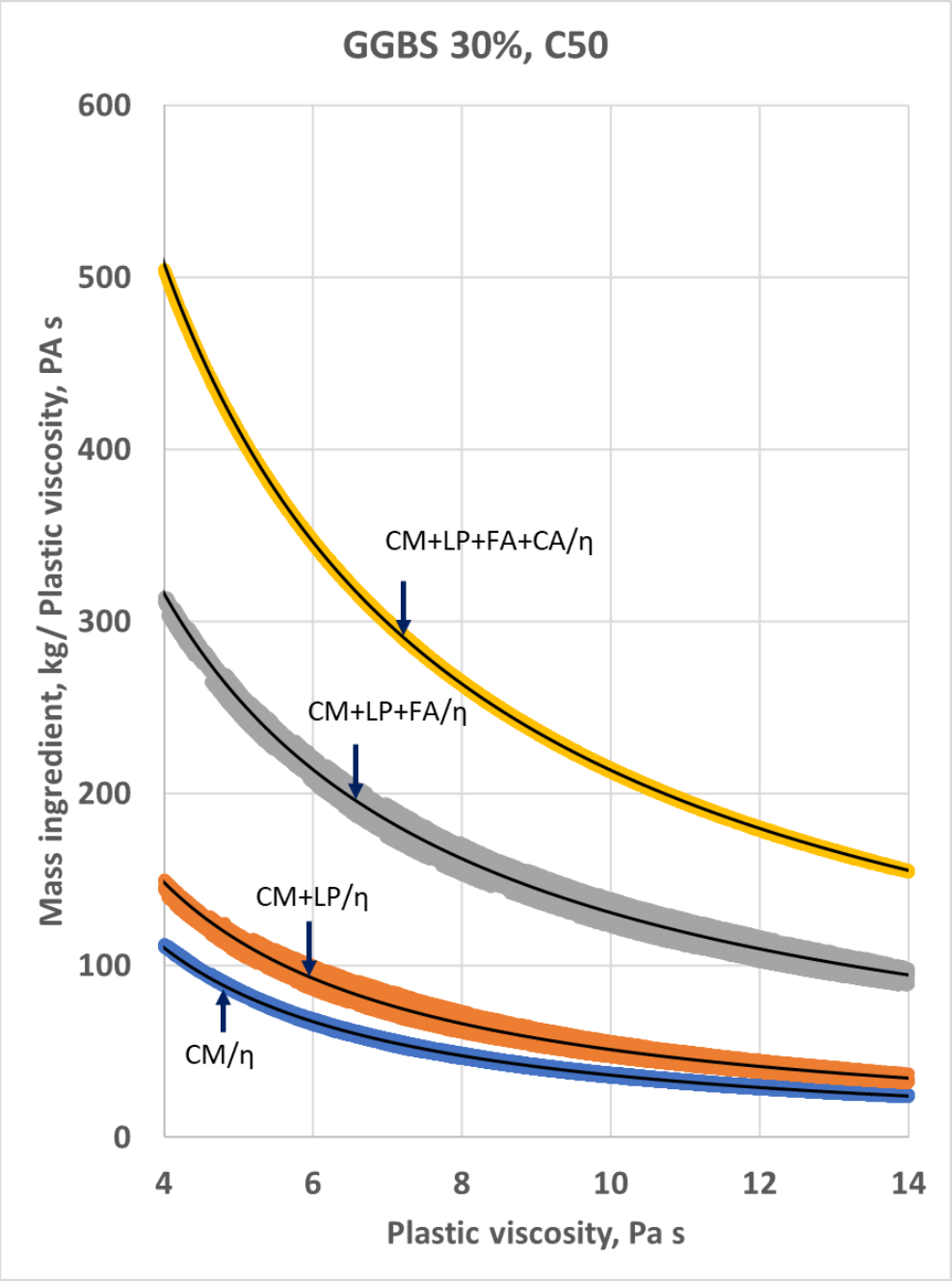

Figure G3 Ingredient mass (kg) normalised by mix plastic viscosity vs. plastic viscosity for ggbs 30% and compressive strength 50MPa mix

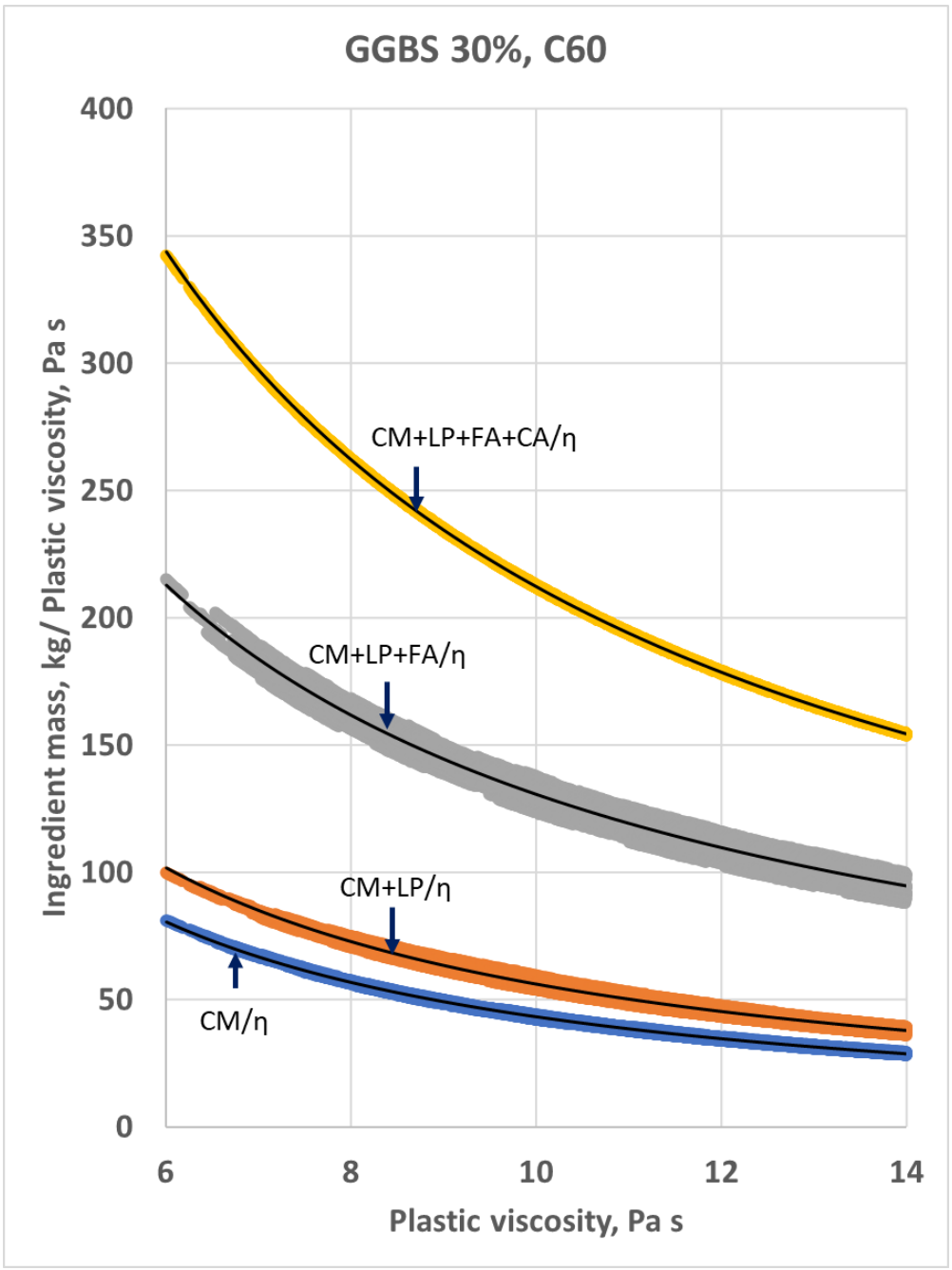

Figure G4 Ingredient mass (kg) normalised by mix plastic viscosity vs. plastic viscosity for ggbs 30% and compressive strength 60MPa mix

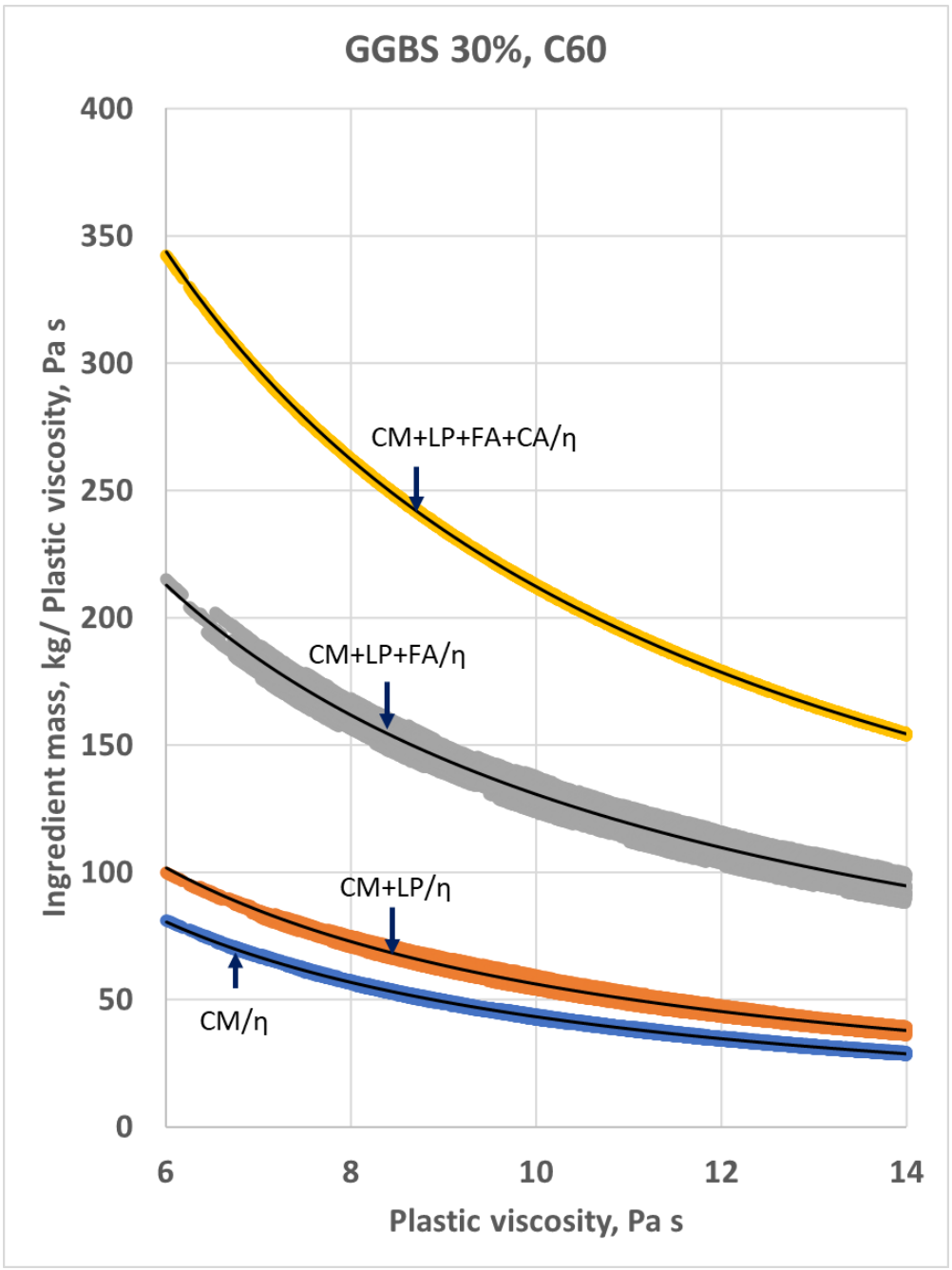

Figure G5 Ingredient mass (kg) normalised by mix plastic viscosity vs. plastic viscosity for ggbs 30% and compressive strength 70MPa mix

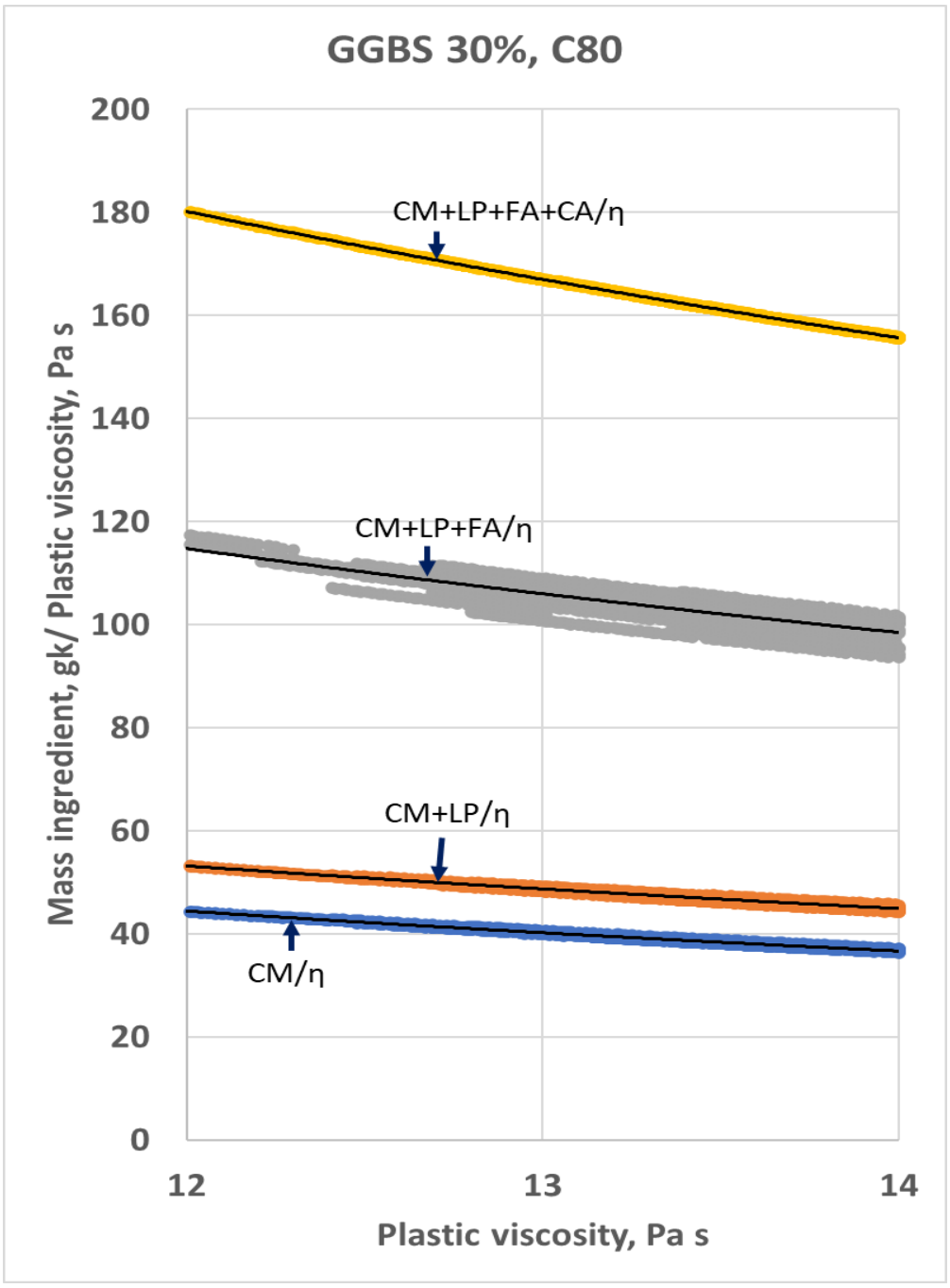

Figure G6 Ingredient mass (kg) normalised by mix plastic viscosity vs. plastic viscosity for ggbs 30% and compressive strength 80MPa mix

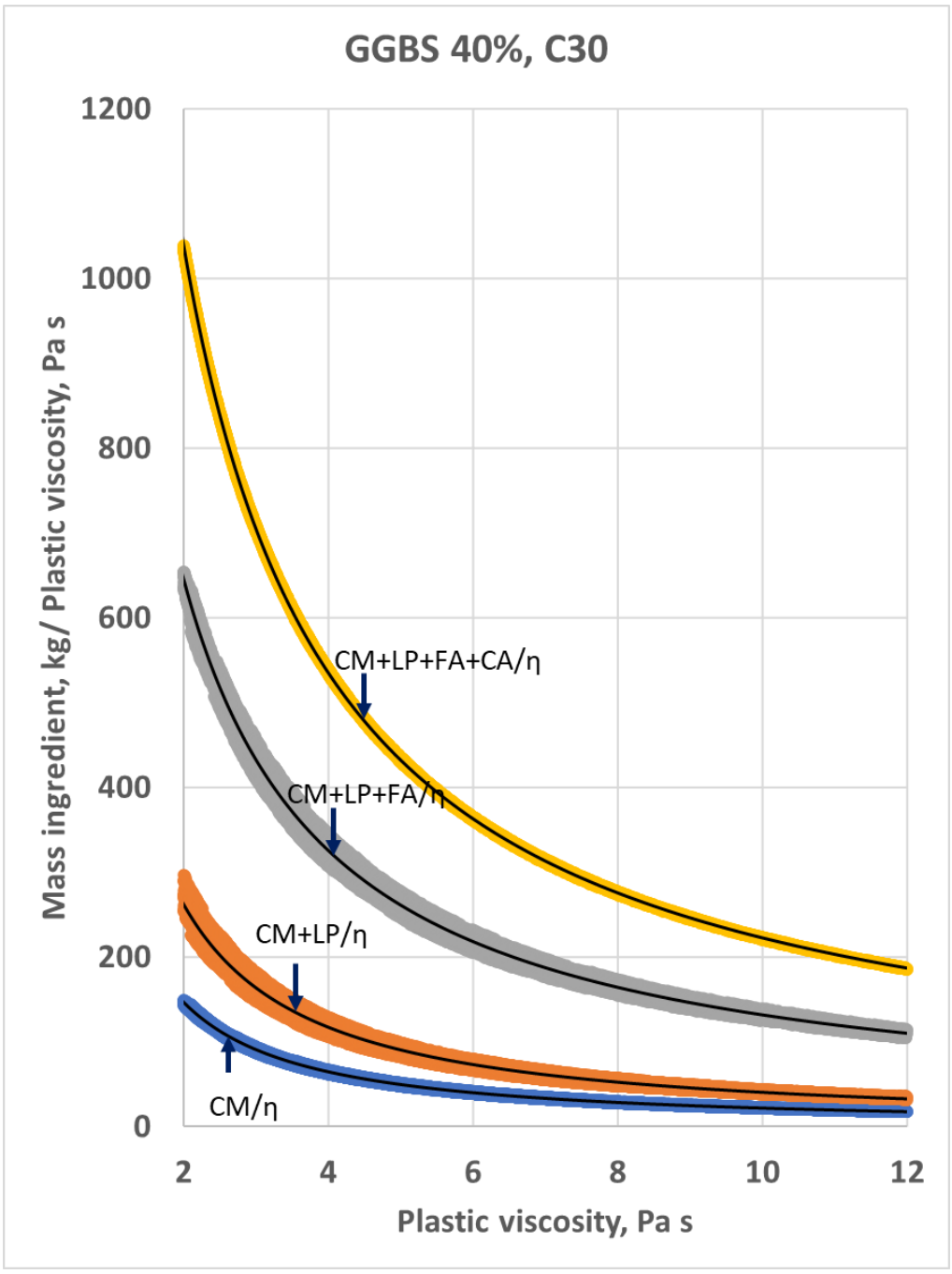

Figure G7 Ingredient mass (kg) normalised by mix plastic viscosity vs. plastic viscosity for ggbs 40% and compressive strength 30MPa mix

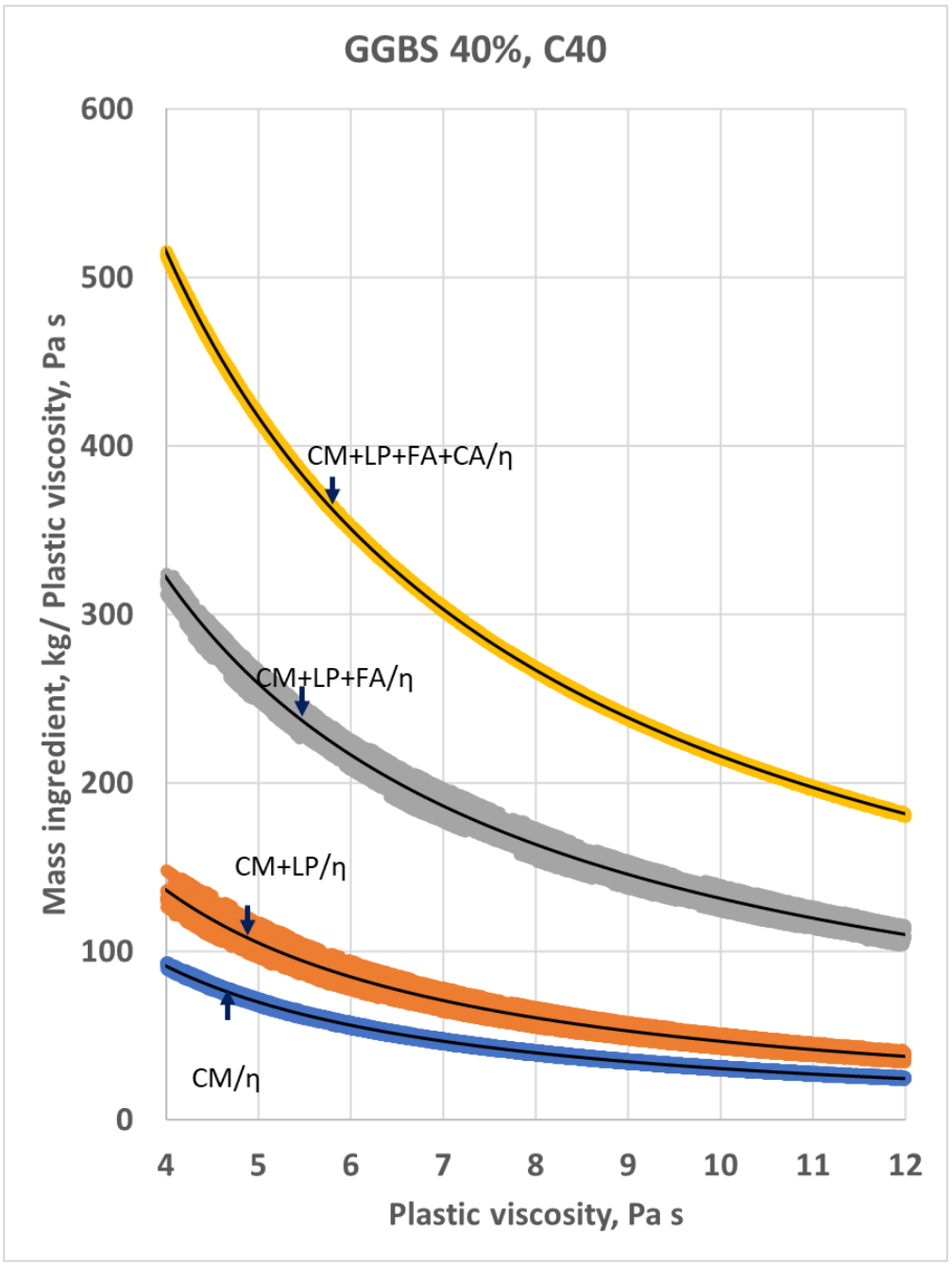

Figure G8 Ingredient mass (kg) normalised by mix plastic viscosity vs. plastic viscosity for ggbs 40% and compressive strength 40MPa mix

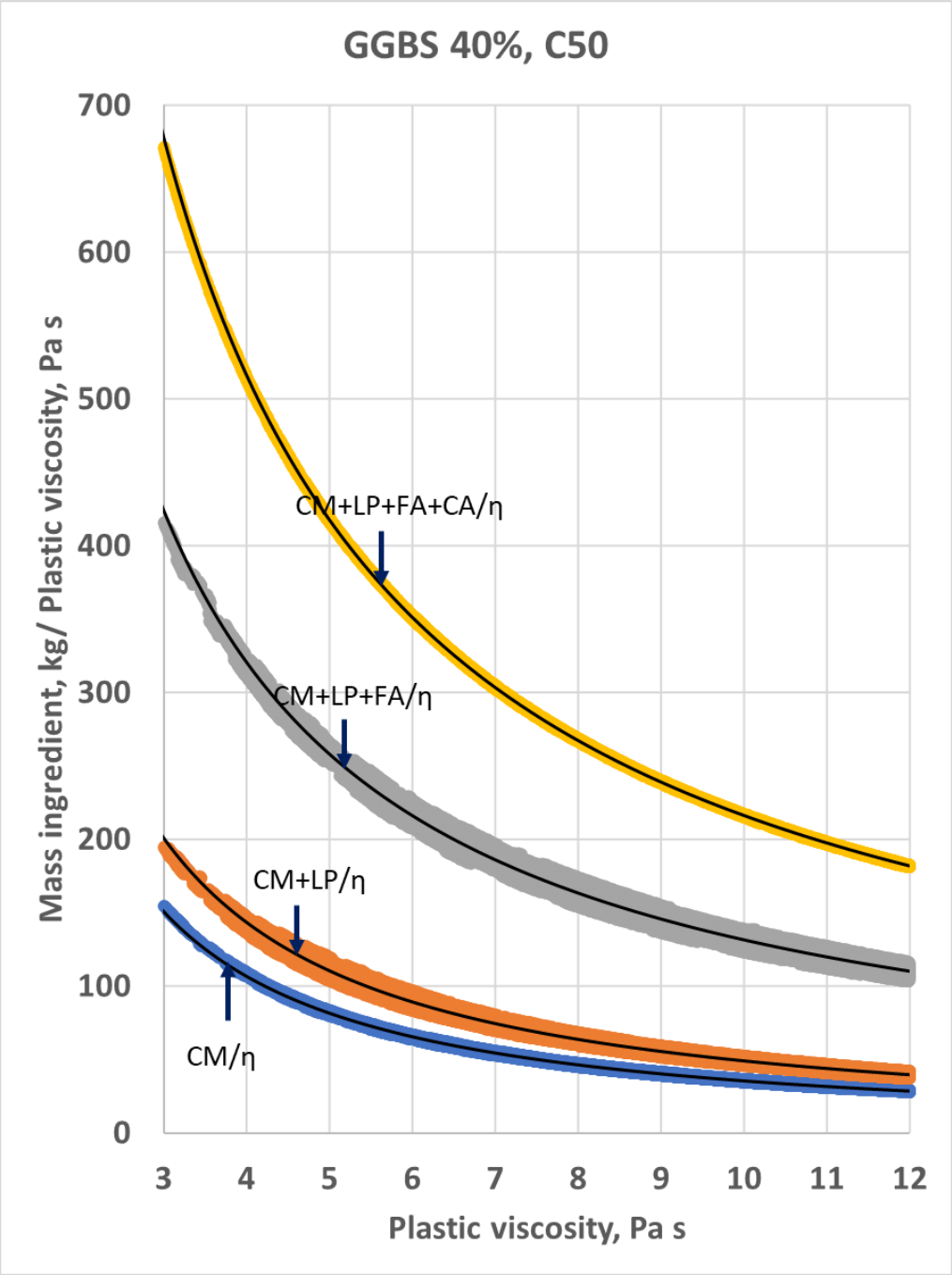

Figure G9 Ingredient mass (kg) normalised by mix plastic viscosity vs. plastic viscosity for ggbs 40% and compressive strength 50MPa mix

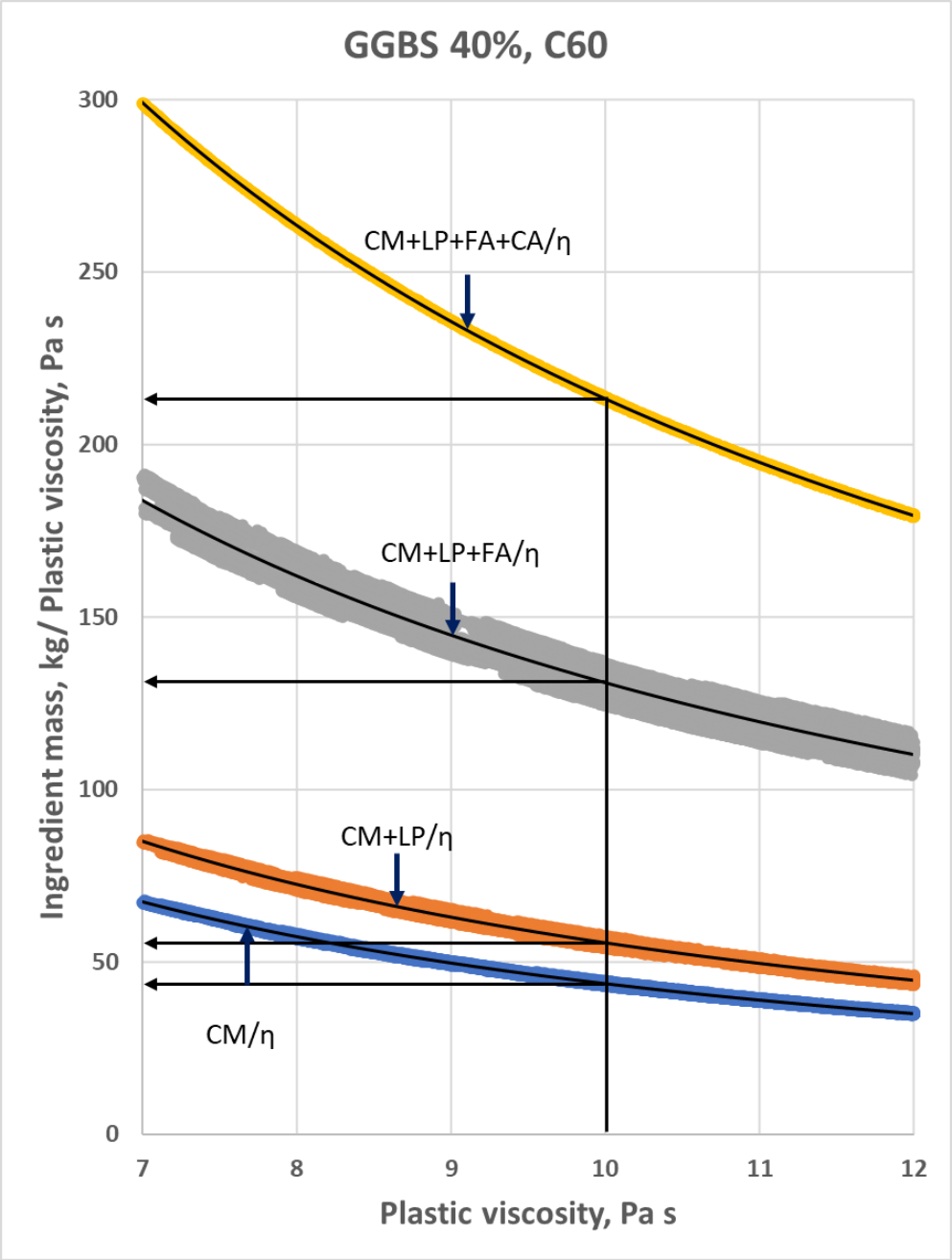

Figure G10 Ingredient mass (kg) normalised by mix plastic viscosity vs. plastic viscosity for ggbs 40% and compressive strength 60MPa mix

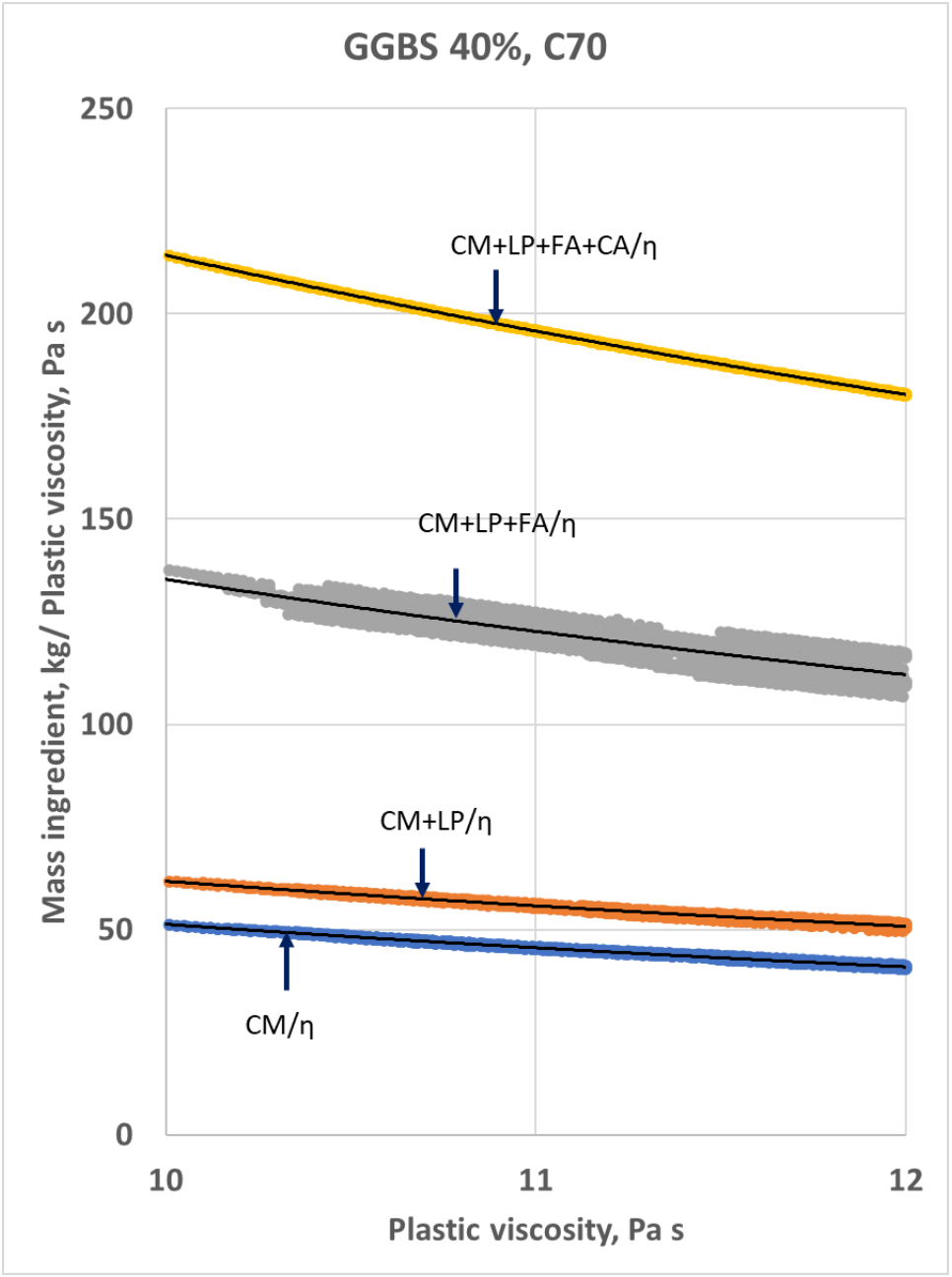

Figure G11

Ingredient mass (kg) normalised by mix plastic viscosity vs. plastic viscosity for ggbs 40% and compressive strength 70MPa mix

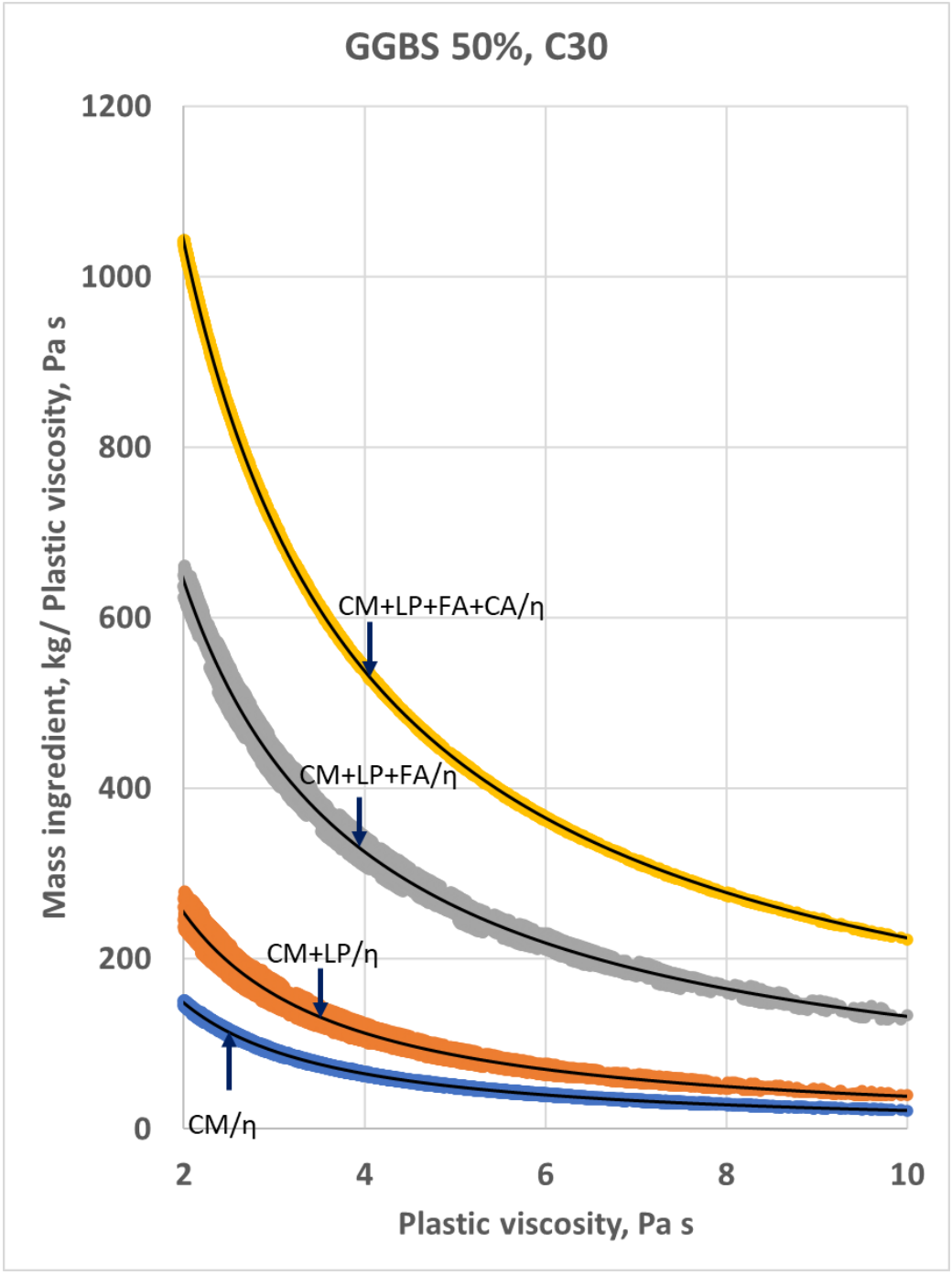

Figure G12 Ingredient mass (kg) normalised by mix plastic viscosity vs. plastic viscosity for ggbs 50% and compressive strength 30MPa mix

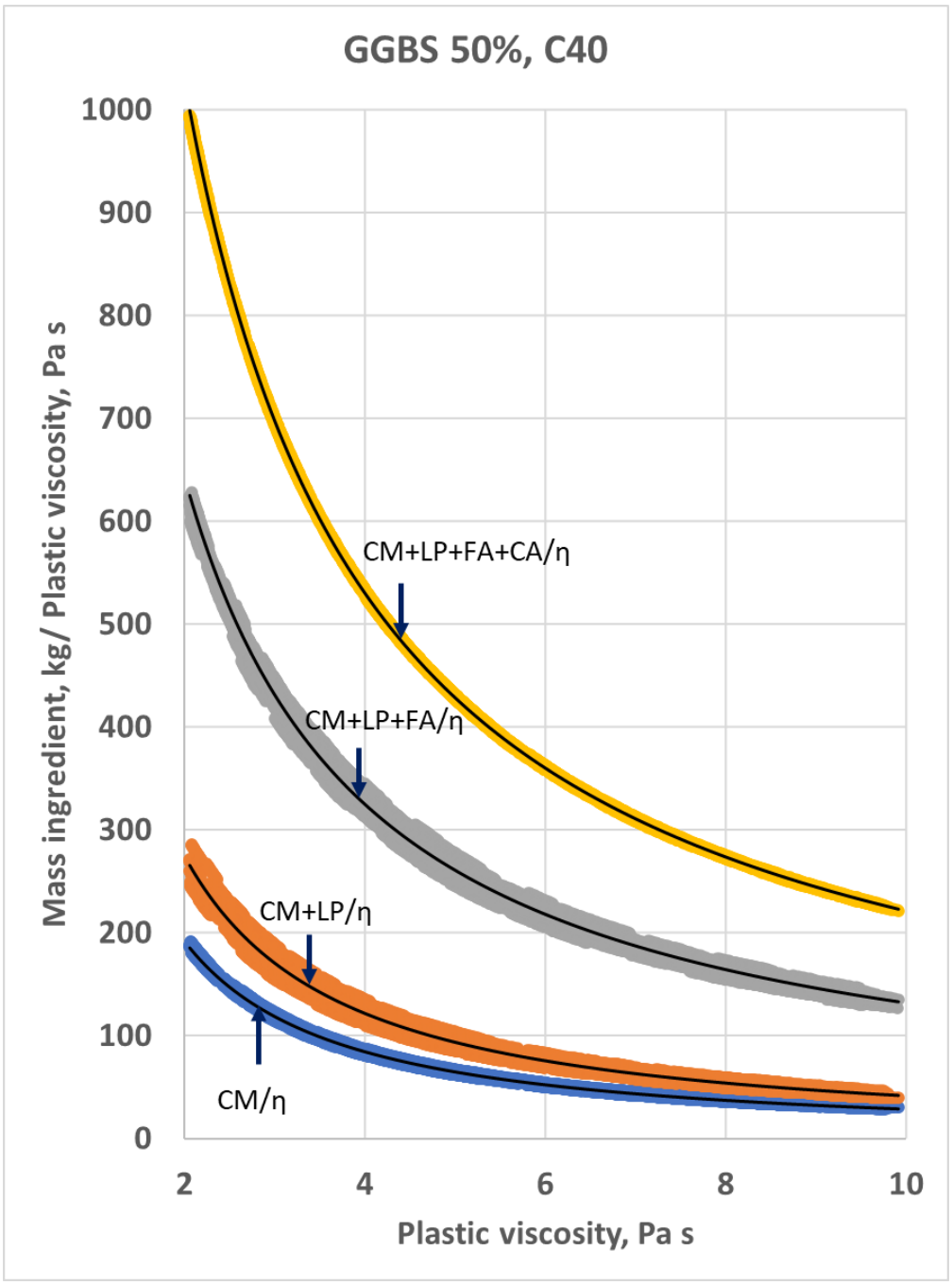

Figure G13 Ingredient mass (kg) normalised by mix plastic viscosity vs. plastic viscosity for ggbs 50% and compressive strength 40MPa mix

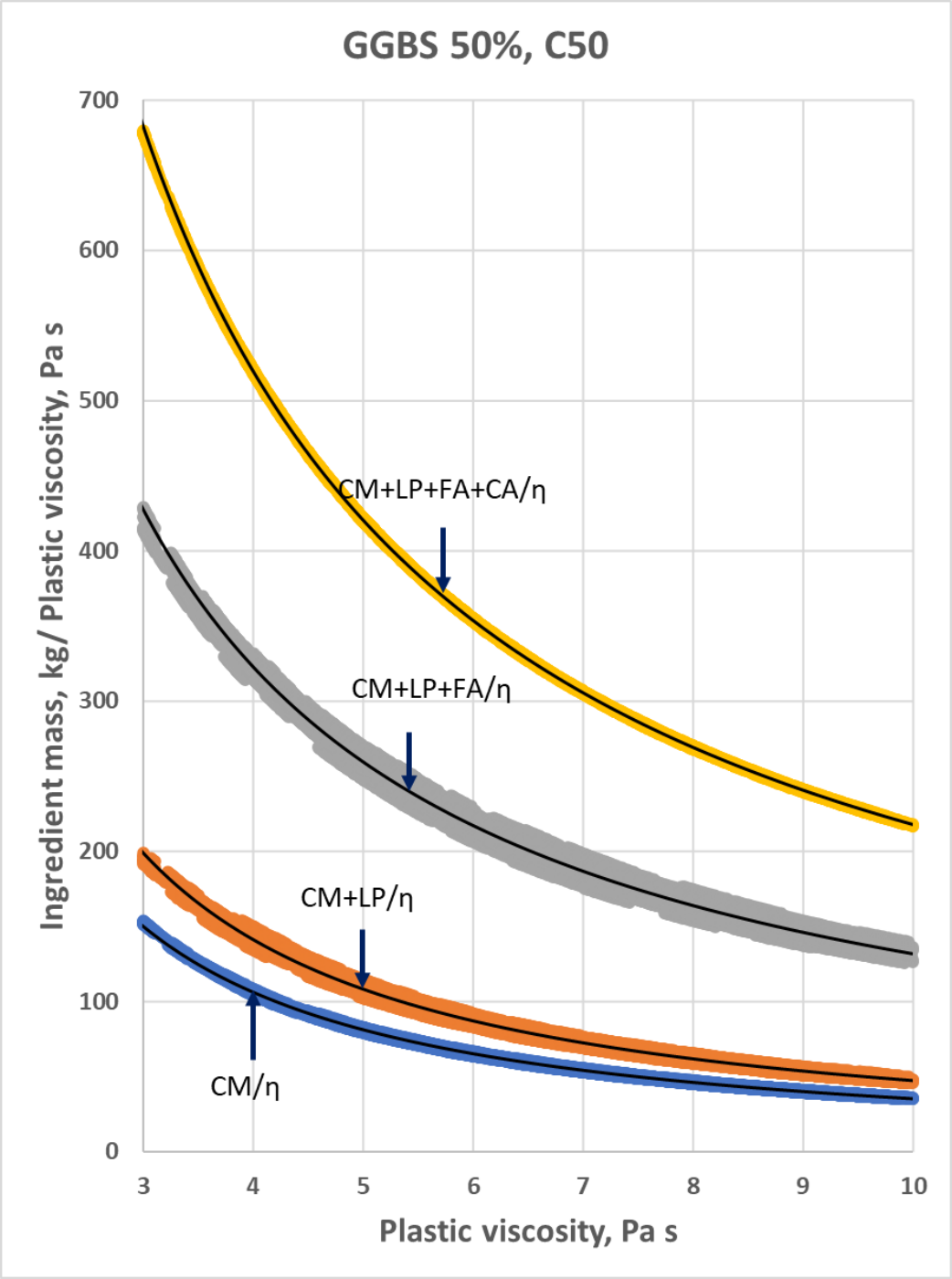

Figure G14 Ingredient mass (kg) normalised by mix plastic viscosity vs. plastic viscosity for ggbs 50% and compressive strength 50MPa mix

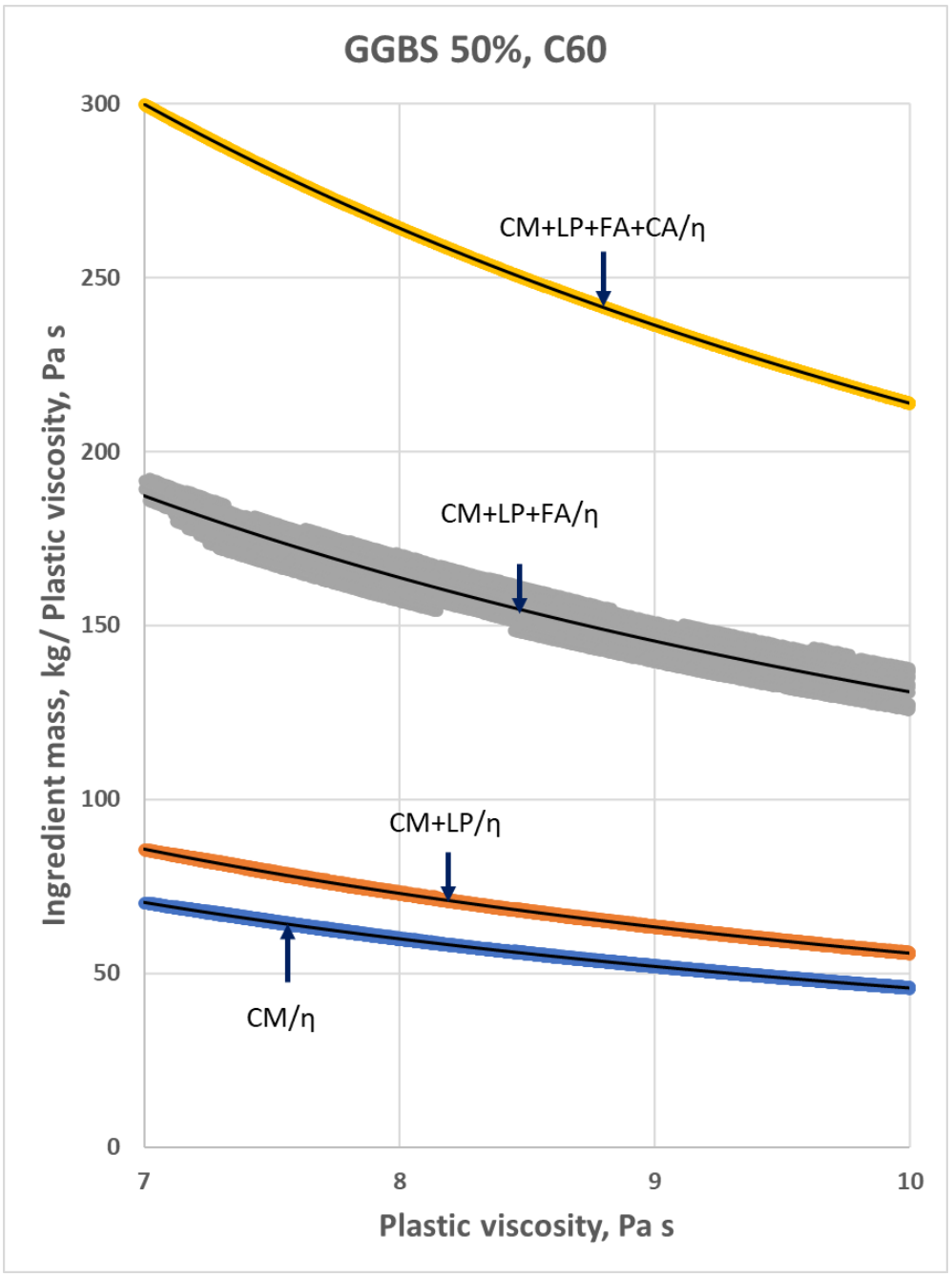

Figure G15 Ingredient mass (kg) normalised by mix plastic viscosity vs. plastic viscosity for ggbs 50% and compressive strength 60MPa mix

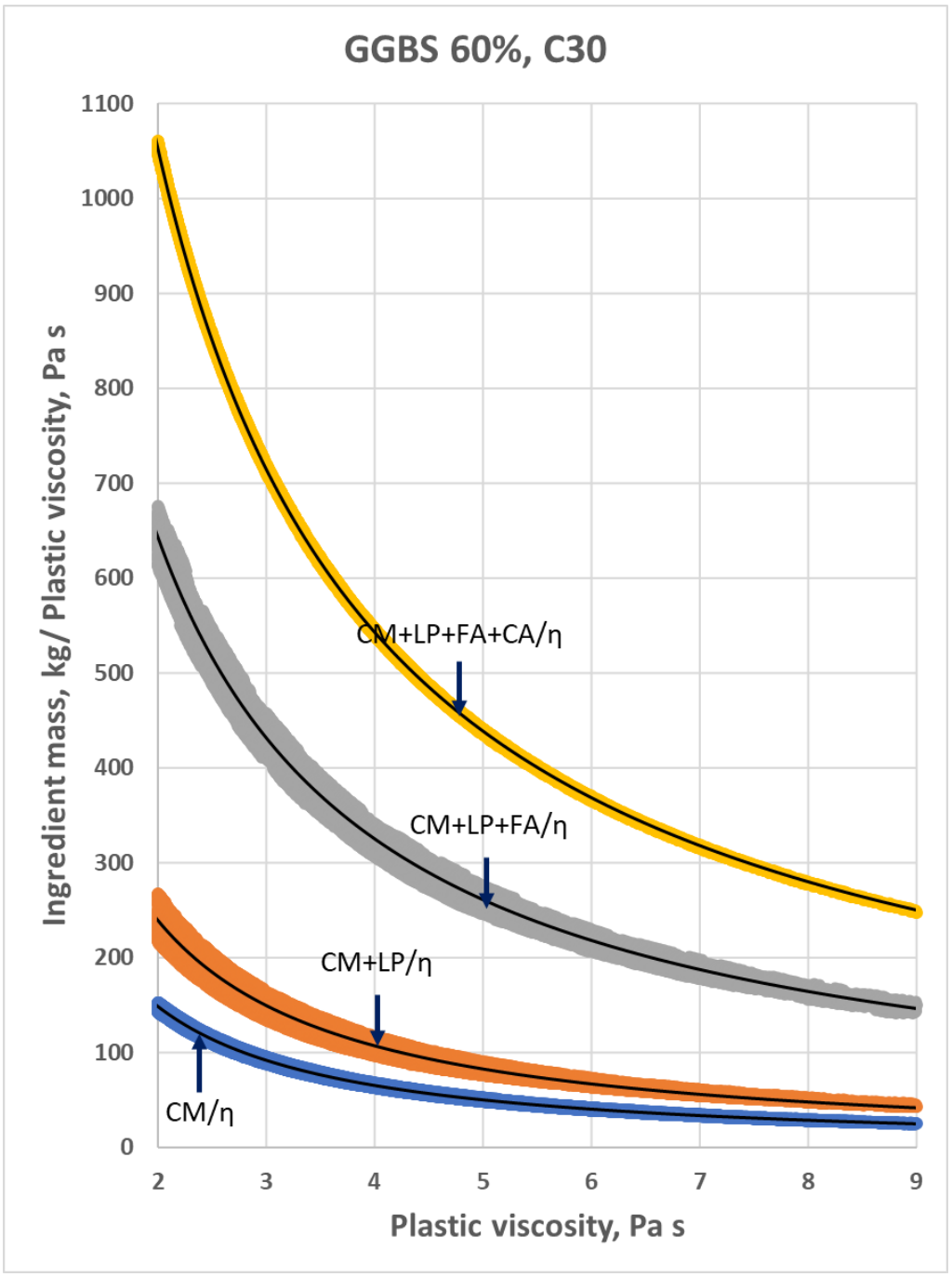

Figure G16 Ingredient mass (kg) normalised by mix plastic viscosity vs. plastic viscosity for ggbs 60% and compressive strength 30MPa mix

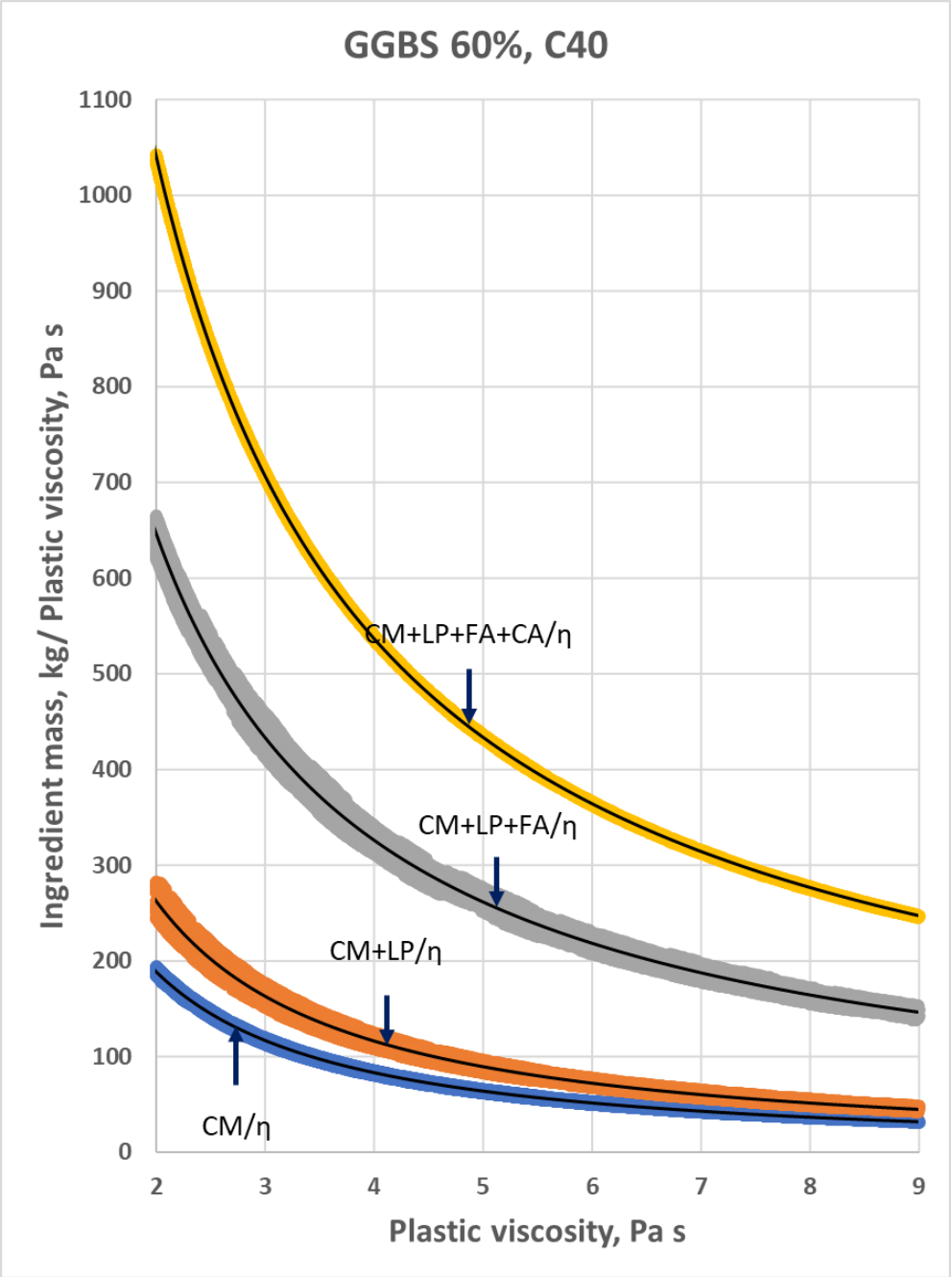

Figure G17 Ingredient mass (kg) normalised by mix plastic viscosity vs. plastic viscosity for ggbs 60% and compressive strength 40MPa mix

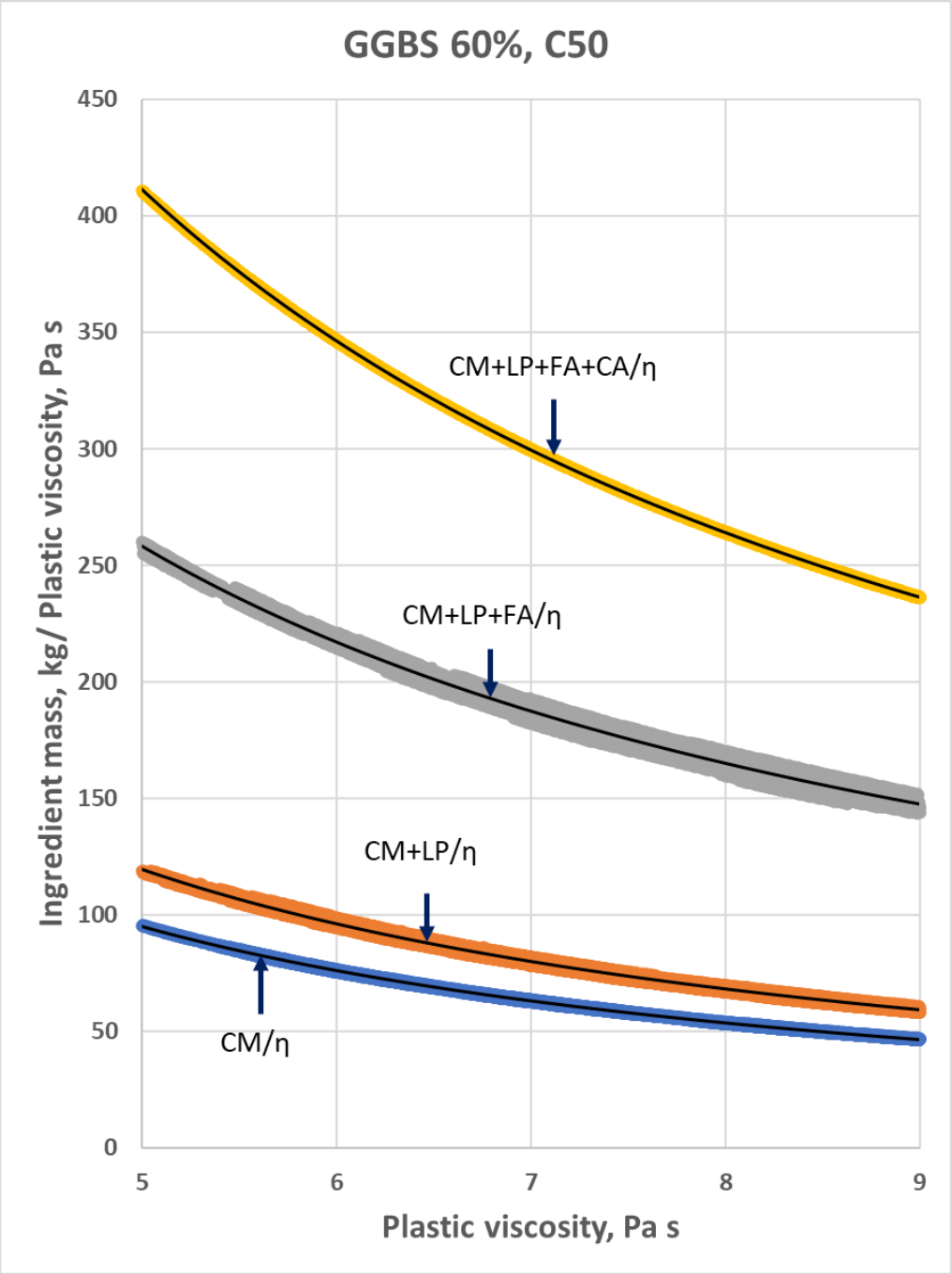

Figure G18 Ingredient mass (kg) normalised by mix plastic viscosity vs. plastic viscosity for ggbs 60% and compressive strength 50MPa mix

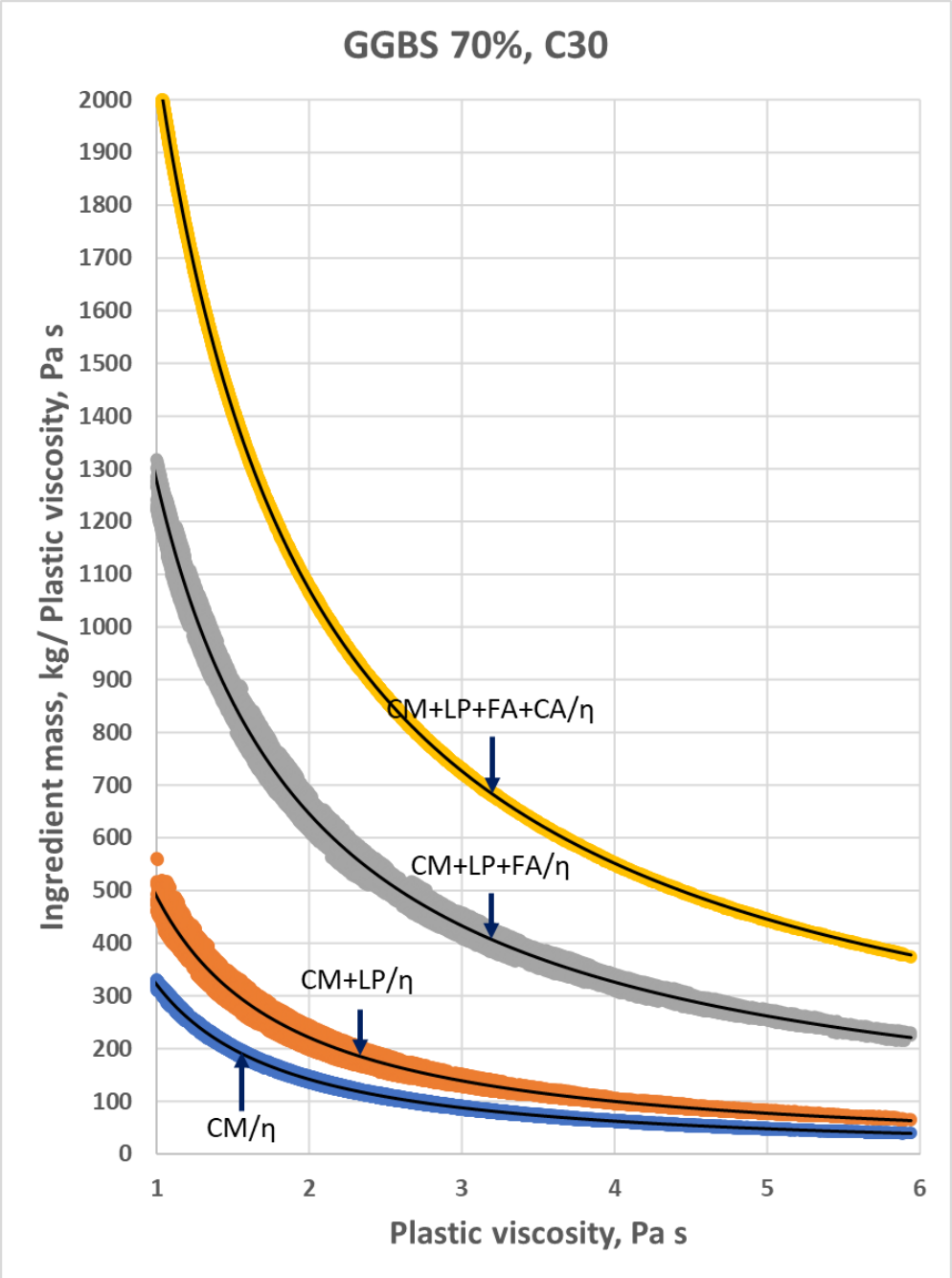

Figure G19 Ingredient mass (kg) normalised by mix plastic viscosity vs. plastic viscosity for ggbs 70% and compressive strength 30MPa mix

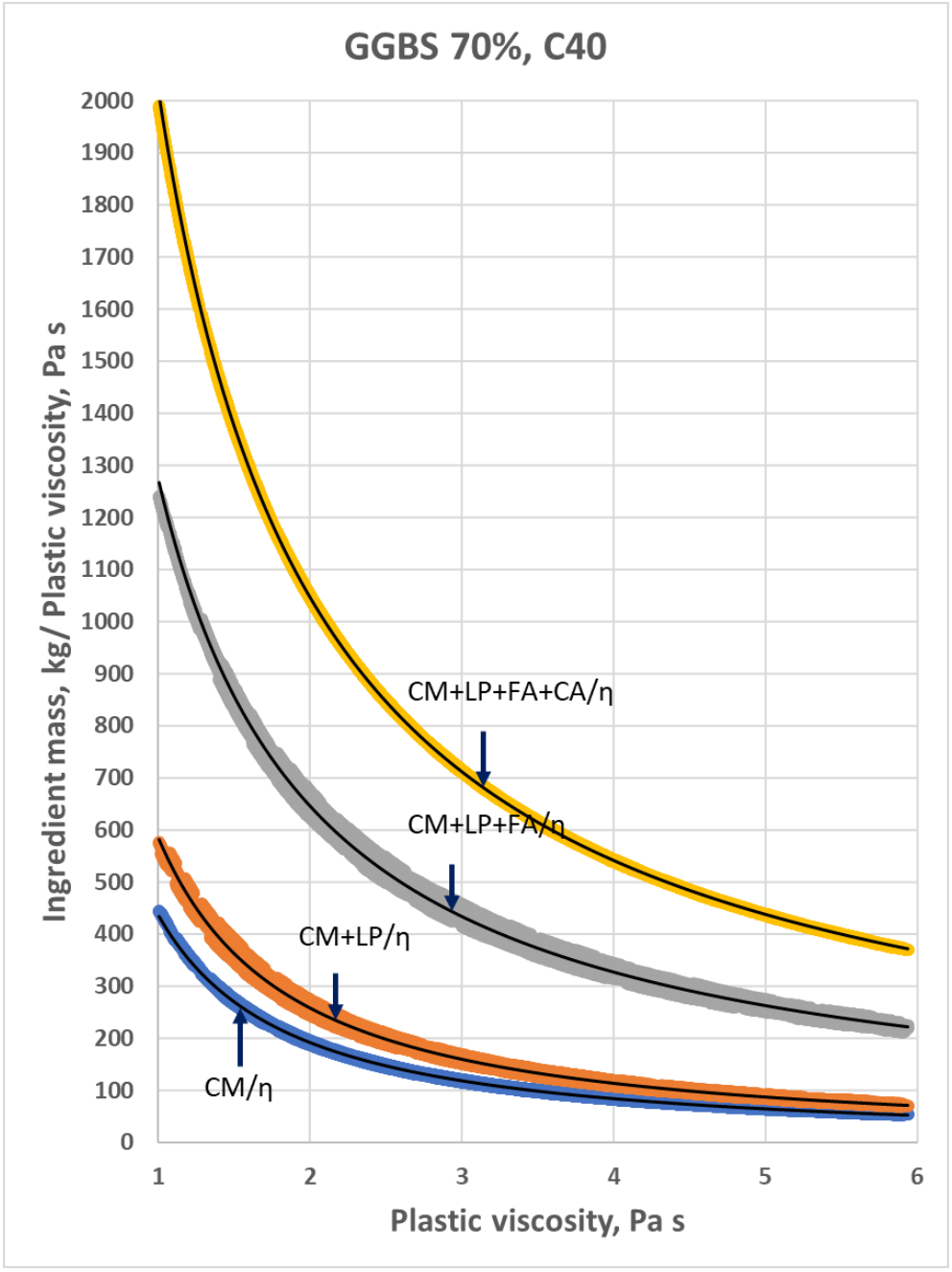

Figure G20 Ingredient mass (kg) normalised by mix plastic viscosity vs. plastic viscosity for ggbs 70% and compressive strength 40MPa mix

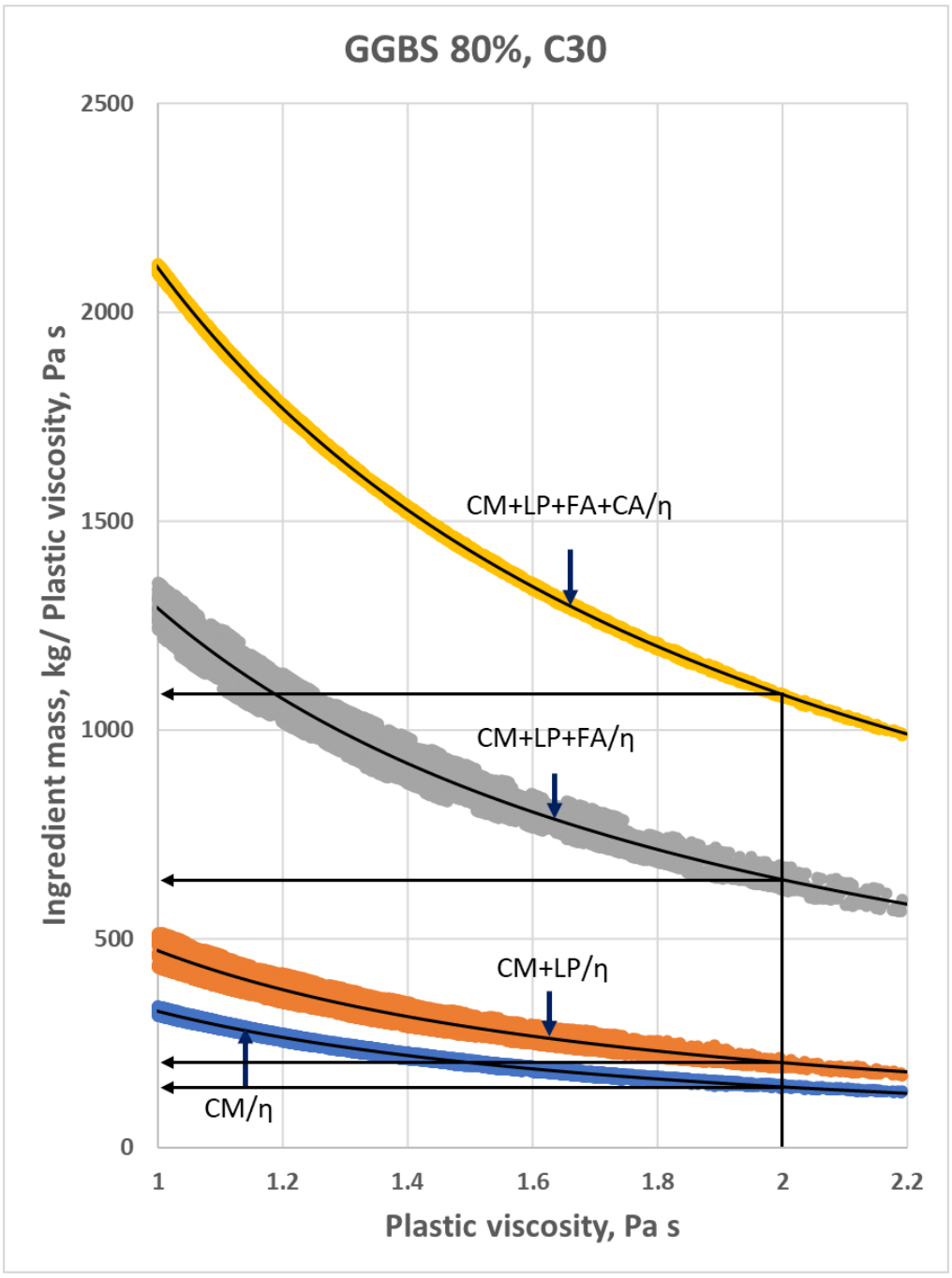

Figure G21 Ingredient mass (kg) normalised by mix plastic viscosity vs. plastic viscosity for ggbs 80% and compressive strength 30MPa mix